Development of human precision cut slices as a novel platform for target identification and validation in the heart

Hannah Louise Paish

Doctor of Philosophy

Newcastle University

Biosciences Institute

September 2022

Abstract

Cardiovascular disease is a term used to broadly describe a range of devastating conditions, each with poor prognosis and limited treatment options. Cardiac fibrosis is one of the primary mechanisms attributed to heart failure and is characterised by cardiomyocyte loss, accumulation of extracellular matrix and increased stiffness of the cardiac muscle, culminating in impaired cardiac function. Widely employed *in vitro* and *in vivo* models used to study mechanisms of cardiac fibrosis have significant limitations and fail to account for the complexity of human heart tissue. Therefore these mechanisms need to be interrogated in more physiologically relevant human models to identify novel therapeutic targets.

Here we describe the development of a novel physiologically relevant *ex vivo* human precision cut heart (PCHS) model for investigating mechanisms of cardiac fibrosis and determining the efficacy of novel therapeutics. Left ventricular tissue was processed to create PCHS and cultured in conventional static culture or using a novel bioreactor system. Differences in PCHS viability and metabolic activity demonstrated the beneficial effects of the bioreactor system on PCHS culture. To investigate inflammation and fibrosis, PCHS were challenged with recombinant human TGF-β1, CTGF, IL-11, Angiotensin II or Galectin-3. Fibrotic and inflammatory responses were assessed through quantification of chemokines, cytokines, ECM and matrix remodelling proteins. Next, unbiased mass-based spectrometry and bulk RNA sequencing was utilised to assess changes in gene and protein expression. Using these methods we discovered that Galectin-3 induced a robust inflammatory response in PCHS, whilst TGF-β1 produced a potent fibrotic response. Ingenuity Pathway Analysis (IPA) identified upstream regulators of inflammation and fibrosis and 32 candidate compounds were selected for assessment as potential novel therapeutics. Of these compounds, n=11 exhibited promising anti-inflammatory effects whilst n=9 exhibited robust anti-fibrotic effects in PCHS. Finally through the use of four distinct cutting-edge molecular biology approaches, we identified number of soluble factors present in the circulation of a well-characterised cohort of patients with a spectrum of severity of cardiac disease. These included 32 differentially expressed proteins, identified by proteomic analysis and 8 markers identified using multi-plex ELISA.

We have optimised and developed a medium throughput culture system of 3D human cardiac tissue. The PCHS are highly reproducible and viable enabling us to interrogate mechanisms regulating inflammation and fibrosis in intact human tissue. We are able to modulate inflammation and fibrosis through the application of novel therapeutic compounds to determine their efficacy in human cardiac tissue. Whilst a small scale study of a well characterised group of female DMD carriers with a range in severity of cardiac involvement has identified a number of potential blood based biomarkers of cardiac fibrosis.

Acknowledgements

I would like to thank my supervisors Dr Lee Borthwick and Professor Derek Mann for their support and encouragement throughout the course of this PhD. Their continued guidance and advice is greatly appreciated and has enabled me to continually develop my scientific knowledge and skills.

Thanks must also be given to Ben Barksby and Rachel Burgoyne who have been great friends and colleagues, even extending offers of help with experiments in the middle of the night. I gratefully acknowledge and thank the many other members of the Newcastle Fibrosis Research Group with whom I have worked with over the course of this PhD. Many thanks also to Dr Laura Sabater, Dr Sandra Murphy, Dr Zoe Hall and Dr Pawel Palmowski for the help given and time taken for the acquisition and generation of the large variety omics datasets which were so integral to this project.

A special thanks must be given to Lucy Bates and John Bourke who were instrumental in the acquisition of the patient samples so key to the success of this project. In addition I am forever grateful to the patients and family members of donors without whom none of this work would have been possible.

The work completed during this PhD was funded by a research grant awarded to Dr Lee Borthwick from Duchenne UK.

Finally I would like to thank my entire family, especially my partner Meg, for their support, encouragement and patience throughout the whole PhD project, and especially over these final few months.

Table of Contents

Table of Contents i
List of Abbreviations v
List of Figures x
List of Tables xiii
1 Introduction 1
1.1 Fibrosis 1
1.1.1 General Fibrosis and wound healing response 1
1.1.2 Cardiac Fibrosis 1
1.1.3 Examples of cardiac fibrosis in disease 4
1.2 Current methods for the Diagnosis of cardiac fibrosis 8
1.2.1 Endomyocardial Biopsy 8
1.2.2 Cardiac magnetic resonance (CMR) Imaging 9
1.2.3 Serum Markers 12
1.3 Pathways involved in Cardiac Fibrosis and the current and emerging therapies targeting them 17
1.3.1 Transforming Growth Factor-β1 (TGF-β1) signalling 18
1.3.2 Targeting the TGF-β1 signalling pathway 20
1.3.3 Renin-Angiotensin-Aldosterone System (RAAS) 22
1.3.4 Endothelin 1 24
1.3.5 Emerging treatments for fibrotic diseases 24
1.4 Current research models for investigating cardiac fibrosis and disease 26
1.4.1 Use of *in vitro* techniques: 2D cell culture, organoids and 3D methods 26
1.4.2 *In vivo* models of cardiac fibrosis: advantages and disadvantages 27
1.5 Use of Precision Cut Slice technology in studying disease 29
1.5.1 Development of Precision Cut Slices as a model for disease 29
2 Study Rationale, Hypothesis and Aims 32
2.1 Study Rationale 32
2.2 Hypothesis 32
2.3 Aims 33
2.3.1 Development of Precision Cut Heart Slice model from human tissue. 33
2.3.2 Investigate the molecular pathways involved in cardiac fibrosis and inflammation. 33
2.3.3 Use established and novel therapeutics to manipulate cardiac fibrosis and inflammation. 33
2.3.4 Identification of a molecular signature of cardiac fibrosis in the blood of patients. 33
3 General materials and methods 34
3.1. Human ethics and tissue acquisition 34

3.1.1. Human heart ethical statement and patient demographics....34
3.2. Processing tissue and generating human precision cut slices (PCHS)....35
3.3. Enzyme Linked ImmunoSorbant Assay (ELISA)....36
3.4. MesoScale Discovery™ (MSD) U-Plex Assay....38
3.5. Lactate Dehydrogenase Assay (LDH)....38
3.6. Resazurin Assay....39
3.6.1. Resazurin on PCHS....39
3.6.2. Resazurin on Cultured Cells....39
3.7. RNA isolation from PCHS....39
3.8. RNA Integrity and Quantification....40
3.9. Cardiac Fibroblast Isolation and Culture....40
3.10. Statistical Analysis....41
4 Precision Cut Heart Slice (PCHS) culture development, optimisation and disease modelling....42
4.1 Introduction....42
4.1.1 Current research methods and disease models of cardiac fibrosis....42
4.1.2 The use of PCS technology in cardiac research and the current limitations of the technology....43
4.2 Rationale, Hypothesis and Objectives....47
4.2.1 Rationale....47
4.2.2 Hypothesis....47
4.2.3 Objectives....47
4.3 Materials and methods....48
4.3.1 Patient Demographics....48
4.3.2 Generation of PCHS and optimisation of long-term culture conditions....48
4.3.3 Treatments for PCHS....49
4.3.4 Enzyme Linked Immunosorbent Assay....50
4.3.5 B-type Natriuretic Peptide Assay....51
4.3.6 Resazurin....51
4.3.7 Statistical Analysis....51
4.4 Results....52
4.4.1 Optimisation of the long-term culture of Precision Cut Heart Slice (PCHS)....52
4.4.2 Bioreactor rocking culture maintains the viability of PCHS compared to static culture....55
4.5 Using the PCHS system to model disease....60
4.5.1 Induction of an inflammatory profile in PCHS....60
4.5.2 Modulation of inflammatory response through the application of therapeutics....63
4.5.3 Induction of a pro-fibrotic response in PCHS after TGF-β1 treatment....66

4.5.4 Modulating the effect of pro-fibrogenic stimuli 70
4.6 Discussion 75
5 Identification of novel targets using proteomics and RNA sequencing 81
5.1 Introduction 81
5.1.1 TGF-β1 81
5.1.2 Angiotensin II 82
5.1.3 Galectin-3 84
5.1.4 Connective Tissue Growth Factor (CTGF) 86
5.1.5 Interleukin-11 (IL-11) 87
5.2 Rationale, Hypothesis and Objectives 90
5.2.1 Rationale 90
5.2.2 Hypothesis 90
5.2.3 Objectives 91
5.3 Materials and methods 92
5.3.1 Treatments for PCHS 92
5.3.2 Treatments of Primary Cardiac Fibroblasts 94
5.3.3 ELISA on conditioned culture media from cardiac fibroblasts and PCHS 96
5.3.4 MesoScale Discovery™ (MSD) analysis of recombinant stimuli 96
5.3.5 RNA Isolation, Integrity and analysis 96
5.3.6 RNA sequencing 96
5.3.7 Proteome sample preparation 97
5.3.8 Downstream analysis of RNA sequencing results 98
5.3.9 Ingenuity Pathway Analysis 99
5.3.10 Statistical Analysis 99
5.4 Results 101
5.4.1 Exploring other pathways involved in Cardiac Fibrosis 101
5.4.2 Effects of exogenous stimuli on PCHS – an unbiased approach 118
5.4.3 Investigating the inhibitory effect of compounds identified through IPA on primary cardiac fibroblasts. 145
5.4.4 IPA Compounds on PCHS 155
5.5 Discussion 171
6 Patient Biomarker Study 177
6.1 Introduction 177
6.1.1 Female Manifesting Carriers 177
6.1.2 Biomarkers 178
6.2 Rationale, Hypothesis and Objectives 180
6.2.1 Rationale 180

6.2.2 Hypothesis 180
6.2.3 Objectives 181
6.3 Materials and Methods 182
6.3.1 Ethical approval and Patient Stratification and Recruitment 182
6.3.2 Sample collection and processing 182
6.3.3 Neoepitopes 185
6.3.4 Mesoscale Discovery™ Multiplex ELISA 185
6.3.5 Lipidomics 185
6.3.6 Proteomics 186
6.3.7 Statistical Analysis 187
6.4 Results 188
6.4.1 Patient Demographics 188
6.4.2 Nordic Neoepitope Biomarkers 188
6.4.3 Multi-plex ELISA to quantify proteins present in patient plasma 192
6.4.4 Lipidomic profiles 195
6.4.5 Proteomic differences between severity of disease 199
6.5 Discussion 212
7 Final Conclusions, Limitations and Future Work 215
7.1 Final Conclusions and Limitations 215
7.2 Future Directions 217
8 References 220

List of Abbreviations

2D	Two dimensional
3D	Three dimensional
AAV	Adeno-associated virus
ACE	Angiotensin-converting enzyme
ADAM	A disintegrin and metalloproteinases
ALK5	Activin receptor like kinase
ADAMTS	ADAMs with a thrombospondin motif
ANOVA	Analysis of variance
ARB	Angiotensin receptor blockers
BDM	2,3-butanedione-monoxime
BMD	Becker's Muscular Dystrophy
BME	Beta Mercaptoethanol
BMP	Bone morphogenetic protein
BNP	B-type natriuretic peptide
BSA	Bovine serum albumin
Ca^{2+}	Calcium
CCL	Chemokine (C-C motif) ligand
CCN	Cellular communication network
cDNA	Complementary DNA
cm	Centimetre
CMRI	Cardiac magnetic resonance imaging
CO2	Carbon dioxide
COL	Collagen
CTGF	Connective tissue growth factor
cTnT	Cardiac troponin T
CVD	Cardiovascular Disease
CXCL	Chemokine (C-X-C motif) ligand
DAMP	Damage associated molecular pattern
DAPC	Dystrophin associated protein complex
DBD	Donation after brain death

DCD	Donation after circulatory death
DMD	Duchenne Muscular Dystrophy
DMSO	Dimethyl sulfoxide
DNA	Deoxyribonucleic acid
dsRNA	Double stranded RNA
ECM	Extracellular matrix
EDTA	Ethylenediaminetetraacetic acid
EGF	Epidermal growth factor
ELISA	Enzyme linked immunosorbent assay
EMB	Endomyocardial biopsy
ET	Endothelin
EU	European Union
FBLN	Fibulin
FDR	False discovery rate
FGF	Fibroblast growth factor
FN	Fibronectin
g	Gram
GAPDH	Glyceraldehyde 3-phosphate dehydrogenase
GBCA	Gadolinium based contrast agents
GM-CSF	Granulocyte-macrophage colony-stimulating factor
HBSS	Hanks' Balanced Salt Solution
HCM	Hypertrophied cardiomyopathy
HEPES	N-(2-Hydroxyethyl) piperazine-N’-(2-ethanesulfonic acid)
hESC	Human embryotic stem cells
HF	Heart Failure
HFpEF	Heart Failure with Preserved Ejection Fraction
HFrEF	Heart Failure with Reduced Ejection Fraction
HHD	Hypertensive heart disease
HRP	Horseradish peroxidase
ICAM	Intracellular adhesion molecule
IFN	Interferon
IGFBP	Insulin-like growth factor binding protein

IHC	Immunohistochemistry
IL	Interleukin
IL-1rl1	Interleukin 1 receptor ligand 1
IPF	Idiopathic pulmonary fibrosis
iPS	Induced pluripotent stemcells
IVS	Intraventricular septum
kDa	Kilodalton
kg	Kilogram
kPa	Kilopascal
L	Litre
LDH	Lactate dehydrogenase
LGE	Late gadolinium enhancement
LPS	Lipopolysaccharide
LV	Left ventricle
LVAD	Left ventricle assistance device
LVEF	Left ventricular ejection fraction
m/z	Mass to charge ratio
MCP	Monocyte chemoattractant protein
MFI	Mean fluorescence intensity
mg	Milligram
MI	Myocardial infarction
MIP1	Macrophage Inflammatory Protein-1
miRNA	MicroRNA
ml	Millilitre
mm	Millimetre
mmol	Millimoles
MMP	Matrix metalloproteinase
MOLLI	Modified Look-Locker sequence
MRA	Mineralocorticoid antagonist
mRNA	Messenger RNA
MSC	Mesenchymal stem cells
MSD	Meso Scale DiscoveryTM

NAFLD	Non-alcoholic fatty liver disease
ncRNA	Non-coding RNA
ng	Nanogram
NHS	National health service
NIDCM	Non-ischemic dilated cardiomyopathy
nm	Nanometre
NSF	Nephrogenic systemic fibrosis
NT-proBNP	N-terminal pro-BNP
O_2	Oxygen
^oC	Degrees Celsius
Padj	Adjusted p value
PAI-1	Plasminogen activator inhibitor 1
PBS	Phosphate-buffered saline
PCA	Principle component analysis
PCHS	Precision cut heart slice
PCR	Polymerase chain reaction
PCS	Precision cut slice
PDGF	Platelet derived growth factor
PDGFR	Platelet derived growth factor receptor
pg	Picogram
PICP	Carboxy-terminal propeptide of pro-collagen I
PIIINP	Amino-terminal propeptide of procollagen type III
POLY:IC	Polyinosinic acid
PRR	Pattern recognition receptor
PTX3	Pentraxin 3
qRT-PCR	Real-time quantitative polymerase chain reaction
QUOD	Quality in Organ Donation
r	Recombinant
RAAS	Renin aldosterone angiotensin system
RAS	Renin-angiotensin system
RD	Reagent diluent
RINTAG	Research, Innovation and Novel Technologies Advisory Group

RNA	Ribonucleic acid
ROS	Reactive oxygen species
rpm	Revolutions per minute
RT	Reverse transcriptase
SASHA	Saturation-recovery single-shot acquisition
Sc	Single cell
scRNA-seq	Single cell RNA sequencing
SEM	Standard error of the mean
siRNA	Small interfering RNA
SMAD	Suppressor of Mothers Against Decapentaplegic
SOD2	Superoxide dismutase 2
ST2	Suppression of Tumorigenicity 2
S-Trap	Suspension trapping
TAC	Transverse aortic constriction
TCL	Total cell lysate
TGF-β	Transforming growth factor - β
TIMP	Tissue inhibitor of metalloproteinases
TLR	Toll-like receptor
TMT	Tandem mass tag
TNF-α	Tumour necrosis factor-alpha
TSP	Thrombospondin
USA	United States of America
α-SMA	Alpha smooth muscle actin
µg	Microgram
µm	Micrometre

List of Figures

Figure 1. Schematic showing the Dystrophin-associated protein complex (DAPC). 8
Figure 2. Overview of TGF-β signalling pathway 19
Figure 3. Schematic showing the Angiotensin signalling pathway 23
Figure 4. Workflow of generation of PCHS 36
Figure 5. ELISA Protocol 37
Figure 6. Precision Cut Liver Slice Viability 44
Figure 7. Induction of fibrogenesis in Precision Cut Liver Slices (PCLS). 45
Figure 8. Precision Cut Kidney Slices induction and attenuation of fibrogenesis 46
Figure 9. Histological examples of the different tissue sources used to generate PCHS 53
Figure 10. Maintenance of tissue architecture post-slicing 54
Figure 11. Metabolic activity is a key measure for the viability of PCHS 56
Figure 12. Media B is unsuitable for the long-term culture of PCHS 57
Figure 13. PCHS cultured in 24 well static plates are unsuitable for long-term culture 58
Figure 14. PCHS cultured in Media A continue to be metabolically active after 144hrs in culture ... 59
Figure 15. Rocked culture improves PCHS viability. 59
Figure 16. IL-1α and IL-1β treatment can induce an inflammatory phenotype in PCHS 61
Figure 17. IL-1α and LPS treatment can induce an inflammatory phenotype in PCHS. 62
Figure 18. IL-1α induced inflammatory phenotype can be modulated through the application of therapeutics 64
Figure 19. LPS induced inflammatory phenotype can be modulated through the application of therapeutics 65
Figure 20. TGF-β1 induces a potent fibrotic phenotype in PCHS from LVAD donors 67
Figure 21. TGF-β1 induces IL-6 but not IL-8 or MCP-1 secretion in PCHS from LVAD donors 68
Figure 22. TGF-β1 induces a potent fibrotic phenotype in PCHS from unused donors 69
Figure 23. TGF-β1 induces IL-6 and MCP-1 but not IL-8 secretion in PCHS from unused donors 70
Figure 24. Attenuation of Collagen 1a1 secretion. 71
Figure 25. Attenuation of inflammatory responses from PCHS 72
Figure 26. Modulation of pro-fibrogenic stimuli through the use of therapeutics. 73
Figure 27. Modulation of inflammation through the use of therapeutics 74
Figure 28. IL-11 signalling in fibrosis 89
Figure 29. Schematic of PCHS treatments and harvest 92
Figure 30. Treatment plan for candidate compounds applied to PCHS 93
Figure 31. Treatment plan for candidate compounds applied to cardiac fibroblasts 94
Figure 32. Galectin-3 induced inflammatory response from Unused donor PCHS 102
Figure 33. Galectin-3 induced inflammatory response from unused donor PCHS 103
Figure 34. Induction of fibrogenic response from Unused Donor PCHS 105
Figure 35. Combination treatment is unable to further induce inflammatory response from PCHS 107
Figure 36. Combination treatment is unable to further induce collagen 1a1 secretion 108
Figure 37. Induction of inflammatory phenotype from LVAD PCHS in response to exogenous challenge 110
Figure 38. Induction of inflammatory phenotype from LVAD PCHS in response to exogenous challenge 111
Figure 39. Induction of fibrotic phenotype from LVAD PCHS in response to exogenous challenge 112
Figure 40. Response of PCHS to treatment highlighting underlying disease pathology. 114
Figure 41. Galectin-3 challenge induces potent inflammatory response in PCHS. 116
Figure 42. TGF-β1 challenge induces potent pro-fibrotic response in PCHS 117

Figure 43. Exogenous TGF-β1 challenge dictates PCHS PCA clustering. 119
Figure 44. TGF-β1 and Galectin-3 treatment induce transcriptional differences in PCHS. 120
Figure 45. Heat map depicting distinct changes in gene expression induced by TGF-β1 challenge.121
Figure 46. Heat map depicting distinct changes in gene expression induced by Galectin-3 challenge 122
Figure 47. Galectin-3 and TGF-β1 challenge produce very distinct profiles in differentially expressed genes 123
Figure 48. Heat map depicting distinct profile caused by TGF-β1 challenge..... 124
Figure 49. Representative graphs of genes upregulated in response to TGF-β1 treatment..... 125
Figure 50. Representative graphs of genes downregulated in response to TGF-β1 treatment 126
Figure 51. Heat map depicting distinct profile caused by Galectin-3 challenge 128
Figure 52. Representative graphs of genes upregulated in response to Galectin-3 treatment 129
Figure 53. Representative graphs of genes downregulated in response to Galectin-3 treatment . 130
Figure 54. Exogenous TGF-β1 and Galectin-3 challenge dictates proteomics PCA clustering 132
Figure 55. TGF-β1 and Galectin-3 treatment induce proteomic differences in PCHS 133
Figure 56. Heat map depicting distinct changes in protein expression induced by TGF-β1 challenge 134
Figure 57. Heat map depicting distinct changes in differential protein changes induced by Galectin-3 challenge 135
Figure 58. Galectin-3 and TGF-β1 challenge produce very distinct profiles in differentially expressed proteins 136
Figure 59. Heat map depicting distinct protein profile caused by TGF-β1 challenge 137
Figure 60. Representative graphs of proteins upregulated in response to TGF-β1 treatment 139
Figure 61. Representative graphs of proteins downregulated in response to TGF-β1 treatment . 140
Figure 62. Heat map depicting distinct protein profile caused by Galectin-3 challenge 142
Figure 63. Representative graphs of proteins upregulated in response to Galectin-3 treatment .. 143
Figure 64. Representative graphs of proteins downregulated in response to Galectin-3 treatment 144
Figure 65. Metabolic activity of cardiac fibroblasts in response to treatment with candidate compounds 149
Figure 66. Collagen 1a1 secretion from cardiac fibroblasts in response to treatment with candidate compounds 151
Figure 67. TIMP-1 secretion from cardiac fibroblasts in response to treatment with candidate compounds. 152
Figure 68. MCP-1 secretion from cardiac fibroblasts in response to treatment with candidate compounds 154
Figure 69. Efficacy and viability testing of candidate compounds identified through Ingenuity Pathway Analysis..... 159
Figure 70. Efficacy and viability testing of candidate compounds identified through Ingenuity Pathway Analysis..... 160
Figure 71. Efficacy and viability testing of candidate compounds identified through Ingenuity Pathway Analysis..... 163
Figure 72. Efficacy and viability testing of candidate compounds identified through Ingenuity Pathway Analysis..... 164
Figure 73. Efficacy and viability testing of candidate compounds identified through Ingenuity Pathway Analysis..... 165
Figure 74. Attenuation of fibrosis by candidate compounds..... 167
Figure 75. Attenuation of inflammation by candidate compounds 168

Figure 76. Mechanistic network of the predicted effects of Dexamethasone identified through Upstream Regulator Function. 169
Figure 77. Differences in response between Cardiac fibroblasts and PCHS 170
Figure 78. Workflow of sample collection and processing from donors 183
Figure 79. Neoepitopes of ECM Degradation 189
Figure 80. Neoepitopes of ECM formation. 190
Figure 81. Ratio of neoepitope degradation/formation markers 191
Figure 82. Heat map depicting the differences in proteins present in patient plasma depending on disease severity 193
Figure 83. Representative graphs of proteins significantly changed in the plasma of female DMD carrier patients 194
Figure 84. Disease severity had no effect on Lipidomic PCA clustering 195
Figure 85. Heat map depicting the differences in lipid profiles between disease severity 196
Figure 86. Comparisons of Total lipid levels between patients with different severities of cardiac disease 197
Figure 87. Changes in the n6/n3 ratio of different lipids depending of the cardiac disease severity of patients 198
Figure 88. Disease severity had no effect on Proteomic PCA clustering 199
Figure 89. Heat map depicting the differences in protein expression between disease severity ... 200
Figure 90. Significantly differentially expressed proteins between Normal and Early CM donors. 202
Figure 91. Representative graphs of proteins significantly downregulated in Early CM donors versus Normal cardiac donors. 203
Figure 92. Representative graphs of proteins significantly upregulated in Early CM donors versus Normal cardiac donors 204
Figure 93. Significantly differentially expressed proteins between Normal and CM Donors 206
Figure 94. Representative graphs of proteins significantly upregulated in CM versus Normal donors 207
Figure 95. Significantly differentially expressed proteins between Early CM and established CM donors 209
Figure 96. Representative graphs of proteins significantly upregulated in established CM donors versus early CM donors 210
Figure 97. Representative graphs of proteins significantly downregulated in CM donors versus CM donors 211

List of Tables

Table 1. Demographics of LVAD donors 34
Table 2. Demographics of Unused donors and perfused heart.....34
Table 3. Details of Slicing buffer used due the isolation of PCHS 35
Table 4. Product details of ELISA kits used 37
Table 5. Components of cell culture media used in the optimisation of PCHS culture**.**.....49
Table 6. Details of Candidate compounds identified from IPA Upstream Regulators.....95
Table 7. Top 20 genes significantly upregulated in response to TGF-β1 treatment.....125
Table 8. Top 20 genes significantly downregulated in response to TGF-β1 treatment.....126
Table 9. Top 20 genes significantly upregulated in response to Galectin-3 treatment.....129
Table 10. Top 20 genes significantly downregulated in response to Galectin-3 treatment.....130
Table 11. Top 20 most significantly upregulated proteins in response to TGF-β1 challenge.....139
Table 12. Top 20 most significantly downregulated proteins in response to TGF-β1 challenge.....140
Table 13. Top 20 most significantly upregulated proteins in response to Galectin-3 challenge.....143
Table 14. Top 20 most significantly downregulated proteins in response to Galectin-3 challenge...144
Table 15. Candidate compounds identified through the upstream regulators function during IPA..146
Table 16. Viability of cardiac fibroblasts in response to treatment with candidate compounds.....148
Table 17. Collagen 1a1 secretion from cardiac fibroblasts in response to treatment with candidate compounds.....150
Table 18. TIMP-1 secretion from cardiac fibroblasts in response to treatment with candidate compounds.....152
Table 19. MCP-1 secretion from cardiac fibroblasts in response to treatment with candidate compound**s**.....153
Table 20. Viability of PCHS in response to treatment with candidate compounds.....157
Table 21. Candidate compounds and their effect on secretion of fibrosis markers 161
Table 22. Candidate compounds and their effect on secretion of inflammatory markers 166
Table 23. Patient information and group stratification. 184
Table 24. Nordic Bioscience Protein Fingerprint™ Technology 185
Table 25. Details of Mesoscale Discovery™ multi-plex ELISAs used. 186
Table 26. Patient demographics 188
Table 27. Details of the analytes which fell below the lower level of quantification (LLOQ) and were therefore excluded from the results**.**.....192

1 Introduction

1.1 Fibrosis

1.1.1 General Fibrosis and wound healing response

Fibrosis is the wide reaching term for the dysregulation of the wound healing response, leading to the excess deposition of extracellular matrix (ECM) proteins. Under normal physiological wound healing conditions damage will occur to a tissue resulting in acute inflammatory response and the release of chemokines and cytokines involved in resolving the damage, the recruitment of neutrophils and other granulocytes followed by monocytes(1). Fibroblasts, cells of mesenchymal origin, become activated and differentiate into contractile, secretory cells termed myofibroblasts. It is these activated cells that are responsible for the deposition of scar tissue, ECM and the release of other pro-fibrotic factors that lead to the involvement of other cell types required for the repair of the injury. Normally this process halts once the wound is repaired and the stimuli has been removed. Myofibroblasts will undergo apoptosis and be cleared from the site of injury(1). Fibrosis occurs when this process becomes pathological, continuing even in the absence of the initial injury. This leads to a build-up of the ECM, the continued proliferation and migration of myofibroblasts, increased secretion of pro-inflammatory and pro-fibrotic markers and therefore the recruitment of other inflammatory cells and proliferation of fibroblasts(1–3). This cycle continues unchecked in the organ with increased levels of scar being deposited until integrity and function of the organ is severely compromised. The culmination of this process is the loss of function of the organ and due to the lack of effective treatment, ultimately results in the need for transplantation of the organ. In the western world up to 45% of deaths can be linked to fibrotic diseases(3), thus highlighting the importance of meeting the current unmet need for the development of anti-fibrotic therapies.

1.1.2 Cardiac Fibrosis

In the heart, fibrosis, known as myocardial fibrosis, is the common pathophysiology which underpins numerous cardiovascular diseases (CVD), including arrythmias, hypertension and myocardial infarction, many of which culminate with heart failure and death. In the USA in 2012 1 in 9 deaths could be attributed to heart failure(4). Whilst in Europe is it thought up to 49 million people are living with CVD, at a cost of €210 million a year(5). This highlights the huge healthcare and economic burden of cardiovascular diseases. Similar to fibrosis present

within other organs, myocardial fibrosis can be characterised by activation of myofibroblasts resulting in alterations of the extracellular matrix. The initiation of the fibrogenic signals which lead to the development of fibrosis can also be driven by cardiomyocyte damage, necrosis or apoptosis and the replacement of myocytes with a collagen-rich scar(6,41). This type of fibrosis, termed replacement fibrosis, is the result of the sudden loss of a large number myocytes resulting in acute damage caused by myocardial infarction or myocarditis.

Alterations in the rate of synthesis and degradation of ECM proteins, such as collagens, and variations in the ratio between different types of collagen fibres, results in changes to ventricular stiffness, force generation and myocardial contractility. The most abundant component of the ECM proteins in the heart are the fibrillar collagens type I and type III. Type I collagen is a large diameter, highly cross-linked fibre making up about 80% of cardiac collagen(6). It plays an important role in providing structural support for cardiac myocytes in the normal functioning heart, ensuring myocyte alignment is maintained, as well as conferring tensile strength(7). Type III collagen is the second most abundant form of collagen present, responsible for around 11% of cardiac collagen(6). It is termed a free collagen, and unlike type I collagen, type III forms thin fibres which are key in maintaining the elasticity of the extracellular matrix(7). Both type I and type III collagen are synthesised and regulated by cardiac fibroblasts. Under conditions of homeostasis, collagen and other structural ECM proteins, such as elastin and fibronectin are continually synthesised and degraded. Their degradation is tightly controlled by ECM-regulatory proteins, also produced by cardiac fibroblasts, called matrix metalloproteinases (MMPs) and their inhibitors, tissue inhibitors of metalloproteinases (TIMPs). Upon cardiac injury fibroblasts become activated. These phenotypically changed fibroblasts, termed myofibroblasts are responsible for the increase in the synthesis and secretion of procollagen chains, which are then cleaved to form type I and III collagen fibrils. Upon the development of fibrosis the ratio between type I and III fibres present within the myocardium alters. There is an increase in type I collagen fibres present, resulting in an increase in cross-linking between type I fibres, myocardial stiffness and a detrimental effect on the contractility of myocytes.

Cardiac fibrosis can be categorised into two distinct types, reactive interstitial fibrosis or replacement fibrosis. Reactive fibrosis, also known as interstitial fibrosis due to its development in the interstitium, initiates around the microvasculature before spreading

throughout the interstitial space. It is characterised by a dysregulation in collagen turnover driven by myofibroblasts. The resultant increase in collagen synthesis by the myofibroblasts is confounded by unchanged or reduced degradation, although, importantly it does not result in the significant loss of cardiomyocytes(8). Used as an indicator of disease severity it is often seen prior to the development of irreversible replacement fibrosis. Reactive fibrosis is present in a number of diseases including hypertension and diabetes mellitus as well as idiopathic dilated cardiomyopathy and in the aging heart(9,10).

Replacement fibrosis occurs after cardiac injury triggers the apoptosis or necrosis of myocytes, resulting in the deposition of type I collagen in their place and the formation of a collagen-rich scar. The development of the scar acts to maintain the structural integrity of the myocardium after the loss of myocytes although due to the changes in structure of the myocardium this is ultimately responsible for the loss of function of the cardiac muscle(11). Replacement fibrosis may remain localised to the site of myocardial infarction or be diffuse within the muscle following conditions such as viral myocarditis.

Cardiac fibroblasts account for <20% of cells in the developed murine heart(12), with 20-35% attributed to cardiomyocytes(13) and endothelial cells are thought to make up around 60% of the non-myocyte cell types in the adult heart(12). Due to the limited regenerative capacity in the adult heart, the loss of cardiomyocytes can have profound effects on the functionality of the heart with necrotic cardiomyocytes being replaced by fibrotic scar deposited by activated cardiac fibroblasts.

Cardiac fibroblasts are not only responsible for ECM production in the heart, they are thought to have a number of other functions including distribution of mechanical forces throughout the tissue and cardiac electrophysiology. Through the deposition of ECM between adjoining myocytes, termed annulus fibrosis, they are able to block the electrical signals that pass through the heart to ensure the sequential contraction of the atria and ventricles(14). Cardiac fibroblasts have also been found to be connected directly to myocytes through the gap junctions connexin-43 and connexin-45(15,16). Research by Gaudesius *et al* confirmed the expression of connexin-43 and connexin-45 by both fibroblasts and cardiomyocytes and demonstrated that fibroblasts had the ability to synchronise long-range electrical activity between the two cell types(16), not just through short-range direct interactions(17). The

deposition of new ECM due to fibrosis could have major implications in disrupting the balance of electrical signalling in the heart, not only between myocytes but between myocytes and cardiac fibroblasts, leading to impaired and dysregulated contraction. The increase in ECM as well as the inability to break down and clear this excess fibrosis also results in increased stiffness of the cardiac muscle, with the eventual result of this process being impaired cardiac function and ultimately heart failure(16,17).

The origin of the cardiac myofibroblasts involved during fibrotic disease development remains a constantly evolving and controversial area of research. Traditionally, it was believed that a homogeneous population of fibroblasts resident within the cardiac tissue responded to signals within the circulation to become activated matrix-producing cells(18,19). However, through the use of cellular tracking studies over the last 10-15 years, evidence is emerging identifying the recruitment of a heterogeneous population of cells from other cellular sources. One of the most highly researched cellular sources of cardiac fibroblasts includes endothelial cells, via endothelial-to-mesenchymal transition (EndMT)(20). Fate mapping studies have suggested up to 30% of activated fibroblasts in the damaged heart originate from endothelial cells(20) whereas in the normal heart they are provide a negligible contribution to fibroblast population(21–23). In addition to EndMT, other fibroblast origins include pericytes(24), bone-marrow derived progenitor cells(25,26), macrophages(27) and fibrocytes(28–31).

1.1.3 Examples of cardiac fibrosis in disease

1.1.3.1 Heart Failure with Preserved Ejection Fraction (HFpEF)

Heart failure with preserved ejection fraction (HFpEF) is the most common form of heart failure (HF), estimated to be responsible for >50% of HF cases(32). Whilst HF is most commonly associated with a loss of function of the cardiac muscle, HFpEF usually presents with sustained systolic function however diastolic filling and relaxation of the heart is impaired(33). Patients often have a number of comorbidities including diabetes, obesity and non-alcoholic fatty liver disease (NAFLD), with age a major risk factor for HFpEF(34,35). Unlike for heart failure with reduced ejection fraction (HFrEF) patients, there are no therapies to effectively treat HFpEF patients. HFpEF does not represent a single pathological process, there are a number of different disease mechanisms which contribute to the development of heart failure. These include inflammation, RAAS activation, endothelial dysfunction and ROS activation. Whilst

these all play in important role in the development of disease, arguably the most common pathway present, irrespective of the aetiology, is fibrosis. Whilst replacement fibrosis is primarily associated post-myocardial infarction (MI), in HFpEF patients interstitial fibrosis is the primary type present. Patients with confirmed fibrosis have increased prevalence of arrythmias, hospitalisation and even death(36,37). For this reason reversing the pathological remodelling caused by fibrosis has become a target for the development of new therapies to treat HFpEF patients. One such hope was the mineralocorticoid antagonist (MRAs), Spironolactone, already shown the be effective in reducing mortality in HFrEF patients(38). However currently trials testing its use in HFpEF patients have failed to show similar positive effects. In the large TOPCAT trial, HF patients given Spironolactone treatment for 3 years failed to see any improvement in the primary outcomes of the trial, including incidence of death or hospitalisation(38,39).

The complex nature of both the causes of HFpEF including the many intertwined disease mechanisms which lead to its progression, along with the poor prognosis of patients, highlights the importance of continued research into the disease.

1.1.3.2 Myocardial Infarction

Myocardial infarction (MI) is a major cause of the replacement fibrosis present in ischaemic cardiomyopathy. MI results in cardiac remodelling due to the death of cardiomyocytes, which once cleared from the site of injury, are replaced with large amounts of fibrous tissue. The cellular response to the injury caused by MI can, simply, be split into three overlapping phases, inflammatory, proliferative and maturation phases(40,41). Innate immune pathways are rapidly activated upon cardiomyocyte death, leading to the secretion of cytokines and chemokines and the recruitment of leukocytes to the infarct site(42). The proliferative phase begins upon the clearance of dead cells from the wound site, and the activation of fibroblasts to myofibroblasts by macrophages(43). Activated myofibroblasts secrete large amounts of ECM, whilst a microvasculature network is formed by the activation of angiogenic pathways(44,45). Upon transition to the maturation phase, once the infarct site is filled with matrix, myofibroblasts become quiescent and cleared by apoptosis(46). Finally cross-linking of collagen fibrils occurs providing strength and stability to the scar however due to increased

stiffness of the cardiac muscle it also contributes to diastolic dysfunction often observed in patients post-MI(47).

1.1.3.3 Duchenne Muscular Dystrophy

Duchenne Muscular Dystrophy (DMD) is an X-linked recessive neuromuscular disorder affecting 1/5000 males(48). It is characterised by inherited or spontaneous mutations in the dystrophin gene that encodes the cytoplasmic protein dystrophin in striated muscle. Dystrophin is vital in ensuring the stability of the plasma membrane through the anchoring of the extracellular matrix and membrane proteins to the cytoskeleton forming part of the larger dystrophin-associated protein complex (DAPC) **(Figure 1)**(49). The absence of dystrophin has been thought to increase the susceptibility of the muscle fibre membrane to contraction-induced damage resulting in an influx of Ca^{2+} into the cell and eventual cell death(50). In contrast to the highly organised fibres present in healthy muscle, in DMD patients the fibres are disorganised with inflammation, myocyte hypertrophy and evidence of extensive deposition of fat and connective tissue(51).

DMD is usually first identified in patients between 3-5 years of age firstly with the onset of clinical signs such as performing Gower's manoeuvre and calf muscle pseudohypertrophy(52,53). Diagnosis is usually then confirmed by elevated Creatine Kinase levels in the blood, muscle biopsy and DNA test. The progression of DMD can occur rapidly after initial diagnosis with the loss of independent walking by 10 years, followed by respiratory dysfunction by 20 years and the onset of cardiovascular manifestations(52). Evidence of cardiac abnormalities first present at an early age in patients through abnormal echocardiograms and the presence of sinus tachycardia(54). However it is not until later in life that the presence of cardiac fibrosis is observed. This is characterised by thinning followed by the enlargement of the left ventricular wall resulting in a loss of contractile function and heart failure. DMD patients most commonly suffer from dilated cardiomyopathy with a number of patients developing arrhythmias, which can be a marker of the deterioration in myocardial function(55).

The effect of the DMD mutation on the cardiac muscle is still not fully understood, with it being unclear whether the same effects observed in the skeletal muscle stands true for the

cardiac muscle. Studies have shown no correlation between the severity of the skeletal muscle myopathy and the degree of cardiomyopathy(54). In Becker Muscular Dystrophy (BMD) the locus of the mutation in the dystrophin gene has been shown to be important regarding the onset of cardiomyopathy; however it is unknown whether this holds true for DMD patients(56).

Until recently treatments for DMD patients have focused on improving both their muscle strength and pulmonary function. Steroids, namely glucocorticoids, are prescribed to boys from the age of 5, improving the function and strength of muscles as well as pulmonary function. Spinal stabilisation and pulmonary support have helped increase the life expectancy of DMD patients to the late twenties and into their early thirties(57). Due to the improvements in the treatment of the respiratory-related disorders, cardiomyopathies have now become the leading cause of death for DMD patients(58,59). In patients aged over 18 years, over 90% have evidence of cardiac dysfunction, with 20% of deaths being accounted for by heart failure(55,59). In DMD patients the cardiac involvement presents itself through progressive interstitial fibrosis and the deposition of adipose tissue in the ventricles and atria. This may lead to cardiomyopathy, arrhythmias and conduction defects(58). Currently treatments for these patients are limited to steroids, ACE inhibitors and β-blockers with screening at time of diagnosis and continued monitoring of disease progression(58). Due to the increasing numbers of DMD patients suffering from cardiomyopathies, preventing the cardiac fibrosis that occurs has an unmet urgent clinical need.

DMD research can be broadly grouped into two different categories, firstly strategies that target the primary defect of the disease. This includes research involving gene therapy, such as AAV and CRISPR/Cas9 genome editing, or exon skipping(60–63). Secondly, approaches that look to mitigate the secondary and downstream pathological mechanisms that are the result of the primary defect of the dystrophin gene. The development of membrane sealants such as Poloxamer 188 (P188) is an example of this approach(64). P188 is been shown to improve the membrane stability of the myocytes to help prevent and repair the damage that occurs due to the loss of the dystrophin protein. Research into the cardiac fibrosis that DMD patients develop and the potential to provide a treatment to this in the form of an anti-fibrotic therapy is another of the downstream responses that can be investigated.

The long term goal of treating patients with Duchenne Muscular Dystrophy will undoubtedly be to correct the defect, whether that is to restore dystrophin gene expression or the functionality of the dystrophin protein, however it is still beneficial to patients to investigate ways to treat the secondary effects of the disease, such as cardiac fibrosis.

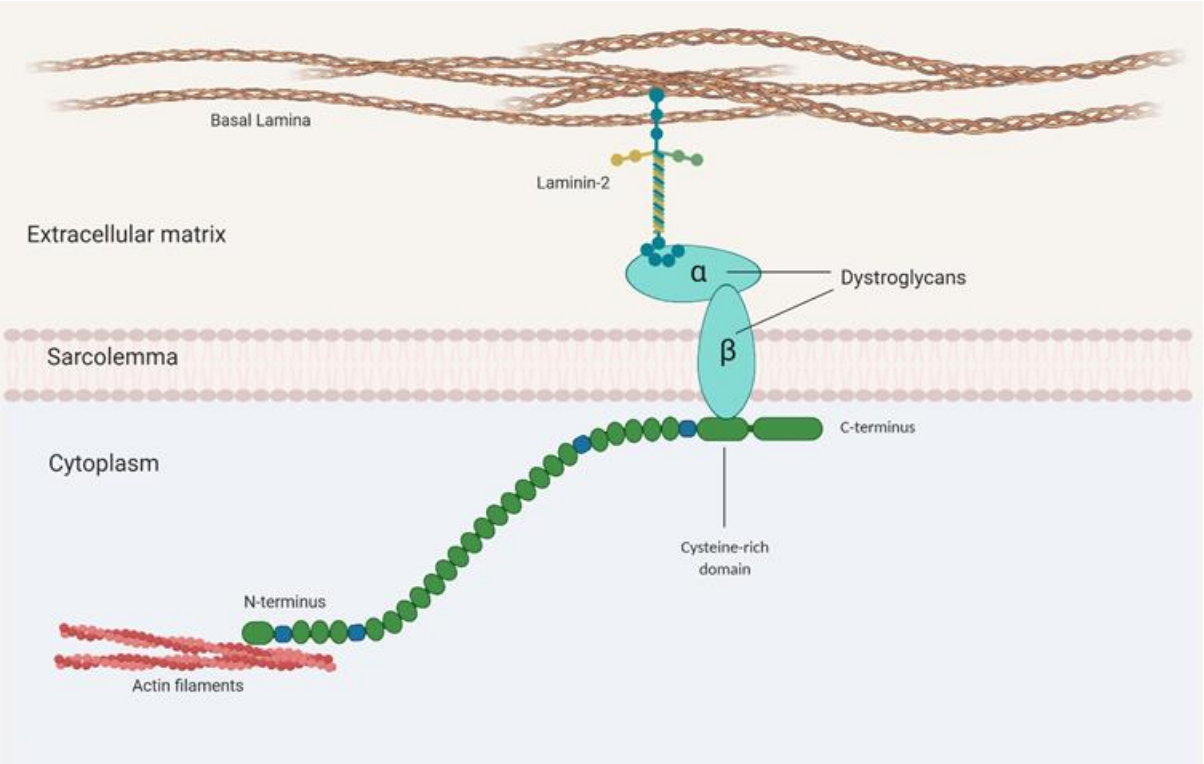

Figure 1. Schematic showing the Dystrophin-associated protein complex (DAPC). Adapted from Fairclough *et al* (2013)(49). The dystrophin protein (green) is shown as an important link between the cytoplasmic actin filaments and dystroglycan complexes at the sarcolemma.

1.2 Current methods for the Diagnosis of cardiac fibrosis

1.2.1 Endomyocardial Biopsy

The current gold standard for the diagnosis of cardiac fibrosis is through the use of endomyocardial biopsies (EMB) to quantify the amounts of interstitial collagen present within the interventricular septum. The first reports of the procedure being carried out date back to 1958(65) with it becoming more commonplace throughout the 1960s(66,67). Biopsy samples were initially processed and haematoxylin-eosin staining performed. Recently the accuracy has increased enabling its use more widely.

Despite this, due to the invasive nature of the procedure performing endomyocardial biopsies is not without risk, with a complication rate reported of <1% in over 4000 biopsies performed(68). Highlighting the careful consideration required prior to the use of EMB for the diagnosis and treatment of patients with cardiovascular diseases. Using a bioptome, access to the heart is *via* a sheath inserted into the right internal jugular or femoral vein which is then tracked using fluoroscopy or echocardiography into the heart chambers. For accurate diagnosis between 5-10 samples, 1-2mm^3 in size, need to be collected from the right intraventricular septum (IVS) of patients. Whilst still defined as the gold standard for the diagnosis of cardiac fibrosis, other non-invasive techniques are becoming to preferred diagnostic tool for doctors.

1.2.2 Cardiac magnetic resonance (CMR) Imaging

For a number of years magnetic resonance imaging (MRI) has been the preferred non-invasive technique used to help diagnosis cardiac fibrosis in heart failure patients by assessing LV volume and mass(69,70). The benefits of using MRI over invasive biopsies include the ability to provide both accurate and reproducible measures of changes in fibrosis for both the right and left ventricles. The capability to non-invasively image the hearts of patients within a 60 minute period allows for the opportunity to continually monitor disease progression with repeated imaging at follow-up appointments. This is a continually advancing field, with more accurate and detailed imaging techniques being developed, such as the use of T1 mapping and measurement of late gadolinium enhancement (LGE), further highlighting its value as both a diagnostic and prognostic tool(70).

1.2.2.1 Measurement of late gadolinium enhancement (LGE) in patients

The measurement of late gadolinium enhancement (LGE) is often used in patients who have suffered MI due to its ability to assess the amount of replacement fibrosis present within the tissue(71). The imaging of the scar area is achieved through the application of gadolinium based contrast agents (GBCAs), the distribution of them within the myocardium is then imaged using CMR(72). GBCAs passively accumulate within the ECM in areas of expansion or within damaged cells with leaky cell membranes. Once accumulated the GBCAs take longer to be 'washed out' of fibrotic areas, therefore on images regions of replacement fibrosis show up as bright areas whilst healthy myocardium shows up dark(69). Initial studies verifying the

accuracy of LGE-CMR were performed in animal models of MI. Work by Judd *et al* was some of the first to using contrast agents to demonstrate the damage caused after MI and reperfusion(73). Building on this work, Kim *et al* were able to show the ability to distinguish between reversible (injured but viable myocardium not hyperenhanced but with contractile dysfunction), irreversible ischemic injury (acute myocardial infarction showing hyperenhanced and with contractile dysfunction) and normal myocardium (not hyperenhanced and with normal function)(71,74). Flacke *et al* confirmed these findings in human patients, identifying areas of infarct tissue which were still viable(75). In more recent years CMR with LGE has been shown to also be beneficial for predicting the risk stratification of patients in routine clinical practice. Therefore allowing doctors to more accurately predict the risk of all-cause mortality or cardiac transplant and death enabling the optimisation of patient care(76). Beyond its use in the treatment of MI patients, CMR with LGE has also demonstrated the ability to assess myocardial fibrosis in a range of other cardiomyopathies including non-ischemic dilated cardiomyopathy (NIDCM) and hypertrophied cardiomyopathy (HCM)(77,78).

Whilst CMR with LGE clearly has many benefits, especially for patients after MI, as with most techniques, there are a number of limitations which need to be taken into account. The main problem with this technique is whilst able to accurately assess and measure the extent of replacement fibrosis its sensitivity is still relatively limited for measurements of diffuse interstitial fibrosis. Due to the diffuse nature of interstitial fibrosis, it is difficult to accurately quantify the signal intensities between fibrotic areas and normal myocardium. In recent years questions have also been raised regarding the safety of the GBCAs, with some clinicians identifying an increased risk of developing nephrogenic systemic fibrosis (NSF) or the identification of gadolinium deposits in the brain of patients receiving multiple doses of GBCAS. Work by Monti *et al* and Alfano *et al* demonstrated that either by decreasing the dose of gadobutrol or using a macrocyclic GBCA these safety concerns could be addressed without a reduction in the quality of image produced(79,80).

1.2.2.2 T1 Mapping

In order to allow for the more accurate assessment of diffuse and interstitial cardiac fibrosis, a newer CMR technique, T1 mapping has started to be employed(72). T1 mapping involves the quantification of the T1 relaxation time of tissue in a pixel-by-pixel basis after the administration of a gadolinium contrast agent(70). While normal myocardial tissue displays as predictable T1 relaxation time, fibrotic tissues deviate from this. In areas of fibrosis there is a build-up of the contrast agent, resulting in the quicker relaxation of adject protons and therefore T1 shortening. A baseline reading of the T1 relaxation times are taken prior to the administration of the contrast agent, therefore allowing even slight variations in T1 times to be identified making it possible to assess diffuse fibrosis in the heart(72). In recent years there have been a number of different techniques developed, each with their own advantages and limitations. The modified Look-Locker sequence (MOLLI) is the most widely used clinical technique for T1 mapping(81). This technique has been shown to be highly reproducible and requires a shorter acquisition time compared to earlier versions, resulting in patients reducing the time in which they need to hold their breath during the measurement(82). The shortened modified Look-Locker technique (shMOLLI) reduced the patient breath-hold time further still without having detrimental effects on the accuracy of the results(83).

Limitations of T1 mapping include the relatively expensive cost of CMR, the lack of suitability for patients with metallic implants and intracardiac devices as well as the requirement for multiple breath-holds which some patients are unable to manage. Recent work by Garg *et al* and Chow *et al* has hoped to reduce this through the development of free breathing T1 mapping sequences called high-contrast Saturation-recovery single-shot acquisition (SASHA)(84,85). Finally, despite attempts to introduce standardised T1 mapping protocols, these currently have not been universally adopted therefore differences in inter-centre and inter-scanner variabilities still exist(86). Despite these problems, T1 mapping still offers a highly sensitive method for the quantification of interstitial and diffuse fibrosis. Whilst continued research will continue to improve the technique further for both clinicians and patients.

1.2.3 Serum Markers

1.2.3.1 N-terminal-Pro B-type natriuretic peptide (NT-ProBNP)

Pro-BNP is a peptide secreted by cardiomyocytes usually in response to myocardial stretch and/or pressure overload(87,88). It is then cleaved into two fragments, the biologically active B-type natriuretic peptide (BNP) and the inert N-terminal pro-BNP (NT-proBNP). Both of these fragments are found in the plasma of patients making them attractive potential biomarkers(89). Whilst BNP only has a half-life of approximately 20 minutes, NT-proBNP is able to circulate in the blood for 1-2 hours before being cleared by the kidney(88). Measurement of NT-proBNP are routinely used in the clinic to diagnose and monitor HF progression(90,91). However its relationship to myocardial fibrosis is still to be fully elucidated. Work by Lui *et al* in the Multi-Ethnic Study of Atherosclerosis (MESA) study (NCT00005487) compared serum NT-proBNP with CMR with T1 mapping confirmed myocardial fibrosis(92). They confirmed elevated NT-proBNP was associated with diffuse fibrosis as confirmed by CMR. The current gold standard for myocardial fibrosis diagnosis is the use of endomyocardial biopsies. In the Hisayama study, serum NT-proBNP levels were found to be positively correlated with histopathologically confirmed myocardial fibrosis in patients without apparent cardiac diseases(93). Both these studies highlight the possibility to expand the use of serum NT-proBNP to offer a non-invasive and cheaper diagnosis of cardiac fibrosis in asymptomatic individuals.

1.2.3.2 High sensitivity cardiac troponin T (hs-cTnT)

Troponin T is part of the larger troponin complex which regulates the contraction of striated muscle. In addition to troponin T, the troponin complex contains two other subunits, troponin I and troponin C(94). Cardiac troponin is mostly bound to myofilaments on cardiomyocytes, with only 3-8% free in the cytosol. However upon injury and disruption of the cardiomyocyte sarcolemma, cytoplasmic troponin is released from the cells and if damage continues troponin is also released from deteriorating myofilaments. Cardiac troponin levels become elevated in the circulation 3-4 hours after the initial damage and can remain increased for up to 14 days(95,96). Of the three troponin subunits cardiac troponin T (cTnT) is used to assess damage to cardiomyocytes. A recent modification to the assay has enabled detection of cTnT at much higher sensitivity compared to previous versions, allowing for the detection of more subtle elevations symptomatic of cardiac injury(97,98). In the clinic high sensitivity cTnT (hs-cTnT)

assays are used to diagnose MI in patients(99). Recently though cTnT levels in the serum are being investigated as potential biomarkers for cardiac fibrosis and prognosis in a number of other cardiac diseases(100,101). Kawasaki *et al* demonstrated elevated serum levels of cTnT to be a marker of myocardial fibrosis in patients with hypertrophic cardiomyopathy(102). LGE-CMR was used to confirm fibrosis in patients, which when combined with hs-cTnT level had sensitivity of 96%. An exciting study which highlighted the potential of hs-cTnT for use as a biomarker in asymptomatic subjects. Higher baseline cTnT was associated with a longitudinal increase in LV mass >12% and LGE as confirmed by CMR in follow up studies(103). This study demonstrates the ability of hs-cTnT to identify subclinical heart disease, allowing for either earlier interventions or prolonged monitoring of these patients.

1.2.3.3 Matrix metalloproteinase 9 (MMP-9), ST-2 and Galectin-3

Galectin-3, a β-galactoside-binding lectin, is predominantly expressed by monocytes and activated macrophages(104). It is only expressed in low levels in healthy tissue, however becomes upregulated upon the initiation of both inflammatory and fibrotic responses. As well as having a role in driving disease Galectin-3 has also been investigated as a potential biomarker for fibrosis in heart failure progression(105). Serum levels of Galectin-3 have been demonstrated to be elevated in heart failure patients. Lok *et al* showed its potential as a prognostic marker in heart failure patients enrolled in the DEAL-HF study(106). Galectin-3 was shown to be a significant predictor of mortality in patients, especially in those who had high baseline levels of both Galectin-3 and NT-proBNP, highlighting its potential as a prognostic marker(106). These findings were confirmed using data from two large cohorts, the Controlled Rosuvastatin Multinational Trial in Heart Failure (CORONA) and Coordinating Study Evaluating Outcomes of Advising and Counselling Failure (COACH) trials, with Galectin-3 levels identifying patients with increased risk of future HF morbidity and mortality(107). In 2013 the American College of Cardiology Foundation/American Heart Association added Galectin-3, along with soluble ST2 to their recommendations for myocardial fibrosis assessment in HF patients, although it is worth noting this was not recommended by the European Society of Cardiology(108). However Galectin-3 had no predictive value in acute MI in patients, with no correlation found with serum Galectin-3 levels and LV remodelling(109). Although it was found to be correlated with a number of biomarkers involved in ECM turnover, including MMP-3 and MCP-1. The ability of Galectin-3 as a prognostic biomarker in HF patients initially generated

immense interest and hope in its success, however conflicting evidence has tempered initial excitement. A systematic review of 27 studies investigating Galectin-3 concluded that whilst used alone it does not appear to be able to predict mortality, there may be some prognostic benefits for using it as part of a multi-biomarker panel for heart failure patients(110).

Suppression of Tumorigenicity 2 (ST2), also known as IL-1 receptor ligand 1 (IL-1rl1) is a member of the IL-1 receptor family, and exists in two forms. Firstly as a membrane-bound cellular receptor for IL-33, and also in a soluble form (sST2), acting as a decoy receptor(111,112). After myocardial damage sST2 is transcribed and secreted into the circulation by cardiomyocytes and endothelial cells. Once in the circulation sST2 prevents the binding of IL-33 to membrane-bound ST2, thereby blocking the cardioprotective mechanism of the ST2L-IL33 pathway. sST2 has been proposed as a potential biomarker in HF patients. Early work by Weinberg *et al* first demonstrated its potential for use as a biomarker(113). They found sST2 to be elevated in the serum of patients one day after MI, and this increase was positively correlated with the damage marker creatine kinase. In the case of chronic heart failure ST2 levels were able to predict risk of death or transplantation in patients who were part of the larger Penn Heart Failure Study (PHFS)(114). In addition when combined with NT-proBNP it enabled patients to be reclassified into more appropriate risk categories. The Barcelona study compared the effectiveness of sST2 and Galectin-3 as potential fibrosis biomarkers(115). Whilst both sST2 and Galectin-3 were associated with an increase in all-cause mortality, only sST2 predicted cardiovascular associated deaths. In order to assess the suitability of sST2 and other potential biomarkers Wu *et al* measured their levels in healthy subjects over an 8 week period(116). Their data showed sST2 levels to have the smallest variations over the 8 week period compared to Galectin-3 and NT-proBNP, highlighting the suitability of ST2 for serial measurements and as a monitoring biomarker for HF patients. Despite promising data with regard to predicting HF progression, conflicting data failed to find a correlation between sST2 levels and myocardial fibrosis in HCM patients(117). Quick *et al* combined sST2 readouts with CMRI in order to assess the accuracy of sST2 at predicting myocardial scar formation(118). They found no correlation between identification of scar through LGE and levels of sST2, whereas biomarker NT-proBNP was found to be correlated with myocardial scar.

Matrix metalloproteinases (MMPs) are enzymes involved in the regulation of the ECM specifically collagen turnover. The dysregulation of the deposition/degradation axis of the ECM can lead to an imbalance in the ratio of factors which degrade the ECM versus those which increase ECM content. MMP-9 has been proposed as a potential biomarker of fibrosis. In a study of 54 HCM patients serum quantification of MMP-1, -2, -3 and -9 were analysed(119). Results were cross-referenced with LGE-CMR, which had been used to confirm the presence of cardiac fibrosis in patients. The data showed that only MMP-9 was associated with fibrosis in female, but not male, HCM patients. The TOPCAT study took a multi-marker approach to investigate circulation biomarkers with the aim of improving the risk stratification in HFpEF patients(120). MMP-9 was among a panel of 49 markers tested, they found no relationship between levels of circulating MMP-9 and prognosis. Associations were observed for ST2, NT-proBNP and MMP-7 with the risk of either all-cause death or heart failure-related hospital admission (DHFA).

Further larger-scale studies are required to further assess the success and accuracy of these potential biomarkers for both the diagnosis of cardiac fibrosis and the prognosis of cardiovascular diseases.

1.2.3.4 Markers of collagen synthesis

Collagen is the major component of the ECM, during the fibrotic process its production and secretion is significantly upregulated leading to the formation of an area of scar. Collagen type I and type III are initially synthesised as a pro-collagen chain by fibroblasts and myofibroblasts that is subsequently converted to either collagen type I or collagen type III by proteinases(121,122). During this process amino-terminal and carboxyl-terminal propeptides for both collagen type I and III are cleaved from the collagen molecule and secreted into the blood, whilst the individual collagen molecules are able to self-assemble initially into collagen fibrils prior to their aggregation to form the larger collagen fibres(123,124). The ability to measure the now cleaved carboxy-terminal propeptide of pro-collagen I (PICP) and amino-terminal propeptide of procollagen type III (PIIINP) in the circulation of patients has made them both attractive targets as fibrosis biomarkers(125,126). PICP is a particularly attractive option for a circulating biomarker due to the 1:1 stoichiometric ratio of PICP and collagen type

1 molecule formation(126,127). An early study assessing the relationship between PICP and histological assessment of collagen in the myocardium of hypertensive heart disease (HHD) patients found an association between myocardial collagen accumulation and circulatory PICP levels(127). In addition to these findings their results showed PICP was secreted via the coronary sinus into the circulation of HHD patients. PICP was able to have good prognostic value in DCM patients when combined with LGE-CMR, identifying patients with elevated levels of PICP combined with fibrosis-positive LGE-CMR were at increased risk of death, heart transplantation or heart failure hospitalisation(128). Raafs and colleagues then went on to evaluate the transcriptome in these patients, discovering expression of pro-inflammatory and pro-fibrotic transcriptomic profiles in PICP/LGE-CMR positive patients. This study also assessed the effectiveness of PIIINP as a prognostic marker, finding that it had no prognostic value(128). This study highlights the potential of PICP to be used as a non-invasive biomarker in DCM patients. The HOMAGE clinical trial demonstrated PICP's potential to monitor cardiac fibrosis in response to anti-fibrotic therapies. Spironolactone, a mineralocorticoid receptor antagonist, significantly reduced circulating levels of both PICP and NT-proBNP whilst having no effect on PIIICP(129,130). This was also in conjunction with an improvement in cardiac remodelling as demonstrated by reductions in LV volume and increased LVEF. Despite these results more data is required to discover whether these changes in PICP only apply to collagen turnover or whether they will eventually also lead to a reduction in collagen mass within the heart(130).

1.2.3.5 MicroRNAs

The presence of microRNAs (miRNAs) was first discovered in 1993, initially they were considered as 'junk DNA' with no functions due to being only 17-25 nucleotides in length and described as non-coding RNA(131). However since their discovery research has highlighted a number of important roles including gene regulation through their interactions with messenger RNAs (mRNA)(132). miRNAs are able to bind to 3'-untranslated regions of target mRNAs, initiating either their degradation or repression at a post-translational stage. What makes miRNAs particularly interesting is their ability to effect not just one gene, but to target entire networks involved in particular biological functions. Whilst miRNAs have effects in a wide range of cellular processes across a number of diseases, their apparent important role in

cardiovascular diseases has resulted in investigations assess to their suitability as non-invasive biomarkers for myocardial fibrosis and disease progression(133,134).

Of particular interest are circulating miRNAs. Fang *et al* evaluated the expression of circulating miRNAs in HCM patients with diffuse myocardial fibrosis(135). An initial panel of 84 miRNAs was screened to assess expression levels with a smaller panel of 16 being taken forward for in-depth investigation. They found individual miRNAs only had a limited prognostic value, whereas a panel of 14 miRNAs were able to provide predictive values for diffuse fibrosis as confirmed by T1 mapping. Interestingly their results showed that markers of collagen turnover, PINP and PIIINP, had no predictive value(135). One of the miRNAs identified miR-21 is the most extensively studied for its involvement in myocardial fibrosis(136–138). It has been shown to regulate fibroblast survival and induces fibrosis through its regulation of the TGF-β1 signalling pathway. Work by Villar *et al* further confirmed the biomarker potential of miR-21, showing both myocardial and circulating levels of miR-21 were positively correlated with expression levels of genes involved in ECM remodelling and TGF-β1 signalling in the left ventricle(139).

Other circulating miRNAs proposed as biomarkers of myocardial fibrosis include miR-29b, miR-122, miR-133a and miR-499-5p. However evidence is still lacking to prove levels of these circulating miRNAs are associated with histologically proven myocardial fibrosis. Therefore further research is needed before any of these miRNAs would be able to be used as a fibrosis biomarker in the clinic.

1.3 Pathways involved in Cardiac Fibrosis and the current and emerging therapies targeting them

Cardiac fibrosis is a complex process with no single cause or solution. There are a number of different pathways that are thought to be involved in cardiac fibrosis to varying degrees. Identifying and targeting specific components of these pathways provides an exciting potential for the modulation of these signals through the development and application of novel therapeutics.

1.3.1 Transforming Growth Factor-β1 (TGF-β1) signalling

TGF-β1 is a member of the much larger TGF-β family of growth factors which are involved in multiple aspects of cell growth and differentiation, consisting of TGFβs, bone morphogenetic proteins (BMPs), as well as activins and inhibins(140). TGF-β exists as three different isotypes in mammals, TGF-β1, TGF-β2 and TGF-β3, although TGF-β1 is the predominant isotype involved in organ fibrosis. TGF-β1 is one of the most extensively investigated and well defined pathways involved in fibrotic disease and is known to be involved in fibroblast activation and fibrosis in the liver, lungs, kidneys as well as the heart(140,141). TGF-β1 is not secreted in its active form, but as part of a complex with latent TGF-β-binding proteins, thus preventing its activity. Upon proteolytic cleavage TGF-β1 is free to bind to TGF-β receptor type II (TGF-β RII), initiating the phosphorylation and recruitment of TGF-β receptor type I also known as activin receptor-like kinase 5 (ALK5). Activation of ALK5 initiates both canonical and non-canonical signalling cascades within fibroblasts, resulting in myofibroblast activation. The activation of the SMAD-dependant canonical pathway is thought to be the most potent inducer of TGF-β1 driven fibrosis **(Figure 2)**. Once activated ALK5 phosphorylates SMAD2/3, which binds to its co-mediator SMAD4, this complex then translocates to the nucleus where it binds to promotors of genes involved in ECM production and fibrosis, resulting in their upregulation. The importance of the SMAD2/3 dependent pro-fibrotic pathway was confirmed during experiments using fibroblasts isolated from the hearts of $Smad3^{-/-}$ mice(142). Fibroblasts isolated from these $SMAD3^{-/-}$ animals had significantly reduced levels of α-SMA gene expression compared to WT fibroblasts. The $SMAD3^{-/-}$ cells also showed a reduction in cardiac fibroblast migration and a decrease in expression of ECM proteins including Collagen I, Collagen III and Connective Tissue Growth Factor (CTFG). Finally, *in vivo* these mice also showed resistance to TGF-β1-induced fibrosis with a reduction in α-SMA positive staining and collagen deposition. These results indicate to the involvement and importance of the TGF-β1/SMAD3-dependant pathway in cardiac fibrosis.

The involvement of the non-canonical TGF-β1 pathway in cardiac fibrosis has recently started to come to the fore with research highlighting it may be more important in driving fibrosis than previously thought. Like the canonical pathway TGF-β signals primarily through TGFβRII, however, it does so without the involvement of ALK5. TGFβRII then activates a number of kinases including TAK1, RhoA, TRAF, ERK and p38 MAPKs(140). A number of these kinases have become the focus for the development of novel therapeutic targets, TAK1 inhibition

attenuated TGF-β1 induced ECM production whilst p38 inhibition in fibroblasts isolated from WT mice reduced expression of α-SMA and ECM components such as collagens and fibronectin(143,144).

Whilst TGF-β1 is most widely associated with activation of cardiac fibroblasts and ECM deposition, it is also involved in the upregulation of matrix-preserving proteins. Tissue inhibitor of metalloproteinases (TIMPs) are enzymes which can inhibit the activity of matrix degrading enzymes, such as matrix metalloproteinases (MMPs), a disintegrin and metalloproteinases (ADAMs) and ADAMs with a thrombospondin motif (ADAMTS). Picard *et al* found elevated levels of TIMP-1 mRNA in the biopsies from patients with dilated cardiomyopathy(145). This finding was further confirmed in hypertensive patients, with increased TIMP-1 correlating with diastolic dysfunction and left ventricular fibrosis(146). Through the inhibition of MMP activity by TIMPs, the ECM is unable to be degraded at the rate in which it is produced, thereby leading to the accumulation of excessive ECM, the hallmark of fibrosis.

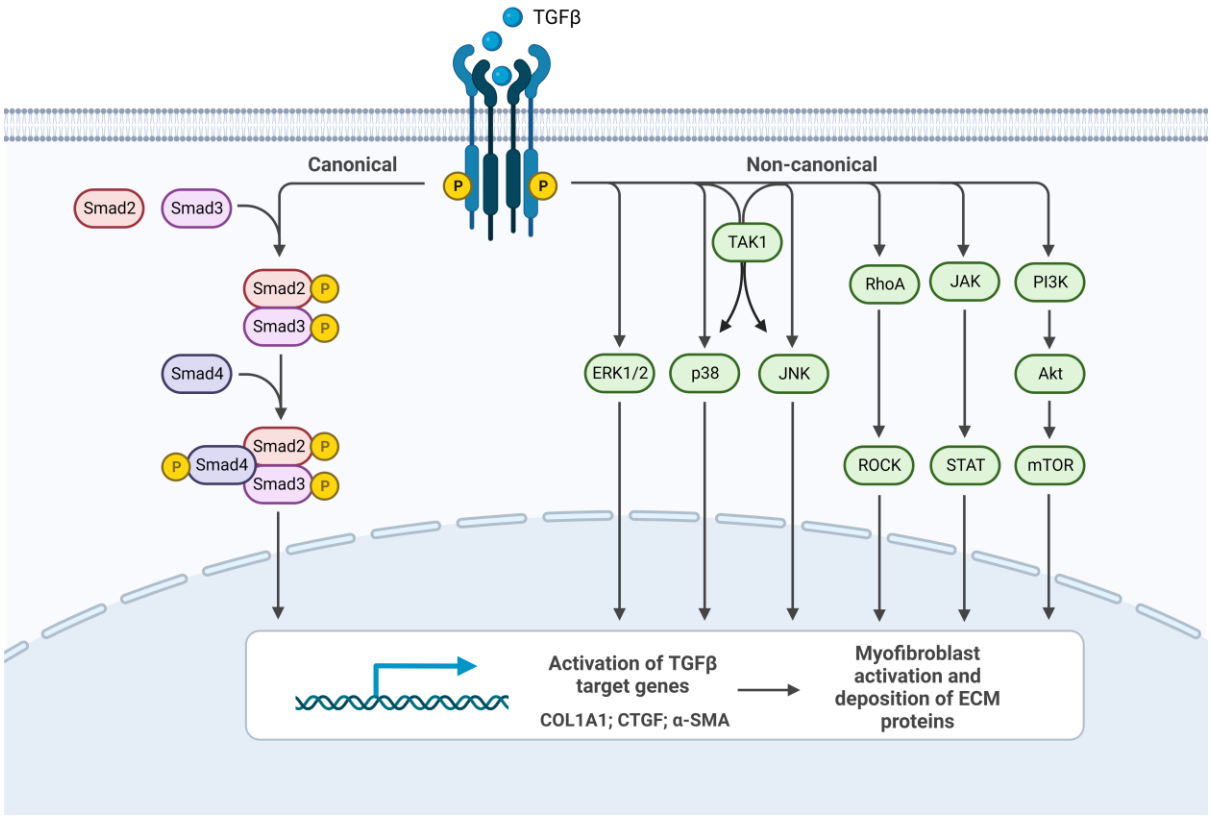

Figure 2. Overview of TGF-β signalling pathway – TGF-β signalling occurs via both SMAD-dependent canonical and non-canonical signalling pathways such as Rho-associated coiled-coil containing protein kinases (ROCKs), TAK1, p38 and JAK/STAT. Phosphorylated SMAD and non-canonical signalling translocate to the nucleus upon which activation of TGF-β target genes leading to the activation of myofibroblasts and deposition of ECM proteins. Adapted from and created with BioRender.com

1.3.2 Targeting the TGF-β1 signalling pathway

Due to the important role that TGF-β1 signalling plays in cardiac remodelling and the development of fibrosis, it has long been thought of as a potential target for novel anti-fibrotic therapies. These therapies are able to split into four different categories 1) small-molecule inhibitors of TGF-β-receptor kinases, 2) antibodies which bind to the TGF-β receptors, 3) ligand traps, which are able to bind to TGF-β, sequestering it and preventing its binding to the receptor and finally 4) preventing TGF-β1 activation through the use of small molecules or antibodies(147). Due to the diverse role of TGF-β1 in both health and disease, so far the direct inhibition of either TGF-β1 or its receptor has proved controversial. In animal models of MI inhibition of TGF-β1 directly after MI has been show to increase the risk of cardiac dysfunction and mortality. Work by Frantz and colleagues treated mice both pre- and post-MI with a TGF-β neutralising antibody. Whilst there was reduced collagen production and an increase in MMPs they also observed an increase in mortality of anti-TGF-β treated mice(148). However, there are a number of conflicting studies regarding the inhibition of TGF-β activity in pre-clinical animal models of cardiac fibrosis. Application of an anti-TGF-beta neutralising antibody inhibited fibroblast activation and collagen deposition along with reversing diastolic dysfunction in pressure-overload rats(149). Whilst use of an ALK5 inhibitor, GW788388 in rats after MI attenuated systolic dysfunction and left ventricular remodelling(150). Interestingly Frazier *et al* found that GW788388 treatment induced physeal dysplasia in rats undergoing toxicology studies(151). This highlights the risk of targeting TGF-β isoforms or their receptors, likely due to the importance of TGF-β and its signalling in health as well as disease. In a TGF-β1 knockout mouse model, mice died either in utero or by the 4 week after birth due to uncontrolled multi-organ inflammation. Whilst patients treated with fresolimumab, an anti-TGF-β human monoclonal antibody, had increased incidence of keratoacanthomas thought to be due to the loss of TGF-βs inhibitory effects on the proliferation of keratinocytes(152). TGF-β1 plays an important role in the regulation of the immune system, including its anti-inflammatory effects and the ability to suppress cells of the innate immune system. Therefore targeting the TGF-β signalling pathway using novel therapies risks causing disruption to the many important roles TGF-β performs.

1.3.2.1 Pirfenidone

Pirfenidone, an oral anti-fibrotic agent approved for use in IPF patients, inhibits TGF-β1 through one of its many unknown mechanisms of action. Initial research using animal models have tested its efficacy in attenuating cardiac fibrosis in a number of different cardiac disease models. Anti-fibrotic effects have been observed in rat MI models(153), diabetic rat models(154) and in hypertensive rats(155). Yamagami *et al* demonstrated cardioprotective effects, such as suppression of myocardial fibrosis and increased survival, in a murine pressure-overload model after Pirfenidone treatment. Finally, as well as exhibiting anti-fibrotic effects, Pirfenidone is also able to reduce inflammation. These properties were evident in a model of TAC-induced fibrosis. Mice exposed to Pirfenidone treatment had suppressed NLRP3-induced IL-1β synthesis, which in turn, attenuated IL-1β-induced inflammation and fibrosis(156). These promising results in pre-clinical models have supported the transfer into Phase II clinical trials, namely the PIROUETTE study (NCT02932566)(157). This study investigated the effects of Pirfenidone treatment in HFpEF (heart failure with preserved ejection fraction) patients. Results appear to indicate Pirfenidone treatment to be beneficial to patients, with treatment associated with reduced myocardial fibrosis(158). Despite these promising results, further larger patients trials are required to fully elucidate the therapeutic potential of Pirfenidone as a treatment for cardiac fibrosis.

1.3.2.2 Tranilast

Tranilast was initially developed to treat allergic disorders such as asthma and allergic rhinitis, however in recent years there have been studies investigating the effects of repurposing the drug to treat various forms of cardiac fibrosis(159–161). An early animal study by Martin *et al* demonstrated Tranilast's ability to attenuate cardiac matrix deposition through the inhibition of TGF-β1 in (mRen2)27 diabetic rats(160). Similar findings were presented by Kagitani *et al* whose work also demonstrated the ability of tranilast to reduce mRNA levels of PAI-1, MCP-1, IL-6 and TGF-β1 as well as the procollagens I and III(161). In tandem to the mRNA changes, collagen accumulation was supressed and myocardial fibrosis and monocyte infiltration reduced. Tranilast has undergone a Phase III clinical trial the PRESTO study, investigating whether there was a beneficial effect on reducing the incidence of restenosis after percutaneous coronary intervention (PCI)(162). However, results indicated no difference between placebo or tranilast groups.

1.3.3 Renin-Angiotensin-Aldosterone System (RAAS)

Angiotensin II (Ang II) is an important part of the renin-angiotensin system (RAS) involved in the regulation of blood volume and systemic vascular resistance(163). Initially it was believed Ang II's effects were limited to those as a circulating vasopressor through RAS, however research over the last 20 years now point to its importance in a wide range of pathological functions across multiple organs(164). Angiotensinogen, initially produced in the liver, is converted to Angiotensin I (Ang I) by the enzyme renin before Ang II is produced through the cleavage of Ang I by angiotensin-converting enzyme 1 (ACE1)**(Figure 3)**. In the case of fibrosis, Angiotensin II then binds to AT1 receptors on the surface of fibroblasts, resulting in the synthesis of ECM products and cellular proliferation and migration(165)(Murphy et al., 2015)(Murphy et al., 2015). In the heart levels of Angiotensin II have been observed to be elevated after injury(166)(Gao et al., 2009)(Gao et al., 2009). Gao *et al* showed that cardiac fibroblasts treated with Angiotensin II were able to increased collagen I expression as well as expression of the pro-fibrotic cytokine TGF-β1. Research by Schultz *et al* provided the definitive evidence for a link between Angiotensin II and TGF-β1 signalling in the heart(167). They demonstrated that Angiotensin II treatment was unable to induce cardiac fibrosis or cytokine infiltration in TGF-β knockout mice. In addition to inducing TGF-β1 secretion, the other indirect effects of Angiotensin II on cardiac fibroblasts are thought to include the induction of endothelin-1 and IL-6(168).

In recent years the 'protective arm' of RAS has been explored further, resulting in the identification of two separate pathways. The signalling of Angiotensin II through its AT2 receptor has been shown to inhibit the pro-fibrotic actions of the AT1 pathway, although the relationship between AT1, AT2 and their interactions with Angiotensin II still require further research. The second protective pathway involves Angiotensin 1-7, a heptapeptide during by the conversion of Angiotensin I by ACE2. Angiotensin 1-7 is thought to bind to the Mas receptor inhibiting the release of growth factors, reducing collagen synthesis and other Angiotensin II-induced effects on cardiac fibroblasts(169).

Due to the important role of Angiotensin II and evidence of crosstalk between it and TGF-β1 in cardiac fibrosis it has become a target for treatments looking to block AT1 receptors,

increased Angiotensin II affinity to the protective AT2 receptor and increased ACE2 conversion of Angiotensin I and Angiotensin II to Angiotensin 1-7.

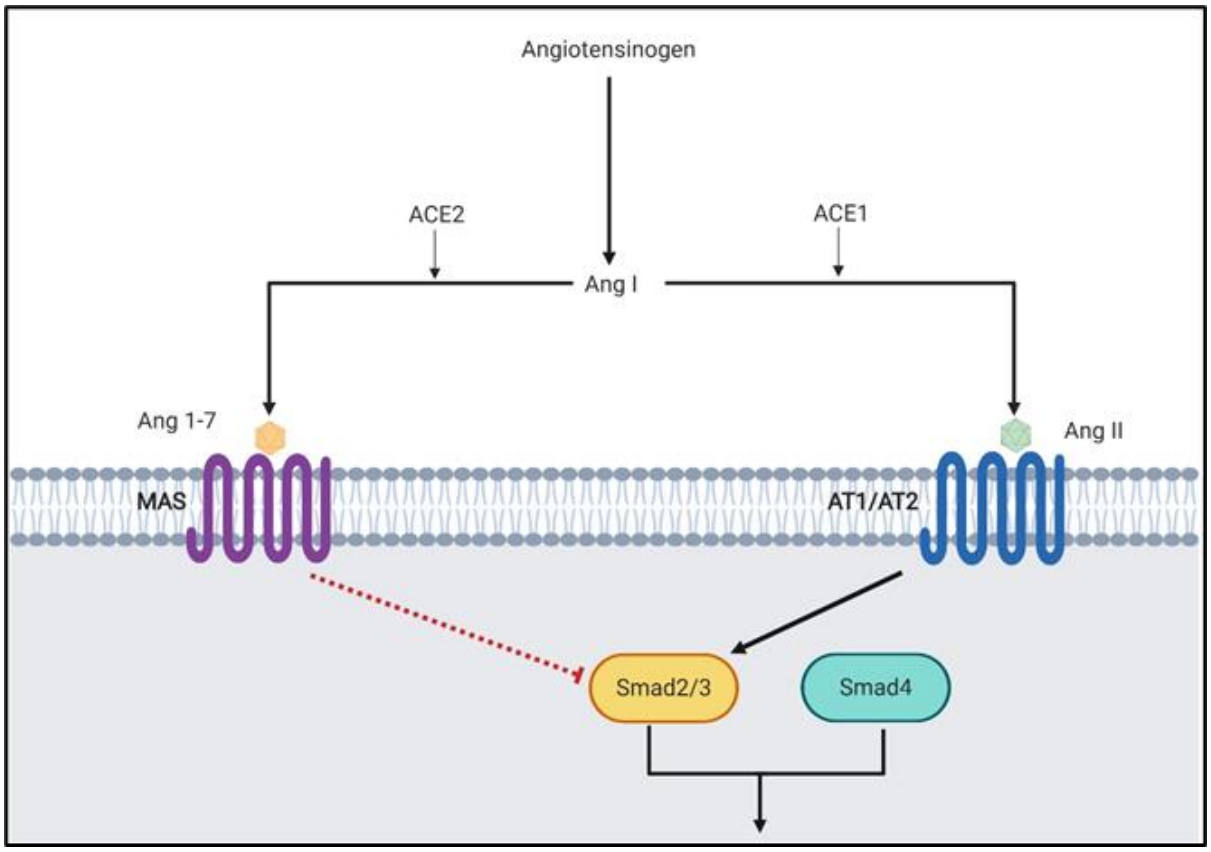

Figure 3. Schematic showing the Angiotensin signalling pathway - Ang II acts through AT1/AT2 receptors on the cell surface. Ang 1-7 is proposed to signal through MAS receptors to induce its Ang II regulatory effects – Created with BioRender.com.

1.3.3.1 Therapies targeting the Renin-Angiotensin-Aldosterone System (RAAS) – ACE inhibitors and angiotensin receptor blockers (ARBs)

Targeting the effects of Angiotensin II has long been a method employed to try and develop anti-fibrotic therapies. There are already a number of approved therapies for the treatment of hypertension, heart failure and renal disease through the inhibition of various components of the RAAS signalling pathway(170,171). Due to the pro-fibrotic effects of Angiotensin II in cardiac fibrosis, many of these therapies have been studied for their impact on cardiac fibrosis. In both animal models and patients with heart failure, treatment with ACE inhibitors or angiotensin receptor blockers (ARB) have already shown some effect at reducing cardiac fibrosis(141). One drug of particular interest losartan, an ARB, has already demonstrated the ability to attenuate fibrosis in patients with hypertrophic cardiomyopathy(172)(Shimada et al., 2013)(Shimada et al., 2013). Losartan is believed to inhibit Endothelial to mesenchymal

transition (EndMT) by preventing Angiotensin II induced phosphorylation of ERK1/2 after TGF-β1 activation(173). Angiotensin converting enzyme (ACE) inhibitors, which prevent the conversion of Angiotensin I to Angiotensin II have ever increasing evidence of their ability to attenuate cardiac fibrosis. Lisinopril was prescribed to patients with hypertensive heart disease for 6 months. When compared to baseline measurements those treated with Lisinopril had regressed myocardial fibrosis and improved LV diastolic function(174). Other studies using rodent models of fibrosis investigated both Lisinopril and another ACE inhibitor Trandolapril also confirmed their ability to reduced cardiac fibrosis and improved heart function(175,176).

1.3.4 Endothelin 1

Endothelin-1, once thought to only be secreted by endothelial cells, is increasingly recognised as an important peptide in promoting tissue fibrosis. Its effects have been observed in the lungs, kidneys and heart(177–179). The receptors for ET-1, Endothelin-A (ET_A) and Endothelin-B (ET_B), have been found to be expressed on numerous cell types including cardiac fibroblasts, cardiomyocytes and macrophages(141,177). Research by Shi-wen *et al* showed that TGF-β1 induced ET-1 mediated fibrosis could be blocked through the use of an ET_A/ET_B antagonist Bosentan resulting in reduced mRNA expression of Col1a1, αSMA and TIMP3 and fibroblast contraction(179). Due to its suspected position downstream of TGF-β1 and Ang II, ET-1 is a potential link between fibrosis and inflammation in the injured heart(180,181). Macrophages are known to secrete ET-1 and in research by Alveraz *et al* this secreted ET-1 was shown to act on cardiac fibroblast via ET_A/ET_B receptors promoting their transdifferentiation to myofibroblasts through subsequent TGF-β1 release(181).

1.3.5 Emerging treatments for fibrotic diseases

1.3.5.1 Non-coding RNAs

In addition to miRNAs being proposed as biomarkers of cardiac fibrosis, there is an ever-expanding body of literature targeting miRNAs as a novel therapeutic target(182,183). miRNAs have a number of mRNA targets, with the ability to regulate expression of multiple genes at the post-transcriptional level. Whilst having been shown to play a key role in ensuring the formation of a normal and functioning heart during cardiac development. The pathogenic mechanisms of miRNAs initially identified in animal models, but further investigated in human disease provides compelling evidence that miRNAs are actively involved in the onset of cardiac

fibrosis and progression of heart failure. Two of the most intensively studied miRNAs in cardiac fibrosis initiation and progression are miR-21 and miR-29(184,185). Quantification of miR-21 levels in the circulation have been suggested as a potential biomarker for cardiac fibrosis however, overexpression of miR-21 has been shown to activate a number of pathways, including TGF-β signalling, leading to increased cardiac fibrosis(184). In response to cardiac injury, in regard to TGF-β signalling, miR-21 expression becomes upregulated. It in turn inhibits the cardioprotective actions of TGF-βIII, resulting in its downregulation(186). Inhibition of TGF-βIII leads to the upregulation of TGF-β1, prior to activation of TGF-β1-induced SMAD signalling. Work by Liang *et al* demonstrated this pathway resulted in an increase in collagen content and cardiac remodelling both in fibroblasts *in vitro* and in an *in vivo* mouse model(186). MicroRNA-21 has also been shown to drive fibrosis through the stimulation of MAP kinase signalling in fibroblasts. Application of an antimir, a chemically modified antisense oligonucleotide which can inhibit miRNA function, silenced miR-21 and reduced ERK-MAP kinase activity(184). This in turn reduced cardiac fibrosis and preserved heart function. The use of antimirs have shown promise in larger animal models, however these have mainly focused on fibrosis after myocardial infarction. An antimir-21 treatment in an ischemia/reperfusion pig model suppressed miR-21 associated remodelling including reductions in both fibroblast and monocyte numbers(187).

In addition to miRNAs having detrimental effects on cardiac fibrosis, there are a large number of cardio-protective miRNAs including the miR-29 family(185). MircoRNA-29 has a number of target genes involved in the regulation of the ECM. Over expression of miR-29 can downregulate fibrosis-related genes such as COL1A1, fibrillin-1 and elastin(185). Angiotensin-II induced cardiac fibrosis could be prevented by the over expression of miR-29b *in vivo*(188). Other miRNAs with anti-fibrotic effects include miR-1(189), miR-133(190–192) and miR-30(192).

A major stumbling block for the use of miRNAs and antimirs to treat diseases is the need to develop organ specific delivery systems. This could in part be alleviated by targeting miRNAs which are specific only to the heart, such as miR-133 and miR-208, in order to reduce unwanted side effects(193). Delivery to the myocardium is particularly difficult, with currently

cardiac catheterisation the most effective method of delivery(194). The development of a PGMA-based nanovector has been trialled in mice to deliver miR-29b to the heart after IV injection(195). The miR-29b was successfully delivered to the heart tissue and significantly inhibiting cardiac fibrosis. Most importantly there also appeared to be no off target toxic effects in other organs therefore increasing its potential clinical application.

1.4 Current research models for investigating cardiac fibrosis and disease

1.4.1 Use of *in vitro* techniques: 2D cell culture, organoids and 3D methods

Cardiac fibrosis research has for many years centred on the use of *in vitro* techniques to investigate the molecular mechanisms driving fibrosis. Much of this research has taken place using 2D monocultures of cardiac fibroblasts due to their role as the main cell type responsible for driving fibrosis(196). These provide a cheap and easily reproducible model, especially useful in large-scale toxicology screening studies. However, these 2D models are unable to accurately recapitulate the intricate mechanisms present within disease. Cells are cultured on plastic or glass in a monolayer exposing them to shear stresses much higher than those present within the body. Fibroblasts in 2D culture have been shown to become activated in response to culture on plastic, quickly differentiating from quiescent fibroblasts to the activated myofibroblast(197). *In vivo* cells exist within the complex scaffold of the ECM, which not only supplies structural support but is also important for signalling between the multiple cell types presence in the tissues. In recent years attempts have been made to address this limitation through the development of hydrogels enabling the 3D culture cells(198). In this method cells are encapsulated within the hydrogel which acts as a scaffold, providing mechanical support to the cells but lacking signals for other cell types.

Recent years has also seen the development of more complex 3D *in vitro* models for the investigation of cardiac fibrosis. Spheroid culture has been a popular model for cardiac fibrosis research for a number of years. Initial spheroids were simple fibroblast or cardiomyocyte monocultures, formed using the hanging droplet under gravity technique or in cell-repellent or ultra-low attachment plates. Whilst having benefits over 2D culture due to the lack of adherence to plastic, the use of only one cell type assured these advantages were limited. Within the last 10 years more complex spheroid cultures have been developed. Spheroids

containing human coronary artery endothelial cells, iPS-derived cardiac fibroblasts and iPS-derived cardiomyocytes were developed to create a more physiologically relevant model(199,200). The spheroids displayed the ability to mimic the molecular composition of cardiac tissue, with the cardiomyocytes displaying spontaneous beating within the culture(200). Lee *et al* used a similar technique to create 3D cardiac spheroids to model cardiac fibrosis(201). The spheroids consisted of human embryotic stem cell (hESC)-derived cardiomyocytes (CM) and mesenchymal stem cells (MSC), which once formed into a sphere were challenged with TGF-β1. They demonstrated the ability of the MSCs to generate fibroblasts which further transdifferentiated to myofibroblasts upon TGF-β1 stimulation and these myofibroblasts displayed classical fibrotic features including collagen deposition. The 'human cardiac fibrosis-on-a-chip' (hcf-on-a-chip) model utilises human induced pluripotent stem-cell (hiPSC) derived cardiomyocytes in co-culture with cardiac fibroblasts within a fibrin gel(202). This model displayed increased collagen and BNP secretion, impaired functional capacity and a 'fibrotic' transcriptional signature, these markers of fibrosis were able to be attenuated with both Losartan and Pirfenidone treatment.

Whilst these models are no doubt an improvement on simple 2D cultures, and despite their ability to mimic tissue conditions, these 3D models still have a number of significant limitations. In the case of spheroid cultures, care has to be taken to ensure nutrients are to penetrate within the spheroid to prevent the formation of a necrotic core. Despite the ability to co-culture different cell types, these models still do not accurately mimic the structure and composition of native tissue.

1.4.2 *In vivo* models of cardiac fibrosis: advantages and disadvantages

Myocardial fibrosis is the culmination of the dysregulation of a number of different signalling pathways. These are often complex physiological and pathological processes which require investigation in models able to mirror the complex interplay occurring between cell types within the heart but to also enable research to be focused into manageable research questions(203). Currently animal models provide the ability to reproduce these interactions in a disease specific way. The most widely used animal models are mice and rats, although in recent years research has focused mainly on mouse models. The advantages of using mouse

models in cardiac research include the short gestational period, extensive characterisation of their genome and the ability to genetically alter them through gene-targeted knockouts and transgenic overexpression experiments.

Cardiac fibrosis is not caused by one singular aetiology, therefore to account for this there are several rodent models which aim to reproduce the different causes of fibrosis and heart failure. For example the chronic infusion of Angiotensin II in mice is able to be model interstitial fibrosis and cardiac hypertrophy. This model of hypertension was key in highlighting the ability of sildenafil, an approved pulmonary hypertension treatment, to improve LV performance through a reduction in adverse remodelling and infiltration of immune cells(204). However a study published soon after found that in HFpEF patients there were no positive effects of sildenafil on exercise capability of participants(205). A large number of mouse models of heart failure are based upon inducing disease phenotype through surgical intervention. Pressure and volume overload mouse models utilising either minimally invasive aortic banding (MTAB) or transverse aortic constriction (TAC) to mimic cardiac remodelling in pressure overload induced heart failure(206,207). Whilst surgical models of heart failure and fibrosis are able to recapitulate very specific cardiac conditions, the majority of heart failure cases seen clinically are from a mix of different diseases. Therefore raising questions of the biological accuracy of the models produced. A further limitation of using mouse models is that they are often induced in young animals whereas the majority of patients presenting with cardiac fibrosis are older due to the slow disease progression of heart failure. In addition to surgical models of fibrosis, utilising animal models enables the genetic modification of mice to either mimic genetic diseases such as Duchenne Muscular Dystrophy (DMD) or to allow for the investigation into the impact of specific genes on cellular and molecular pathways in heart failure. The *mdx* mouse, which arose from a spontaneous mutation in C57BL mice, has been successfully used in the research of Duchenne Muscular Dystrophy(208). As with DMD patients, these mice completely lack the dystrophin protein, however in contrast to patients the phenotype they display is less severe with mice having a near normal lifespan(209). Despite this many studies have demonstrated it as an appropriate model to investigate dystrophic cardiomyopathy which includes the development of cardiac fibrosis(210–214).

In order to address a number of the limitations of rodent models, larger animal models have also be utilised, in general for use within translational studies(215). The advantages of using larger animals such as dogs and pigs includes their longer lifespans, enabling longitudinal studies to be performed(215,216). They also have a greater genetic homology with humans, allowing for the greater confidence in findings being replicated in humans. Due to the similarities in the circulatory systems of pigs and humans, they are well suited to translational study, especially those investigating gene-editing based therapies(217). However use of larger animals to investigate disease not only results in increased costs and space required to house them but their use is more controversial despite their greater translational potential.

1.5 Use of Precision Cut Slice technology in studying disease

1.5.1 Development of Precision Cut Slices as a model for disease

Precision cut tissue slices have been used for many years for drug toxicology screening only as early models were hampered by poor reproducibility and limited viability and longevity of the tissue slices(218). The tissue slices are either human or animal derived 3D explants which can be produced from a variety of organs including the liver, kidney, lungs and heart. Whilst the initial studies produced tissue slices by hand using a razor blade there has since been the development of a number of different specialised tissue slicers(218,219). The Krumdieck tissue slicer was a the first to enable greater control and accuracy over thickness of the slices produced(220,221). Cylindrical cores of tissue are produced from the organ of interest and subsequently placed within the slicer. A weight is placed above the tissue and tissue slices produced by advancing the core over an oscillating blade(221). Due to the use of a weight to determine tissue thickness, slices produced, whilst more accurate than previous methods, do vary in thickness between each sample(222). Within the last 15 years the development of the Leica VT1200S vibrating blade microtome has sought to further improve the earlier slice methodology. Whereas using the Krumdieck tissue slicer only allows for the accurate control of the speed at which tissue slices are cut, the Leica VT is completely automated and allows the user to accurately set tissue thickness, sectioning speed and oscillation amplitude(222).

Precision cut tissue slices (PCTS) present an exciting translational prospect to bridge the gap between pre-clinical models and patients. PCTS have been used extensively to investigate liver

fibrosis, from its early onset to modelling end-stage disease(223). Slices cultured for up to 96 hours showed activation of fibrotic pathways demonstrated by increased mRNA expression of collagens, MMPs and TGF-β1. Addition of exogenous compounds such as ethanol, bile acids and TGF-β1 have enabled the modelling of a range induced fibrotic diseases(223–225).

Myocardial slices have been used in varying forms of cardiac research for many years, however over the last 10 years research into improving the culture conditions has occurred in earnest. Parrish *et al* were the first to utilise the myocardial slice system over 25 years ago. They demonstrated the ability to keep rat heart slices viable for 24 hours using a roller culture system to investigate the effects of Doxorubicin and Allylamine during toxicology studies(218,219). Further more recent studies have used mouse and larger mammal (such as pig) hearts to continue to develop the culture system. Due to the ability to only maintain tissue viability for up to 24 hours these slices were mainly used for electrophysiology studies or short-term toxicology experiments(226–228). A major limitation for the use of human myocardial slices to investigate cardiac fibrosis is the difficulty accessing donor tissue. This has resulted in the speed of the development of cardiac models being slower than in other organs such as the liver and kidney. Brandenburger *et al* published some of the first results using human samples in 2012(229). Tissue was used from patients undergoing Myectomy during aortic or mitral valve replacement surgery. Slices were prepared using Leica's VT1200S vibratome and a slicing buffer of Tyrode's solution containing an excitation-contraction uncoupler 2,3-butanedione-monoxime (BDM) to ensure less damage occurred to the tissue during the slicing process. Other studies have built on this work, including adding both mechanical load or electrical stimulation to the culture protocol(230–232). Whilst these advancements have improved the viability of the slice cultures, in some cases claiming the slices to remain viable in culture for up to 4 months, the number of tissue slices either able to be produced but also cultured is limited by the specialised equipment required(232). Thus limiting their use to smaller scale studies and those investigating the genetic manipulation of the tissue. To date only work by Perbellini and colleagues have used this system to investigate cardiac fibrosis. Interestingly they were unable to induce fibrotic changes in the slices despite the application of either TGF-β1 or Angiotensin II(233).

The use of precision cut heart slices highlights an exciting development in cardiac research, offering an exciting opportunity to revolutionise the landscape of translational research. Whilst there has been rapid improvements in the culture conditions and length of viable culture in recent years an area in which further studies are required is for the modelling of fibrotic disease in the heart. Currently other groups have been unable to induce fibrosis in their PCHS cultures, thereby limiting their use. This presents itself with the tantalising opportunity to create a human tissue model for the investigation of the pathways involved in cardiac fibrosis and the identification of novel therapeutic targets.

2 Study Rationale, Hypothesis and Aims

2.1 Study Rationale

Current research into cardiac fibrosis has focused on the use of *in vitro* 2D cell culture and *in vivo* animal models. Whilst these two techniques have proved invaluable in the development of our understanding of the fibrotic process, the use of precision cut tissue slices from human tissue provides the potential missing link between animal work, human disease and drug trials. Work by Perbellini and colleagues has paved the way for the use of PCS in cardiac tissue, however as yet they have been unable to model fibrotic disease in PCHS.

The NFRG has many years of experience investigating fibrosis across a number of different organs, including the heart, and has vast expertise in the PCS technology. During this PhD we will seek to use the novel aspects of the culture system developed within the laboratory to firstly optimise the culture conditions required for PCHS and secondly look to model fibrotic disease in the tissue with the overall aim to identify targets for the testing of novel therapeutics.

2.2 Hypothesis

Cardiac fibrosis is a complex disease with wide reaching effects. Researchers currently rely overwhelmingly on the use of *in vivo* animal models or *in vitro* cell cultures isolated from either rodent or human tissue to investigate disease mechanism and identify biomarkers of disease progression. Whilst these models have undoubtedly improved our understanding of disease progression, they do not accurately recapitulate the complex microenvironment of human tissue and have thus far failed to translate to clinical benefit.

We hypothesise that the development of a novel *ex vivo* precision cut slice model combined with a broad omics approach will identify novel biomarkers and molecular mechanisms driving fibrogenesis with direct relevance to the human heart. Through the application of novel therapeutics we will be able to develop a greater understanding of the mechanisms critically involved in fibrosis in the human heart with the overarching goal to identify novel therapies for translation into the clinic.

2.3 Aims

2.3.1 Development of Precision Cut Heart Slice model from human tissue.

Precision Cut Heart slices will be generated from left ventricular tissue donated by patients undergoing Left Ventricular Assistance Device implant surgery, explanted hearts from patients undergoing heart transplantation or from donor hearts unsuitable for transplant. Viability of PCHS will be assessed over 6 days in culture to investigate differences in viability of PCHS depending on tissue culture medium and the use of a bioreactor rocking system versus static/conventional culture conditions.

2.3.2 Investigate the molecular pathways involved in cardiac fibrosis and inflammation.

PCHS will be challenged with proposed drivers of cardiac fibrosis to explore inflammation and fibrosis. This will include exogenous challenge of PCHS with TGF-β1, Angiotensin II, CTGF, galectin 3 and IL-11. Samples will be analysed using in-house methods such as RT-PCR and ELISA to assess inflammation and fibrosis, as well as by a broad 'omics' approach to identify targets of interest. Exogenous challenge of PCHS by pro-inflammatory stimuli such as IL-1α, IL-1β, LPS and poly-IC will also be explored.

2.3.3 Use established and novel therapeutics to manipulate cardiac fibrosis and inflammation.

Established and novel anti-inflammatory and anti-fibrotic therapies will be utilised to investigate the abrogation of fibrogenesis and inflammation in PCHS. Through the use of downstream IPA analysis targets and molecules of interest will be identified and tested in both 2D primary cell culture and *ex vivo* PCHS model.

2.3.4 Identification of a molecular signature of cardiac fibrosis in the blood of patients.

Samples will be collected from a well-characterised cohort of female DMD carriers with a spectrum of disease-state, including those with normal cardiac function to those with extensive cardiac fibrosis with or without left ventricular dysfunction as confirmed by MRI. The molecular signature of the samples will be elucidated using the cutting-edge approaches of proteomic analysis, lipidomic analysis, multiplex ELISA and neoepitope assays.

3 General materials and methods

3.1. Human ethics and tissue acquisition

3.1.1. Human heart ethical statement and patient demographics

Human cardiac tissue for the generation of PCHS and isolation cardiac fibroblasts was obtained under ethical approval from a number of different sources. Initial tissue samples were collected either from patients undergoing Left Ventricle Assistance Device implantation surgery or cardiac transplantation (IOT038). Whole hearts which had been declined for transplant were also accessed through the Newcastle transplant tissue biobank (IOT061). Collection of hearts was facilitated through both Research, Innovation and Novel Technologies Advisory Group (RINTAG) and the Quality in Organ Donation (QUOD) biobank.

Donor number	Tissue Type	Reason for LVAD	Age	Sex	PCHS and/or Cardiac Fibroblasts
NHH010	LVAD	Dilated Cardiomyopathy	71	Male	PCHS
NHH011	LVAD	Transposition of the great arteries	59	Male	PCHS
NHH012	LVAD	Ischaemic cardiomyopathy	59	Male	PCHS
NHH014	LVAD	Ischaemic cardiomyopathy	59	Male	PCHS
NHH019	LVAD	Dilated Cardiomyopathy	59	Male	PCHS
NHH020	LVAD	Ischaemic cardiomyopathy	55	Male	Both
NHH022	LVAD	Dilated Cardiomyopathy	55	Male	Both

Table 1. Demographics of LVAD donors

Donor number	Tissue Type	DCD or DBD	Age	Sex	Reason for Transplant decline	PCHS and/or Cardiac Fibroblasts
NHH017	Perfused Heart	DCD	56	F	PMH	PCHS
NHH018	Perfused Heart	DBD	63	F	Size and PF	Both
NHH021	Perfused Heart	DBD	18	F	Size and PF	Both
NHH024	Perfused Heart	DBD	67	F	Age	PCHS
NHH025	Perfused Heart	DCD	55	F	Age	PCHS
NHH027	Unused Donor	DCD	31	M	Size	PCHS
NHH028	Unused Donor	DBD	71	F	Age	PCHS
NHH029	Unused Donor	DBD	54	F	HLA/ABO Type	PCHS
NHH030	Unused Donor	DCD	59	M	Age	PCHS
NHH031	Unused Donor	DCD	66	M	Not give; Age	PCHS
NHH035	Unused Donor	DBD	52	F	PMH	Cardiac Fibroblasts
NHH036	Perfused Heart	DCD	65	F	PMH	PCHS
NHH037	Unused Donor	DCD	61	M	Poor Function	PCHS
NHH039	Unused Donor	DBD	41	M	PMH	PCHS
NHH040	Perfused Heart	DBD	20	M	HLA/ABO Type	PCHS
NHH041	Unused Donor	DBD	44	F	PMH	PCHS

Table 2. Demographics of Unused donors and perfused heart – DBD: Death after Brain Death; DCD: Death after Circulatory Death; F: Female; M: Male; PMH: Past Medical History

3.2. Processing tissue and generating human precision cut slices (PCHS)

Tissue from the left ventricle was transported to the Newcastle Fibrosis Research Group laboratory in 4°C saline solution. Prior to processing, the sample was incubated for a short period of time in 4°C 'Slicing Buffer' consisting of Tyrode's solution containing 30mM of 2,3-Butanedione monoxime (BDM), an excitation-contraction uncoupler **(Table 3)**. Tissue was washed thoroughly in slicing buffer prior to being cut into blocks 1cm in depth, both endocardial and epicardial tissue was trimmed from the tissue block leaving myocardial tissue only **(Figure 4)**. Tissue cores were generated using a 6mm biopsy punch from the block. Tissue cores were next placed in cold slicing buffer for 10 minutes. Six cores were then dried using tissue and placed in metal histology tray on ice before 3% low melting agarose was poured into the tray until all cores were covered. The tray was kept on ice until the agarose was fully set. Once set the agarose block containing tissue cores was cut out, superglued to a specimen stand and left until the glue was set. The tissue block was placed attached to the Leica VT1200S Vibratome (Leica Biosystems) and completely submerged with 4°C slicing buffer. Precision Cut Heart Slices (PCHS) were cut at a speed of 0.3mm/sec and a thickness of 250µm. Slices were removed from the buffer tray using tweezers and incubated in a Petri dish on ice containing slicing buffer until enough slices had been collected. PCHS were then transferred into 8µm-pore inserts (Greiner Bio) in 12-well BioReactor (rocked) plates with 1.5ml per well of Smooth Muscle Cell Medium (PromoCell) supplemented with Penicillin (100IU/ml) - Streptomycin (100µg/ml) and 2% glutamine/pyruvate and cultured at 37°C supplemented with 5% CO_2. Media was changed daily thereafter.

Slicing Buffer – Tyrode's Solution		
Solid Reagents		
	Mass (g)	**Final Concentration (mM)**
2,3-Butanedione monoxime (BDM)	3.00	30.00
Glucose	1.86	1.00
HEPES	2.38	10.00
Potassium chloride	0.45	6.00
Sodium chloride	8.18	140.00
Solutions		
	Volume (ml)	**Final Concentration (mM)**
1M Magnesium chloride	1.00	1.00
1M Calcium chloride	1.80	1.80

Table 3. Details of Slicing buffer used due the isolation of PCHS

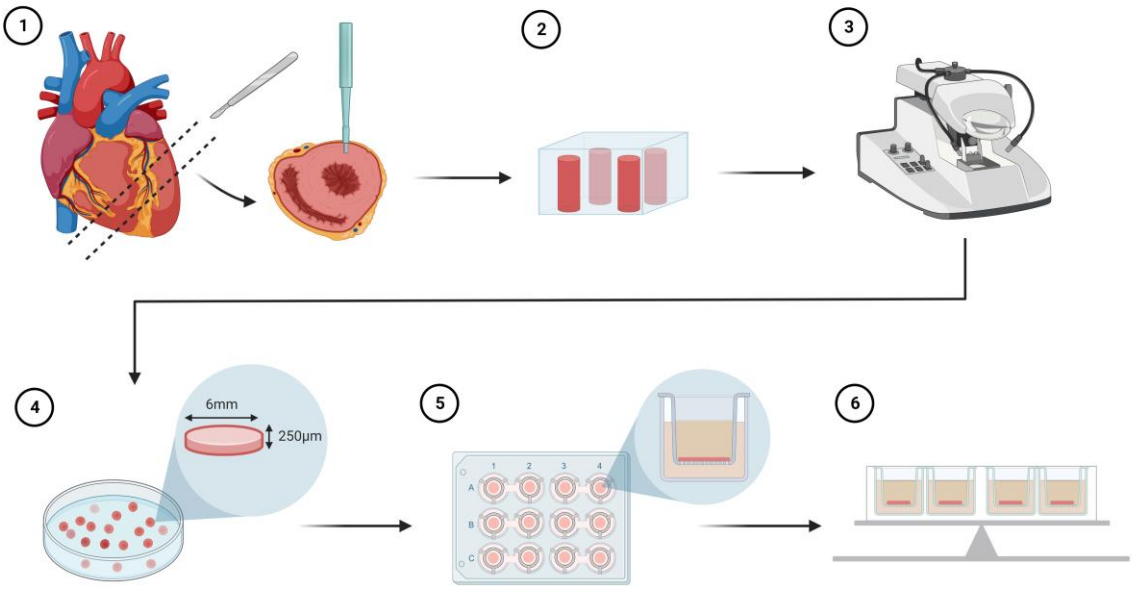

Figure 4. Workflow of generation of PCHS – **1)** Heart tissue was dissected and processed to generate 6mm tissue cores using a biopsy punch; **2)** Tissue cores were set in 3% agarose scaffold; **3)** Leica VT1200S vibratome was used to slice cores at a speed of 0.3mm/sec and thickness of 250µm; **4)** Tissue slices 6mm x 250µm were stored in 4°C Tyrode's Buffer + BDM until required; **5)** Slices were transferred to transwell inserts within specialised 12-well culture plates; **6)** Plates were placed upon Bioreactor Rocking platform and cultured at 37°C and 5% CO_2 for up to 6 days.

3.3. Enzyme Linked ImmunoSorbant Assay (ELISA)

Sandwich ELISA was performed using DuoSet ELISA Kits (R&D Systems) on samples removed from treated heart slices to measure the secretion of Collagen 1a1, TIMP1, IL-11, CTGF, IL-6, IL-8 and MCP-1 **(Table 4)** as per manufacturer's instructions **(Figure 5)**. Briefly, Capture antibodies diluted in PBS were added to a 96 well half area plate (Corning) and incubated overnight with rocking. Plates were blocked using reagent diluent (1% BSA + PBS) for 1 hour at room temperature. Standards were prepared by diluting recombinant protein to a concentration of; Collagen 1a1 (2000pg/ml), IL-6 (600pg/ml), IL-8 (500pg/ml), MCP-1 (1000pg/ml), CTGF (2000pg/ml), IL-11 (2000pg/ml) and TIMP1 (2000pg/ml). A 6 step 2-fold serial dilution was then performed with the eighth standard containing reagent diluent (RD) only. Samples were diluted in RD to a final assay dependant concentration. The plate was washed 3 times with 1x PBS + 0.05% Tween prior to addition of samples and standards. The plate was rocked at room temperature for 2 hours. Samples were washed off and detection antibodies were then applied to the plate for 2 hours at room temperature with rocking. Streptavidin conjugated to horseradish protein (HRP) was added and plate incubated in the dark for 20 minutes. Plates were washed for the final time prior to application of substrate solution (1:1 ratio). Colour change was stopped when the standard curve was clearly defined

by adding stop solution (1M H_2SO_4). The optical density was measured at 450nm and 570nm. Sample concentrations were calculated using the 7-point standard curve.

Marker	Reference Number	Supplier
Collagen 1a1	DY6220	R&D
TIMP-1	DY970	R&D
IL-6	DY206	R&D
IL-8/CXCL8	DY208	R&D
MCP-1/CCL2	DY279	R&D
IL-11	DY218	R&D
CTGF/CNN2	DY9190	R&D

Table 4. Product details of ELISA kits used

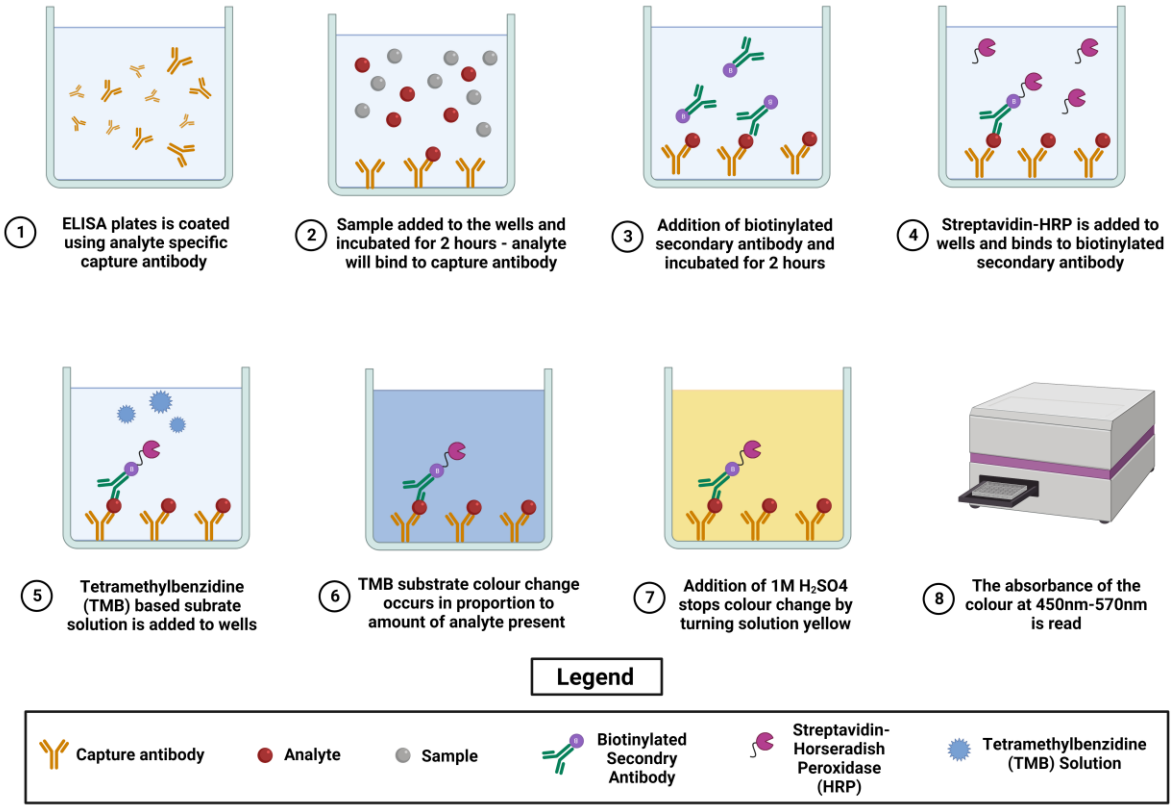

Figure 5. ELISA Protocol – **1)** Capture antibodies diluted in PBS were applied to microtest plates, after overnight incubation any unbound antibodies were washed off, **2)** Samples and standards diluted in Reagent diluent (RD) were applied to the plate, the analyte within the sample will bind to its specific capture antibody, unbound sample was washed off after a 2 hour incubation **3)** The secondary biotinylated antibody was added to the plate for 2 hours prior washing **4)** Streptavidin-HRP was added to the plate and binds to the biotinylated secondary antibody, excess was washed off after 20 minute incubation **5)** A TMB based substrate solution was applied and the plate was incubated in the dark **6)** The colorimetric change occurs, samples and standards are visualised **7)** 1M H_2SO_4 was applied to stop colour change and prevent over saturation of the samples and standards **8)** Optical density was measured at 450nm and 570nm. Figure created using BioRender.com

3.4. MesoScale Discovery™ (MSD) U-Plex Assay

MSD biomarker assays were performed on samples using U-Plex Multi-Spot Assay System (MesoScale Discovery™). The biomarkers present in each kit were GM-CSF, IL-6, IL-8, TNF-α, Eotaxin, MCP-1, MIP-1α and TNF-α. The assay was performed as per manufacturer's protocol. Briefly, U-plex plates were coated with the appropriate Linker-coupled capture antibodies, sealed and left for 1 hour with shaking at room temperature. Following this the plates were washed 3 times using 1X MSD wash buffer (PBS/0.05% Tween20) before the prepared samples, calibrator or controls were applied to the plate and incubated at room temperature with shaking for 1 hour. Plates were washed before detection antibodies were applied and incubated for a final time at room temperature for 1 hour with shaking. Plates were washed prior to Read Buffer T being added to each well and the plate read using MesoScale Discovery™ Sector imager 2400 plate reader (MSD™). Analysis of results was performed using the MSD Discovery Workbench 4.0 analysis software.

3.5. Lactate Dehydrogenase Assay (LDH)

Lactate dehydrogenase (LDH) assay was performed on tissue culture media collected from heart slices. Pierce LDH cytotoxicity Assay Kit (Thermo Scientific) was used following manufacturer's instructions. Briefly, Reaction Mixture was made by adding Substrate Mix to ultrapure water and dissolved by gentle mixing before the Assay Buffer was added. A PCHS positive control was prepared by adding 200µl of 20% Triton X to 1.3ml of culture media containing a tissue slice. This mixture was left to incubate at room temperature and vortexed at intervals to ensure maximal cellular death before being added in duplicate to 96 well plate (Corning). Samples and a negative control (media blank) were added in duplicate to the plate. The plate was placed in the dark and incubated for 30 minutes prior to the addition of stop solution. Absorbance was read at 490nm and 680nm using spectrophotometer plate reader (Thermo Scientific), with LDH activity determined by subtracting the values produced at 490nm from values at 680nm prior to the subtraction of the negative control value. Data was normalised against the positive control to give final measurements as a percentage of control.

3.6. Resazurin Assay

3.6.1. Resazurin on PCHS

To assess the metabolic activity of the tissue slices a resazurin assay was performed at the time of slicing (t=0) and subsequently at Day 2, Day 4 and Day 6 in culture. Briefly 4.5mM resazurin stock solution was mixed with each media type to produce a 450µM resazurin working solution. PCHS were then incubated in 100µl of the working solution in 96 well tissue culture plates for 1 hour in a cell culture incubator at 37°C supplemented with 5% CO_2. A media blank for each media type tested was cultured alongside. After the incubation, 50µl from all wells was transferred to white 96 well plate and read for fluorescence at excitation 535nm and emission 595nm. Media blank values were subtracted from matched tissue values.

3.6.2. Resazurin on Cultured Cells

Metabolic activity of cultured fibroblasts in 96 well plates was assessed using the resazurin assay as described above with the following amendments. Cells were incubated in 50µl of 450µM resazurin media working stock for 1 hour in tissue culture incubator supplemented with 5% CO_2 at 37°C. Following the incubation 49µl from all wells was transferred into white 96 well plates and fluorescence measured as previously described.

3.7. RNA isolation from PCHS

Total ribonucleic acid (RNA) from snap frozen PCHS was isolated using the MagMAX-96 Total RNA Isolation Kit (Invitrogen, AM1830) as per the manufacturer's instructions. In order to isolate higher yields of RNA 2-4 PCHS were pooled for each treatment condition at PCHS harvest, snap frozen and stored at -80°C until required. Tissue was lysed in 100µl Lysis Binding Solution (AM8500) plus 0.7µl β-Mercaptoethanol using the Tissue Lyser II bead homogeniser. Lysate was spun for 2 minutes at 8000G, the supernatant transferred into 96-well plate and 60µl isopropanol added to each sample. The plate was rocked on an orbital shaker for 1 minute. Magnetic bead mixture was added to the samples and plate the returned to the shaker for 5 minutes. The plate was placed onto magnetic block for 3 minutes, the supernatant was removed without disturbing the pellet, prior to the plate being removed from the block and Wash Solution 1 (AM8504) added. The plate was put onto a shaker for 1 minute prior to 3 minute incubation on the magnetic block. The supernatant was removed and Wash Solution II (AM8640) added. The shaking and supernatant removal step was repeated prior to the

application of a DNase Solution. After 15 minutes RNA Rebinding Solution was applied and the plate incubated with shaking for a further 3 minutes before placing onto the magnetic block, and the supernatant was removed and Wash Solution II added. The plate was incubated with shaking for a further 1 minute, prior to the removal of the supernatant and this process repeated once more. After removal of the supernatant, pellets were dried for 2 minutes on the shaker before the addition of 30µl of Elution Buffer. Samples were incubated for 3-5 minutes on the shaker, then placed onto the magnetic block to allow magnetic beads to form a pellet. The supernatant was removed and placed into Eppendorfs and stored at -80^{o}C until required.

3.8. RNA Integrity and Quantification

Quantity and purity of RNA was measured spectrophotometrically using an IMPLEN nanophotometer. After blanking with RNAase-free water, 1µl of RNA was pipetted onto the sample surface and absorbance measured at the wavelengths 260nm and 280nm. A 260/280 ratio of ≥2 was used to indicate minimal protein contamination.

3.9. Cardiac Fibroblast Isolation and Culture

Isolation of cardiac fibroblasts was performed using a method adapted from Agocha *et al*(234) from LVAD **(Table 1)** and Unused or perfused **(Table 2)** left ventricular donor tissue. Firstly tissue was washed 3 times in cold PBS before being separated into 50mg chunks and minced to 1mm^3 pieces to increase the surface area of the tissue. The minced tissue was placed into separate 50ml falcon tubes before addition of 10ml of digestion buffer (200u/L Collagenase B, 0.1% Trypsin and DNase I). The tubes were then incubated at 37^{o}C for 10mins with constant shaking. The supernatant was then discarded to remove red blood cells and cellular debris, leaving the tissue in the bottom before another 10ml of digestion buffer was added and the process repeated once more. A further 10ml of digestion buffer was added for a final time and incubated for a further 30 minutes. After this digestion the entire contents of the tube (buffer and tissue) was placed through a 100µm filter. Tissue was disrupted and washed with HBSS+. This process was repeated for all tubes ensuring they all contained equal volumes before being centrifuged at 1400rpm for 5 minutes. The supernatant was discarded and the pellets resuspended in 1ml of Fibroblast Media 3 (PromoCell) supplemented with 1%

penicillin/streptomycin and 2% glutamine/pyruvate and added to T-75 flasks containing 12ml media. Flasks were incubated at 37°C supplemented with 5% CO_2. Media was changed after overnight incubation and then every 3-4 days thereafter.

Once cells reached ~85% confluence they were split *via* trypsinisation. Culture media was discarded and cells washed using PBS warmed to 37°C. Cells were detached using Trypsin/EDTA (0.04%/0.03%) Solution (PromoCell) prior to neutralisation with Trypsin Neutralising Solution (PromoCell), containing 0.05% Trypsin inhibitor in 0.1% BSA. Cell suspension was centrifuged at 1400rpm for 5 mins, supernatant was discarded and pellet resuspended in either 1ml Fibroblast Media 3 or at a density of 1 million cells per 0.5ml in Cryo-SFM freezing medium (PromoCell) if being prepared for long-term storage. Cells in Cryo-SFM were aliquoted into cryovials, transferred into a Mr Frosty™ and frozen at a rate of -1°C per minute. Once frozen, vials were transferred to liquid nitrogen for long-term storage.

3.10. Statistical Analysis

Statistical analysis was performed on datasets using GraphPad Prism 9.4.1. Results are presented as mean ± standard error of the mean (SEM). Statistical analysis comprised of either paired t-tests, paired t-test with multiple comparisons or ANOVA mixed effects analysis with Dunnett's multiple comparisons. Data were considered statistically significant with a p value ≤0.05 *, p≤0.01 **, p≤0.001 *** and p≤0.0001 ****.

4 Precision Cut Heart Slice (PCHS) culture development, optimisation and disease modelling

4.1 Introduction

4.1.1 Current research methods and disease models of cardiac fibrosis

A large proportion of current research into cardiac fibrosis, including its initiation and the pathways involved, is performed using animal models or *in vitro* 2D cell cultures of either mouse or human derived fibroblasts. These techniques have been instrumental in advancing our understanding of cardiac fibrosis and are widely accepted as the 'gold standard' approaches. Without *in vivo* mouse models evidence about fibroblast and myofibroblast origins, as well as systemic causes and effects of cardiac fibrosis could not have been discovered. However despite this there are still significant limitations when using both *in vitro* cell cultures and *in vivo* models to discern the cellular and molecular changes that occur during fibrosis and to identify/test potential targets for drug discovery.

A major limitation of 2D cell culture centres around the conventional methodology of culturing cells in a 2D monolayer on solid, flat surfaces. This increases the level of sheer stress that the cells are exposed to when compared to levels they would experience *in vivo*. Fibroblasts cultured in 2D monolayers are exposed to supra-physiological levels of stiffness, changing their function, phenotype and viability(235). Due to the fact these cells are also cultured in a monolayer they are restricted in their ability to communicate to surrounding cells, limited only to their periphery. Whereas in tissue, cells form a multi-directional structure, communicating to neighbouring cells in a far more complex manner than that of 2D monolayers. This limitation can have a detrimental effect when it comes to drug discovery, potentially providing either false negative or positives during drug screening(196). In recent years advances in technology has led to the development of 3D cell culture systems to attempt to allay a number of the limitations of 2D cultures(236). In these structures cells are able to form interactions with neighbouring cells to more accurately reflect those seen *in vivo*, this enables the ability to provide more insights into the crosstalk between cells. Despite these techniques being an improvement compared to 2D cultures, 3D systems still mostly use only two different cell types, therefore still oversimplifying the complex interactions between multiple cell types present in tissues, such as the heart(12).

In vivo animal models are able to overcome a number of the issues of 2D and 3D culture, multiple cell to cell interactions are present, as well as the ability to look at the effects of disease and/or drug therapies on the animal as a whole, not just a specific organ or cell type. However, there still remains limitations in translating the findings discovered through the use of animal models into patients. The obvious limitation of *in vivo* models is the differences between animals and human patients in terms of biology and that what is observed in rodents *in vivo* may not translate when tested in humans.

4.1.2 The use of PCS technology in cardiac research and the current limitations of the technology

Precision cut tissue slices (PCTS) are becoming an increasingly popular tool to study the multi-cellular interactions present in many diseases. They provide a unique insight into the interactions occurring between multiple cell types present in an organ, something that could prove invaluable for testing of novel therapeutics, providing the missing link between *in vivo* animal models and testing compounds in intact human tissue(237). Precision cut tissue slices are now being utilised across a number of different organs and tissues including lung(238), liver(223,237), kidney(239) and heart(240,241). Despite being derived from human tissue, PCTS do have their own limitations. There is, at present, the inability to model the effects of circulating immune cells during progression of diseases. Secondly, the effects of drug therapies on the tissue would not highlight potential side effects on other organs of the body. Despite this PCTS derived from human tissue still hold the potential to provide the missing link in drug discovery, helping to inform pre-clinical decisions and potentially highlighting therapies which may be more or less likely to work when tested in patients. Currently only <10% of novel therapies progress from Phase I trials to approval, the use of PCTS in this process could help to improve the preclinical research and bridge the translational gap in drug discovery research and the clinic(242).

Initial studies using precision cut heart slices (PCHS) focused on the use of the tissue in electrophysiological studies(243,244), whilst more recent work by Perbellini *et al* has looked to develop longer term culture of PCHS to enable their use in drug toxicology studies and the investigation of cardiac fibroblasts(241). Work by Watson, Perbellini *et al* was key in developing a protocol for the acquisition of viable PCHS for longer-term culture(240).

Our laboratory has significant experience of PCTS technology, producing tissue slices across a range of organs including liver(223) **(Figures 6 and 7)** and kidney(245) **(Figure 8)**. Importantly in the case of tissue slices produced from liver and kidney, the development of our novel bioreactor technology has increased the viability of tissue slices from these organs and has enabled us to model fibrotic disease(223). We believe our experience in fibrotic diseases and development of PCTS as well as our patented novel bioreactor technology will allow us to develop this technology in human heart tissue, leading to the investigation of cardiac fibrosis and the testing of novel therapeutics.

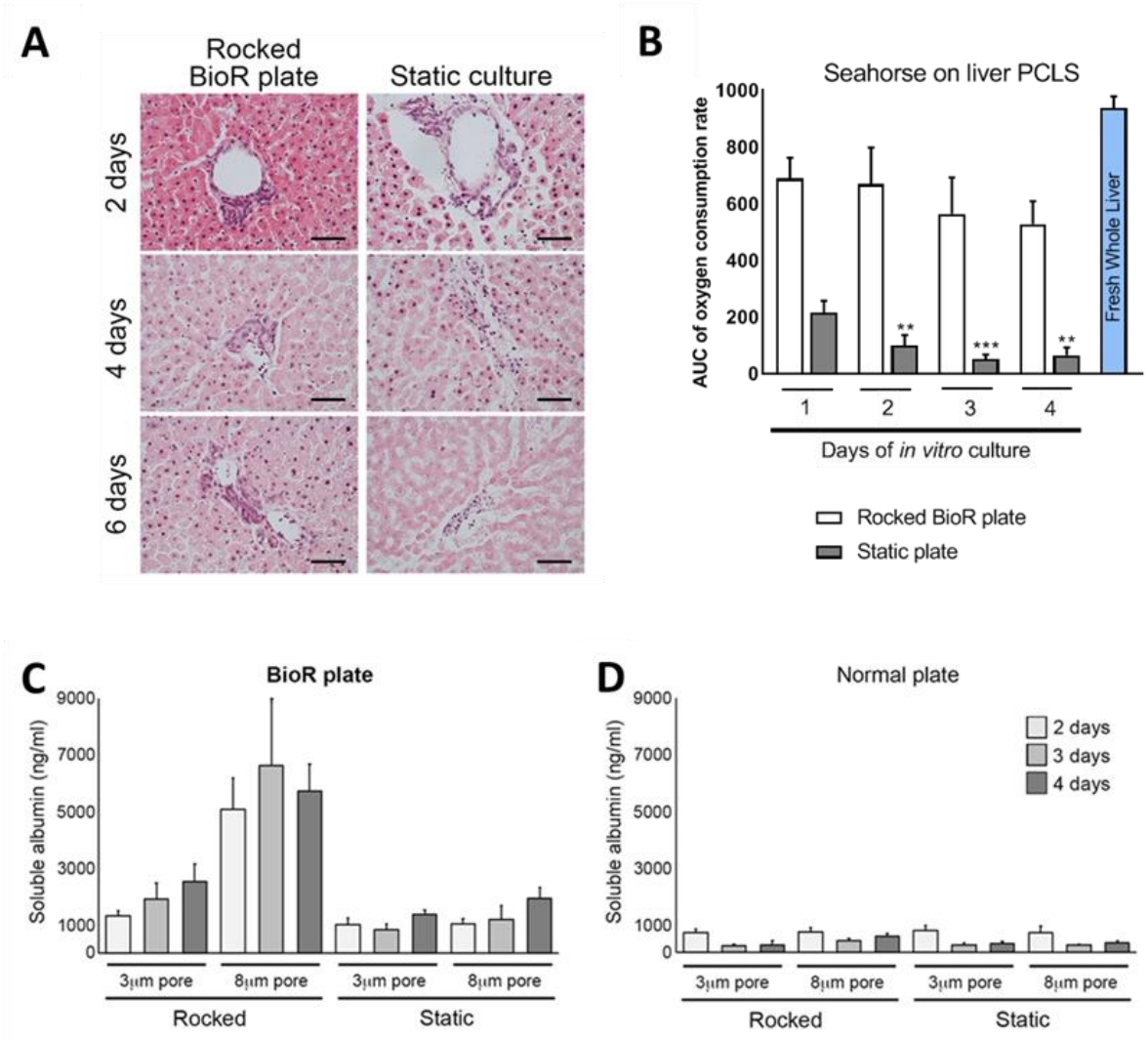

Figure 6. Precision Cut Liver Slice Viability - Figure taken from Paish *et a*l (2019) paper to show the increased viability of slices cultured in our bioreactor plate and rocker compared to tissue cultured in normal 12 well tissue culture plates(223). **A)** Representative images of Haematoxylin and Eosin staining **B)** Metabolic activity of PCLS shown as Area under the curve (AUC) over 4 days in culture**. C–D)** Soluble albumin data of the effect of different pore size of transwell inserts and rocking vs static over 4 days in culture.

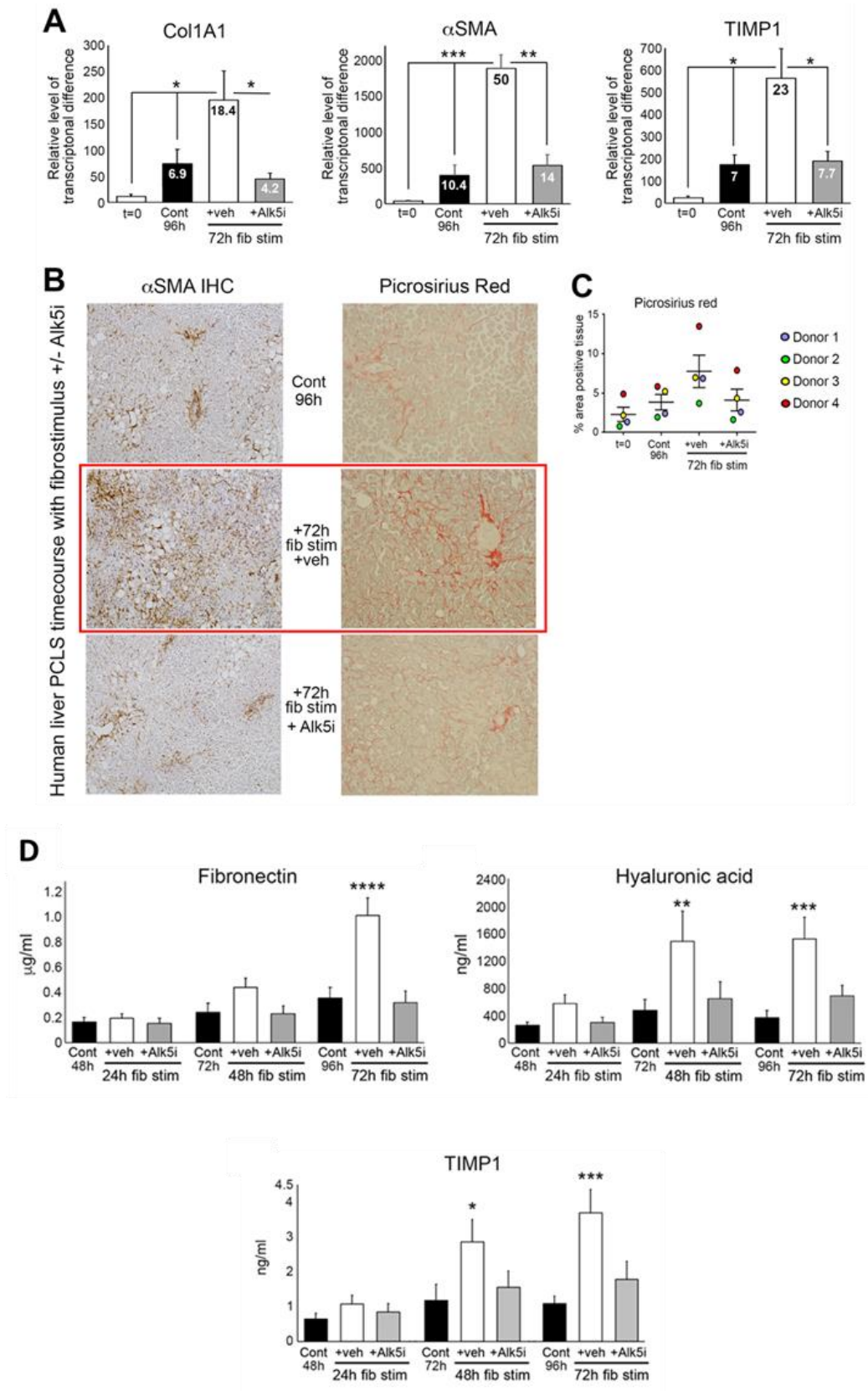

Figure 7. Induction of fibrogenesis in Precision Cut Liver Slices (PCLS). Taken from Paish *et al* (2019) to highlight the ability to induce fibrogenesis in PCLS stimulated with TGF-β1 and attenuate it with use of an ALK5 inhibitor(223). **A)** RT-PCR measuring RLTD of the fibrotic marker genes Collagen 1a1, αSMA and TIMP1. **B)** Representative images of αSMA and Picrosirius Red IHC of slices treated +/- TGF-β1 and ALK5i **C)** quantified results of Picrosirius Red staining. **D)** Secretion of soluble proteins measured by ELISA.

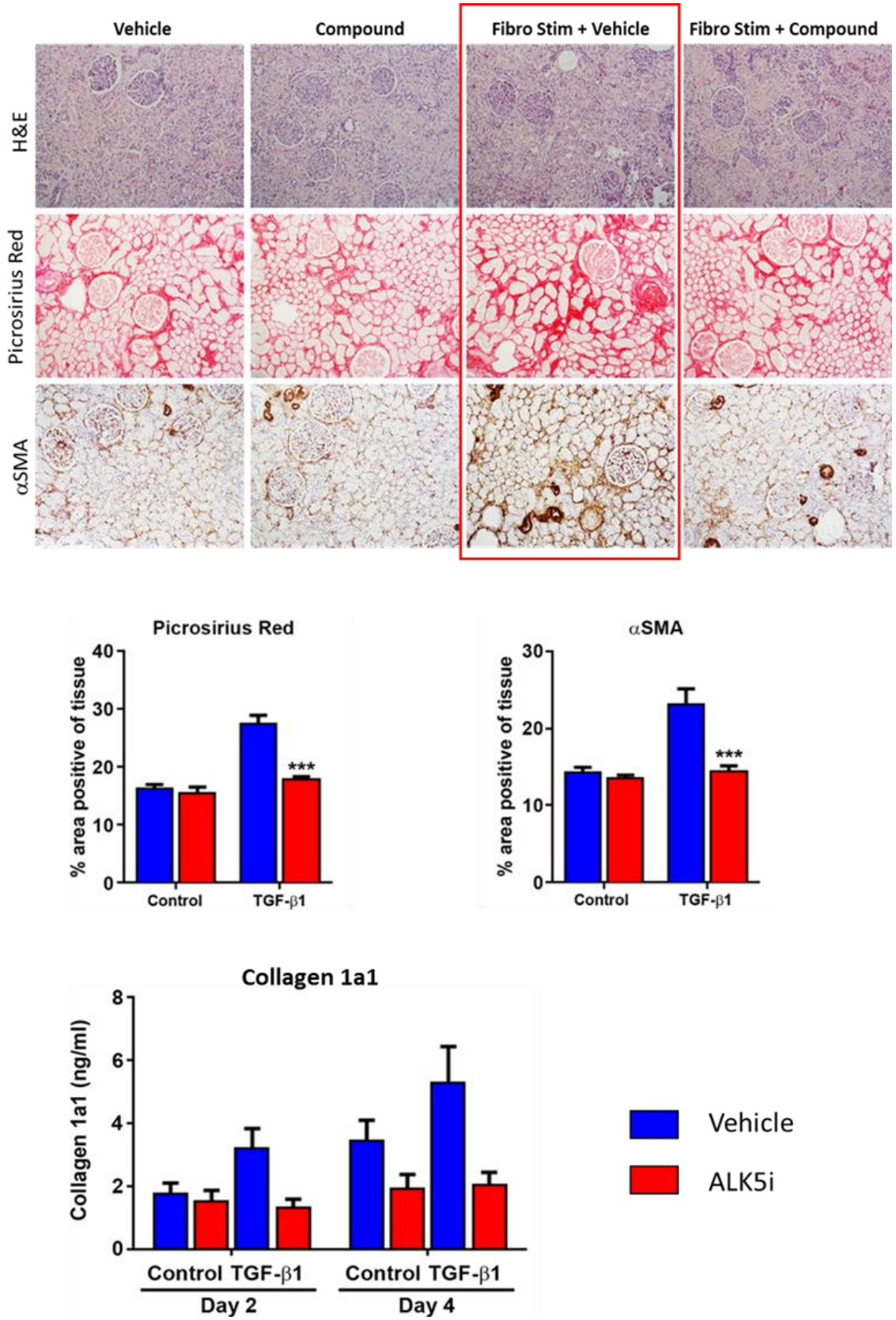

Figure 8. Precision Cut Kidney Slices induction and attenuation of fibrogenesis – Published data from our laboratory (Leslie *et al* (245)) showing the induction of fibrosis by TGF-β1 treatment and attenuation with use of ALK5 inhibitor in precision cut kidney slices (PCKS). **A)** Representative images of Haematoxylin & Eosin, Picrosirius Red and αSMA immunohistochemistry of slices treated ± TGF-β1 and ALK5 inhibitor. **B-C)** quantified results of Picrosirius Red and αSMA staining **D)** Secretion of soluble Collagen 1a1 quantified *via* ELISA.

4.2 Rationale, Hypothesis and Objectives

4.2.1 Rationale

Currently research methods for the study of cardiac fibrosis centre around the use of either animal models or 2D cell and organoid cultures. Whilst these techniques have been instrumental in investigating and providing an understanding of the processes which drive cardiac fibrosis they are unable to accurately recapitulate the cellular compositions and interactions present within the whole human heart. In recent years there has been an ever expanding field of research which utilises intact human tissue from organs to create precision cut tissue slices. These tissue slices retain the cellular composition present in the tissue at the time of processing.

4.2.2 Hypothesis

We hypothesise that the use of our novel bioreactor system will improve the functionality and viability of PCHS compared to current culture methods. We suggest that the application of known pro-inflammatory and fibrotic recombinant proteins will drive inflammation and fibrosis in PCHS. Finally, we propose the inflammatory and fibrotic phenotypes induced within the PCHS system can be modulated through the application of know anti-inflammatory and anti-fibrotic compounds.

4.2.3 Objectives

1) Investigate the feasibility of producing human Precision Cut Heart slices from left ventricular tissue.
2) Explore different culture conditions, including the use of our novel bioreactor, and test different tissue culture medium in order to improve the long-term viability of PCHS.
3) Challenge PCHS with recombinant proteins to model inflammation (IL-1α, IL-1β or LPS) and fibrosis (TGF-β1).
4) Modulate inflammation and fibrotic responses in PCHS through the application of known anti-inflammatory or anti-fibrotic compounds.

4.3 Materials and methods

4.3.1 Patient Demographics

This project received approval is detailed in **Chapter 3**. Briefly approval was granted by the Newcastle Transplant Tissue Biobank and informed written consent was obtained from all patients prior to their involvement in the study. Tissue was collected at the Freeman Hospital, Newcastle upon Tyne from patients who underwent either Left Ventricular Assistance Device (LVAD) implantation or explanted heart tissue from heart transplantation surgery. Whole hearts which had been declined for transplant were also accessed through the Newcastle transplant tissue biobank. Collection of hearts was facilitated through RINTAG or QUOD.

4.3.2 Generation of PCHS and optimisation of long-term culture conditions

Human PCHS were generated as described in **Chapter 3**. For initial experiments PCHS were cultured on 8µm transwell inserts in either specialised 12 well BioReactor plates with an interconnected paired well or standard 24 well cell culture plates. The BioReactor plates were cultured on the bioreactor rocking platform (EU16787549.1, US15770106, and IN201827011946), and will be referred to as 'rocked plates'. For comparison PCHS were cultured in either 500µl medium in 24 well static plates or in 3ml medium per paired well in the 12 well rocked BioReactor plates. The culture medium tested were Smooth Muscle Cell Media 2 (PromoCell C-22066), Endothelial Cell Media MV (PromoCell C-22020), Endothelial Cell Media MV2 (PromoCell C-22022), Myocyte Media (PromoCell C-22070), Fibroblast Media 3 (PromoCell C-23025). All medium were supplemented with their relevant supplement packs **(see Table 5)**, Penicillin (100IU/ml) - Streptomycin (100µg/ml) and 2% glutamine pyruvate. PCHS were incubated at 37°C supplemented with 5% CO_2 and media refreshed daily.

In-house Code	Product code	Cell Culture Media	Media Supplements	
Media A	C-22062	Smooth Muscle Cell Growth Medium 2	Foetal Calf Serum	0.05ml/ml
			Epidermal Growth Factor	0.5ng/ml
			Basic Fibroblast Growth Factor	2ng/ml
			Insulin	5µg/ml
			Glutamine-Pyruvate	1mM
			Penicillin	100IU/ml
			Streptomycin	100µg/ml
Media B	C-22020	Endothelial Cell Growth Medium MV	Foetal Calf Serum	0.05ml/ml
			Endothelial Cell Growth Supplement	0.004ml/ml
			Epidermal Growth Factor	10ng/ml
			Heparin	90µg/ml
			Hydrocortisone	1µg/ml
			Glutamine-Pyruvate	1mM
			Penicillin	100IU/ml
			Streptomycin	100µg/ml
Media C	C-22022	Endothelial Cell Growth Medium MV 2	Foetal Calf Serum	0.05ml/ml
			Epidermal Growth Factor	5ng/ml
			Basic Fibroblast Growth Factor	10ng/ml
			Insulin-like Growth Factor (Long R3 IGF)	20ng/ml
			Vascular Endothelial Growth Factor 165	0.5ng/ml
			Ascorbic Acid	1µg/ml
			Hydrocortisone	0.2µg/ml
			Glutamine-Pyruvate	1mM
			Penicillin	100IU/ml
			Streptomycin	100µg/ml
Media D	C-22070	Myocyte Growth Medium	Foetal Calf Serum	0.05ml/ml
			Epidermal Growth Factor	0.5ng/ml
			Basic Fibroblast Growth Factor	2ng/ml
			Insulin	5µg/ml
			Glutamine-Pyruvate	1mM
			Penicillin	100IU/ml
			Streptomycin	100µg/ml
Media E	C-23025	Fibroblast Growth Medium 3	Foetal Calf Serum	0.1ml/ml
			Basic Fibroblast Growth Factor	1ng/ml
			Insulin	5µg/ml
			Glutamine-Pyruvate	1mM
			Penicillin	100IU/ml
			Streptomycin	100µg/ml

Table 5. Components of cell culture media used in the optimisation of PCHS culture. Shown above are the different cell culture medium used for the optimisation of PCHS, each medium is shown with the individual supplements specific for that medium, alongside their reference number.

4.3.3 Treatments for PCHS

4.3.3.1 Known pro-fibrotic recombinant protein stimuli and application of inhibitors

To assess the ability to induce fibrogenesis in PCHS, slices were challenged with recombinant human (rh) TGF-β1. PCHS were initially rested for 24 hours in culture media following the slicing process. Once the rest period was over PCHS were challenged with rhTGF-β1 (10ng/ml)

or control media for a further 72 hours. Media and treatments were refreshed every 24 hours. Media was collected at 24 hour intervals and slices and media collected at the experiment endpoint, snap frozen and stored at -80°C for future analysis. Inhibitor treatments were applied prophylactically. ALK5 inhibitor SB525334 (10µM), Pirfenidone (2.5mM) and Nintedanib (2.5µM) were reapplied either alone or in combination with rhTGF-β1 (10ng/ml) every 24 hours for a total of 72 hours. Media was collected daily and snap frozen prior to storage at -80°C. Tissue slices were snap frozen at terminal endpoint and stored at -80°C for future analysis.

4.3.3.2 Pro-inflammatory stimuli and their inhibitors

To assess the ability for PCHS to respond to inflammatory stimuli, after a 24 hour rest period slices were challenged for 24 hours with IL-1α, IL-1β (both at 10,000pg/ml, 1000pg/ml or 100pg/ml), LPS (1µg/ml, 0.1µg/ml or 0.01µg/ml) and Poly-IC (100µg/ml, 10µg/ml or 1µg/ml) before media and tissue slices were collected, snap frozen and stored at -80°C. Inhibitor treatments were applied prophylactically to PCHS. IKK VIII inhibitor (10µM), Pirfenidone (2.5mM) and Nintedanib (2.5µM) were applied for 24 hours in combination with IL-1α (1ng/ml) or LPS (1µg/ml). At the end of the treatment period media and slices were collected, snap frozen and stored at -80°C for future analysis.

4.3.3.3 Pro-inflammatory stimuli and their inhibitors

To assess the ability for PCHS to respond to inflammatory stimuli, after a 24 hour rest period slices were challenged for 24 hours with IL-1α, IL-1β (both at 10,000pg/ml, 1000pg/ml or 100pg/ml), LPS (1µg/ml, 0.1µg/ml or 0.01µg/ml) and Poly-IC (100µg/ml, 10µg/ml or 1µg/ml) before media and tissue slices were collected, snap frozen and stored at -80°C. Inhibitor treatments were applied prophylactically to PCHS. IKK VIII inhibitor (10µM), Pirfenidone (2.5mM) and Nintedanib (2.5µM) were applied for 24 hours in combination with IL-1α (1ng/ml) or LPS (1µg/ml). At the end of the treatment period media and slices were collected, snap frozen and stored at -80°C for future analysis.

4.3.4 Enzyme Linked Immunosorbent Assay

To assess the response of PCHS to inflammatory and fibrogenic stimuli, ELISA was performed of tissue culture supernatants as described in **Chapter 3**. Sandwich ELISA was performed using

R&D DuoSet kits for the following markers; collagen 1a1, TIMP-1, MCP-1, IL-6, IL-8, CTGF and IL-11 as per the manufacturer's instructions.

4.3.5 B-type Natriuretic Peptide Assay

B-type Natriuretic Peptide EIA kit (RAB0386, Sigma) was performed following manufacturer's instructions on media samples collected from tissue slices every 24 hours for six days of culture. Briefly, anti-BNP antibody was added to all wells of the 96 well plate and incubated at room temperature with rocking for 1.5 hours. During this incubation standards, positive control and samples were prepared. Standards were prepared using Biotinylated BNP peptide at a concentration of 10pg/ml in all standards. The top standard contained 1000pg/ml of BNP whilst the lowest value of the standard contained 0.1pg/ml BNP. After the incubation period the plate was washed 3 times using 1x wash solution buffer prior to addition of standards, samples and positive control. Plate was covered and rocked for 2.5 hours at room temperature. Plate was washed as previously described and prepared HRP-Streptavidin solution was added before the plate was incubated for a further 45 minutes. Plate was washed for the final times prior to addition of TMB One-Step Substrate Reagent to all wells until development of standards and samples was observed. Stop solution was then applied and the plate immediately read at 450nm.

4.3.6 Resazurin

To assess metabolic activity of the PCHS in response to the different culture conditions, resazurin assay was performed on slices as described in **Chapter 3**. Baseline metabolic activity was measured at t=0, with n=2 PCHS for each condition harvested at days 2, 4 and 6 in culture to assess the changes over the culture period.

4.3.7 Statistical Analysis

Statistical analysis was performed on datasets using GraphPad Prism 9.4.1. Results are presented as mean ± standard error of the mean (SEM). Statistical analysis comprised of either paired t-tests, paired t-test with multiple comparisons or ANOVA mixed effects analysis with Dunnett's multiple comparisons. Data were considered statistically significant with a p value ≤ 0.05 *, $p \leq 0.01$ **, $p \leq 0.001$ *** and $p \leq 0.0001$ ****.

4.4 Results

4.4.1 Optimisation of the long-term culture of Precision Cut Heart Slice (PCHS)

4.4.1.1 Characterisation of the different donor tissues

Due to the challenges involved in accessing human left ventricular tissue, PCHS were isolated from donors from wide a range of different disease phenotypes. **Figure 9** shows the t=0 tissue from each of the different disease phenotypes used. Tissue from patients undergoing LVAD implantation had 1 of 3 different pathologies. Picrosirius red enables the visualisation of collagen fibres within the tissue. The tissue from dilated cardiomyopathy patients shows the thickening of collagen fibres around vessels, termed perivascular fibrosis. There is a degree of perivascular fibrosis present in the Ischaemic cardiomyopathy donors, however in addition to this there is also a striking amount of diffuse fibrosis and potentially areas of replacement fibrosis. The Haematoxylin and Eosin staining shows evidence of myocyte disarray and enlarged nuclei in ischaemic cardiomyopathy tissue. In both the perfused and unused donor tissues there is evidence of collagen fibres throughout the tissue, however to a lesser extent to that observed in the LVAD tissue. The age of the donors is likely to be linked to the amount of collagen in the tissue, which NHH021, from an 18 year old donor having very little perivascular or diffuse fibrosis. Whilst there appears to be an increase in the amount of positive collagen staining in donors NHH024 and NHH028, who are aged 67 and 71 years respectively. Haematoxylin and Eosin staining of the unused and perfused donors shows normal alignment and arrangement of myocytes. These images highlight the underlying differences in the tissues accessed during the study.

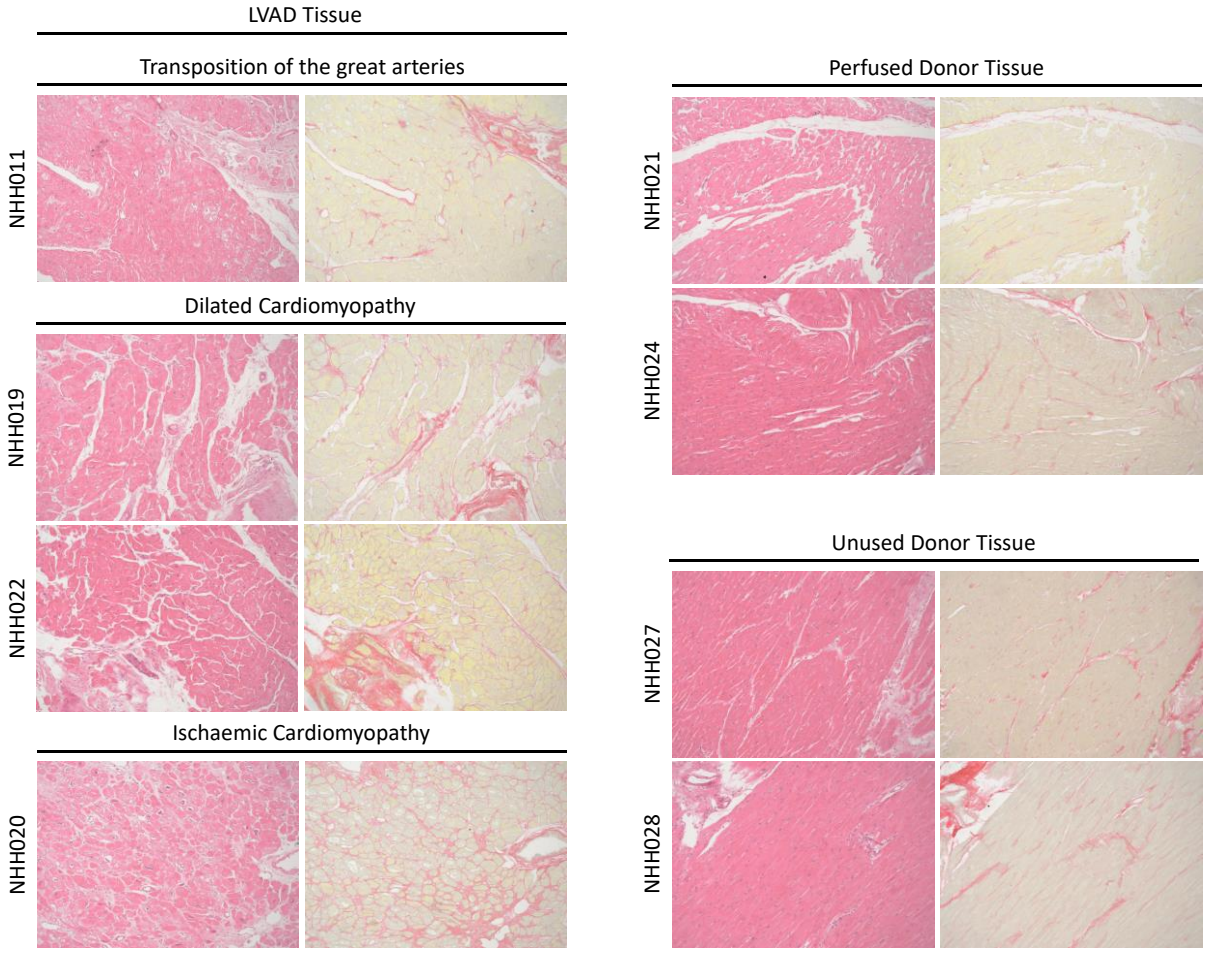

Figure 9. Histological examples of the different tissue sources used to generate PCHS – Representative images of t=0 tissue stained for Haematoxylin & Eosin or Picrosirius Red. LVAD Tissue: NHH011 – Transposition of the great arteries; NHH019 and NHH022 – Dilated Cardiomyopathy; NHH020 – Ischaemic Cardiomyopathy, NHH021 and NHH024 – Perfused Donor Tissue, NHH027 and NHH028 – Unused Donor Tissue. Images taken at magnification 100x.

4.4.1.2 Architecture of heart tissue was maintained in PCHS after the slicing process

The first step in the optimisation of the *ex vivo* precision cut heart slice model was to ensure the integrity of the tissue slices after the initial slicing process. We stained for a number of markers to assess the integrity and structure of the tissue. Representative images **(Figure 10)** show that Connexin-43, a key gap junction present in the heart, important for electrochemical signalling between myocytes and also cardiac fibroblasts and myocytes was still present and in an organised distribution within the tissue. Vimentin identified the presence of cells of mesenchymal origin such as fibroblasts in the tissue. The use of α-SMA, a marker of activated myofibroblasts, showed very few fibroblasts activated in the tissue. Immunohistochemistry also showed the presence of a number of immune cells present within the tissue, as shown by positive CD68 (marker of monocytes and macrophages). The endothelial cell marker CD31 marked the presence of vessels.

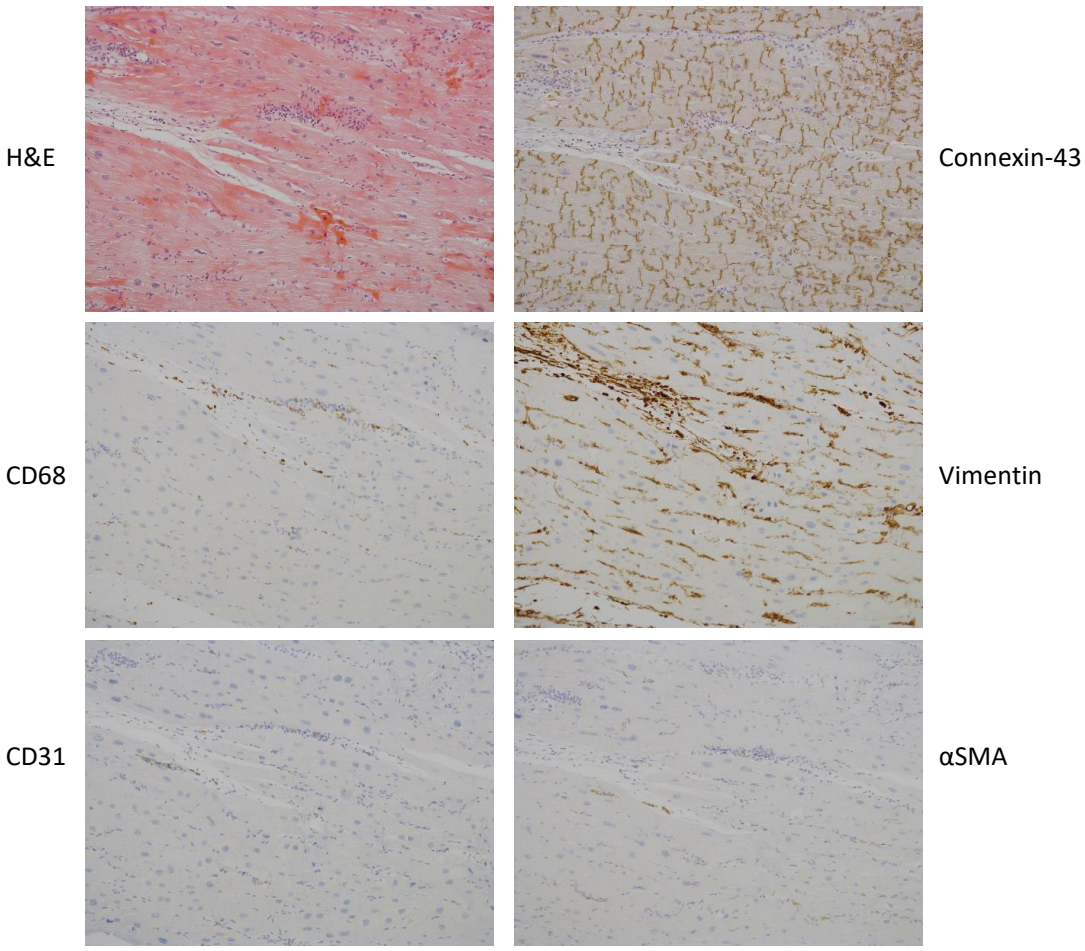

Figure 10. Maintenance of tissue architecture post-slicing - Representative images of PCHS at t=0, tissue stained for haematoxylin & eosin, Connexin-43, CD68, Vimentin, CD31 and αSMA. Magnification 400x.

4.4.2 Bioreactor rocking culture maintains the viability of PCHS compared to static culture

In order to assess the viability of the tissue slices in culture we employed a wide range of outputs measuring soluble markers of cellular death, function and metabolic activity. Experiments were performed using five different media types **(Table 5)**. Over a 6 day culture period secretion of B-type Natriuretic Peptide (BNP) and Collagen 1a1 from the slices was quantified along with the metabolic activity of the tissue, assessed by resazurin assay **(Figure 11)**.

Resazurin is a blue dye which is readily and irreversibly reduced via mitochondrial reductase by viable cells to form the highly fluorescent pink dye resorufin. The greater the number of viable cells the higher the fluorescent signal measured. An important first step in the optimisation of the PCHS model was to ascertain whether the tissue required rocking in our bioreactor system or whether they are viable in static culture. Metabolic activity was instrumental in deciding the most appropriate culture conditions **(Figure 11)**. The metabolic activity of PCHS was measured within an hour slicing this acted as our baseline activity for the PCHS in the different media types. Slices (n=4 per timepoint) were then harvested at 48 hours, 96 hours and 144 hours post-slicing enabling the tracking of the metabolic activity over 6 days of culture.

Media A best maintained the viability of PCHS using rocking culture compared to all other media types and culture conditions over the entirety of the culture period. Culture Media E had fairly similar levels and profiles of metabolic activity between static and rocked plates, whilst Media B appeared to maintain viability in the rocked culture. On the other hand, Media C and D both showed reduced activity in the static and rocked culture conditions compared to the other media types, suggesting that both these media types would be unsuitable for the long term culture of PCHS. Results from these media types were excluded from the other analyses. These results indicate that based on the metabolic activity of the slices, Media A and rocked culture provide the most suitable conditions for long-term PCHS culture.

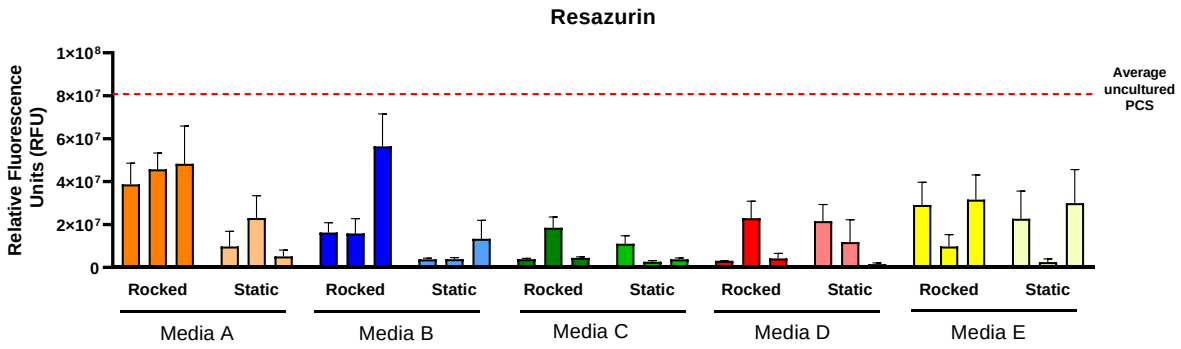

Figure 11. Metabolic activity is a key measure for the viability of PCHS – Metabolic activity of precision cut heart slices cultured in either 12 well rocked plates or 24 well static plates and in 5 different culture media was quantified using Resazurin Assay. Results are shown as relative fluorescence units (RFU). Resazurin assay was performed at 48hrs, 96hrs and 144hrs. Dashed red line denotes average RFU of uncultured PCHS measured at t=0. Data are mean ± SEM from one donor with n=4 slices used at every timepoint per condition.

Next, in order to assess the health of the cardiac myocytes within the PCHS we measured the levels of B-type Natriuretic Peptide (BNP) secreted into the culture media over the 6 day culture period. BNP is secreted by ventricular myocytes and elevated levels have been previously described as a potential biomarker for heart failure in the clinic(246). **Figure 12A** showed that Media B produced hugely elevated levels of BNP secretion, especially from the static cultured slices, compared to all the other media types and culture conditions. Levels of BNP in the media from PCHS cultured statically in Media B were over 10-fold higher than that of the next highest static cultured slices. Due to the high levels of BNP measured from Media B cultured slices the differences between the other media tested was unable to be ascertained. **Figure 11B** depicts the results from the BNP assay when Media B has been excluded. Overall within the different media types there was not much variation between BNP levels in static or rocked culture. These data suggest that Media B, both static and rocked would be an unsuitable media to use for the long-term culture of PCHS, it was therefore excluded from further analysis.

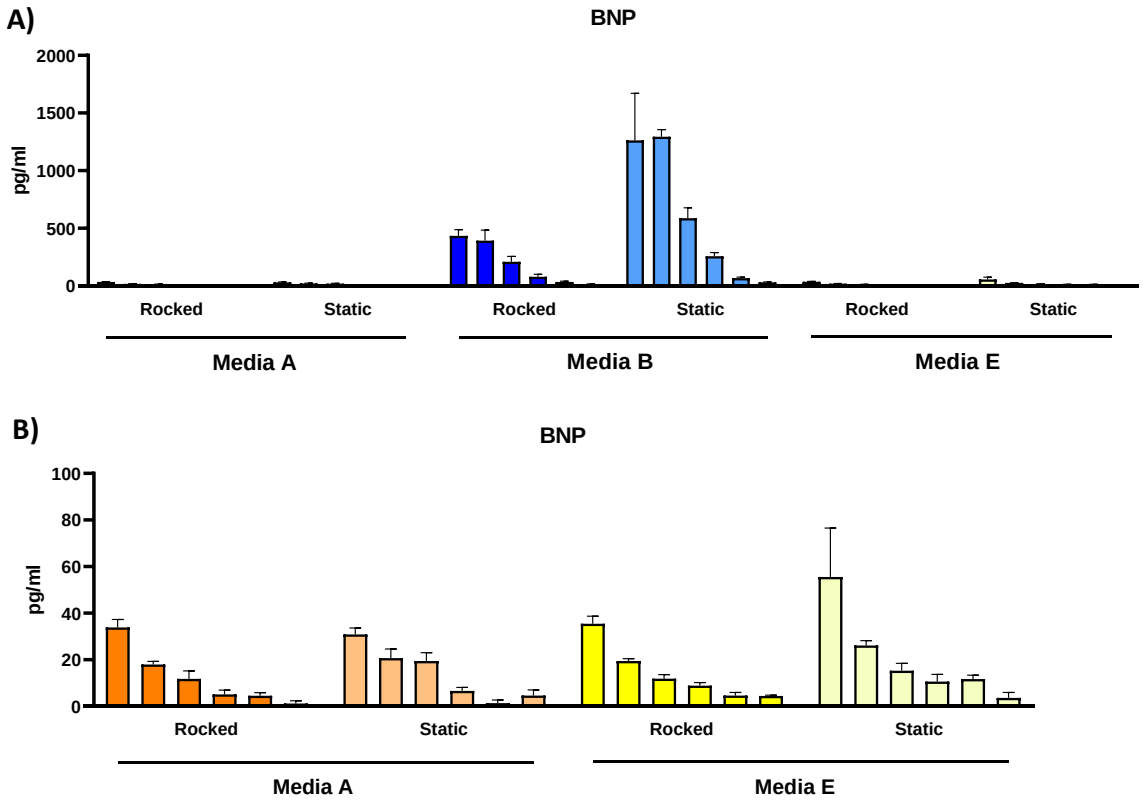

Figure 12. Media B is unsuitable for the long-term culture of PCHS – Graphs show B-type Natriuretic Peptide (BNP) secretion from PCHS cultured in either 12 well rocked plates or 24 well static plates and in 3 different culture media **(A)**, Media B was excluded from **(B)** in order to visualize BNP levels from the other media types. Culture media was harvested at 24hrs, 48hrs, 72hrs, 96hrs, 120hrs and 144hrs and quantified using BNP Enzyme Immunoassay (EIA) kit. Data are mean ± SEM from one donor with n=4 slices used at every timepoint per condition.

Finally, we measured Collagen 1a1 protein secretion into the tissue culture media in the form of ELISA to assess basal levels of function. In previous experiments in our laboratory, Collagen1a1 secretion has been shown to be a good indicator of tissue function within the slice culture system. Collagen 1a1 secretion for Media A static culture showed extremely low levels of secretion **(Figure 13)**. Media E showed more erratic levels of secretion, with the static culture having the highest levels and biggest increases over the six days. The erratic nature of the secretion indicates increased stress and death between the individual slices. PCHS cultured in Media A and rocked culture had a steady increase of Collagen 1a1 levels over the 6 days.

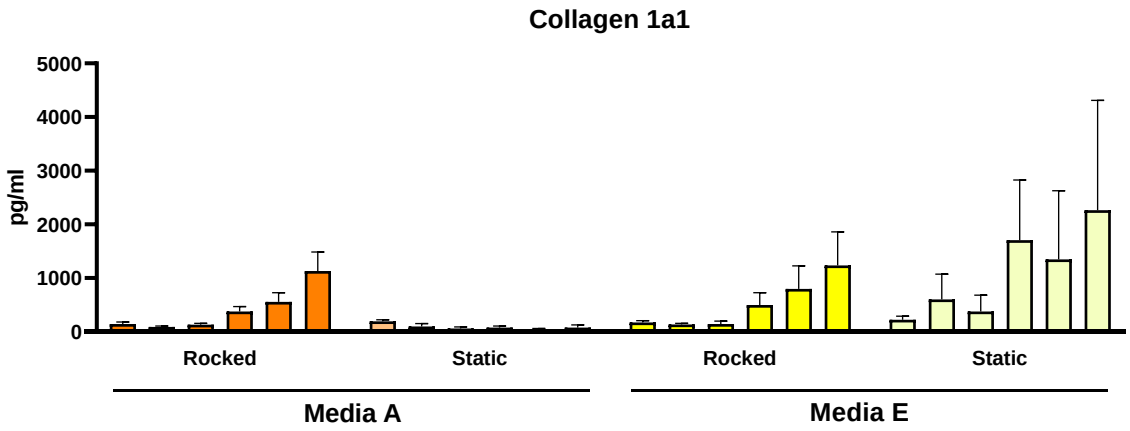

Figure 13. PCHS cultured in 24 well static plates are unsuitable for long-term culture – Graph depicts Collagen 1a1 secretion from PCHS cultured in either 12 well rocked plates or 24 well static plates. Culture media was harvested at 24hrs, 48hrs, 72hrs, 96hrs, 120hrs and 144hrs and quantified using DuoSet ELISA. Data are mean ± SEM from one donor with n=4 slices used at every timepoint per condition.

The results across these different assays confirmed that the optimal culture conditions for PCHS is using our rocked bioreactor system. This was particularly evident when assessing the differences in metabolic activity of PCHS in the different systems and BNP secretion which was elevated in all media types when compared to the rocked matched media type.

4.4.2.1 Different media types resulted in differences between soluble viability readouts

In order to confirm that Media A is the most suitable for the long-term culture of PCHS we assessed Medias A, C, D and E on a further 3 donors by resazurin assay **(Figure 14)**. Media A had increased metabolic activity compared to the other media types with the elevated activity maintained over the six days in culture. Media D saw a drop off in activity by day 6, as well as being reduced compared to both Media A at all times points and when compared to the basal activity at t=0. Whilst Media C and E both showed more stable activity over the time course their metabolic activity was around 40-50% lower when compared to Media A. The activity of the slices was compared to baseline activity of an uncultured PCHS taken at t=0.

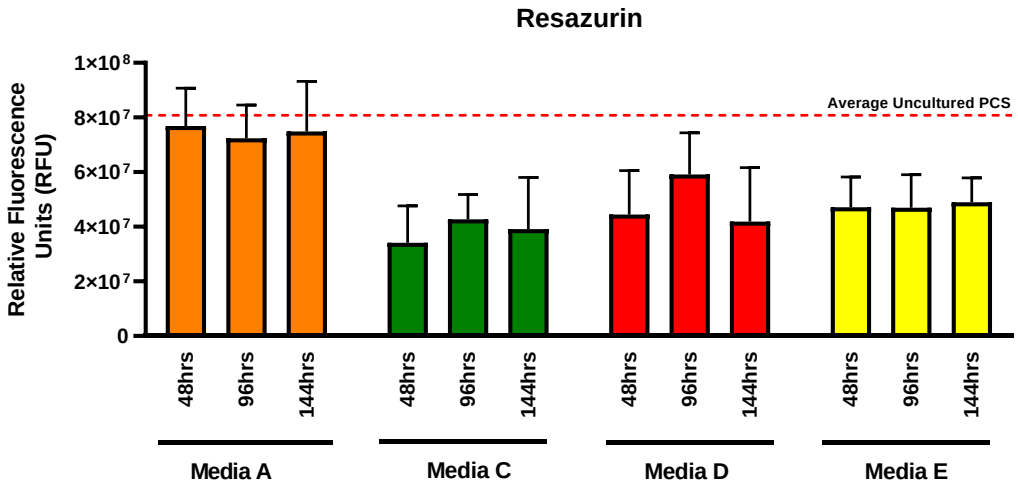

Figure 14. PCHS cultured in Media A continue to be metabolically active after 144hrs in culture – Graph depicts metabolic activity from PCHS cultured in 4 different culture media types. Results are shown as relative fluorescence units (RFU). Resazurin assay was performed using n=4 donors at 48hrs, 96hrs and 144hrs. Dashed red line denotes average RFU of uncultured PCHS measured at t=0. Data are mean ± SEM.

Media A was deemed the best media for the long-term culture of PCHS. **Figure 15** depicts the metabolic activity from four donors with PCHS cultured using Media A. Despite varying levels of activity observed between donors all four donors assessed remained stable between 48 and 96 hours in culture **(Figure 15A)**. One donor did have a slight reduction in metabolic activity by the 144 hour timepoint. Therefore to ensure the viability of the PCHS remains high and to create the optimal conditions for the extended culture of PCHS we limited the culture period to 96 hours in future experiments. **Figure 15B** depicts the increased viability of the PCHS cultured using the 12 well rocked culture conditions versus static, further confirming our earlier findings that this provides the optimal culture conditions for PCHS.

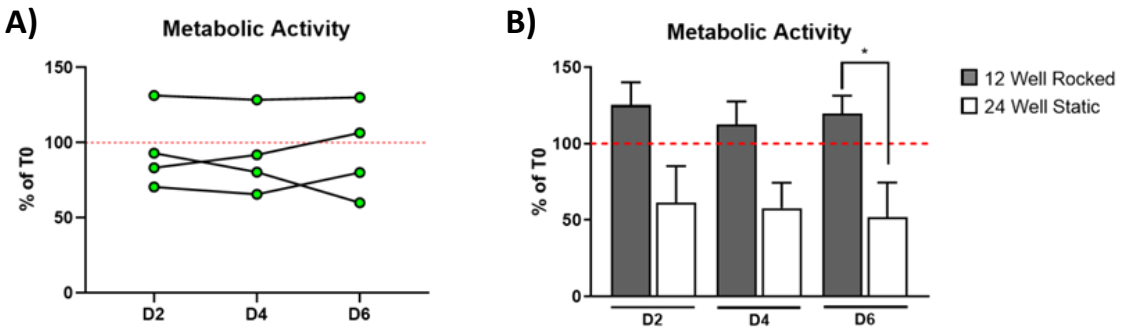

Figure 15. Rocked culture improves PCHS viability – Graphs depict metabolic activity assessed by resazurin assay over 6 days in culture. Data is presented as a % of T=0 with T=0 marked by red dashed line at 100%. Data are mean ± SEM from n=4 donors. p values were calculated using paired student t-tests. Data were considered statistically significant with a p value ≤0.05 *.

4.5 Using the PCHS system to model disease

4.5.1 Induction of an inflammatory profile in PCHS

Unresolved inflammatory responses are known to be involved in the initiation of fibrosis. In order to investigate whether PCHS could be used to investigate inflammatory responses in the human heart we developed an acute model whereby PCHS were challenged for 24 hours with recombinant proteins known to initiate acute inflammation *in vivo*. The recombinant proteins used mimic a wide range of cellular actions involved in the acute inflammatory response. Interleukin-1α (IL-1α) is secreted from damaged cells and act as an alarmin or damage-associated molecular pattern (DAMP) with the ability to bind to its IL-1R1 on numerous cell types(112). IL-1β is produced in response to microbial products in its inactive pro-IL-1β form requiring cleavage by caspase-1 for its activation(112). Lipopolysaccharides (LPS) are a major component of bacterial cell walls and is used *in vitro* to mimic responses to bacterial infection and has been shown to be involved in sepsis induced cardiomyopathies(247,248). Poly-IC is a synthetic double-stranded RNA which mimics the ds-RNA present in some viruses. It is able to induce the response of cells to a viral infection *in vitro* through recognition by Toll-like Receptor 3 (TLR3)(248,249).

Prior to treatment, PCHS were rested for 24 hours after the slicing process to allow the tissue to recover. Media was then removed and replenished with media containing different recombinant proteins. **Figure 16** shows the dose dependant response to IL-1α (10000pg/ml, 1000pg/ml, 100pg/ml), IL-1β (10000pg/ml, 1000pg/ml, 100pg/ml), LPS (1μg/ml, 0.1μg/ml, 0.01μg/ml) and Poly IC (100μg/ml, 10μg/ml, 1μg/ml) treatment. PCHS stimulated with the highest doses of IL-1α and IL-1β strongly induced the secretion of IL-6 and IL-8. This response was also dose dependant with a stepwise increase in levels of IL-6 and IL-8 secretion with increasing concentrations of IL-1α and IL-1β. In response to LPS stimulation, IL-6 and IL-8 were elevated slightly, however the increasing treatment dose had little to no effect on the magnitude of IL-6 or IL-8 secretion. Finally, Poly-IC treatment resulted in a modest dose dependent induction of IL-6 and IL-8 secretion.

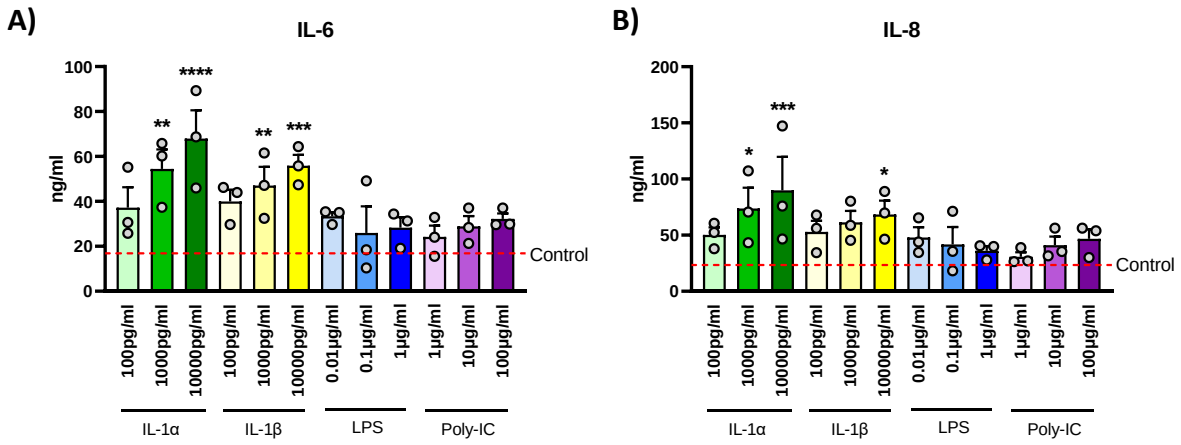

Figure 16. IL-1α and IL-1β treatment can induce an inflammatory phenotype in PCHS – (A) IL-6 and **(B)** IL-8 secretion after acute 24hr challenge with IL-1α (100pg/ml, 1000pg/ml or 10,000pg/ml), IL-1β (100pg/ml, 1000pg/ml or 10,000pg/ml), LPS (0.01µg/ml, 0.1µg/ml or 1µg/ml) and Poly-IC (1µg/ml, 10µg/ml or 100µg/ml). N=3 donors. Data are mean ± SEM. p values were calculated using ANOVA mixed effects analysis with Dunnett's multiple comparisons. Data were considered statistically significant with a p value ≤0.05 *, p≤0.01 **, p≤0.001 *** and p≤0.0001 ****.

We next proceeded to investigate more broadly the inflammatory profile from PCHS in response to IL-1α or LPS challenge only. PCHS were initially rested for 24 hours after slicing prior to treatment for 24 hours with control media, IL-1α (1000pg/ml) or LPS (1µg/ml). Supernatants were collected after the treatment period and secretion of the pro-inflammatory markers IL-6, IL-8, MCP-1, GM-CSF, Eotaxin and GRO-α quantified via multi-plex ELISA (MesoScale Discovery™) **(Figure 17)**. The induction of secretion from the slices across all markers was dramatic after either IL-1α or LPS treatment. IL-6 and IL-8 secretion was induced 20-fold and 16-fold by IL-1α, whilst GM-CSF and GRO-α saw the greatest inductions of 31-fold and 32-fold respectively. Interestingly the LPS induced-inflammatory response is lower in magnitude compared to the response to IL-1α stimulation for all markers measured except TNF-α. Despite this LPS challenge still resulted in elevated secretion of all the markers.

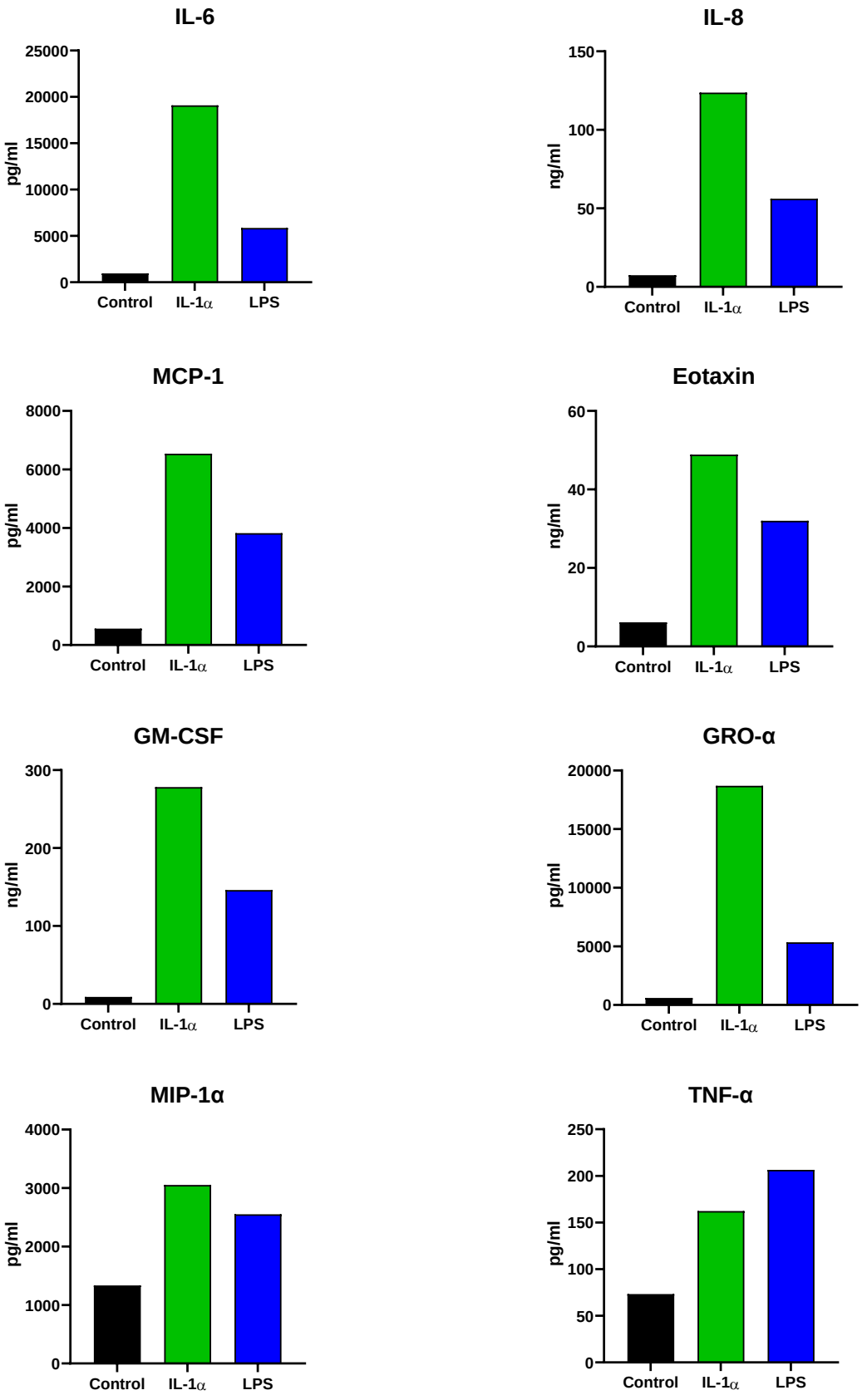

Figure 17. IL-1α and LPS treatment can induce an inflammatory phenotype in PCHS – Quantification of secreted inflammatory chemokines and growth factors from PCHS harvested after acute 24hr challenge with IL-1α (1ng/ml) or LPS (1µg/ml). Data is presented as mean from n=1 donor.

4.5.2 Modulation of inflammatory response through the application of therapeutics

Having demonstrated the ability to induce an acute pro-inflammatory response in the PCHS, the next step was to attempt to attenuate this response. PCHS were treated with control media, IL-1α (1000pg/ml) or LPS (1µg/ml) alone or in combination with Pirfenidone (2.5mM), Nintedanib (2.5µM) or IKK-2 inhibitor VIII (10µM) for 24 hours **(Figures 18 and 19)**. Pirfenidone and Nintedanib are approved anti-fibrotic therapies for the treatment of Idiopathic Pulmonary Fibrosis (IPF). Pirfenidone has already shown some efficacy in animal models of cardiac fibrosis(250). Recently the results of a Phase 2 clinical trial investigating the effects of Pirfenidone treatment in heart failure patients with preserved ejection fraction (HFpEF) have been published(157). Nintedanib is a tyrosine kinase inhibitor which targets a number of growth factors, including FGF/FGFR, PDGF-α/β and VEGF/VEGRF(251). They are currently the only clinically approved therapies for the treatment of a fibrotic disease. These therapies were compared to the small molecule inhibitor IKK-2 inhibitor VIII which is well documented to have strong anti-inflammatory effects *in vitro*(252,253). We applied these drugs to PCHS in order to ascertain whether an effect would also be observed in heart tissue. After the acute 24 hour treatment, media was collected and MSD assay performed on the supernatants **(Figure 18)**. The data shows that the IKK-2 inhibitor VIII was able to strongly block the IL-1α induced secretion of all the pro-inflammatory markers measured. Pirfenidone was as effective as IKK-2 inhibitor VIII, blocking IL-6, IL-8, MCP-1 and GRO-α secretion by nearly 50%. Interestingly Nintedanib showed no attenuating effect on IL-1α induced inflammatory responses on PCHS.

We next investigated the ability of Nintedanib, Pirfenidone and IKK-2 inhibitor VIII to block the inflammatory response upon stimulation with LPS **(Figure 19)**. Unlike IL-1α, LPS was less potent in its ability to induce the secretion of pro-inflammatory markers again Nintedanib had little to no anti-inflammatory effect on inflammation. IKK-2 inhibitor VIII successfully attenuated secretion of MCP-1, GM-CSF and GRO-α, with MCP-1 and GRO-α levels returned to that of the control treated slices. It had less of an effect on preventing the secretion of Eotaxin, whilst reducing the levels of IL-6 and IL-8 secretion by around a third. Pirfenidone was able to reduce GM-CSF, IL-8 and to a lesser extent IL-6 secretion in response to LPS treatment. However it had little to no effect on Eotaxin and GRO-α secretion. These data have shown that along with being able to induce an acute pro-inflammatory response in our PCHS system we are able to modulate it through the use of known anti-inflammatory compounds Pirfenidone and IKK-2 inhibitor VIII.

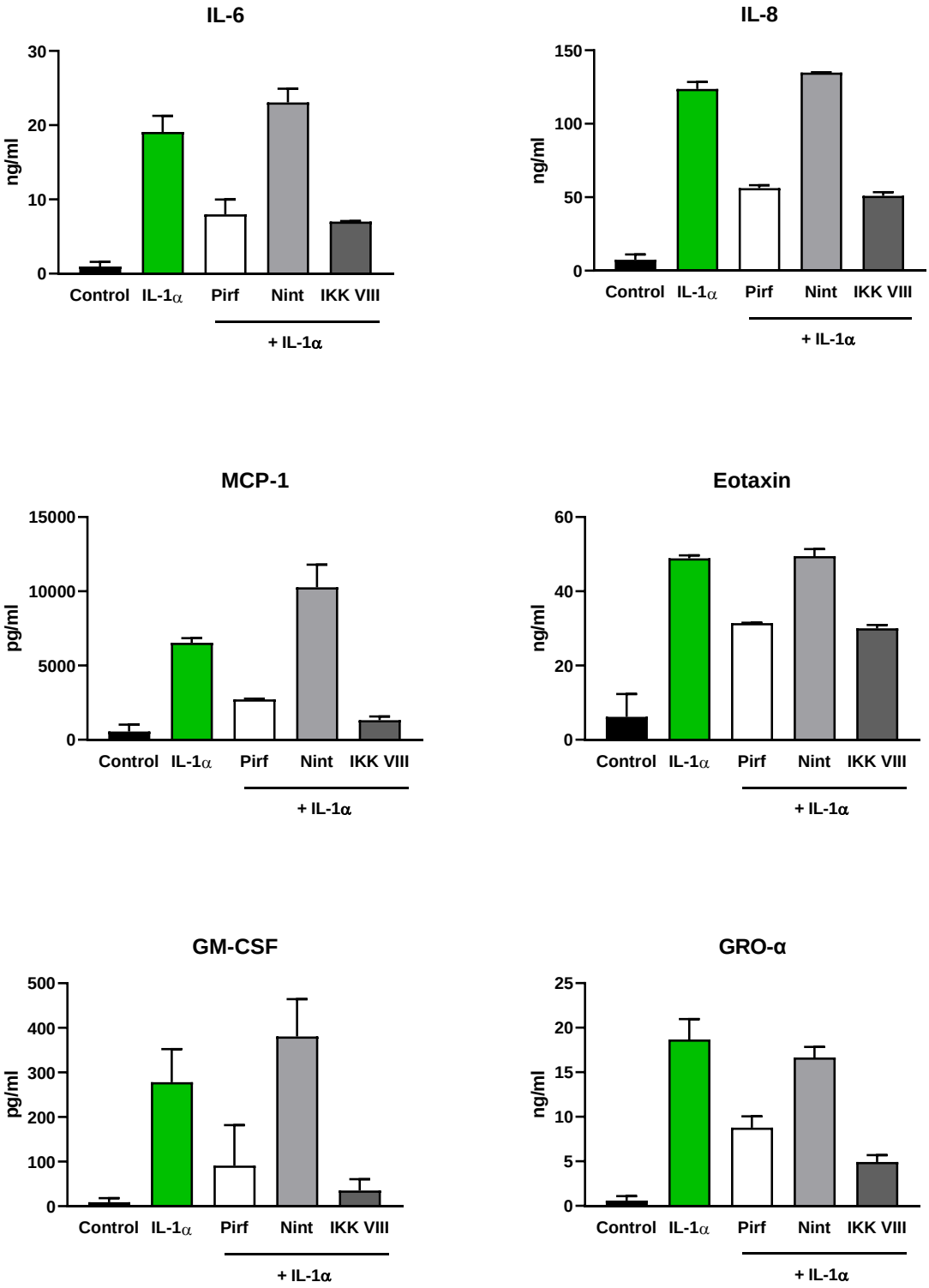

Figure 18. IL-1α induced inflammatory phenotype can be modulated through the application of therapeutics - After a 24 hour rest period PCHS were treated with either control media, IL-1α (1000pg/ml) alone or in combination with Pirfenidone (2.5mM), Nintedanib (2.5μM) or IKK-2 inhibitor VIII (10μM) for 24 hours. Culture media was harvested and inflammatory response quantified using multi-plex ELISA (MSD). Data is mean ± SEM from n=2 media samples from n=1 donor.

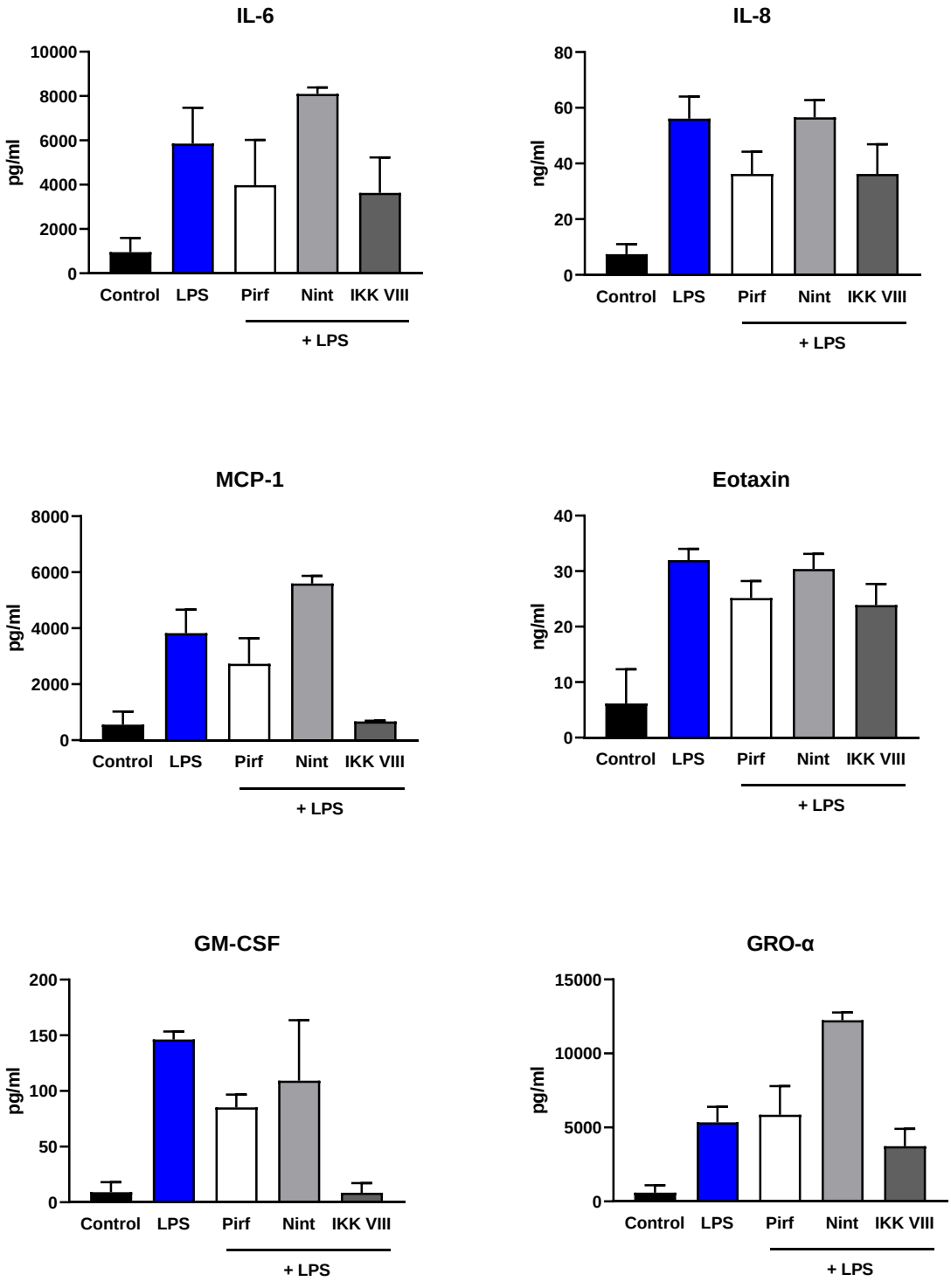

Figure 19. LPS induced inflammatory phenotype can be modulated through the application of therapeutics - After a 24 hour rest period PCHS were treated with either control media, LPS (1µg/ml) alone or in combination with Pirfenidone (2.5mM), Nintedanib (2.5µM) or IKK-2 inhibitor VIII (10µM) for 24 hours. Culture media was harvested and inflammatory response quantified using multi-plex ELISA (MSD). Data is mean ± SEM from n=2 media samples from n=1 donor.

4.5.3 Induction of a pro-fibrotic response in PCHS after TGF-β1 treatment

The TGF-β signalling pathway is arguably one of the most important in the development of fibrosis in the heart, therefore the next step in the development of the PCHS culture system was to attempt to induce a pro-fibrogenic response in slices via treatment with TGF-β1 (10ng/ml). To achieve this tissue from n=7 donors undergoing LVAD surgery were used to produce PCHS. After a 24 hour rest period, PCHS were treated with either control media (unstimulated) or TGF-β1 (10ng/ml) for a further 72 hours. Supernatants from the slices were collected and protein secretion of markers of fibrogenesis and inflammation was assessed using DuoSet ELISA.

Figure 20 shows the effect of TGF-β1 stimulation on the secretion of a number of pro-fibrotic markers in comparison to unstimulated slices over 72 hours of treatment. Collagen 1a1 secretion was significantly induced (>50%) by TGF-β1 stimulation in culture **(Figure 20A)**. Tissue Inhibitor Metalloproteinase Inhibitor-1 (TIMP-1) secretion increased over the 96 hours in culture in both the control and TGF-β1 treated slices **(Figure 20B)**. Whilst TIMP-1 secretion was increased at both 72 and 96 hours it did not reach statistical significance, likely due to interpatient variability. However spontaneous TIMP-1 secretion from PCHS was significantly elevated at both T72 and T96 versus T48 slices. The matricellular protein CTGF, thought to be a modulator of fibrosis, is significantly elevated 3-fold with TGF-β1 stimulation **(Figure 20C)**. Whilst the spontaneous release of CTGF over the 96 hours is less pronounced than that of TIMP-1, it still equates to a 22-fold increase at 96 hours in culture. The final soluble marker of fibrogenesis we measured was IL-11 **(Figure 20D)**. IL-11 has recently been shown in a paper by Schafer *et al* (2017) to play a potentially important role in TGF-β1 induced cardiac fibrosis(254). Results show sustained secretion of IL-11 in response to TGF-β1 treatment at all time points.

These data show that in our PCHS system TGF-β1 can modulate know promoters of fibrosis. We also show that in regard to Collagen 1a1, TIMP-1 and CTGF secretion from unstimulated PCHS increases in a time dependent manner. Both the spontaneous and induced secretion of fibrotic markers allows for the exciting prospect of attenuating these responses using novel therapies and inhibitors in the future.

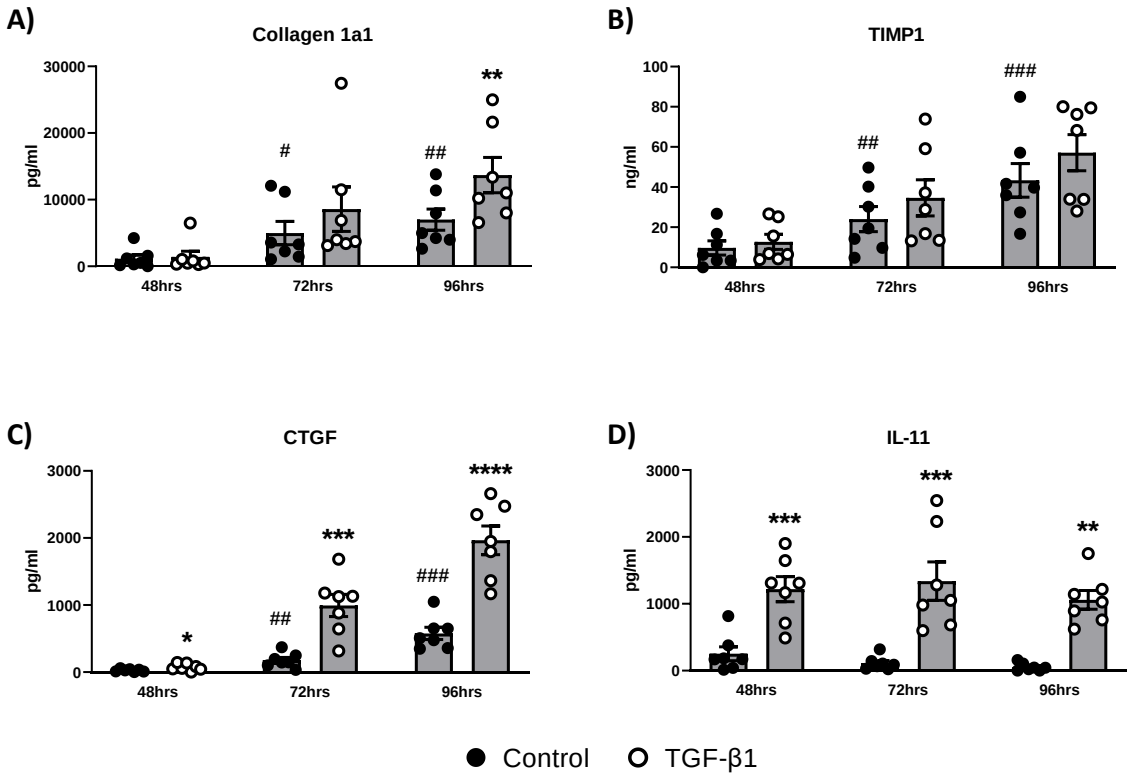

Figure 20. TGF-β1 induces a potent fibrotic phenotype in PCHS from LVAD donors – After a 24 hour rest period, PCHS were treated with either control media (unstimulated) or TGF-β1 (10ng/ml) for a further 72 hours. Media was collected and treatments refreshed daily. Supernatants from the slices were collected and protein secretion of markers of fibrogenesis was measured using DuoSet ELISA. N=7 donors. Data are mean ± SEM. Statistical analysis comprised of paired t-tests. * or # p<0.05, ** or ## p<0.01, *** or ### p<0.001, ****p<0.0001.

Whilst mostly being associated with causing the release of pro-fibrogenic molecules involved in the deposition of excess ECM, TGF-β1 binding to fibroblasts has also been shown to effect the secretion of a number of pro-inflammatory cytokines, therefore we measured the secretion of IL-6, IL-8 and MCP-1 in response to TGF-β1 treatment **(Figure 21A-C)**. IL-8 secretion was not able to be induced by TGF-β1 treatment. Results show that IL-6 secretion is inducible by TGF-β1 stimulation. Monocyte chemoattractant protein 1 (MCP-1) is one of the better studied chemokines involved in cardiac fibrosis. MCP-1 is involved in the recruitment of monocytes to areas of damage. MCP-1 may also have a direct effect on cardiac fibroblasts, inducing fibroblast proliferation and differentiation to myofibroblasts. Results showed no induction of MCP-1 secretion in TGF-β1 stimulated PCHS **(Figure 21C)**. Levels of MCP-1 remained stable over the 96 hours in culture in both the TGF-β1 and control slices.

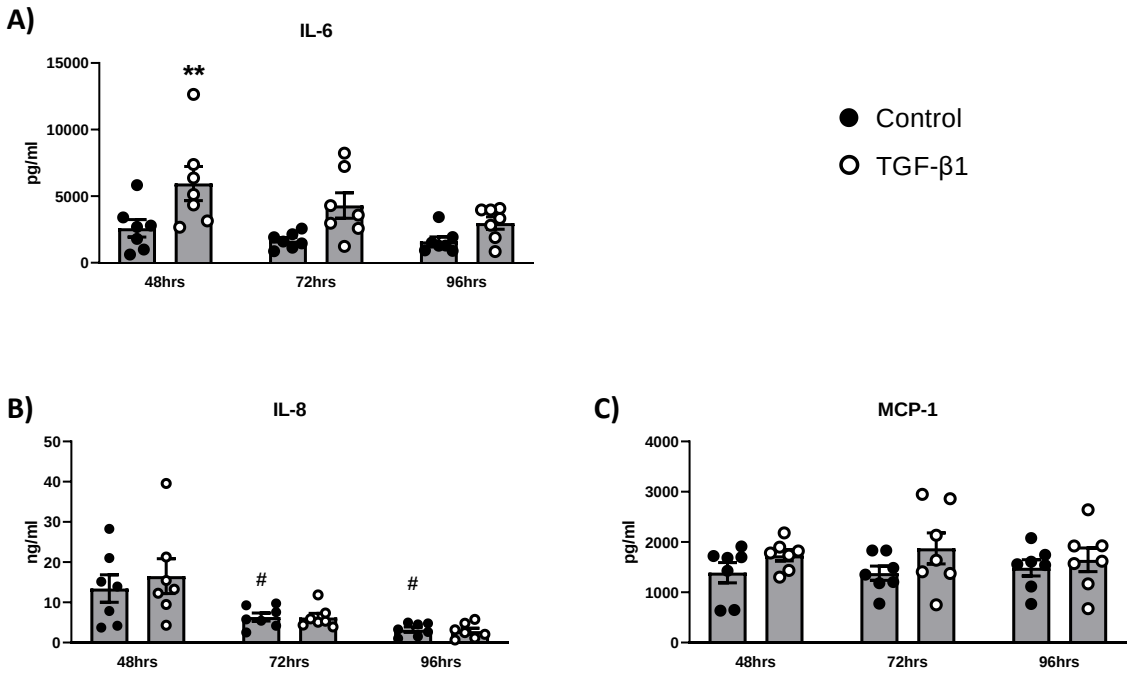

Figure 21. TGF-β1 induces IL-6 but not IL-8 or MCP-1 secretion in PCHS from LVAD donors – After a 24 hour rest period, PCHS were treated with either control media (unstimulated) or TGF-β1 (10ng/ml) for a further 72 hours. Media was collected and treatments refreshed daily. Supernatants from the slices were collected and protein secretion of markers of fibrogenesis was measured using DuoSet ELISA. N=7 donors. Data are mean ± SEM. Statistical analysis comprised of paired t-tests. #p<0.05, **p<0.01.

In order to investigate further whether the disease state of the tissue could affect the ability to induce TGF-β1 driven fibrosis we compared the response of PCHS prepared from 6 unused donor hearts **(Figures 22-23)**. As with the slices from LVAD donors, tissue was rested for 24 hours prior to three challenges with TGF-β1 over the subsequent 72 hours. **Figure 22** shows that TGF-β1 was able to significantly induce Collagen 1a1, TIMP-1, CTGF and IL-11 secretion by 96 hours in culture. Unlike LVAD PCHS, slices from unused donors were able to significantly induce TIMP-1 secretion by 96 hours in response to TGF-β1, resulting in a 1.8-fold increase **(Figure 22B)**. Untreated control PCHS were able to secrete collagen 1a1, TIMP-1 and CTGF without TGF-β1 stimulation. Levels of IL-11 measured in the media from unstimulated control PCHS significantly reduced over the 96 hour culture period when compared to 48 hour untreated slices **(Figure 22D)**.

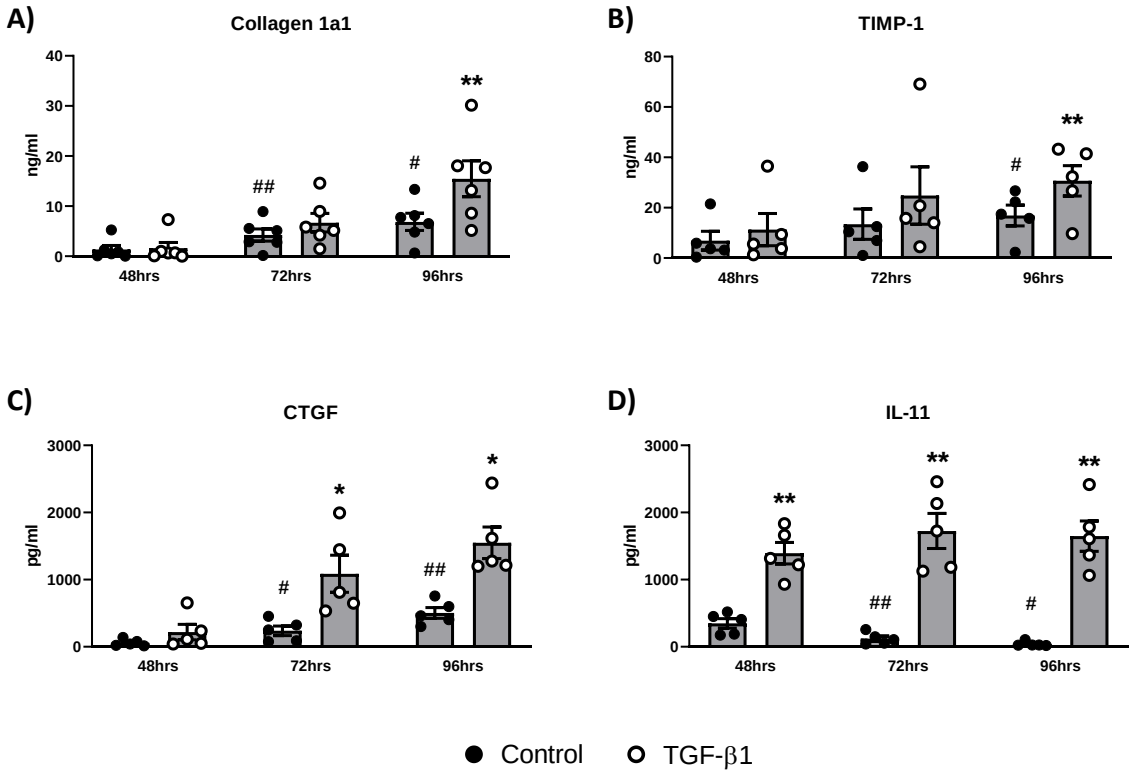

Figure 22. TGF-β1 induces a potent fibrotic phenotype in PCHS from unused donors – After a 24 hour rest period, PCHS were treated with either control media (unstimulated) or TGF-β1 (10ng/ml) for a further 72 hours. Media was collected and treatments refreshed daily. Supernatants from the slices were collected and protein secretion of markers of fibrogenesis was measured using DuoSet ELISA. N=6 donors for Collagen, N=5 for other markers. Data are mean ± SEM. Statistical analysis comprised of paired t-tests. * or # p<0.05, ** or ## p<0.01.

Finally we assessed the secretion of markers of inflammation from TGF-β1 challenged unused donor PCHS. Whilst the amount of IL-6 secreted from unstimulated control PCHS reduced over the culture period, at both 72 and 96 hours TGF-β1 treatment resulted in significantly increased IL-6 secretion **(Figure 23A)**. There was no effect of TGF-β1 challenge on IL-8 secretion, whereas MCP-1 secretion was modestly induced after 72 and 96 hours **(Figure 23B-C)**. Spontaneous MCP-1 secretion was significantly reduced over the 96 hours in culture.

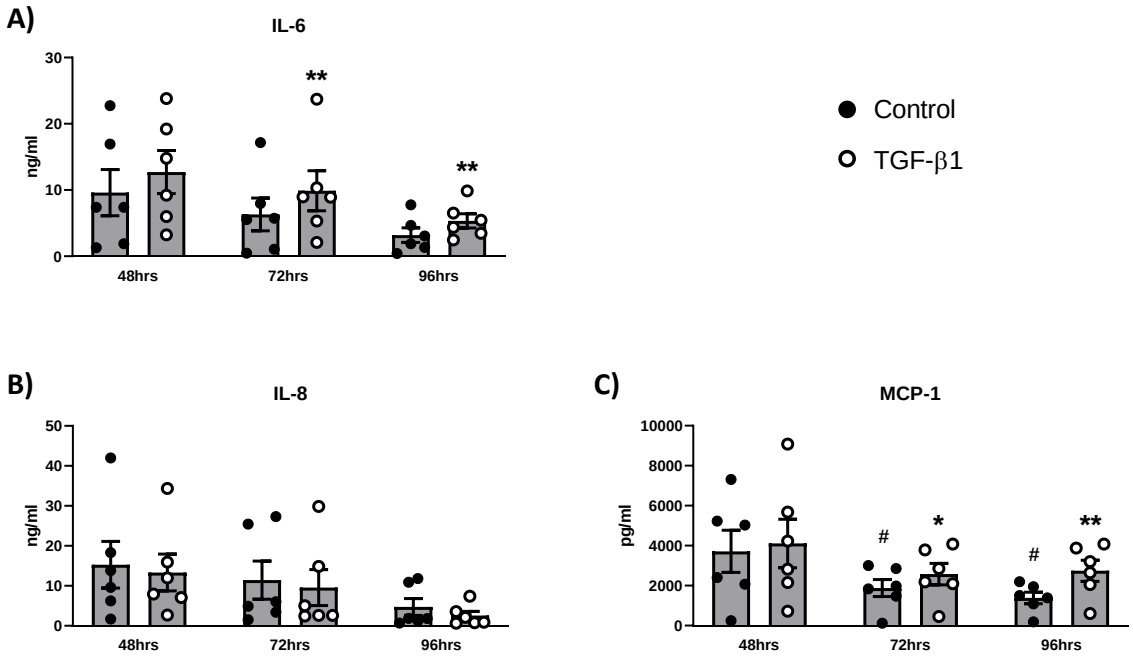

Figure 23. TGF-β1 induces IL-6 and MCP-1 but not IL-8 secretion in PCHS from unused donors – After a 24 hour rest period, PCHS were treated with either control media (unstimulated) or TGF-β1 (10ng/ml) for a further 72 hours. Media was collected and treatments refreshed daily. Supernatants from the slices were collected and protein secretion of markers of fibrogenesis was measured using DuoSet ELISA. N=6 donors. Data are mean ± SEM. Statistical analysis comprised of paired t-tests. * or # p<0.05, **p<0.01.

4.5.4 Modulating the effect of pro-fibrogenic stimuli

The next step was to try and modulate the spontaneous secretion of pro-fibrotic and pro-inflammatory markers observed in PCHS. After the initial 24 hour rest period slices from n=6 donors were challenged with ALK5 inhibitor SB-525334 (10µM), Pirfenidone (2.5mM) or Nintedanib (2.5µM) for a further 72 hours. Supernatants were collected and ELISA used to quantify levels of Collagen 1a1, TIMP-1, IL-6, IL-8 and MCP-1 secretion. Despite variation between donors, **Figure 24A** highlights the striking effect of both Nintedanib and ALK5i to attenuate collagen 1a1 secretion. Both interventions resulted in a 65% (ALK5i) and 70% (Nintedanib) reduction at 96 hours. Pirfenidone was also able to significantly reduce spontaneous collagen 1a1 secretion, albeit a lesser percent. Pirfenidone and Nintedanib were unable to significantly reduce TIMP-1 secretion **(Figure 24B)**. However, despite not reaching statistical significance, ALK5i appears to reduce TIMP-1 at 96 hours.

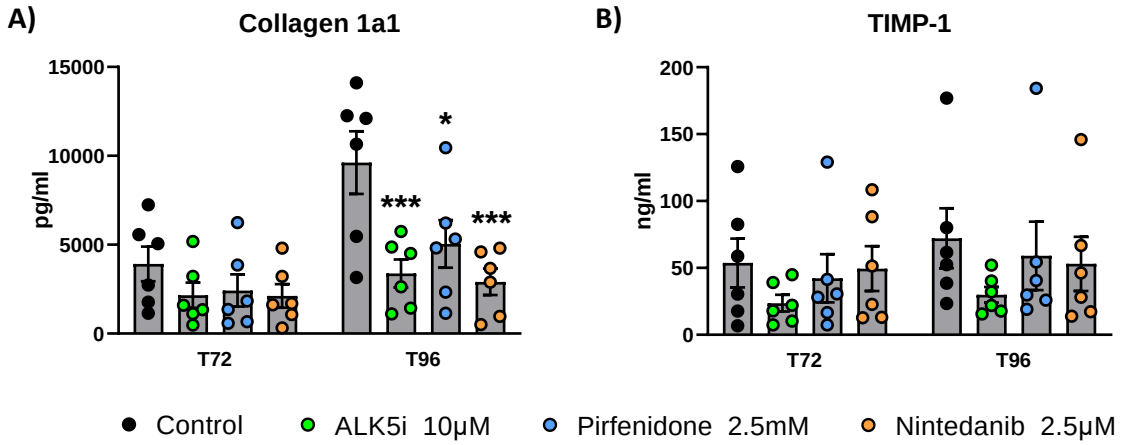

Figure 24. Attenuation of Collagen 1a1 secretion – After a 24 hour rest period, PCHS were treated with either control media (unstimulated) or ALK5 inhibitor SB-525334 (10µM), Pirfenidone (2.5mM) or Nintedanib (2.5µM) for a further 72 hours. Media was collected and treatments refreshed daily. Supernatants from the slices were collected and protein secretion of markers of fibrogenesis was measured using DuoSet ELISA. N=6 donors. Data are mean ± SEM; p values were calculated using ANOVA mixed effects analysis with Dunnett's multiple comparisons. Data were considered statistically significant with a p value * $p<0.05$, *** $p<0.001$.

Next we investigated the ability of the inhibitors to attenuate inflammatory responses in PCHS. **Figure 25** shows ALK5i was able to significantly reduce IL-6 secretion by 65% at 72 hours and 73% by 96 hours. Despite appearing to reduce MCP-1 secretion at both 72 and 96 hours, statistical significance was not reach, whilst it was also ineffective at attenuating IL-8 secretion. Pirfenidone displayed the strongest anti-inflammatory effects, significantly reducing IL-6 by % and % at 72 and 96 hours respectively. Whilst also attenuating both IL-8 by % at 72 hours and MCP-1 secretion by 57% at 96 hours **(Figure 25B-C)**. Nintedanib had no effect on attenuating secretion of any of the inflammatory markers.

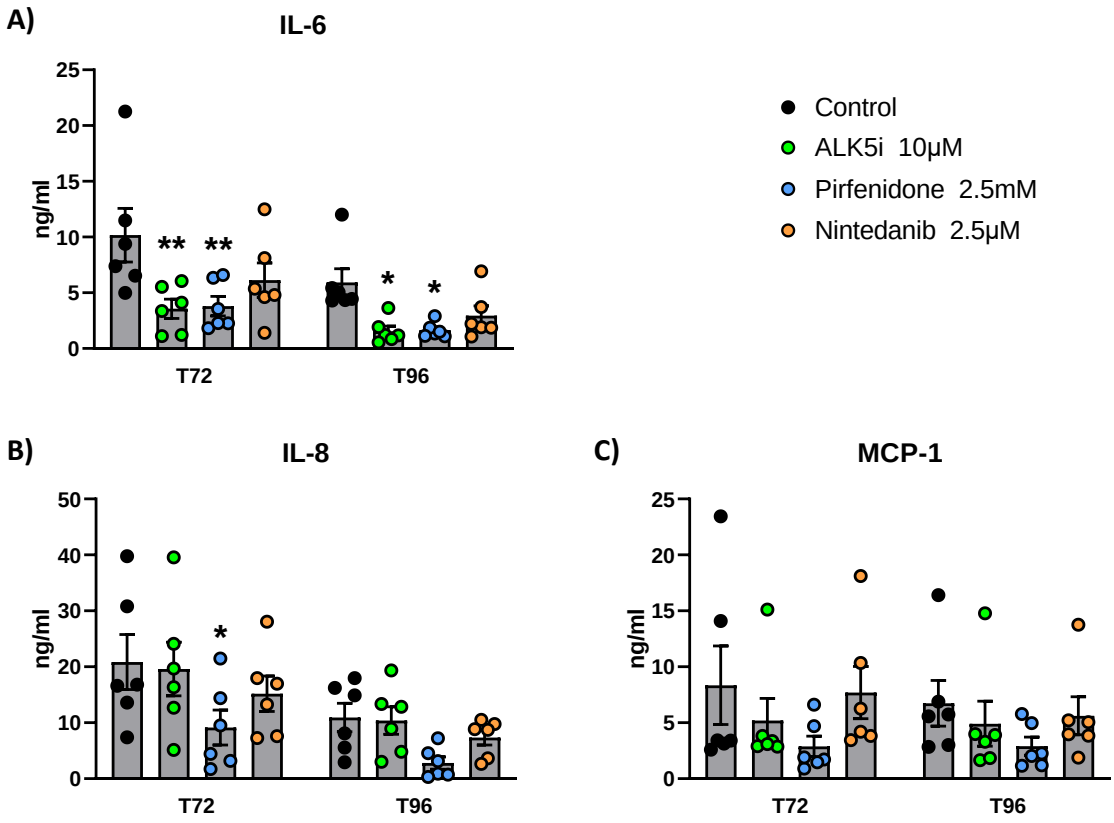

Figure 25. Attenuation of inflammatory responses from PCHS – After a 24 hour rest period, PCHS were treated with either control media (unstimulated) or ALK5 inhibitor SB-525334 (10µM), Pirfenidone (2.5mM) or Nintedanib (2.5µM) for a further 72 hours. Media was collected and treatments refreshed daily. Supernatants from the slices were collected and protein secretion of markers of fibrogenesis was measured using DuoSet ELISA. N=6 donors. Data are mean ± SEM; p values were calculated using ANOVA mixed effects analysis with Dunnett's multiple comparisons. Data were considered statistically significant with a p value. * $p<0.05$; ** $p<0.01$.

Next we investigated the ability to attenuate pro-fibrotic and inflammatory responses from TGF-β1 challenged PCHS using an ALK5 inhibitor (10µM), Nintedanib (2.5µM) and Pirfenidone (2.5mM). TGF-β1 stimulated secretion of collagen 1a1 and TIMP was reduced by treatment with all three inhibitors **(Figure 26A-B)**. However, only Nintedanib significantly attenuated secretion of both Collagen 1a1 and TIMP1. It was also able to potently reduce IL-11 secretion however it proved ineffective at inhibiting CTGF secretion. The ALK5i potently blocked CTGF and IL-11 secretion from PCHS. IL-11 was attenuated the most by all the inhibitors tested. At both 72 hours and 96 hours ALK5i and Nintedanib reduced IL-11 secretion in response to TGF-β1 challenge. Pirfenidone treatment was only able to significantly attenuate IL-11 levels, with no effect on CTGF secretion from PCHS.

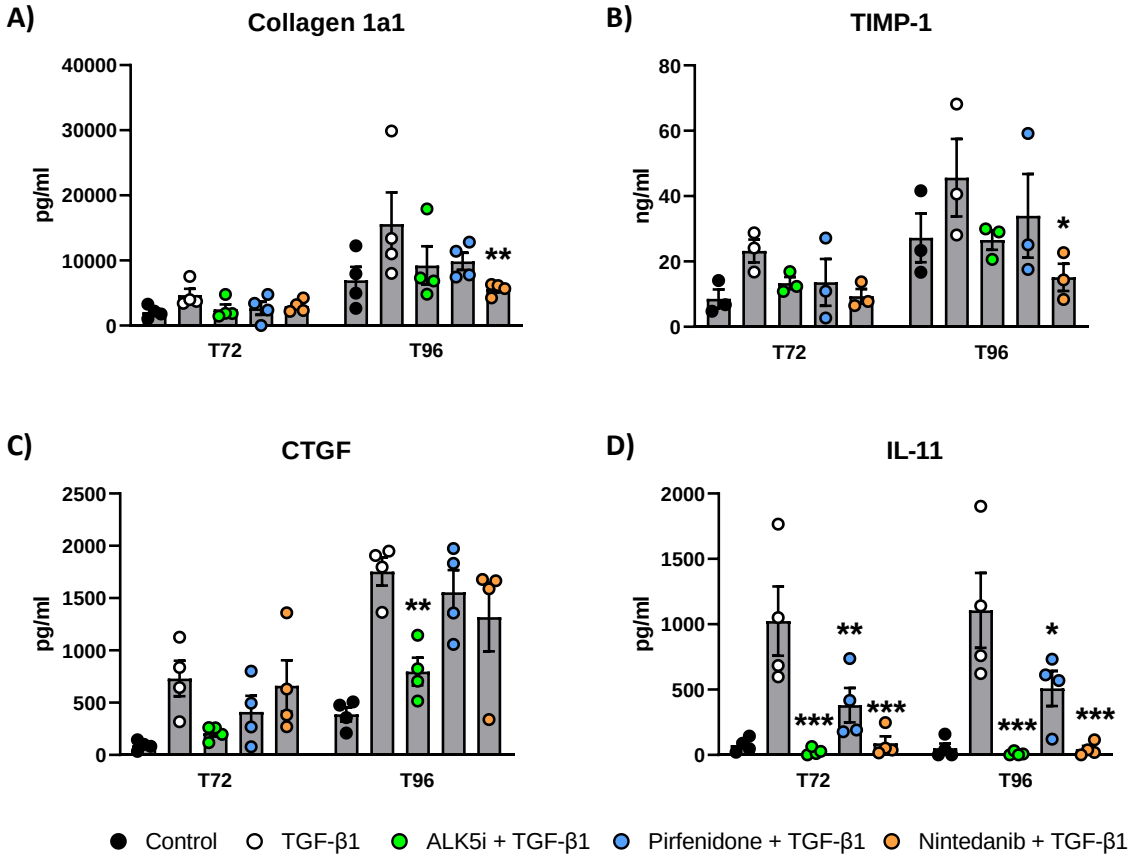

Figure 26. Modulation of pro-fibrogenic stimuli through the use of therapeutics – After a 24 hour rest period, PCHS were treated with either control media (unstimulated), TGF-β1 (10ng/ml) alone or in combination with ALK5 inhibitor SB-525334 (10µM), Pirfenidone (2.5mM) or Nintedanib (2.5µM) for a further 72 hours. Media was collected and treatments refreshed daily. Supernatants from the slices were collected and protein secretion of markers of fibrogenesis was measured using DuoSet ELISA. N=4 donors. Data are mean ± SEM; p values were calculated using ANOVA mixed effects analysis with Dunnett's multiple comparisons. Data were considered statistically significant with a p value * p<0.05, **p<0.01, ***p<0.001.

Finally, the ability to attenuate TGF-β1 induced inflammatory responses were assessed **(Figure 27)**. The ALK5i was ineffective at inhibiting IL-8 and MCP-1 secretion, whilst it was able to reduce IL-6 secretion despite failing to reach statistical significance. Both Pirfenidone and Nintedanib were able to significantly attenuate IL-8 secretion at 72 hours and MCP-1 secretion at 96 hours. However, much like the ALK5 inhibitor, Nintedanib and Pirfenidone displayed inhibitory effects on IL-6 secretion despite statistical significance not being achieved.

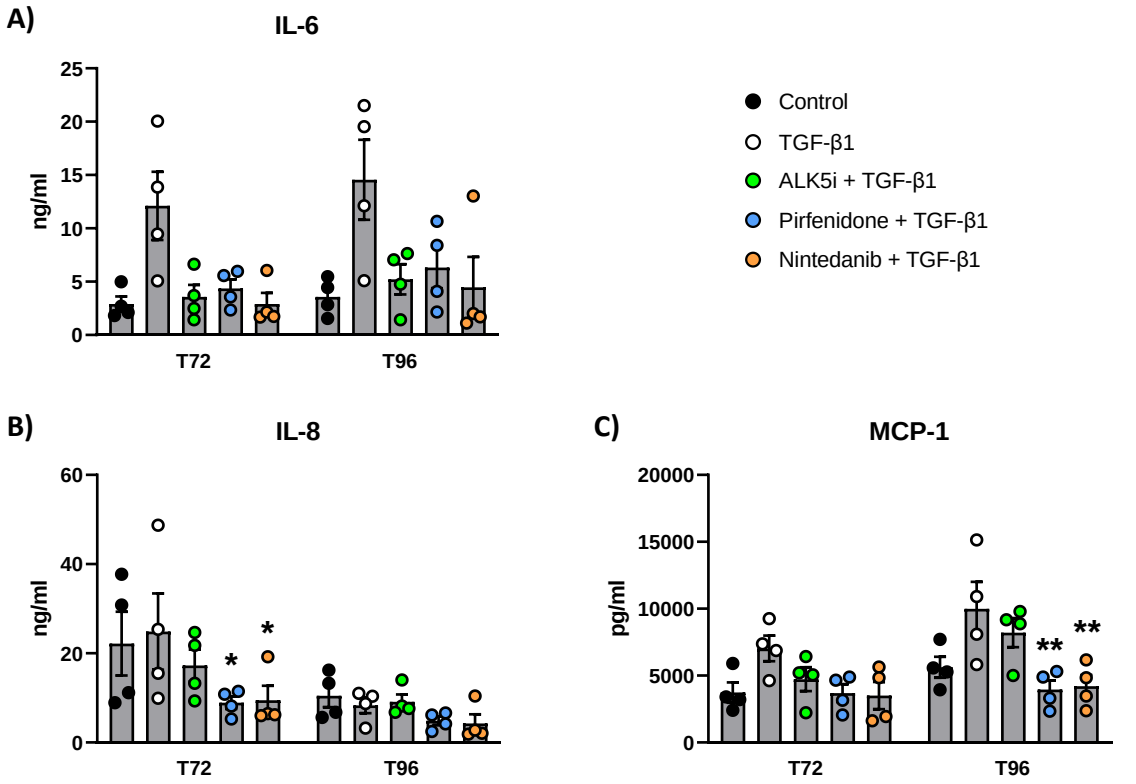

Figure 27. Modulation of inflammation through the use of therapeutics – After a 24 hour rest period, PCHS were treated with either control media (unstimulated), TGF-β1 (10ng/ml) alone or in combination with ALK5 inhibitor SB-525334 (10μM), Pirfenidone (2.5mM) or Nintedanib (2.5μM) for a further 72 hours. Media was collected and treatments refreshed daily. Supernatants from the slices were collected and protein secretion of markers of fibrogenesis was measured using DuoSet ELISA. N=4 donors. Data are mean ± SEM; p values were calculated using ANOVA mixed effects analysis with Dunnett's multiple comparisons. Data were considered statistically significant with a p value * $p<0.05$, ** $p<0.01$.

We have shown that both spontaneous inflammatory and fibrotic responses as well as those induced by TGF-β1 challenge are able to be attenuated by ALK5 inhibitor, Pirfenidone and Nintedanib. These results provide an exciting starting point in the work to develop as system in which novel therapeutics can be trialled before use in human patients.

4.6 Discussion

Myocardial fibrosis is a major pathological disorder which is common to a wide range of cardiac diseases, often culminating in the development of chronic heart failure. Fibrosis occurs after cardiac injury leading to pathological remodelling and dysregulation of normal processes within the ECM. The cardiac ECM plays an important role in normal heart function. Disturbance to the fine balance of proteins in the ECM during the development of fibrosis can lead to a number of problems including disruption of electrical signalling, dysfunction of the microvasculature and stiffening of the cardiac muscle. Despite a number of heart failure treatments, which may indirectly target the pathways involved in the progression of myocardial fibrosis, currently there are no therapies approved for the use in patients that are able to directly target fibrosis. Due to cardiovascular diseases being a leading cause of deaths globally there is a current unmet clinical need for the development of experimental systems which can aid the understanding of the pathogenesis behind myocardial fibrosis and for the testing of novel therapies for its treatment. The development of new drugs is extremely expensive and time consuming, with many potential treatments failing to reach clinical trials or for those which do many either exhibit a lack of efficacy in patients or unanticipated adverse effects. With as many as 28% of drug withdrawals in the USA due to unexpected cardiotoxicity(255).

There is a currently expanding field of research aiming to utilise whole human tissue to generate 3D precision cut tissue slices(223,237,239,240). These tissue slices share the complex structure and multicellular interactions present within the whole organ. Our laboratory has developed a patented bioreactor plate and rocking platform which successfully increases the viability of human liver and kidney slices compared to other slice culture systems(223,245). With the clear need to develop a suitable experimental system using human cardiac tissue, the primary aim of this chapter was to explore the feasibility to use our patented bioreactor system to generate viable cardiac slice cultures and to attempt to model disease pathways using drivers of inflammation and fibrosis within our system.

To investigate the requirements of PCHS for long-term *ex vivo* culture we tested a range of different media types, each developed for specific cells types present within the intact left

ventricular tissue. The presence of multiple cell types meant it was important to use a cell culture media which was able to complement and ensure the viability of the whole cellular composition of the LV. We therefore selected commercially available media specifically formulated for use with primary human cell culture. Early experiments also investigated the effects of our bioreactor system on PCHS viability. This was key to the optimisation of the system, as a number of current culture methods for precision cut slices are in static tissue culture plates at an air liquid interface(256,257) or require the use of supplemented oxygen into the culture media(258). In our own laboratory we have demonstrated that liver and kidney slices require culturing in our bioreactor(223,245), and therefore for this reason it was important to investigate the need for rocking within our system for heart slice viability(223). An area in which we could further improve our system would be through the measurement of a number of functional endpoints, such as force measurements, Ca^{2+} transients and action potentials. Despite this, our results demonstrate the need to culture PCHS using our bioreactor system the ensure long-term viability of the tissue.

Having developed a viable PCHS model the next step was to utilise it to model inflammation and fibrosis. Initially we looked at inducing an acute inflammatory response in the tissue slices. The activation of inflammatory pathways in a number of heart conditions, such as myocardial infarction, diabetes mellitus, myocarditis are well known and often serve as a precursor to acute and chronic heart failure. The development of fibrosis also occurs after an initial acute inflammatory response, with the persistent injury and failure to repair ultimately leading to a dysregulation in fibroblast response. We chose a number of well-established pro-inflammatory drivers which covered a wide range of inflammatory pathways. Using these stimuli we demonstrated the plasticity within the PCHS system, and the ability to induce changes in protein secretion in response to different stimuli.

In order to assess the inflammatory effects of the different stimuli we employed the use of a well-defined panel of markers of inflammation through the quantification of the secretion of cytokines and chemokines measured by ELISA. The chemokine CCL2/MCP-1 has a well-defined literature confirming its role in heart failure(259–261), both through the use of experimental models, highlighting its involvement in adverse remodelling, dysfunction of the cardiac tissue

and fibrosis, but also within the clinic. Chronic heart failure patients were shown to have elevated levels of serum CCL2, those with HFrEF exhibiting the highest levels(262). Work by Damas *et al* showed that increased MCP-1 levels were not just found in the circulation but that there was increased RNA and protein expression of both MCP-1 and its receptor CXCR2 in the failing heart(263). In addition to MCP-1 secretion, we also assessed the ability of our stimuli to affect the secretion of the pleiotropic cytokine IL-6 from the PCHS. Much like MCP-1, IL-6 has long been associated with the pathogenesis of cardiovascular diseases. Whilst acute upregulation of IL-6 is thought to have cardioprotective effects, if IL-6 remains chronically elevated it becomes associated with the exacerbation of chronic inflammation and the development of fibrosis. The final marker of inflammation was quantified was the chemokine IL-8. In disease IL-8 is primarily involved in the recruitment of neutrophils. In the heart IL-8 has been shown to be mainly localised within cardiomyocytes(264). Whilst in disease IL-8 is upregulated in HF patients, with increased levels correlated with worse clinical prognosis(265–268).

We demonstrated that in response to an acute stimulation by LPS PCHS were able to increase the secretion of a wide range of pro-inflammatory markers. The effect of LPS treatment on elevating secretion of IL-6 and TNF-α agrees with work by Kuo *et al* who demonstrated increased mRNA expression of IL-6 and TNF-α in cardiomyocytes exposed to 1μg/ml or 5μg/ml of LPS for up to 24 hours(269). The application of IL-1α to PCHS was to mimic its role as an alarmin *in vivo,* which occurs after damage to epithelial cells, resulting in IL-1α's subsequent release. The secreted IL-1α is able to bind to IL-1R1 on a range of cell types, initiating downstream signalling pathways which ultimately result in the secretion of a number of inflammatory cytokines(112,270,271). Through IL-1α challenge we have shown that we are able to replicate the pro-inflammatory response which occurs *in vivo* within our PCHS system.

The importance of TGF-β1 in the development of fibrosis is well defined(140). It is often described as the 'master regulator' of fibrosis *in vivo* with the downstream signalling pathway often a target for the development of therapies to prevent and reverse fibrosis progression. Therefore it was imperative to the development of an *ex vivo* model of cardiac fibrosis to be able to use TGF-β1 to induce fibrogenesis within the tissue slices. Work utilising PCHS by

Perbellini *et al* attempted to induce a pro-fibrotic phenotype in slices through the application of TGF-β1. Despite using a dose of 20ng/ml, they were unable to induce αSMA expression or cardiac fibroblast proliferation(233). However differences in results observed could be due to the differences in the culture system used, slices were isolated from canine hearts and cultured statically at an air-liquid interface, also the secretion of pro-fibrogenic proteins such collagen 1a1 were not assessed during their study. Our results showed that through the application of TGF-β1 at a concentration of 10ng/ml we were able to significantly increase the secretion of key ECM proteins, such as Collagen 1a1 and CTGF, as well as drivers of fibrogenesis and chronic inflammation, IL-11 and IL-6. Our utilisation of TGF-β1 at 10ng/ml in our study is in agreement with other studies using TGF-β1 challenge *in vitro*, and known to induced αSMA expression in isolated ventricular fibroblast cultures(272). Cardiac fibrosis is often referred to as a 'living scar' due to its presence within the constantly beating heart and exposure to changing biochemical and electrical signals. Despite improvements in the both the viability of PCHS and ability to induce a pro-fibrotic response from TGF-β1 treated PCHS, our model could still be described as an oversimplification of the *in vivo* heart due to the lack of appropriate electrical signalling within the system.

Finally we investigated the effect of applying anti-fibrotic and anti-inflammatory compounds to PCHS. This was done both in combination with either the inflammatory stimuli (IL-1α or LPS) or fibrotic stimuli (TGF-β1) or alone without any stimulation. Pirfenidone and Nintedanib are currently the only approved anti-fibrotic treatments and are licensed for use in Idiopathic Pulmonary Fibrosis (IPF) patients. There have been multiple studies and trials investigating the repurposing of these drugs to treat other fibrotic diseases. The PIROUETTE trial was designed to evaluate the efficacy of Pirfenidone at reducing cardiac fibrosis in HFpEF patients(158). Patients treated with Pirfenidone had reduced myocardial fibrosis and a reduction in NT-proBNP, an established diagnostic test for heart failure. These beneficial effects are in agreement with a number of pre-clinical studies which showed that Pirfenidone treatment is associated with the regression of cardiac fibrosis(273,274). These results are in agreement with our data, in which we observed a significant reduction in spontaneous collagen 1a1 secretion. Pirfenidone treatment was also successful at attenuating IL-11 secretion in our induced model of fibrosis. In addition to its anti-fibrotic effects, Pirfenidone is also known to exhibit pleiotropic effects in reducing inflammation. This has been demonstrated both

through the use of animal models but also in IPF patients, patients with chronic hepatitis C and has been postulated as having therapeutic benefits in patients during and after COVID-19 infection(275–277). Our data was in agreement with studies demonstrating Pirfenidone's anti-inflammatory effects. We showed that Pirfenidone was effective at attenuating secretion of a wide range of inflammatory markers (IL-6, MCP-1, IL-8, GM-CSF and Eotaxin) in response to both an inflammatory (IL-1α) or a pro-fibrogenic (TGF-β1) stimuli as well as inhibiting their spontaneous release from unstimulated control PCHS.

Nintedanib is a tyrosine kinase inhibitor, primarily targeting vascular endothelial growth factor receptors (VEGFR)-1, -2 and -3, fibroblast growth factor receptors (FGFR)-1, -2 and -3 and platelet derived growth factor receptors (PDGFR)-α and -β. Initially used to prevent progression of fibrosis in IPF patients, in 2019, after the success for the INBUILD clinical trial, Nintedanib was also approved for use in ILD patients(278). In fibrosing lung diseases Nintedanib is able to slow the decline of Forced Vital Capacity (FVC) and reduce mortality, it is also currently undergoing a phase 3 clinical trial, NINTECOR, to assess its ability to slow progression of fibrosis in COVID-19 patients. In addition to treating lung fibrosis, there are a number of studies investigating the efficacy of Nintedanib in a number of other fibrotic diseases, including kidney, skin and liver(279–281). *In vitro*, Nintedanib significantly downregulates expression and secretion of ECM components such as collagen 1a1 and fibronectin and has also been shown to block TGF-β1 signalling in primary lung fibroblasts isolated from IPF patients(282). Our data from PCHS treated with TGF-β1 mimicked that of published data, showing the ability of Nintedanib to significantly attenuate collagen 1a1 secretion as well as other fibrogenic factors (IL-11 and CTGF). Interestingly Nintedanib had no effect on reducing inflammation, which is in agreement with unpublished data from our laboratory in Idiopathic Pulmonary Fibrosis (IPF) lung PCS. This is in contradiction to research in mouse models of bleomycin-induced lung inflammation, in which reduced IL-1β levels were observed(283). However, much like in our own study, the anti-inflammatory effects of Nintedanib tend to be much weaker in the clinic than those seen in animal models. This may be due to inter-species differences or to the fact in clinic the inflammatory response has peaked before the intervention of Nintedanib, and therefore potential anti-inflammatory effects are missed. An area of focus for future experiments could centre on the timing of the application of anti-fibrotic therapies. In the early stages after injury TGF-β signalling is involved

in the normal wound healing response. Therefore blockade of this process too early in the wound healing process may in fact lead to aberrant remodelling whilst application once fibrosis is established may reduce the effectiveness of the therapy, as is potentially observed with Nintedanib treatment.

In conclusion, we have developed a novel culture system that enables PCHS to remain viable for up to 6 days in culture. This extended culture period has allowed us to effectively model acute inflammatory responses through IL-1α or LPS challenge or model fibrogenesis through TGF-β1 stimulation. The application of approved anti-fibrotic therapies, Pirfenidone and Nintedanib confirms data observed in patients in the clinic. These findings gives confidence to the PCHS system's ability to model disease and act as a more biologically relevant model for the testing of novel therapeutics prior to their progression to clinical trials.

5 Identification of novel targets using proteomics and RNA sequencing

5.1 Introduction

We performed a detailed review of the literature to identify several candidate proteins which are proposed to have a role in the initiation and progression of cardiac inflammation and fibrosis both *in vivo* and *in vitro*. As well as identifying a number of well described proteins, such as TGF-β1 and Angiotensin II, we have also identified a number of candidates with emerging evidence including Galectin-3, IL-11 and CTGF.

5.1.1 TGF-β1

TGF-β1 is a multifunctional cytokine synonymous with fibrosis and fibrotic diseases, including cardiac fibrosis. It is one of three isoforms which are part of a larger superfamily of proteins key in development and homeostasis. The three TGF-β isoforms (TGFβ-1, TGFβ-2 and TGFβ-3) signal through the same receptor signalling pathways. TGF-β is initially synthesised as an inactive precursor, furin is required for enzymatic cleavage to produce a latent complex of TGF-β(284). The mature TGF-β is blocked by the latency-associated peptide (LAP) regions folding around the mature peptide, preventing its binding to its receptor. This complex is then trafficked out of the cell where it can be sequestered to the ECM through the binding of latent TGF-β binding protein (LTBP), forming a large latent complex (LLC). In order for TGF-β signalling to occur the protein requires activation and release from the ECM(284). Binding of thrombospondin 1 to the LAP prevents its association with the mature TGF-β peptide, therefore allowing its release from the ECM. Further cleavage by serine proteases releases TGF-β from its latent form, allowing it to bind to its receptor on the cell surface. In addition to the activation of TGF-β signalling by thrombospondin, integrins, a family of cross-membrane receptors, are able to modulate TGF-β activation and signalling cascade through either a protease dependent or independent manner(285).

TGF-β1 signals through the TGF-β receptor complex, a tetrameric structure initially composed of a dimer of TGF-βRII which upon TGF-β1 binding recruits a dimer of TGF-βRI (ALK5). Upon formation of the TGF-β receptor complex TGF-βR1 undergoes phosphorylation, activating the downstream TGF-β signalling pathways. In cardiac fibrosis TGF-β1 is proposed to signal

through either SMAD dependant or non-SMAD dependant pathways(286). Phosphorylation of SMAD2/3 and their oligomerisation with SMAD4 leads to their translocation into the nucleus, and upregulation of TGF-β1 dependent genes. Upregulated pro-fibrotic genes include α-smooth muscle actin (α-SMA), a large number of collagens (COL1A1, COL3A1, COL6A1 and COL6A3), PAI-1, and CTGF to name a few(286–288). Work by Khan *et al* demonstrated the upregulation of TGF-β1 in the myocardium of patients with dilated cardiomyopathy (DCM) and ischemic cardiomyopathy (ICM) compared to non-failing hearts(289). The increased TGF-β1 was also significantly positively correlated with both phosphorylated SMAD2 and the presence of Collagen type I and Collagen type III. Through aberrant non-canonical signalling, TGF-β1 has been show to activate three pathways including various branches of the mitogen-activated protein kinases (MAPK) pathway, such as ERK1/ERK2 signalling, JNK/p38 activation and JAK/STAT3 activation(290,291). The two other pathways activated through non-canonical TGF-β1 signalling are the phosphoinositide-3-kinase (PI3K)/protein kinase B (Akt) pathway and RhoA-ROCK axis. Activation of the RhoA-ROCK axis appears to play a potentially important role in cardiac fibrosis. ROCKs, also known as Rho-associated protein kinases are coiled-coil-containing protein kinases known to be involved in the regulation of a number of cellular functions, particularly in the development of cardiac fibrosis. Inhibition of ROCK using the inhibitor Y27632 limited cardiac fibrosis and pathological remodelling in mouse models of cardiac fibrosis(292).

5.1.2 Angiotensin II

Angiotensin II, a hormonal peptide, is most commonly associated with the Renin Angiotensin Aldosterone System (RAAS). Through RAAS, Angiotensin II can be produced both systemically, in response to low blood pressure, and locally within an organ, including the heart, kidney and brain. Angiotensin II is the product from the final step of the RAAS pathway. In the case of cardiac fibrosis, Renin is initially secreted from stressed cardiomyocytes, immune cells and fibroblasts, and catalysed by Angiotensinogen to Angiotensin I. Following which Angiotensin I is converted to Angiotensin II by Angiotensin Converting Enzyme (ACE). Once produced and secreted into the cardiac interstitium, Angiotensin II is able to bind to AT_1 and AT_2 receptors on the surface of a variety of cell types, including cardiomyocytes, fibroblasts and endothelial cells(293–295). These two receptors both have very distinct functions upon Angiotensin II binding. Signalling through AT_2 acts in a cardioprotective role through the suppression of the

pro-fibrotic actions of the AT_1 receptor(296–298). Conversely, activation of AT_1 receptors results in cardiac fibroblast proliferation and migration, ECM synthesis and apoptosis. It is believed that the signalling actions downstream of the AT_1 receptor are mediated through a variety of different cascades, such as ERK, p38/MAPK and protein kinase C (PKC)(299,300). The result of this signalling is the elevated transcription of pro-fibrotic genes such as Collagen I and III. In addition to Angiotensin II inducing fibrosis alone, some actions require either stimulation with TGF-β1 or need TGF-β1 to become activated. For example work by Zhou *et al* showed that Angiotensin II induced thrombospondin secretion was key in activating TGF-β1 signalling and exacerbating cardiac and renal fibrosis(301).

Angiotensin II induced cardiac fibrosis has long been a target for anti-fibrotic therapies. Currently there are a number of angiotensin receptor blockers (ARBs) being tested both in animal models and clinical trials, one of the most well-known being Losartan. Sopel *et al* demonstrated the infusion of Angiotensin II in a mouse model of heart failure resulted in an increase in the deposition of ECM from areas high in myofibroblasts and that these responses could be attenuated and reversed somewhat by the application of Losartan(302). The anti-fibrotic effects for ARBs and also ACE inhibitors (ACEi) have been shown in patients in small-scale clinical trials(303). Biopsies from hearts demonstrated reduction in myocardial collagen content and LV chamber stiffness after Losartan treatment in patients with severe fibrosis. A therapy which is neither an ARB or ACEi but appears to show some efficacy in animal models is the approved IPF drug, Pirfenidone. This was shown to be effective at attenuating Angiotensin II-induced cardiac hypertrophy(304).

Whilst targeting the AT_1 receptor has shown promise, including the anti-fibrotic effects of ARB and ACEi treatments, the combination of these therapies to provide a dual RAAS inhibition and maximise any anti-fibrotic effects in the clinic, proved to have adverse effects(305,306). This was to such an extent that dual RAAS inhibition is contraindicated in guidelines for cardiovascular treatments. Therefore more recently attention has shifted to other ways in which to attenuate Angiotensin II's pro-fibrotic effects. One of these methods involved utilising the anti-fibrotic effects of signalling through the AT_2 receptor. The AT_2 receptor is postulated to induce anti-fibrotic and anti-inflammatory pathways in response to the pathophysiological effects of AT_1 activation. In healthy patients AT_2 receptors are expressed at low levels, however, due to its subsequent upregulation in a number of pathological

conditions, including myocardial infarction, it has become a target for the development of new anti-fibrotic therapies. The first AT_2 receptor agonist identified was the non-peptide Compound 21 (C21)(307). This has shown efficacy in animal models of hypertension, with Rehman *et al* demonstrating its ability to reduce collagen content and myocardial fibrosis(308). The anti-fibrotic effects were also confirmed in a rat model of MI, once again reduced collagen content in the LV was observed but also reduced expression of TGF-β1, MMP-2 and MMP-9, a finding also confirmed in cardiac fibroblast cultures(309).

5.1.3 Galectin-3

Galectin-3 is a β-galactoside-binding leptin and member of the wider galectin superfamily, with 15 galectins currently described and categorised into 3 subtypes. Galectin-3, the only chimaera type galectin, is unique in its structure compared to other galectins, containing not only a C-terminal Carbohydrate Recognition Domain (CRD) but also a large N-terminal (NT) protein binding domain. The N-terminal, rich in proline and glycine, allows for the formation of oligomers between Galectin-3 monomers, unique within the galectin family.

Galectin-3 has been shown to be predominantly found within the cytosol of cells where it participates in a number of important intracellular events. This includes cell survival, effecting proliferation, differentiation and apoptosis but also the growth of connective tissues and bone and cartilage development. Nuclear Galectin-3 has a wide range of functions. Both Dagher *et al* and Park *et a*l showed its importance in promoting pre-mRNA splicing(310,311). Whilst work by Nakahara *et al* highlighted its role in the regulation of gene expression in cancer(312). Galectin-3 is synthesised on free ribosomes located within the cytosol, in order to be secreted Galectin-3 bypasses the reticulum-Golgi apparatus and is secreted through an incompletely understood non-classical pathway(313). Secreted Galectin-3 can either be membrane-associated or free within the ECM. This enables it to interact with a number of ECM proteins such as laminin, fibronectin and tenascin and also macrophage surface antigens, highlighting key roles in both cell-cell interactions and cell-matrix adhesion.

There is now a growing body of evidence for the involvement of Galectin-3 in cardiac fibrosis, with the role of galectins in the heart ranging from cell proliferation to regulation of immune and inflammatory responses(314). Work by Sharma *et al* provided the first evidence for a

potential role of Galectin-3 in heart failure(315). Through the use of a rat model of hypertension they identified Galectin-3 as the most significantly expressed gene compared to healthy controls. Also showing its localisation to activated macrophages in areas of fibrosis in heart failure (HF) rats and the ability for exogenous Galectin-3 to induce collagen 1a1 from cardiac fibroblasts *in vitro*. Importantly these observations were also confirmed in human patient biopsies, with increased mRNA expression in myocardial biopsies from HF patients. Later studies continued to build on evidence that Galectin-3 is thought to be secreted and able to act on macrophages and fibroblasts during cardiac fibrosis. Lui *et al* (2009) showed that Galectin-3 induced macrophage infiltration, as well as the activation of the TGF-β1/SMAD3 signalling pathways leading to enhanced cardiac fibrosis(316)(Liu et al., 2009)(Liu et al., 2009). In a paper by Yu *et al* (2013) Galectin-3 knockout mice were shown to be protected from cardiac fibrosis when subjected to either Angiotensin II infusion or transverse aortic constriction(317). The same study also showed the ability to attenuate fibrosis in REN2 rats through the use of the Galectin-3 inhibitor N-acetyllactosamine(317).

Galectin-3 has been described as a potential biomarker for disease severity in patients. A number of studies, including in the large PREVEND (Prevention of REnal and Vascular ENd-stage Disease) cohort, have demonstrated that increased serum levels of Galectin-3 are positively correlated with increased risk of hospitalisation and death in heart failure patients(318–320). However despite these data, the use of Galectin-3 as a biomarker remains controversial. A number of smaller studies have found conflicting results, including a systemic review of the literature by Srivastan *et al* showing that serum Galectin-3 was a poor predictor of mortality(321). Despite these conflictions, in 2010 Galectin-3 was approved for use as a biomarker for predicting cardiovascular adverse effects, when used in conjunction with other clinical measures, by the U.S. Food and Drug Administration (FDA)(322).

The role of Galectin-3 in cardiac fibrosis and disease progression still requires further study. The mechanisms by which it is involved in the early inflammatory response and the subsequent progression into fibrosis remains to be fully elucidated. Further studies are therefore required both to fully illuminate its mechanisms and to confirm its effectiveness as both a biomarker of cardiac fibrosis severity and progression in patients.

5.1.4 Connective Tissue Growth Factor (CTGF)

Connective tissue growth factor (CTFG), also known as CCN2, is a 36-38kDa matricellular protein. It is one of 6 members of the multifunctional CNN family of proteins (CNN1-6), characterised by their highly conserved disulphide bonding pattern. CTGF contains 4 functional domains, insulin-like growth factor binding protein (IGFBP), von Willebrand factor type C repeat (VWC), thrombospondin type-1 repeat (TSP1 or TSR), and cysteine knot-containing domain (CT). These allow for binding with other proteins, such as TGF-β1, insulin-like growth factors (IGFs) and integrins(323). Due to the range of different proteins CTGF can interact with, it participates in a number of complex biological processes, including angiogenesis, wound healing, adhesion and tumorigenesis(323).

Despite being described as an ECM protein, CTGF does not have an obvious structural role within the extracellular matrix. Instead it functions to modulate cellular responses with the matrix due to changes in the cellular and ECM environment. Whilst rarely found in heathy individuals or tissues, it is shown to be significantly upregulated in a number of different diseases(324,325), and is rapidly induced during the tissue repair process. The role of CTGF in fibrotic diseases has been significantly studied, especially in response to TGF-β1. The aberrant expression of CTGF in response to injury has been observed in a number of renal fibrosis disorders, including diabetic nephropathy. FG-3019, is a humanized monoclonal antibody proposed as a potential therapy(326). Phase I clinical trials that have taken place in patients with diabetic nephropathy showed that FG-3019 treatment was well-tolerated in participants and associated with a reduction of albuminuria(326). This is one of a number of clinical trials, covering a range of fibrotic disorders, investigating the efficacy and tolerability of FG-3019 (ClinicalTrials.gov identifier: NCT01262001; NCT00754143; NCT00913393; NCT01217632). In the liver, CTGF in patient serums correlated with fibrotic activity(327). Whilst targeting CTGF in the liver has also shown potential in reducing CCL4-induced liver fibrosis. This was achieved through the use of siRNA to knockdown CTGF expression, resulting in a 40% reduction in collagen 1a1 expression *in vivo*(328). Interestingly, studies in a number animal models overexpressing the CTGF transgene alone in the kidney, liver and heart failed to elicit a pro-fibrotic response(329). Exacerbation of fibrosis was only observed in transgene mice after chronic treatments with the hepatoxic compounds CCL4 or thioacetamide(329,330).

In the injured heart CTGF expression is induced by TGF-β1 (331–333). Work by Chen *et al* (2000) showed that TGF-β1 stimulation was able to increase the expression of CTGF in both cardiac fibroblasts and cardiac myocytes(333). Conversely, transgenic mice overexpressing CTGF, did not develop cardiac hypertrophy at baseline, however in response to injury, in this case pressure overload, there was a significant increase in cardiac fibrosis(334). The inability of CTGF to drive fibrosis alone was also confirmed in recent work by Accornero *et al*. They demonstrated that cardiomyocyte specific deletion of CTGF had no effect at reducing cardiac remodelling in a TAC-model of fibrosis(335). Interestingly CTGF has also been suggested as a co-factor for TGF-β1, enabling maximal pro-fibrotic effects whereas it is thought to have limited ability to induce a strong fibrotic response alone(331,336)(Leask, 2010, Mori et al., 1999)(Leask, 2010, Mori et al., 1999).

5.1.5 Interleukin-11 (IL-11)

Interleukin-11 (IL-11) is a member of the IL-6 family of cytokines. In order for signal transduction, IL-11RA requires co-expression with the subunit glycoprotein 130 (gp130). It was initially thought that IL-11 signalling would then occur through the STAT pathway, much like that of IL-6, which also forms a complex with gp130. However recent studies in fibroblasts have demonstrated that whilst recombinant IL-11 treatment causes STAT3 activation, there are no downstream effects on transcription. Instead signalling appears to be dependent on ERK phosphorylation for its activation. Prior to its recently discovered role in driving fibrosis, IL-11 was primarily used as a therapy to reduce treatment-associated thrombocytopenia in patients undergoing chemotherapy(337). However a more recent study by Lui *et al* investigated the cardiovascular events in leukaemia patients undergoing IL-11 treatment for chemotherapy-induced thrombocytopenia. Their results showed increased BNP-levels, atrial arrythmia and in some cases acute left ventricular failure in these patients(338,339).

In the heart IL-11RA is expressed on the surface of both cardiac fibroblasts and cardiomyocytes. Initially IL-11 was thought to be cardioprotective. Obana *et al* reported IL-11 attenuated cardiac fibrosis in a mouse model of myocardial infarction (MI)(340). Whilst IL-11 infusion protected against ischemia-reperfusion injury in rats(341). However more recently a potentially important role for IL-11 in cardiovascular fibrosis has been highlighted in a paper by Schafer *et al* (2017). They found that IL-11 is the dominant transcriptional response to

cardiac fibroblasts treated with TGF-β1(254)(Schafer et al., 2017)(Schafer et al., 2017). In their proposed pathway of IL-11 signalling, IL-11 released in response to TGF-β1, trafficked out of the cell and was able to act in an autocrine fashion resulting in elevated translation of both IL-11 and other pro-fibrotic proteins including collagens, α-smooth muscle actin and periostin **(Figure 28)**. The pro-fibrotic effects of IL-11 have also been observed in the clinic. In heart failure patients serum levels of IL-11 were elevated in comparison to control, and they correlated with symptoms, NT-pro BNP levels and adverse cardiac events(342). Disparity between the pro-fibrotic and cardioprotective roles of IL-11 has been postulated by some to be due to the use of non-species specific recombinant IL-11, as for many years recombinant human (rh) IL-11 was used in animal models to investigate IL-11 effects(340,341,343,344). Work by Schafer *et al* was key in demonstrating the species specific effects of recombinant IL-11 on cardiac fibroblasts(254). They showed no effect of rhIL-11 on primary mouse cardiac fibroblasts, whereas treatment with recombinant mouse IL-11 induced a potent pro-fibrotic response.

These conflicting results highlight the need for further research into the effects of IL-11 in the development of cardiac fibrosis and the pathways by which it signals.

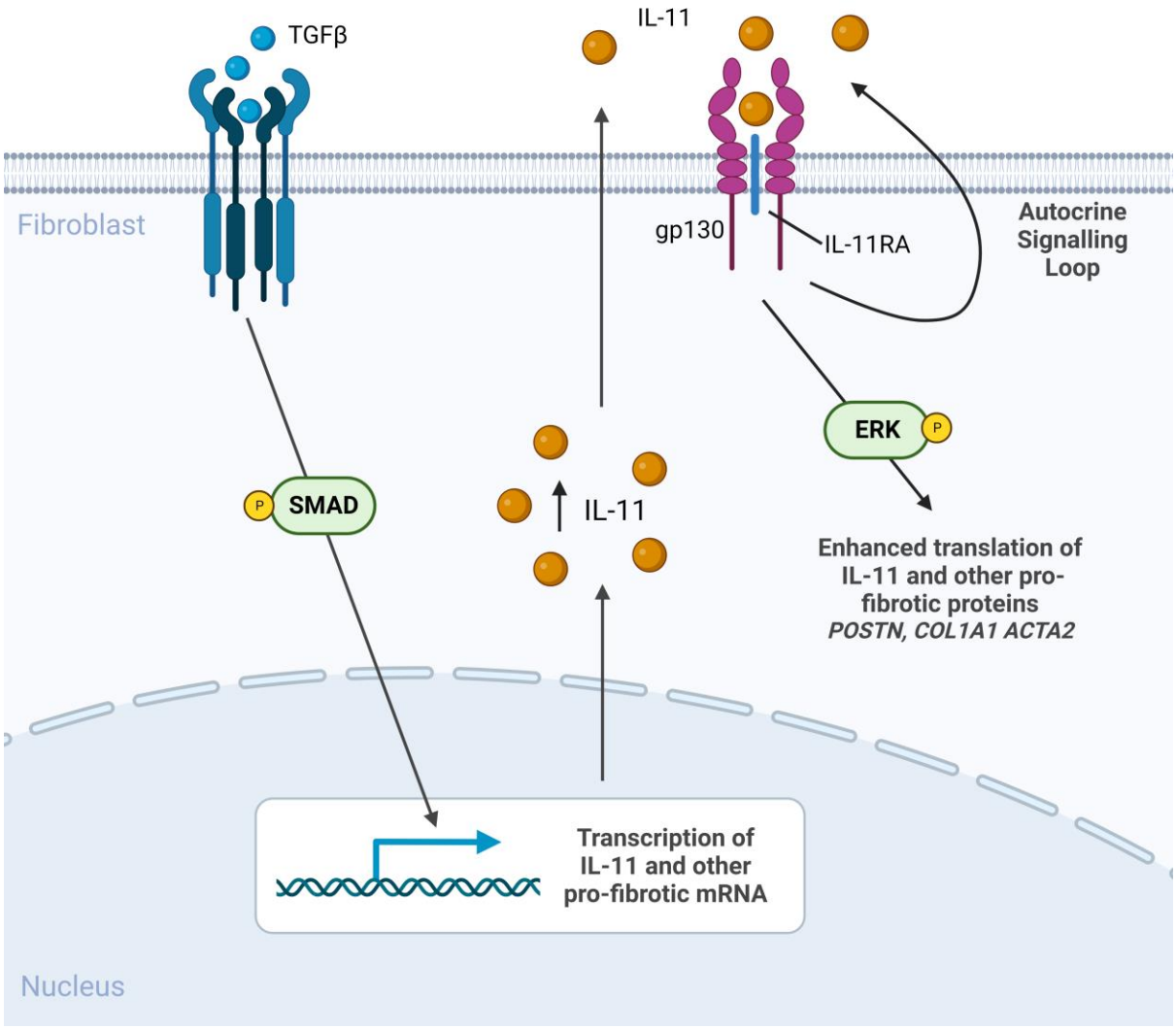

Figure 28. IL-11 signalling in fibrosis – TGF-β1 signalling through SMAD-dependent pathway leads in an increase in the transcription of IL-11 and other pro-fibrotic mRNA. IL-11 is secreted and binds to gp130/IL-11RA complex. Activation of ERK leads to the enhanced translation of IL-11 and other pro-fibrotic proteins including POSTN, COL1A1 and ACTA2. IL-11 autocrine signalling loop further enhance IL-11 ERK-dependent fibrotic protein translation. ERK: extracellular signal-regulated kinase; SMAD: mothers against decapentaplegic homolog; gp130: glycoprotein 130; IL-11RA: interleukin 11 receptor subunit alpha; POSTN: Periostin; COL1A1: Collagen 1a1; ACTA2: Alpha smooth muscle actin. Created with BioRender.com

5.2 Rationale, Hypothesis and Objectives

5.2.1 Rationale

Though current models of cardiac fibrosis have increased our understanding of disease pathways involved in cardiac fibrosis, there is still an unmet need for the development of more physiologically relevant models to aid the advancement of novel therapies. Cardiac fibrosis is the culmination of a number of different pathophysiological conditions, and therefore in order to fully understand the mechanisms driving the disease it is important to develop PCHS models able to recapitulate the disease pathways occurring in patients. We have identified a range of potential proteins proposed, from research using rodent models and *in vitro* culture, to drive cardiac inflammation and fibrosis. This therefore raises the question as to whether these finding hold true in human PCHS.

Whilst it is important to further investigate proteins and signalling pathways of interest in myocardial fibrosis, better models are required to identify novel mechanisms. Whilst data generated directly from patients is the 'Gold Standard' samples are in short supply and in order to fully understand any novel mechanisms discovery experiments using *ex vivo* human tissue are sorely needed. Finally, the current pre-clinical models used to test candidate therapies prior to clinical trials still result in the majority of treatments failing once they reach Phase I and II trials, largely in part due to the use of inappropriate pre-clinical models. Therefore there is a current unmet need for the development of more complex models, such as Precision cut slices, in order to confirm research identified in rodent and *in vitro* cultures and to provide a translational bridge for the testing of novel therapies.

5.2.2 Hypothesis

We hypothesise that through the application of recombinant proteins to PCHS we will be able to more accurately determine those with direct pro-inflammatory or pro-fibrotic effects within intact human heart tissue. Moreover, we believe a broad 'omics' approach using PCHS will enable us to identify novel signalling pathways leading to the identification of candidate inhibitors to test in PCHS. The development of a more accurate pre-clinical model will help increase the number of therapies which succeed in making it to patients in the clinic.

5.2.3 Objectives

To achieve this we will:

1) Challenge PCHS with proposed cardiac specific drivers of disease (recombinant human TGF-β1, CTGF, Angiotensin II, Galectin-3 or IL-11) for up to 96 hours in culture and quantify inflammation and fibrosis.
2) Unbiased analysis will be performed using RNA sequencing and proteomics to assess the success of inducing inflammation and fibrosis in PCHS.
3) Downstream analysis through the use of IPA will be utilised to identify potential candidate compounds to treat cardiac inflammation and fibrosis.
4) Toxicity and efficacy of candidate compounds will be quantified in cardiac fibroblasts and PCHS.

5.3 Materials and methods

5.3.1 Treatments for PCHS

5.3.1.1 Known pro-fibrotic recombinant protein stimuli

Left ventricular tissue either from patients undergoing LVAD surgery or from Unused Donors was used to produce PCHS as described in **Chapter 3**. After a 24hr rest period PCHS were stimulated with recombinant human TGF-β1 (10ng/ml), Angiotensin II (100nM), CTGF (50ng/ml), Galectin-3 (5µg/ml) or IL-11 (5ng/ml) **(Figure 29)**. Treatments were reapplied at 24hr intervals for a total of 72hrs. Media harvested at each time-point was snap frozen and stored for future analysis. PCHS were harvested at the terminal time-point, snap frozen and stored at -80°C for future analysis. In order to prepare PCHS for proteomic and RNA sequencing slices were washed 3 times using PBS warmed to 37°C. After the final wash, PBS was discarded and replaced with serum free media. Plates were then returned to the incubator and cultured for a further 3 hours at 37°C. After the incubation period PCHS were washed again in PBS prior to being snap frozen and stored at -80°C for either RNA sequencing or proteomic analysis.

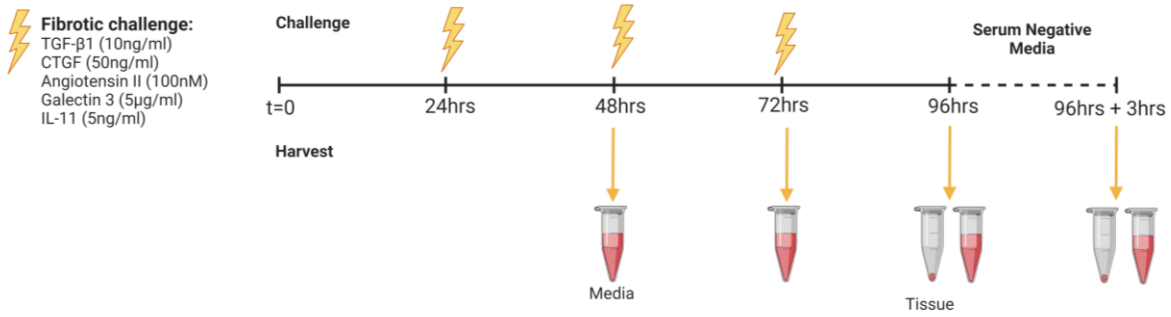

Figure 29. Schematic of PCHS treatments and harvest – Precision cut heart slices are cultured for 24 hours prior to application of any treatments. After 24hr rest period, culture media is removed and replaced with fresh media containing one of the following exogenous challenges: TGF-β1 (10ng/ml), CTGF (50ng/ml), Angiotensin II (100nM), Galectin-3 (5µg/ml) or IL-11 (5ng/ml) and cultured for a further 72 hours. Media is harvested and replenished containing fresh treatments every 24 hours until 96 hours of culture where media is harvested, snap frozen and stored at -80°C for future analysis. At 96 hours PCHS are washed 3 times in warmed PBS prior to further 3 hour culture in serum negative media, after which media and slices are harvested and snap frozen for transcriptomic and proteomic analysis – Created with BioRender.com

5.3.1.2 *Combination treatments on PCHS*

Slices were produced as previously described in **Chapter 3**. using Unused Donor tissue. Briefly, PCHS were rested for 24hrs prior to challenge with Angiotensin II (100nM), CTGF (50ng/ml), Galectin 3 (5µg/ml) or IL-11 (5ng/ml) either alone or in combination with TGF-β1 (10ng/ml). Treatments were reapplied at 24hr intervals for a total of 72hrs. Media was collected and snap frozen at each time point and tissue slices harvests at the terminal time point and stored at -80°C for future analysis.

5.3.1.3 *Application of Novel Compounds*

Human PCHS were generated from n=4 unused donors as previously described in **Chapter 3** and treatments detailed in **Figure 30**. Briefly, after an initial 24hr rest period slices were treated in the absence of exogenous challenge, with either control media alone, or control media containing either ALK5 inhibitor SB525334 (10µM), Pirfenidone (2.5mM) or Nintedanib (2.5µM) or one of the compounds described in **Table 6.** (10µM, 1µM or 0.1µM). Treatments were reapplied every 24hrs for a total of 72hrs of culture. Media was collected at each time-point and snap frozen then stored at -80°C for future analysis.

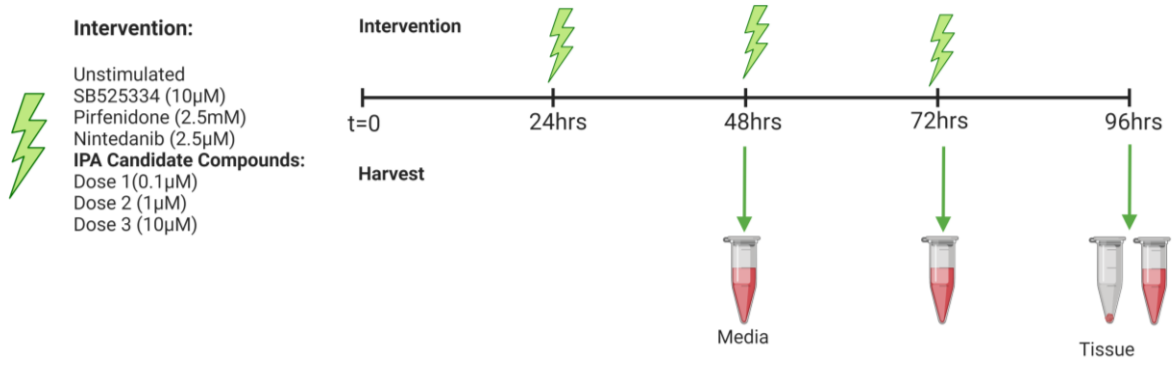

Figure 30. Treatment plan for candidate compounds applied to PCHS – Precision cut heart slices are cultured for 24 hours prior to application of any inhibitors or candidate compounds. After 24hr rest period, culture media is removed and replaced with fresh media containing IPA Candidate compounds (0.1µM, 1µM or 10µM) or positive control inhibitors; SB525334 (10µM), Pirfenidone (2.5mM) or Nintedanib (2.5µM) and cultured for a further 24 hours. Media is harvested and replenished containing fresh treatments every 24 hours until 96 hours of culture where both media and PCHS are harvested, snap frozen and stored at -80°C for future analysis - Created with BioRender.com

5.3.2 Treatments of Primary Cardiac Fibroblasts

5.3.2.1 Application of compounds identified from IPA

Human cardiac fibroblasts from n=5 donors were cultured in T-175 flasks until 85% confluent. Cells were split as described in **Chapter 3**, seeded into 96-well plates at a density of 5000 cells/well and cultured overnight at 37°C and 5% CO_2. Media was discarded and cells washed in warmed PBS prior to application of Serum free media, and cultured overnight **(Figure 31)**. Cells were treated for 24 hours with control media, SB525334 (10µM, 1µM or 0.1µM), Pirfenidone (2.5mM, 0.25mM or 0.025mM), Nintedanib (2.5µM, 0.25µM or 0.025µM) or IPA compounds (10µM, 1µM or 0.1µM) detailed in **Table 6**. All treatments were made up using serum free media. Following treatment, media was transferred into a round bottom 96-well plate and stored at -80°C for future analysis.

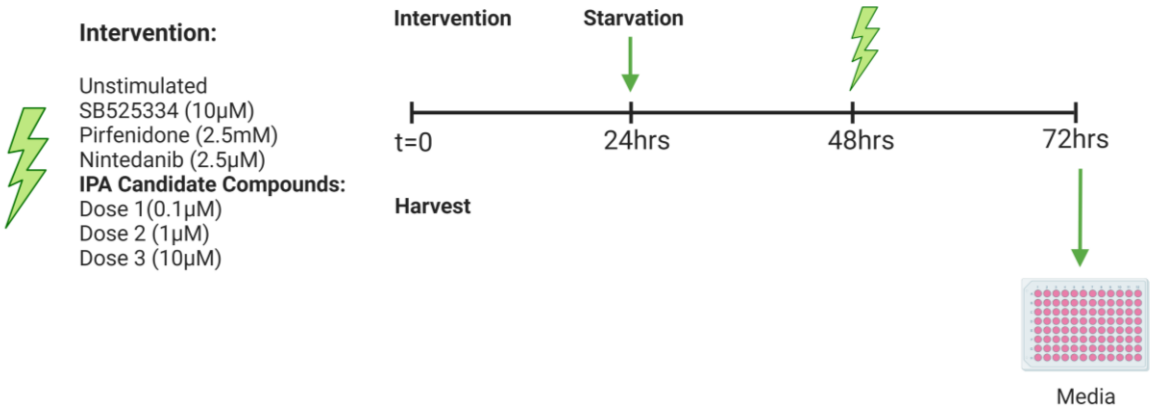

Figure 31. Treatment plan for candidate compounds applied to cardiac fibroblasts – Cardiac fibroblasts are cultured for 24 hours in serum free starvation media prior to application of inhibitors and candidate compounds. After 24hr starvation period, culture media is removed and replaced with fresh media containing IPA Candidate compounds (0.1µM, 1µM or 10µM) or positive control inhibitors; SB525334 (10µM), Pirfenidone (2.5mM) or Nintedanib (2.5µM) and cultured for a further 24 hours. Media is harvested, snap frozen and stored at -80°C for future analysis - Created with BioRender.com

Compound name	Target	Supplier	Product Code
GW9662	PPARγ Antagonist	Selleckchem	S2915
BAY 11-7082	NF-κB Inhibitor	Selleckchem	S2913
LY294002	PI3Kα/δ/β Inhibitor	Selleckchem	S1105
GB1107	Galectin-3 Inhibitor	MedChem Express	HY-114409
Paclitaxel/Taxol	Microtubule polymer stabiliser	Selleckchem	S1150
Erlotinib	EGFR Inhibitor	Selleckchem	S7786
PLX5622	CSF-1R Inhibitor	Selleckchem	S8874
Tempol	Superoxide Scavenger	Selleckchem	S2910
Camptothecin	DNA Topoisomerase Inhibitor	Selleckchem	S1288
Cycloheximide	Antifungal Antibiotic	Selleckchem	S7418
Mycophenolic Acid	IMPDH Inhibitor	Selleckchem	S2487
AG-490	EGFR Inhibitor	Selleckchem	S1143
Aspirin	COX1 and COX2 inhibitor	Selleckchem	S3017
Napabucasin	Stat3 Inhibitor	Selleckchem	S7977
Sorafenib	Multikinase Inhibitor	Selleckchem	S7397
Dexamethasone	Glucocorticoid steroid	Selleckchem	S1322
Tamoxifen	Oestrogen receptor	Selleckchem	S1238
Rapamycin	mTOR Inhibitor	Selleckchem	S1039
ABT-737	BH3 mimetic Inhibitor of BCL-2	Selleckchem	S1002
Rottlerin	PKC Inhibitor	Selleckchem	S7862
Ziritaxestat	Selective autotaxin Inhibitor	Selleckchem	S8895
Calcipotriene	Synthetic derivative of calcitriol, a form of vitamin D	Selleckchem	S3739
Resiquimod	TLR7/TLR8 Agonist	Selleckchem	S8133
PMA (Phorbol 12-myristate 13-acetate)	PKC activator	Selleckchem	S7791
Geldanamycin	HSP90 Inhibitor	Selleckchem	S2713
A23187	Calcium ionophore	Tocris	1234
Capsaicin	TRPV1 Agonist	Selleckchem	S1990
Acetaminophen (Paracetamol)	Cyclooxygenase Inhibitor	Tocris	1706
Dorsomorphin	AMPK and BMP type 1 receptor Inhibitor	Selleckchem	S7840
Immethridine Dihydrobromide	Histamine H_3 Receptor Agonist	Tocris	2315
H-7	Protein Kinase Inhibitor	Sigma	I6891

Table 6. Details of Candidate compounds identified from IPA Upstream Regulators – Shown above are the technical details regarding the candidate compounds identified from IPA Upstream Regulator Analysis which were applied to cardiac fibroblasts and PCHS. Product code, supplier and notes regarding their action are detailed.

5.3.3 ELISA on conditioned culture media from cardiac fibroblasts and PCHS

ELISA was performed on conditioned culture media collected from cardiac fibroblasts and PCHS as described previously in **Chapter 3**. R&D DuoSet ELISA kits were used to quantify the secretion of Collagen 1a1, TIMP-1, MCP-1, IL-6 and IL-8.

5.3.4 MesoScale Discovery™ (MSD) analysis of recombinant stimuli

Multiplex ELISA was performed on tissue culture supernatants from PCHS exposed to exogenous challenge (n=7 donors) as described in **Chapter 3**. Samples were analysed using a custom human U-Plex Multi-Spot Assay System (MSD) containing the following biomarkers; IL-6, IL-8, Eotaxin, MCP-1, MIP-1α and GRO-α. Results were analysed using the MSD Discovery Workbench 4.0 analysis software.

5.3.5 RNA Isolation, Integrity and analysis

Isolation of RNA from PCHS was performed as previously described in **Chapter 3**. For each condition n=2 PCHS were pooled (n=5 donors total) and RNA isolated using MagMax-96 Total RNA Isolation Kit (Invitrogen) as per the manufacturer's instructions. Briefly tissue was disrupted using Lysis Binding Solution and washed using isopropanol. Magnetic beads were added and the samples washed multiple times as per manufacturer's instructions. Genomic DNA was removed during DNase incubation following which RNA was eluted using 30µl Elution Buffer. RNA concentrations were assessed using IMPLEN nanophotometer as previously described.

5.3.6 RNA sequencing

1µg of total RNA was used to prepare TruSeq Stranded mRNA libraries (Illumina) as recommended by the manufacturer. Briefly, a total of 1µl of RNA was diluted to a final volume of 50µl in nuclease-free water. Then, mRNA was purified from the total RNA using RNA oligo dT purification beads. Purified mRNA was eluted and the process repeated to minimize non-specific binding. First strand of cDNA was synthesized using random hexamers, followed by generation of the second cDNA strand incorporating dUTPs instead of dTTPs. This way, the polymerase cannot incorporate nucleotides past the dUTPs, making the stranded library. Double strand cDNA was then purified using AMPure XD beads.

A single adenosine nucleotide was added on the 3' end to prevent the fragments from ligating one another. Indexed adapter ligation was done using a corresponding thymine nucleotide on the 3' end of the adapter. Fragments were then purified using AMPure XD beads. Enrichment of DNA library fragments was done by PCR. Then, libraries were validated using Agilent High Sensitivity DNA 1000 chip according to manufacturer instructions. In brief, for the High Sensitivity DNA chip, gel-dye was added into the adequate gel well and allowed to settle across the chip. Then, the ladder, marker and 1µl of library samples are added. The chip was then run in the 2100 Bioanalyser.

Finally, libraries were normalized to 10nM and sequenced for 100 cycles on NovaSeq 6000 system using a NovaSeq S1 cartridge.

5.3.7 Proteome sample preparation

PCHS from n=6 donors were challenged with recombinant proteins and harvested as previously described. Total cell lysate preparation from PCHS and proteomic analysis was performed by Dr Sandra Murphy. PCHS were placed in 200µl SDS lysis buffer (5% SDS, 50mM triethylammonium bicarbonate (TEAB) pH 7.5) then lysed by homogenisation using Qiagen Tissue Lyser II bead homogeniser. Protein concentration was determined by the bicinchoninic acid assay (BCA). A total of 20 µg protein was reduced by incubation with 5mM tris(2-carboxyethyl)phosphine (TCEP) for 20 min at 37°C, and subsequently alkylated with 20mM iodoacetamide for 20 min at room temperature in the dark. Protein digestion was performed as per the manufacturer's guidelines (ProtiFi™, Huntington NY) using the suspension trapping (S-Trap™) sample preparation method. Briefly, 12% phosphoric acid was added to each sample, prior to the addition of 165µl S-Trap binding buffer (90% methanol in 100mM TEAB, pH 7.1). Sample were then added to the S-Trap Micro spin column. Following this samples were centrifuged at 4,000 x g for 2 min and samples passed through a filter. Next, a S-Trap Mini-spin columns were washed by centrifugation (4000xg for 1 min) with S-trap binding buffer. This process was repeated four time. Next, each sample had 50 mM TEAB, pH 8.0 containing trypsin (1:20 ratio of trypsin to protein) added, prior to proteolytic digestion for 4 hours at 47°C using a thermomixer (Eppendorf). Peptides were eluted with 50 mM TEAB pH 8.0 followed by centrifugation at 4,000 x g for 2 min. The elution steps were repeated using

0.2% formic acid and 0.2% formic acid in 50% acetonitrile. A total of three eluates from each sample were combined and dried using a speed-vac prior to storage at -80°C.

Peptides were resuspended in 5% formic acid and each digested sample was analysed on an Orbitrap Fusion Lumos Tribrid mass spectrometer (Thermo Fisher Scientific), connected to a UltiMate 3000 RSLCnano System (Thermo Fisher Scientific). Peptides were injected on an Acclaim PepMap 100 C18 LC trap column (300µm ID × 5 mm, 5µm, 100 Å) followed by separation on an EASY-Spray nanoLC C18 column (75 IDµm × 500 mm, 2µm, 100 Å) at a flow rate of 25 $nlmin^{-1}$. Solvent A was water containing 0.1% formic acid, and solvent B was 80% acetonitrile containing 0.1% formic acid. The gradient used was as follows: solvent B was maintained at 2% for 5 min, followed by an increase from 2 to 35% B in 120min, 35-90% B in 0.5min, maintained at 90% B for 4 min, followed by a decrease to 2% in 0.5min and equilibration at 2% for 10 min. The Orbitrap Fusion Tribrid mass spectrometer was operated in data dependent, positive ion mode. Full scan spectra were acquired in a range from 400 m/z to 1600 m/z, at a resolution of 120,000, with automated gain control (AGC) set to standard and a maximum injection time of 50ms. Precursor ions were isolated with a quadrupole mass filter width of 1.6 m/z and HCD fragmentation was performed in one-step collision energy of 30%. Detection of MS/MS fragments was acquired in the linear ion trap in rapid mode using a Top 3s method, with AGC target set to standard and a dynamic maximum injection time. The dynamic exclusion of previously acquired precursors was enabled for 35s with a tolerance of +/-10 ppm.

MaxQuant (Version 1.6.10.43) was used to analyse all data produced using the SwissProt *homo sapiens* fasta file. Contaminants were identified using a contaminant sequence set provided by MaxQuant. The generation of the Peak list was performed within MaxQuant. A False Discovery Rate of 1% was allowed for both proteins and peptides. The MaxLFQ algorithm was used to calculate the LFQ intensities.

5.3.8 Downstream analysis of RNA sequencing results

Quality control analysis of fastq files was performed using fastQC (Available online at: http://www.bioinformatics.babraham.ac.uk/projects/fastqc/). Sequences were trimmed using trimmomatic software. The trimmed sequences were quality control analysed again, to ensure the sequences had enough quality to be used for further analysis. Mapping and

quantification of sequences was performed using salmon software. First, transcript index was created using Human genome assembly release 31 (gencode.v31.pc_transcripts.fa). Then, pseudo-mapping and quantification of the mRNA sequences were performed. Salmon quantification values were then uploaded into R Studio for differential expression (DE) analysis. DE analysis was performed using R studio (version 1.2.1335). mRNA counts were imported into R using 'tximport' R package; and counts matrix was created using DESeq2 R package. The estimation of the dispersion, normalization and PCA were performed using DESeq2 R package. As mentioned previously, usually for count data the statistical model is the binomial distribution. However, as mRNA sequencing has a variance higher than the mean, the model commonly a negative binomial distribution is used to model RNA count data. In this analysis a negative binomial GLM was applied using DESeq2 R package. mRNA were classified as significant differently expressed when log2 fold change >1.5 and p-value (adjusted) <0.01.

5.3.9 Ingenuity Pathway Analysis

IPA is a bioinformatic tool for the analysis, integration, and interpretation of omics data. Significant data from all comparisons were uploaded in IPA (QIAGEN, version 01.20.04) and core expression analysis was performed using log2 fold change differences for z-score and prediction calculations. Only genes from the ingenuity knowledge base were used as reference and all direct and indirect relations, tissues, node types and data sources from experimentally observed data were considered. All networks were created in IPA and visually modified using its Path Designer tool.

5.3.10 Statistical Analysis

5.3.10.1 Precision Cut Heart Slice cultures

Statistical analysis was performed on datasets using GraphPad Prism 9.4.1. Results are presented as mean ± standard error of the mean (SEM). Statistical analysis comprised of paired t-tests, paired t-test with multiple comparisons or ANOVA mixed effects analysis with Dunnett's multiple comparisons. Data were considered statistically significant with a p value ≤0.05 *, p≤0.01 **, p≤0.001 *** and p≤0.0001 ****.

5.3.10.2 Proteomics

Statistical analysis was performed using R (version 4.0.3). The data was first filtered to remove proteins that matched to a contaminant or a reverse database, or which were only identified by site. Only proteins identified by a minimum of 2 unique peptides were retained. LFQ intensity values were log2 transformed, and data filtered to contain at least 3 valid values in all 6 groups. LIMMA was used for statistical analysis where proteins with a p-value < 0.05 were considered as statistically significant.

5.3.10.3 RNA Sequencing

Significant mRNA values were defined as having a Log2 fold change >1.5 or <1.5 and adjusted P value (Padj) <0.01. GraphPad prism version 9.4.1 was used to create volcano plots and heatmaps.

5.4 Results

5.4.1 Exploring other pathways involved in Cardiac Fibrosis

There are a number of different pathways and molecules hypothesised to be important in the development of cardiac fibrosis. In order to investigate whether a selection of these proposed drivers of cardiac fibrosis would be effective in our PCHS system we exogenously challenged n=6 unused donor hearts with recombinant human proteins of five different stimuli known to be involved in the development of cardiac fibrosis *in vivo*. After an initial 24 hour rest period post-slicing, PCHS were challenged with either control media, TGF-β1 (10ng/ml), connective tissue growth factor (CTGF) (50ng/ml), Angiotensin II (100nM), Galectin-3 (5µg/ml) or IL-11 (5ng/ml). Treatment doses were chosen after careful study of appropriate literature. Slices were challenged for a total of 72 hours, with media harvested and replenished with fresh treatments daily. After 96 hours in culture, media and PCHS were harvested. Culture supernatants were analysed *via* ELISA to assess changes in the secretion of markers of inflammation and fibrosis.

Our initial analysis explored the ability of the five exogenous stimuli to exert a pro-inflammatory response from the PCHS, quantified by the measurement of IL-6, IL-8 and MCP-1 secretion. These three cytokines play important roles in both the recruitment of immune cells to the site of injury but also the exacerbation of chronic inflammation and damage which can eventually lead to the formation of a fibrotic scar. Our data showed that Galectin-3 produced a robust pro-inflammatory response from PCHS, significantly elevating the secretion of IL-6, IL-8 and MCP-1 across the entire culture period **(Figures 32 and 33)**. The magnitude of the induction of secretion of the inflammatory markers was greatest after 48 hours in culture, reducing by 96 hours. The only other exogenous stimuli to elicit an inflammatory response in the PCHS were TGF-β1 and CTGF. Stimulation with TGF-β1 induced IL-6 and MCP-1 secretion by 72 hours in culture, and this increase was sustained at 96 hours. CTGF was the only other stimuli to have an effect on one of the pro-inflammatory markers, significantly increasing MCP-1 levels at 48 and 72 hours in culture.

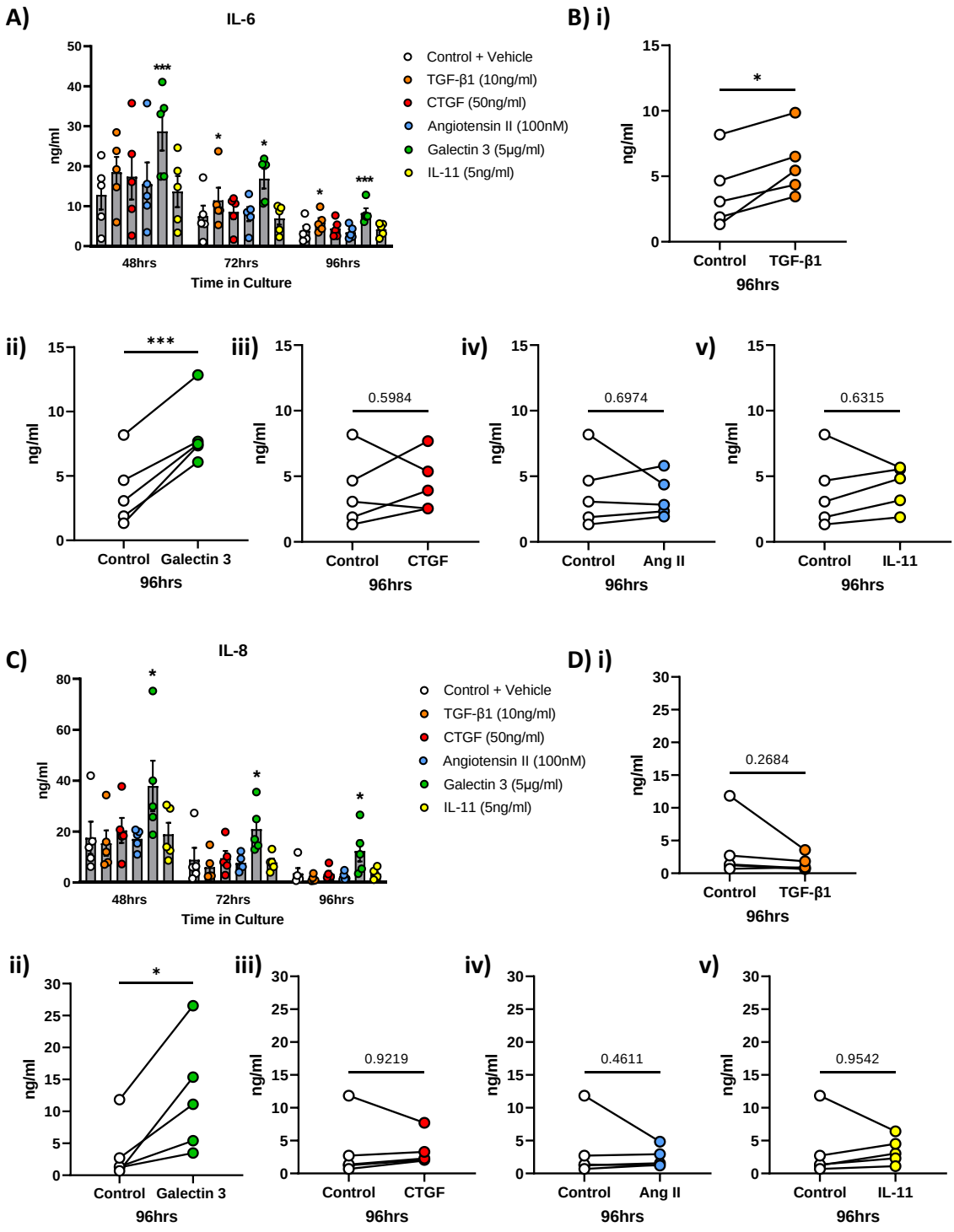

Figure 32. Galectin-3 induced inflammatory response from Unused donor PCHS – After a 24 hour rest period, PCHS were treated with either control media (unstimulated), recombinant human (rh) TGF-β1 (10ng/ml), CTGF (50ng/ml), Angiotensin II (100nM), Galectin-3 (5µg/ml) or IL-11 for a further 72 hours. Media was collected and treatments refreshed daily. Supernatants from the slices were collected and protein secretion of markers of inflammation was measured using DuoSet ELISA. N=5 donors. Data are mean ± SEM. * p<0.05, ***<0.001.

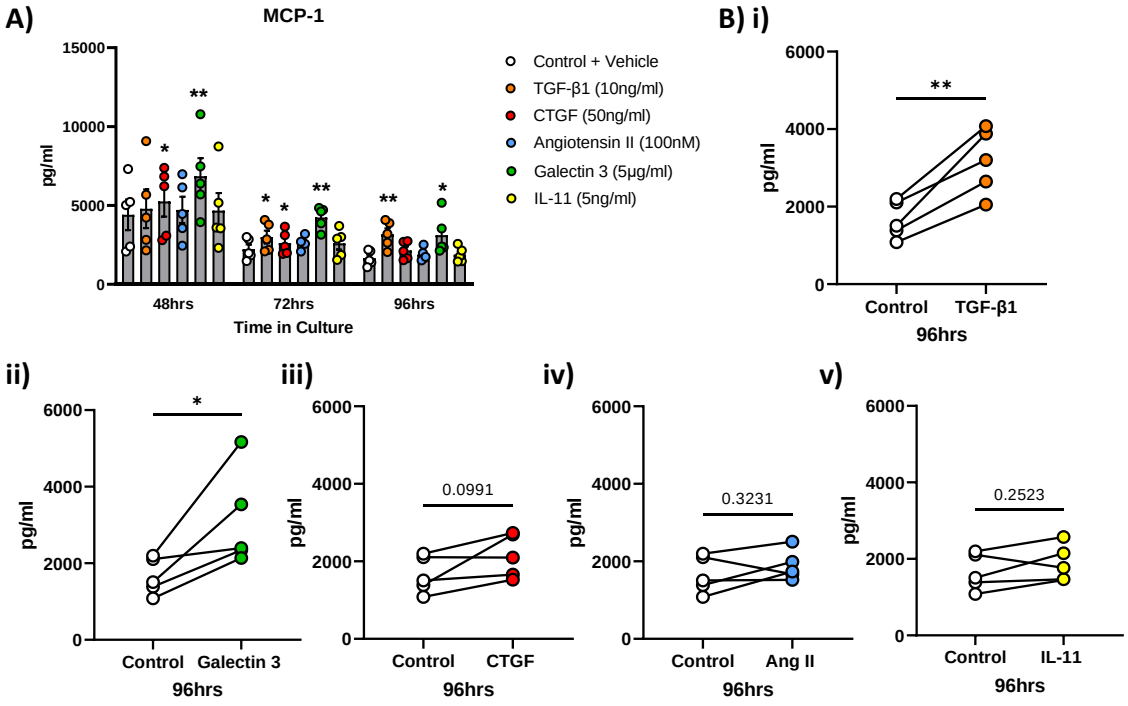

Figure 33. Galectin-3 induced inflammatory response from unused donor PCHS – After a 24 hour rest period, PCHS isolated from unused donor tissue were treated with either control media (unstimulated), recombinant human (rh) TGF-β1 (10ng/ml), CTGF (50ng/ml), Angiotensin II (100nM), Galectin-3 (5µg/ml) or IL-11 (5ng/ml) for a further 72 hours. Media was collected and treatments refreshed daily. Supernatants from the slices were collected and MCP-1 secretion was measured using DuoSet ELISA. N=5 donors. Data are mean ± SEM. * p<0.05, **<0.01.

We next assessed the ability of the exogenous stimuli to induce a pro-fibrotic response from the PCHS through the quantification of Collagen 1a1 and TIMP-1 secretion **(Figure 34)**. The secretion of Collagen 1a1 was significantly elevated from PCHS challenged with TGF-β1 after 96 hours in culture. Collagen 1a1 secretion was also significantly induced after challenge with CTGF and Angiotensin II at the 96 hour time-point only **(Figure 34A iii and iv)**. Despite recent research suggesting the importance of IL-11 in driving fibrosis, it, along with Galectin-3, was unable to induce a significant increase in collagen 1a1 secretion at any time-point. TIMP-1 is an inhibitor of matrix metalloproteinases or MMPs. MMPs are involved in the degradation of ECM, therefore elevated levels of TIMP-1 secretion may result in the inhibition of MMP action and therefore the build-up of ECM proteins. In response to our exogenous stimuli, TIMP-1 secretion was significantly elevated in response to Galectin-3 at 48 and 72 hours in culture, however this response was blunted by 96 hours. Unlike collagen 1a1 secretion, TGF-β1 was unable to significantly induce TIMP-1, despite a trend to increased secretion in five of the six donors after 96 hours in culture. Any significant effects of TGF-β1 on TIMP-1 secretion was blunted by a donor with very high basal levels of TIMP-1 secretion across all time-points but especially at 96 hours (~100ng/ml). As with many of the other secreted markers, IL-11 and Angiotensin II had no effect on TIMP-1 secretion.

These data show that Galectin-3 is able to induce a potent pro-inflammatory response in PCHS, and that whilst unable to induce an increase in components of the ECM (Collagen 1a1), the significant increase in TIMP-1 secretion may suggest a role in the prevention of its degradation. Through the application of TGF-β1 we have shown the ability to drive the PCHS to produce a classical pro-fibrotic response, as characterised by Collagen 1a1 and TIMP-1 secretion. However the effects of the other exogenous proteins were limited.

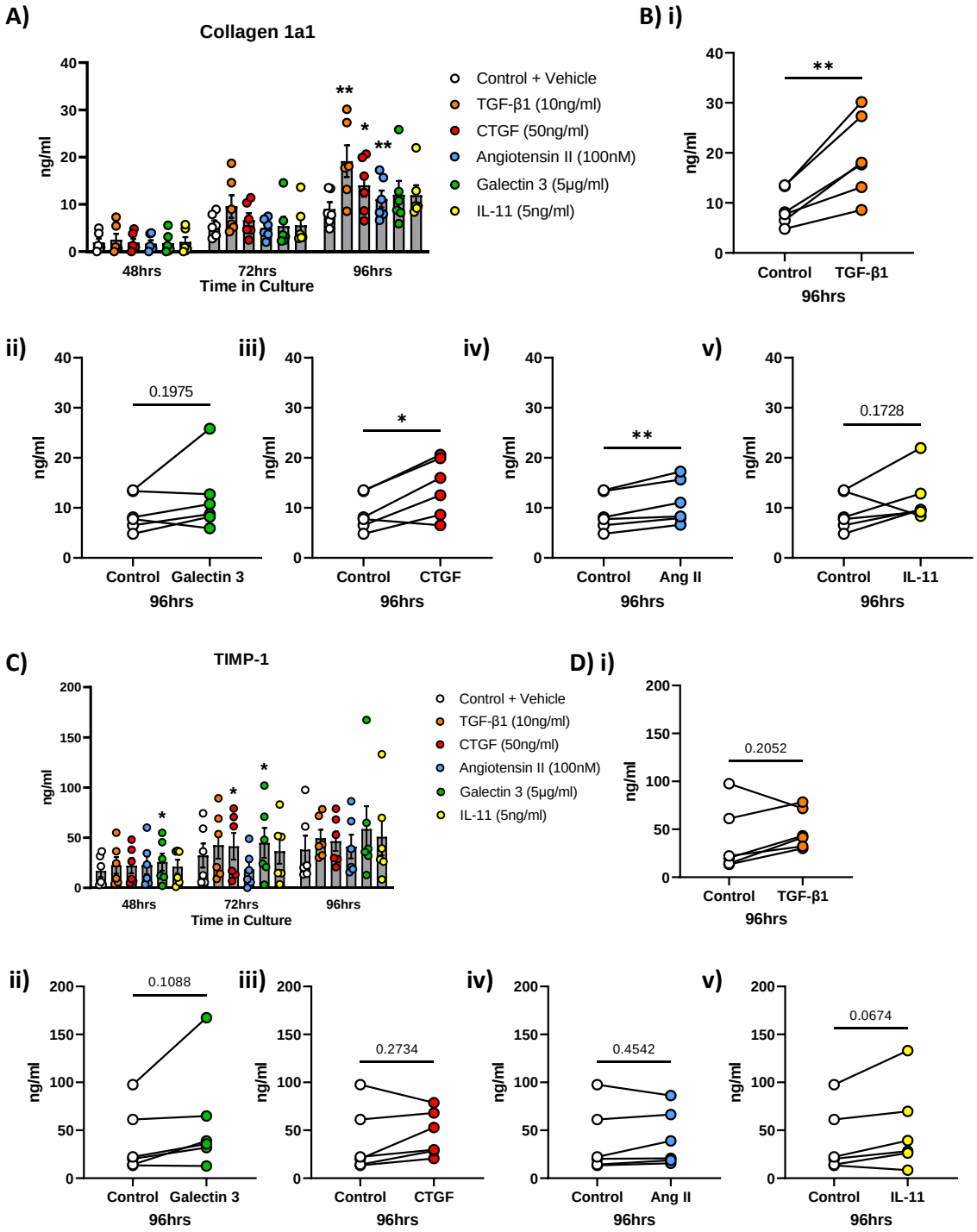

Figure 34. Induction of fibrogenic response from Unused Donor PCHS – After a 24 hour rest period, PCHS isolated from unused donor tissue were treated with either control media (unstimulated), recombinant human (rh) TGF-β1 (10ng/ml), CTGF (50ng/ml), Angiotensin II (100nM), Galectin-3 (5µg/ml) or IL-11 (5ng/ml) for a further 72 hours. Media was collected and treatments refreshed daily. Supernatants from the slices were collected. Collagen 1a1 and TIMP-1 secretion was measured using DuoSet ELISA. N=5 donors. Data are mean ± SEM. * p<0.05, **<0.01.

Next we investigated the protein secretion from PCHS in response to combination treatments of the exogenous stimuli **(Figures 35-36)**. PCHS from n=4 donors were treated with CTGF, Angiotensin II, Galectin-3 or IL-11 alone or in combination with TGF-β1 for a total of 72 hours. Media was harvested at 96 hours and protein secretion quantified by ELISA. Inflammation and fibrosis was assessed through the quantification of IL-6 **(Figure 35)** and collagen 1a1 **(Figure 36)** secretion respectively.

As previously observed, TGF-β1 was able to significantly induce IL-6 secretion compared to control treat slices, interesting IL-11 had a small but significant effect also **(Figure 35D)**. However combination of TGF-β1 with either CTGF, IL-11 or Angiotensin II was unable to further induce IL-6 secretion above that of TGF-β1 treatment alone. Once again Galectin-3 induced a highly significant increase of IL-6 secretion compared to control, whilst also exhibiting an additive effect when in combination with TGF-β1 **(Figure 35C)**. However it is worth noting there was no increase between Galectin-3 alone and the combination treatment. **Figure 36** depicts the effect of combination treatment on collagen 1a1 secretion. As demonstrated with earlier results, CTGF and Angiotensin II were able to significantly induce collagen 1a1 secretion compared to control **(Figure 36A and B)**. Results also show that despite significant increases in collagen 1a1 secretion in response to each of the combination treatments it was unable to induce secretion above levels seen with TGF-β1 treatment alone.

Taken together these results show that there is an additive effect on IL-6 secretion through combinational challenge of the PCHS with Galectin-3 and TGF-β1. However no additional effects were found with any of the combination challenges on Collagen 1a1 secretion, with TGF-β1 treatment providing the maximal response in PCHS.

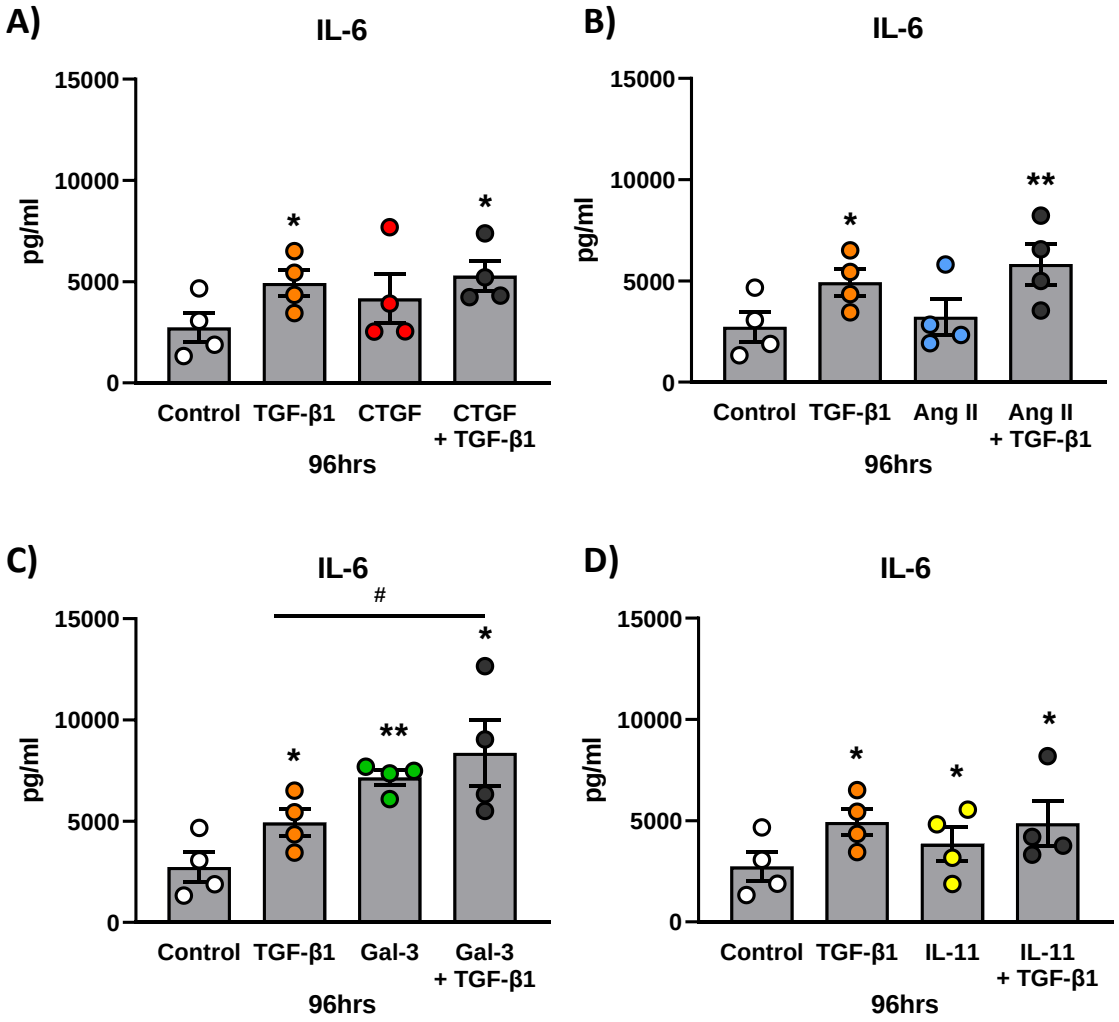

Figure 35. Combination treatment is unable to further induce inflammatory response from PCHS – After a 24 hour rest period, PCHS were treated with either control media (unstimulated), recombinant human (rh) TGF-β1 (10ng/ml), CTGF (50ng/ml), Angiotensin II (100nM), Galectin-3 (5µg/ml) or IL-11 (5ng/ml) alone or in combination with TGF-β1 (10ng/ml) for a further 72 hours. Media was collected and treatments refreshed daily. Supernatants from the slices were harvested and IL-6 secretion was measured using DuoSet ELISA. N=4 donors. Data are mean ± SEM. * p<0.05, **<0.01.

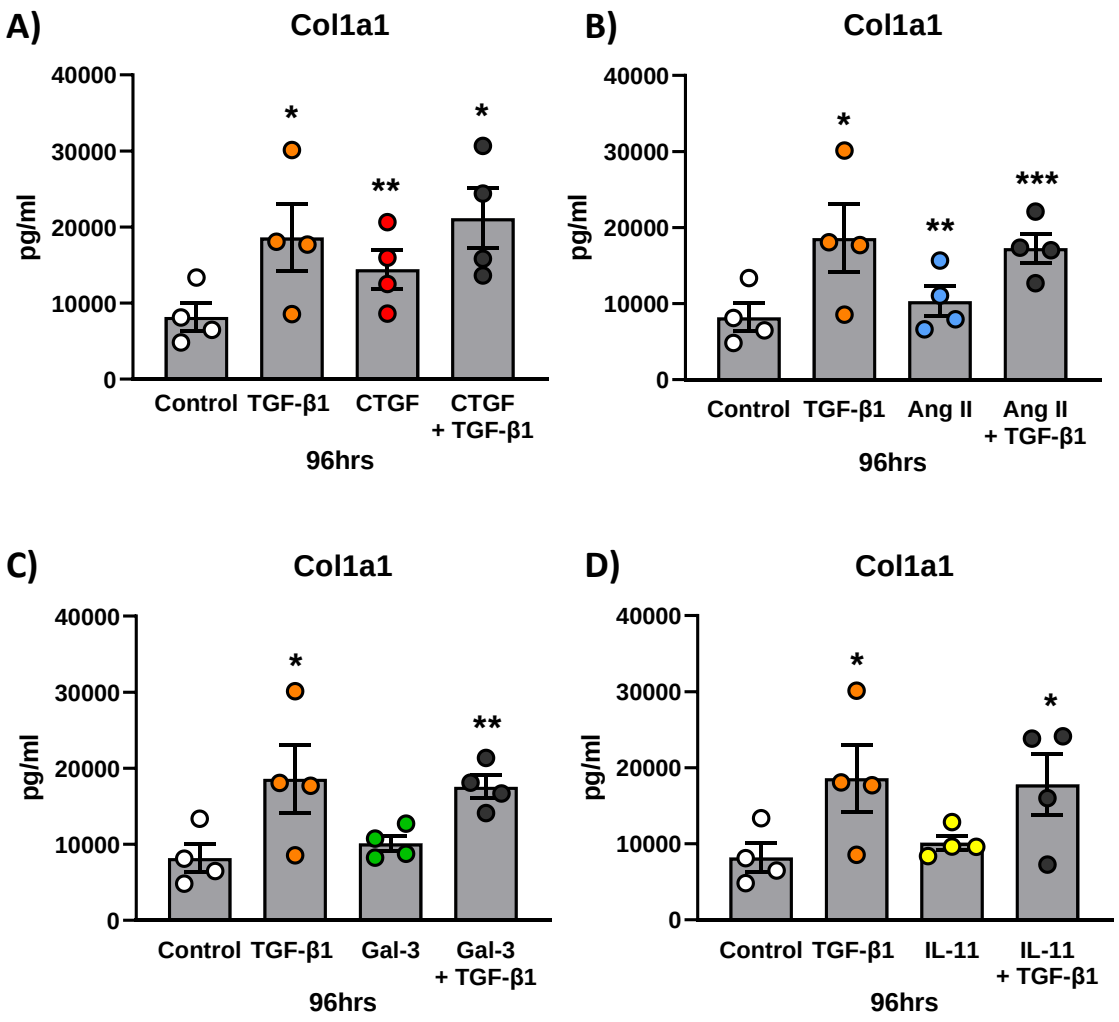

Figure 36. Combination treatment is unable to further induce collagen 1a1 secretion – After a 24 hour rest period, PCHS were treated with either control media (unstimulated), recombinant human (rh) TGF-β1 (10ng/ml), CTGF (50ng/ml), Angiotensin II (100nM), Galectin-3 (5µg/ml) or IL-11 (5ng/ml) alone or in combination with TGF-β1 (10ng/ml) for a further 72 hours. Media was collected and treatments refreshed daily. Supernatants from the slices were harvested and Collagen 1a1 secretion was measured using DuoSet ELISA. N=4 donors. Data are mean ± SEM. * p<0.05, **<0.01.

Having assessed the effect of the exogenous stimuli using hearts deemed unsuitable for transplant we next explored the responses of PCHS from donors undergoing LVAD surgery. This was to investigate any potential differences in the response to exogenous challenge of PCHS from tissue with pre-existing disease and damage. After an initial 24 hour rest period, slices from n=7 donors were challenged with TGF-β1, CTGF, Angiotensin II, Galectin-3 or IL-11 as previously described. Media was collected every 24 hours for analysis of secreted proteins by ELISA and MSD. At the terminal time-point slices were also harvested for analysis by bulk RNA sequencing and proteomics.

Figures 37 and 38 depicts the secretion of inflammatory markers from PCHS in response to the exogenous challenges. IL-6 secretion was highly inducible by Galectin-3 treatment, increasing 6-fold compared to control at 48 hours. The response to Galectin-3 was maintained throughout the treatment period despite reducing from an average of 16.5ng/ml to 5.7ng/ml by 96 hours **(Figure 37A)**. The only other treatment able to induce a change in IL-6 levels was TGF-β1, confirming earlier results. TGF-β1 treatment increased IL-6 by 2.3-fold compared to control at 48 hours. Galectin-3 confirmed its ability to induce a broad inflammatory response from the PCHS by also significantly increasing both IL-8 and MCP-1 secretion, an effect maintained over the entire culture period **(Figures 37C and 38A)**. As observed with IL-6 secretion, both IL-8 and MCP-1 were most strongly induced after 24 hours of treatment, with the magnitude of secretion decreasing over time. All other exogenous stimuli were unable to induce any response in IL-8 or MCP-1 secretion, although TGF-β1 treatment was trending towards a significant induction of MCP-1 secretion after 48 hours in culture **(Figure 38 Bi)**.

Next we proceeded to quantify changes in the secretion of fibrogenesis markers in response to the different stimuli. **Figure 39A** shows the changes in the secretory profile over the entirety of the 96 hour culture period. Much like we demonstrated in the unused donor slices, only at the 96 hour time point were significant increases observed. TGF-β1 induced a 2-fold increase in Collagen 1a1 secretion in response to TGF-β1 **(Figure 39 Bi)**. None of the other exogenous stimuli were able to increase Collagen 1a1 secretion across the culture period. As observed in the unused donor slices, TIMP-1 secretion had greater variation between the different donors **(Figure 39C)**. Once again Galectin-3 was able to induce TIMP-1 secretion, reaching statistical significance by 72 hours in culture. This response was maintained until 96 hours, resulting in a 1.3-fold induction in TIMP-1 secretion **(Figure 39D ii)**. Both TGF-β1 and CTGF were trending towards increased TIMP-1 secretion, however due to high basal levels of TIMP-1 secretion from some of the donors, statistical significance was not attained. IL-11 and Angiotensin II were unable to effect the secretion of Collagen 1a1 or TIMP-1.

These data demonstrate the ability to induce either an inflammatory or fibrotic response in PCHS across the 96 hour culture period. TGF-β1 was able to significantly increase Collagen 1a1 and IL-6 secretion, hallmarks of fibrosis progression, whilst Galectin-3 was a potent inducer of inflammation within the system.

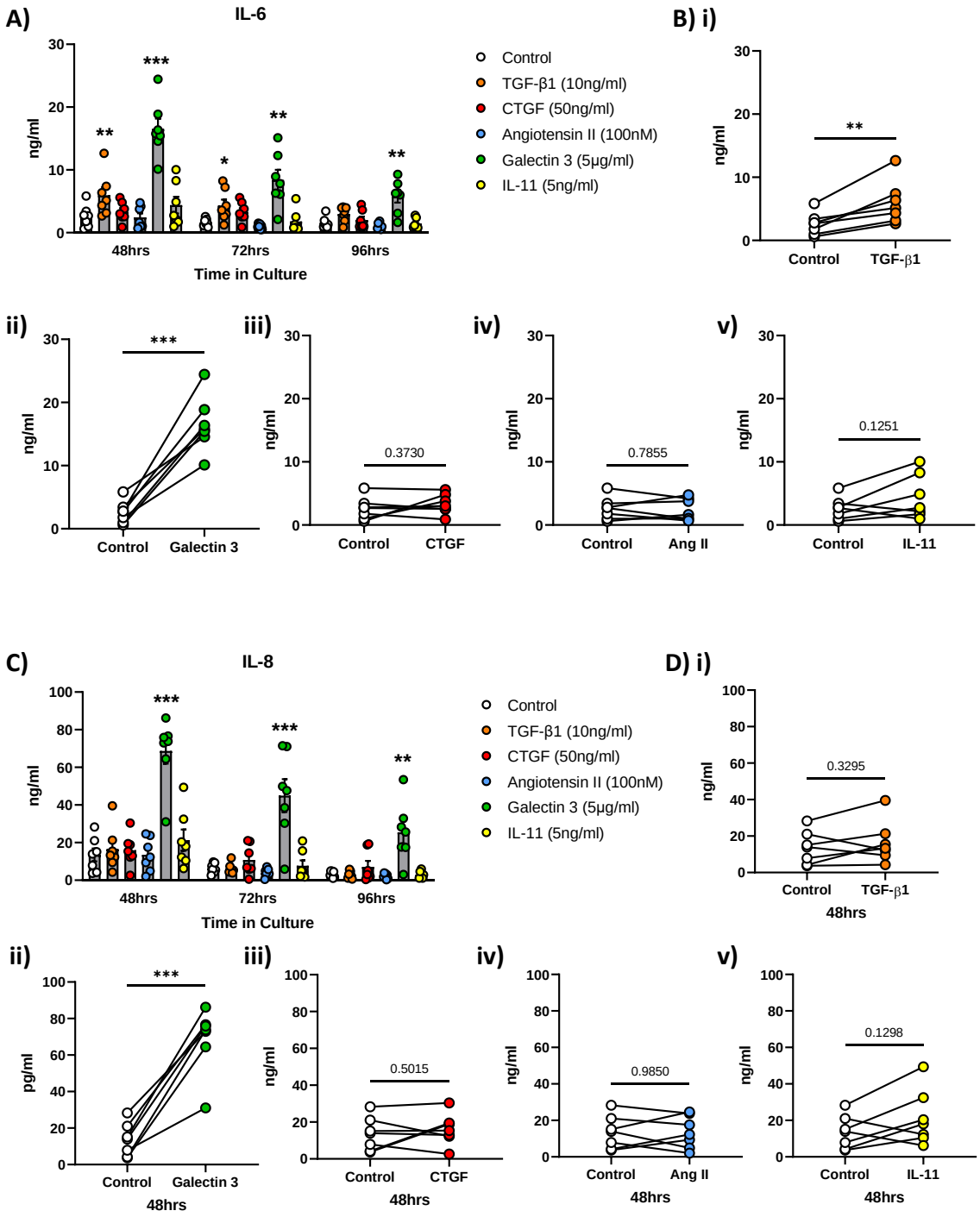

Figure 37. Induction of inflammatory phenotype from LVAD PCHS in response to exogenous challenge – After a 24 hour rest period, PCHS isolated from LVAD donor tissue were treated with either control media (unstimulated), recombinant human (rh) TGF-β1 (10ng/ml), CTGF (50ng/ml), Angiotensin II (100nM), Galectin-3 (5μg/ml) or IL-11 (5ng/ml) for a further 72 hours. Media was collected and treatments refreshed daily. Supernatants from the slices were collected and protein secretion of markers of inflammation were measured using DuoSet ELISA. N=7 LVAD donors. Data are mean ± SEM. *<0.05, **<0.01, ***<0.001.

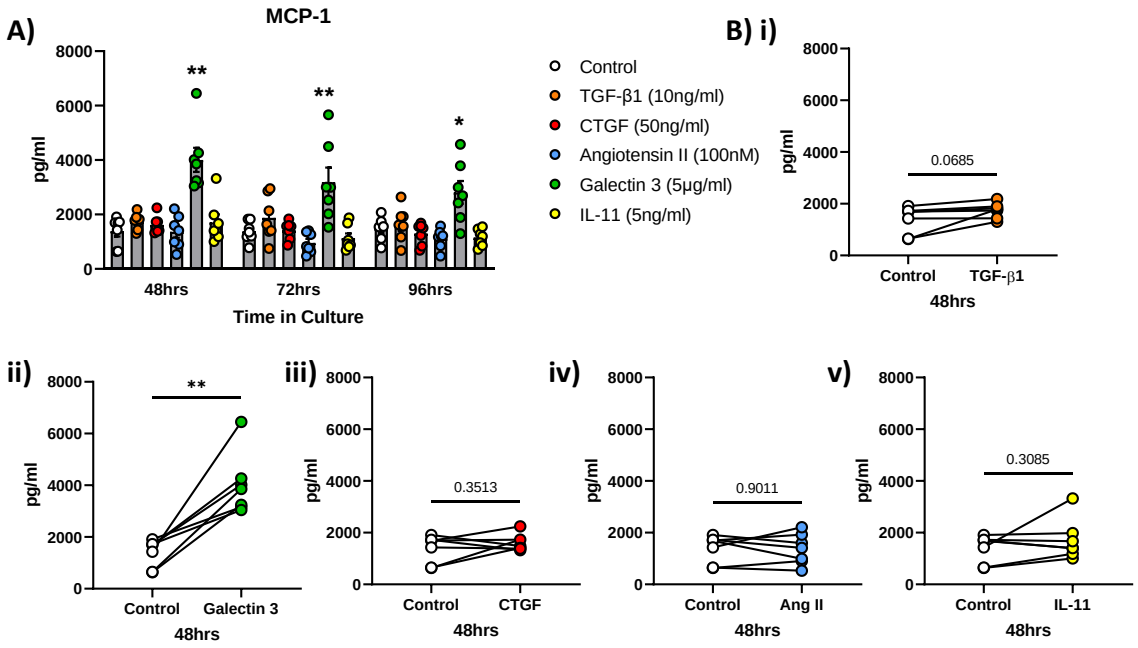

Figure 38. Induction of inflammatory phenotype from LVAD PCHS in response to exogenous challenge – After a 24 hour rest period, PCHS isolated from LVAD donor tissue were treated with either control media (unstimulated), recombinant human (rh) TGF-β1 (10ng/ml), CTGF (50ng/ml), Angiotensin II (100nM), Galectin-3 (5µg/ml) or IL-11 (5ng/ml) for a further 72 hours. Media was collected and treatments refreshed daily. Supernatants from the slices were collected and protein secretion of markers of MCP-1 was measured using DuoSet ELISA. N=7 LVAD donors. Data are mean ± SEM. *<0.05, **<0.01, ***<0.001.

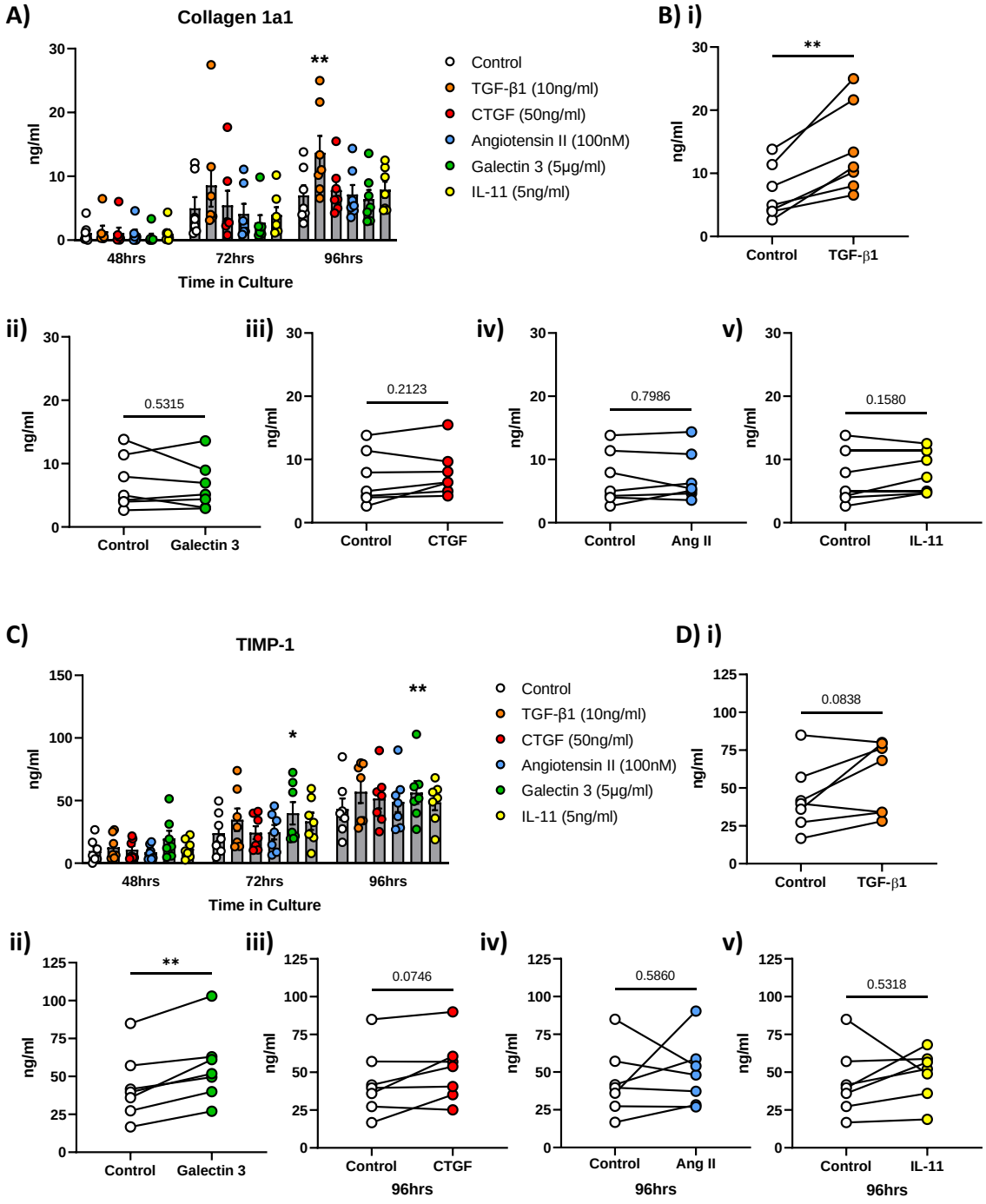

Figure 39. Induction of fibrotic phenotype from LVAD PCHS in response to exogenous challenge – After a 24 hour rest period, PCHS isolated from LVAD donor tissue were treated with either control media (unstimulated), recombinant human (rh) TGF-β1 (10ng/ml), CTGF (50ng/ml), Angiotensin II (100nM), Galectin-3 (5µg/ml) or IL-11 (5ng/ml) for a further 72 hours. Media was collected and treatments refreshed daily. Supernatants from the slices were collected and protein secretion of markers of fibrosis were measured using DuoSet ELISA. N=7 LVAD donors. Data are mean ± SEM. **<0.01.

We next sought to assess whether there were any differences between the disease phenotypes of the LVAD donor tissues in response to either Galectin-3 (at T48) or TGF-β1 (at T96) **(Figure 40)**. Inflammatory responses were assessed by the quantification of IL-8, MCP-1 and IL-6, whilst fibrotic responses were measured by Collagen 1a1, TIMP-1 and IL-6 protein secretion. The acute inflammatory response induced through the treatment of PCHS with Galectin-3 was uniform across the three different disease phenotypes of donor tissue as well as between the 3 different inflammatory markers assessed. In contrast, the response of PCHS after TGF-β1 treatment, measured by TIMP-1 and IL-6 secretion varied between donors. TIMP-1 secretion increased in response to TGF-β1 treatment in 5 of the 7 donors. However, in both the DCM and Ischaemic cardiomyopathy groups there was one donor which had no elevated TIMP-1 secretion as a result of TGF-β1 challenge. Finally the response of Ischaemic cardiomyopathy donor tissue differed to that of tissue from both DCM and other (transposition of the great arteries) donors. In response to TGF-β1, IL-6 secretion was elevated in only one Ischaemic cardiomyopathy donor, whilst in there other two donors a reduction in IL-6 was observed compared to untreated control PCHS.

Whilst these differences in the response of PCHS isolated from different tissue phenotypes could potentially provide important and interesting data regarding disease specific effects, it is important to appreciate the small sample sizes for each group. In order to fully elucidate any disease specific differences, a greater number of donors would be required.

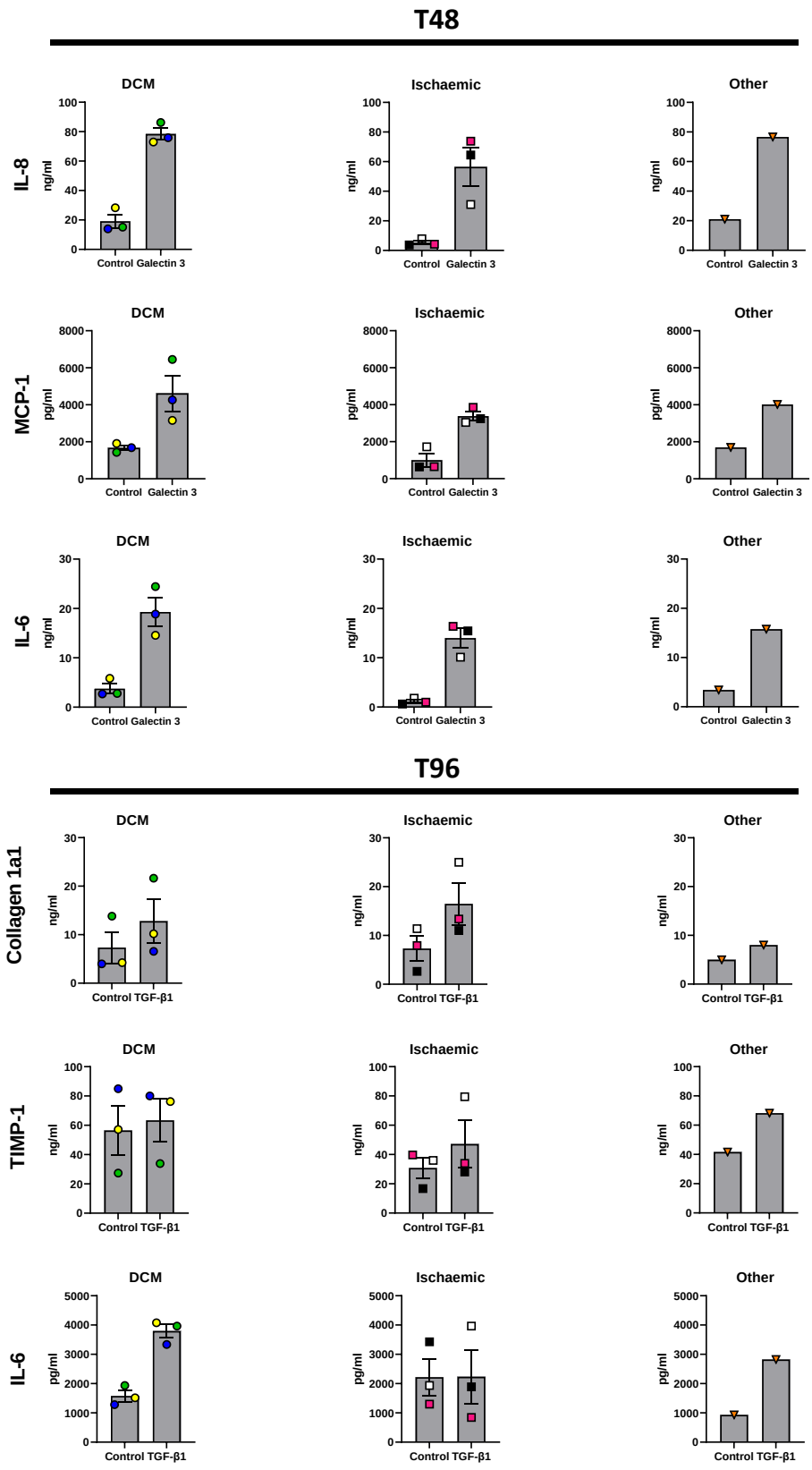

Figure 40. Response of PCHS to treatment highlighting underlying disease pathology – Secretion of soluble proteins were quantified from PCHS isolated from LVAD Donors treated with either Galectin-3 (5µg/ml) or TGF-β1 (10ng/ml). Results are separated depending on underlying disease pathology of LVAD donors. PCHS from the same donor are displayed as the same coloured symbol irrespective of treatment applied. N=3 Dilated Cardiomyopathy (DCM); n=3 Ischaemic Cardiomyopathy or n=1 Other (Transposition of the great arteries). NHH010: Yellow circle; NHH011: Orange triangle; NHH012: Black square; NHH014: Pink square; NHH019: Blue circle; NHH020: White square and NHH022: Green circle. Data are mean ± SEM.

Having demonstrated the ability of Galectin-3 and TGF-β1 to effect the secretion of a small number of selected pro-inflammatory or pro-fibrotic markers it was important to expand the number of markers quantified. Multi-plex ELISA was utilised to quantify changes in the secretion of Eotaxin, GRO-α and MIP-1α in tissue culture supernatants from PCHS challenged with either TGF-β1 or Galectin-3 at 48 hours and 96 hours in culture **(Figure 41)**. The recombinant proteins CTGF, Angiotensin II and IL-11 were excluded from this analysis due to the inability to induce any changes in protein secretion from PCHS. Challenge with recombinant TGF-β1 did not increase secretion of Eotaxin, GRO-α or MIP-1α at either time-point. Levels of these inflammatory markers remained similar to control, with the exception of MIP-1α and GRO-α secretion at 96 hours. **Figure 41 Ci)** shows that TGF-β1 treatment resulted in a significant reduction in MIP-1α secretion, this trend was also observed for GRO-α at 96 hours, although it failed to reach statistical significance. As with the other inflammation markers, Galectin-3 was able to significantly induce secretion of Eotaxin, GRO-α and MIP-1α at both 48 and 96 hours in culture. Despite this the magnitude of response was reduced at 96 hours for all three markers when compared to 48 hours. These data further confirm the ability of Galectin-3 to induce a strong inflammatory signature in the cultured PCHS and the role Galectin-3 may play during the early stages of damage and inflammation during the progression to fibrosis.

The final soluble markers we assessed in response to TGF-β1 and Galectin-3 challenge were IL-11 and CTGF **(Figure 42)**. These two molecules are known to be induced by TGF-β1 *in vivo*, and whilst we did not observe any effects when challenging PCHS with recombinant CTGF or IL-11 it was important to assess whether their expression could be modulated by either TGF-β1 or Galectin-3 within our model. Both CTGF and IL-11 were strongly induced by TGF-β1 treatment, IL-11 secretion remained stable between 48 and 96 hours whilst CTGF increased on average 27-fold between the two time-points. Galectin-3 was unable to increase CTGF production, and levels remained comparable to control slices. Interestingly, IL-11 secretion was able to be induced by Galectin-3 challenge albeit at a much smaller magnitude compared to TGF-β1. This data potentially highlights a role for Galectin-3 in the switch from inflammation to fibrosis.

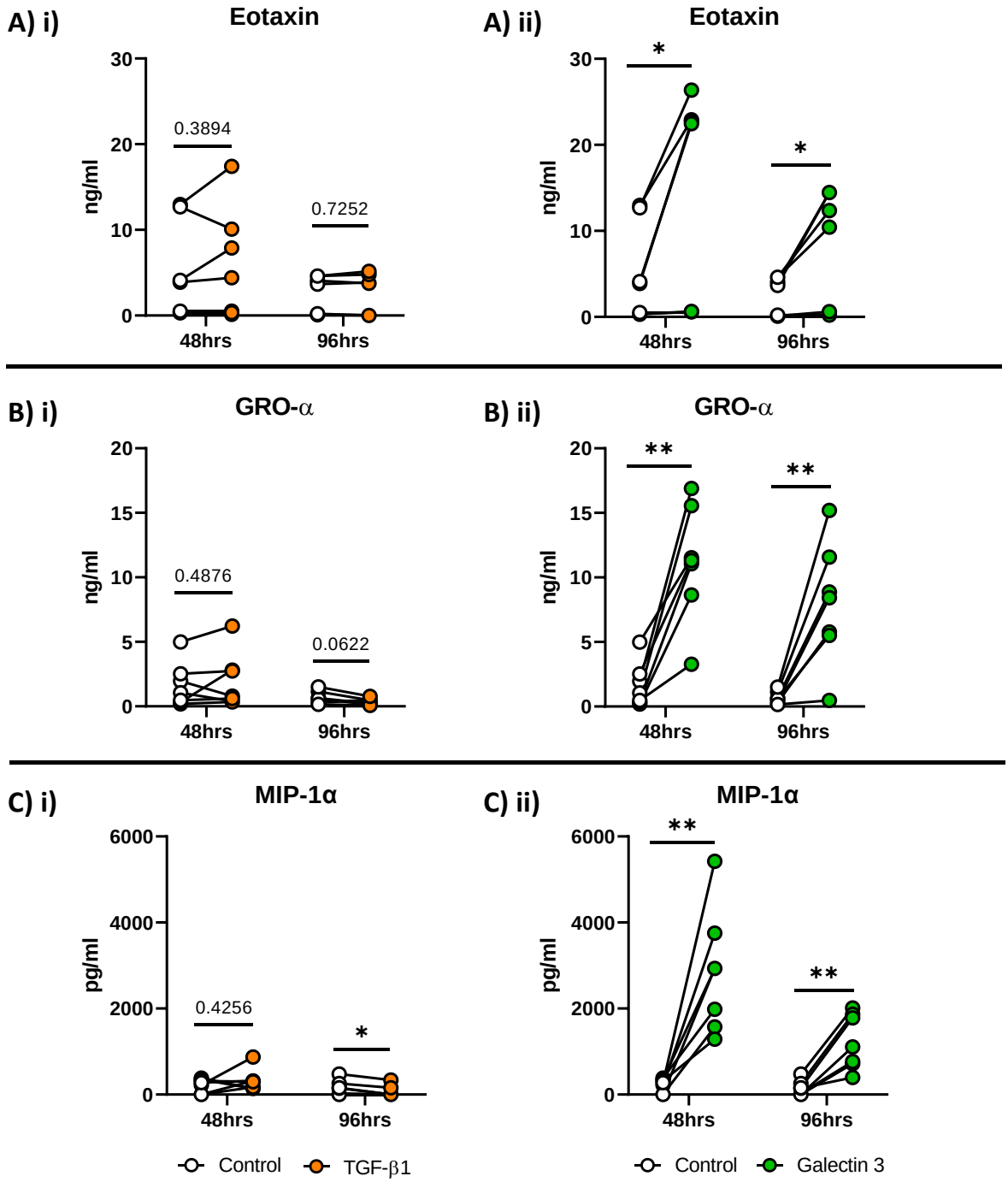

Figure 41. Galectin-3 challenge induces potent inflammatory response in PCHS – Slices (n=7 donors) from LVAD donor tissues were challenged with either control or TGF-β1 (10ng/ml) or Galectin-3 (5µg/ml) media for either 48hrs or 96hrs. Media was harvested and levels of inflammatory cytokine and chemokines were quantified by multiplex ELISA (Eotaxin, GRO-α and MIP-1α). Data are Mean ± SEM p values were calculated by paired student t tests; *p≤0.05; **p≤0.01.

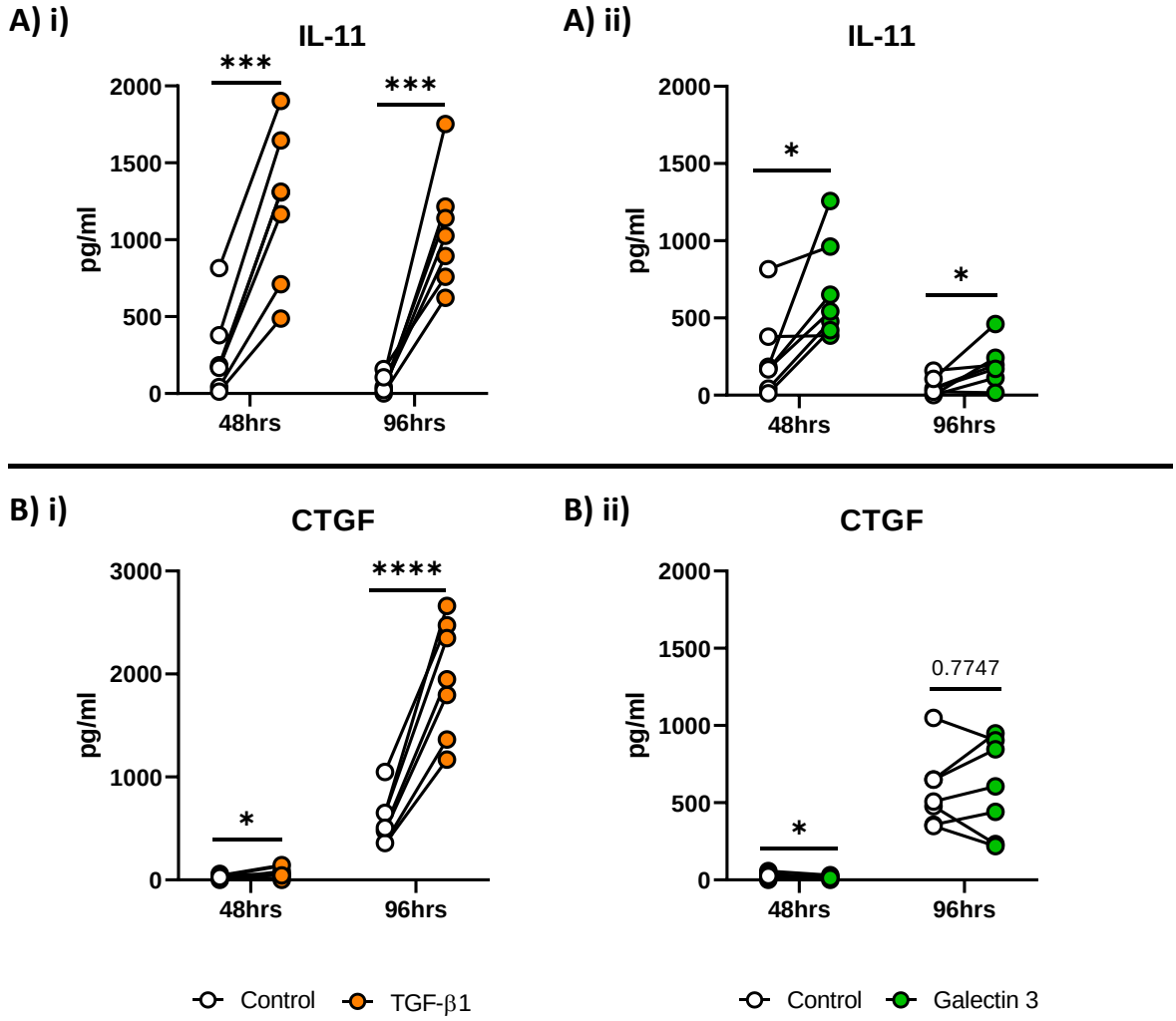

Figure 42. TGF-β1 challenge induces potent pro-fibrotic response in PCHS – Slices (n=7 donors) from LVAD donors tissues were challenged with either control or TGF-β1 (10ng/ml) or Galectin-3 (5µg/ml) media for either 48hrs or 96hrs. Media was harvested and levels of fibrotic markers IL-11 and CTGF were quantified by sandwich ELISA. Data are Mean ± SEM p values were calculated by paired student t tests; *p≤0.05; ***p≤0.001; ****p≤0.0001.

5.4.2 Effects of exogenous stimuli on PCHS – an unbiased approach

5.4.2.1 Precision Cut Heart Slice Transcriptomics

In order to more broadly assess the effect of the exogenous stimuli on PCHS, slices were prepared from n=5 donors and treated with TGF-β1, CTGF, Angiotensin II, Galectin-3 and IL-11 as previously described. After 72 hours of treatment, PCHS were harvested for RNA sequencing or proteomic analysis. Principal Component Analysis (PCA) on RNA sequencing data showed that only TGF-β1 treated PCHS clustered due to the treatment type **(Figure 43)**. The rest of the exogenous stimuli had little to no effect on the clustering, instead clustering was based on the donor. NHH10, 11 and 22 all clustered together, with NHH19 nearby, interestingly NHH20 clustered away from the other donors.

Transcriptomic analysis identified over 57,000 genes present in the PCHS. Treatment of the PCHS with IL-11, CTGF or Angiotensin II resulted in only small number of the genes identified being differentially expressed (Padj <0.01 and fold change >1.5 or >-1.5). Depicted as volcano plots in Figure 42B, Angiotensin II treatment resulted in differential expression of only 11 genes (0.019% of total genes identified), 3 genes significantly reduced and 8 significantly elevated. This was the fewest number of genes identified in response to any of the exogenous challenges. Both IL-11 and CTGF treatment induced significant differences in a greater number of genes than Angiotensin II. IL-11 challenge upregulated 47 (0.082% of total genes), and downregulated 54 genes (0.093% of total genes) **(Figure 44C)** whilst CTGF resulted in 50 genes (0.087% of total genes) increase and 43 decrease (0.074% of total genes) in response to treatment **(Figure 44A)**. Despite IL-11 and CTGF treatment causing a greater number of differentially expressed genes, these numbers are still small compared to the number of genes identified and therefore likely not to be biologically significant.

As we had seen with regard to the secreted proteins, only TGF-β1 and Galectin-3 challenge caused a response of note from the PCHS, and this was also true in regard to RNA-sequencing results. Galectin-3 treatment resulted in the significant differential expression of 285 genes, around 0.5% of the total number of genes identified (161 downregulated and 123 upregulated) with a Padj <0.01 and fold change >1.5 or >-1.5. TGF-β1 stimulation elicited by far the biggest response in PCHS, with 2548 genes differentially regulated **(Figure 44D)**. This accounted for over 4% of total genes identified (1615 downregulated and 933 upregulated) in the total transcriptome.

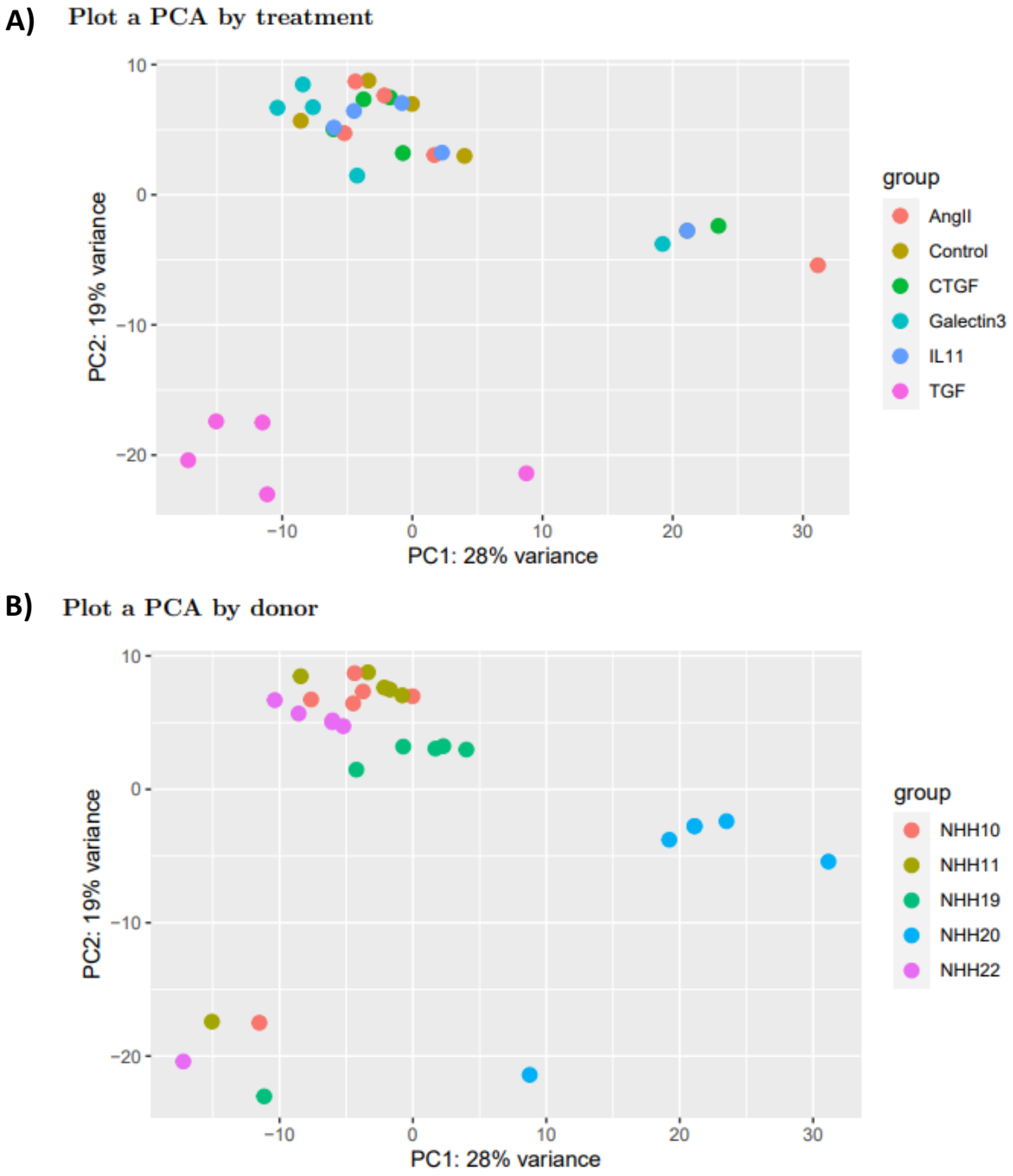

Figure 43. Exogenous TGF-β1 challenge dictates PCHS PCA clustering – PCHS (n=5 donors) were either unchallenged (Control) or treated with TGF-β1, Angiotensin II, CTGF, IL-11 or Galectin-3 for 72 hours prior to harvest of tissue for RNA sequencing analysis. RNA sequencing data is shown as Principle Component Analysis (PCA) according to **A)** treatment applied or **B)** donor.

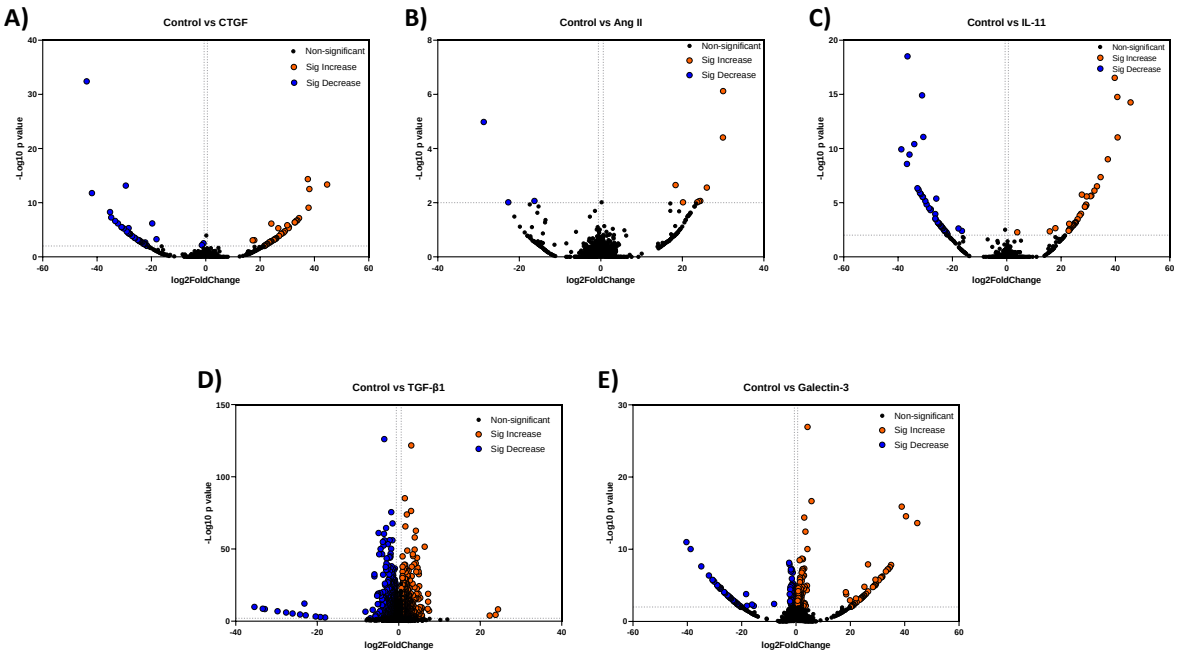

Figure 44. TGF-β1 and Galectin-3 treatment induce transcriptional differences in PCHS – PCHS (n=5 donors) were either unchallenged (Control) or treated with TGF-β1, Angiotensin II, CTGF, IL-11 or Galectin-3 for 72 hours prior to harvest of tissue for RNA sequencing analysis. Transcriptomic data is shown as volcano plots for each treatment versus control. Significantly upregulated genes = orange, significantly downregulated genes = blue and non-significant genes = black. Genes were termed significant by padj≤0.01 and Log 2 Fold Change (FC) ±1.5.

In order the better visualise the differences in gene expression, statistically significant genes with more than 100 reads were z transformed and heat maps produced for either TGF-β1 or Galectin-3 induced changes when compared to control. The other stimuli were also visualised on the heat map for both TGF-β1 and Galectin-3 responses to enable any similarities between expression profiles to be elucidated. **Figure 45** shows that TGF-β1 stimulation induced a very distinct profile of gene change compared to control, and these changes were specific to TGF-β1 alone, with no overlap with the other stimuli. In fact the profile for CTGF, Galectin-3, IL-11 and Angiotensin II matched that of the control slices. When looking at the heat map depicting the significantly differentially expressed genes for Galectin-3 **(Figure 46)** there was a distinct unique profile in regard to the genes upregulated in response to Galectin-3 treatment. However, there is an obvious overlap between the genes downregulated in response to Galectin-3 and TGF-β1 challenge. IL-11, CTGF and Angiotensin II once again had a profile similar to control PCHS. Individual heat maps could not be produced for Angiotensin II, CTGF or IL-11 due to no significant changes in gene expression (p-value <0.01 and FC ±>1.5) having over 100 gene reads.

In addition to the heat maps, Venn diagrams showed that there was very little overlap between TGF-β1 and Galection-3 induced gene expression changes **(Figure 47)**. Only 21 genes were differentially expressed in response to both TGF-β1 and Galectin-3 treatment. Interestingly the highest number of genes in common were those significantly downregulated in response to treatment, with 13 genes common to both TGF-β1 and Galectin-3. These genes included CCL14, COL14A1 and Podocan. The only genes significantly elevated in response to both stimuli were IL-11, IL-6, growth factor receptor bound protein 14 (GRB14) and BTB domain containing 11 (BTBD11).

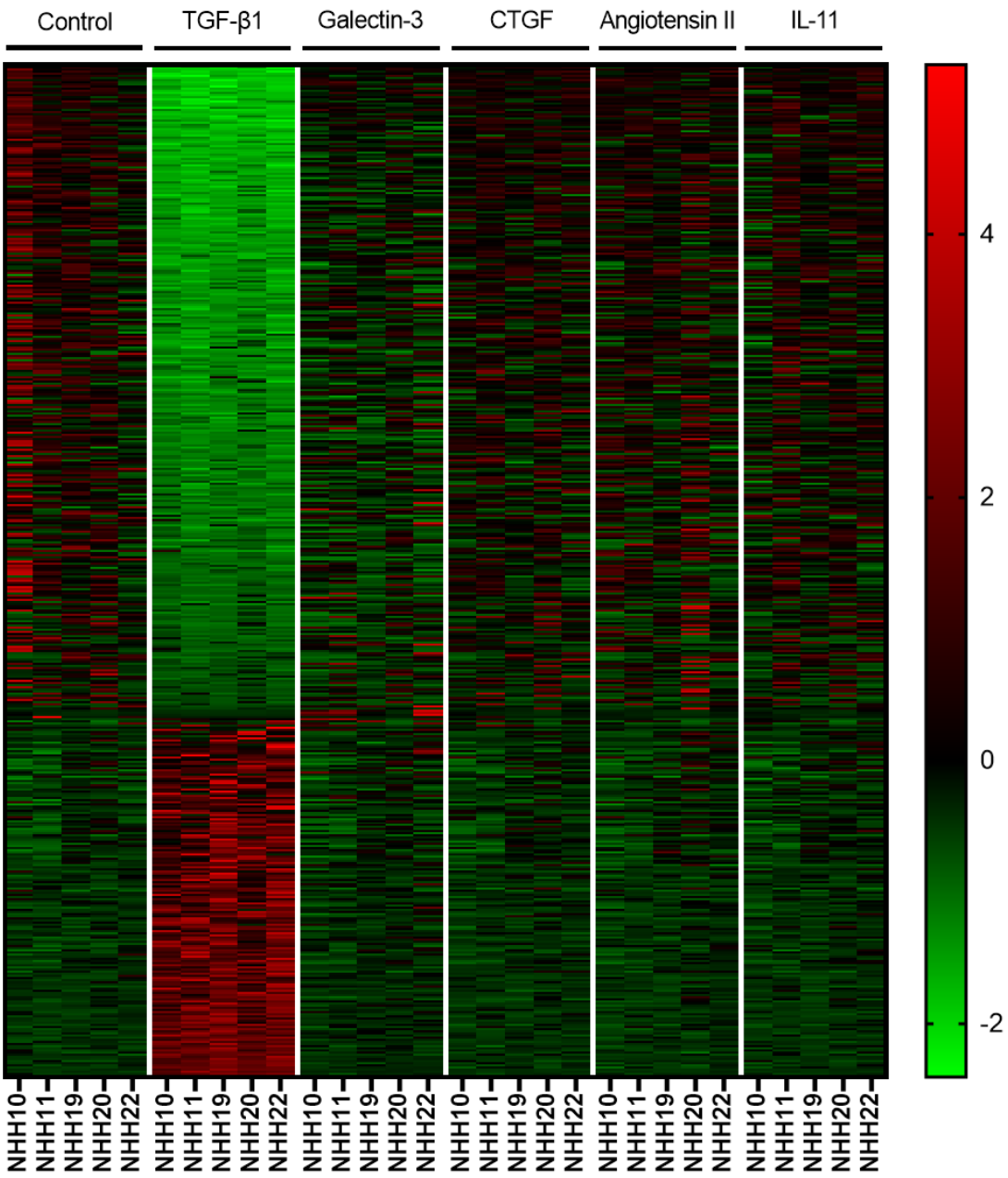

Figure 45. Heat map depicting distinct changes in gene expression induced by TGF-β1 challenge – PCHS (n=5 donors) were either untreated (control) or challenged with TGF-β1, Angiotensin II, CTGF, IL-11 or Galectin-3 for 72 hours prior to harvest of tissue for RNA sequencing analysis. Heat map shows significant changes in gene expression for TGF-β1 versus control. Gene expression was significant if log 2 FC ±>1.5, padj≤0.01 and over 100 counts per gene.

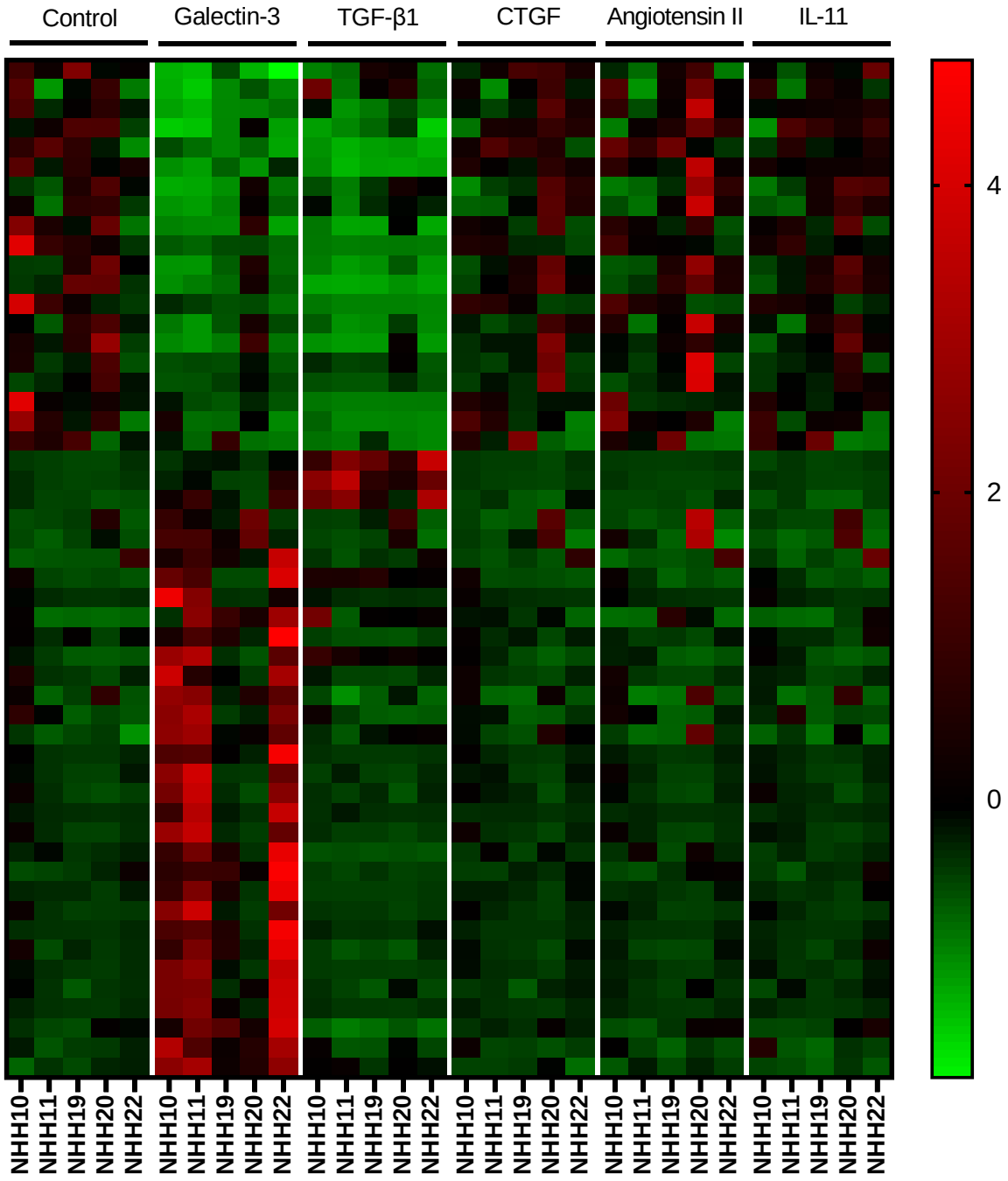

Figure 46. Heat map depicting distinct changes in gene expression induced by Galectin-3 challenge – PCHS (n=5 donors) were either untreated (control) or challenged with TGF-β1, Angiotensin II, CTGF, IL-11 or Galectin-3 for 72 hours prior to harvest of tissue for RNA sequencing analysis. Heat map shows significant changes in gene expression for Galectin-3 versus control. Gene expression was significant if log 2 FC ±>1.5, padj≤0.01 and over 100 counts per gene.

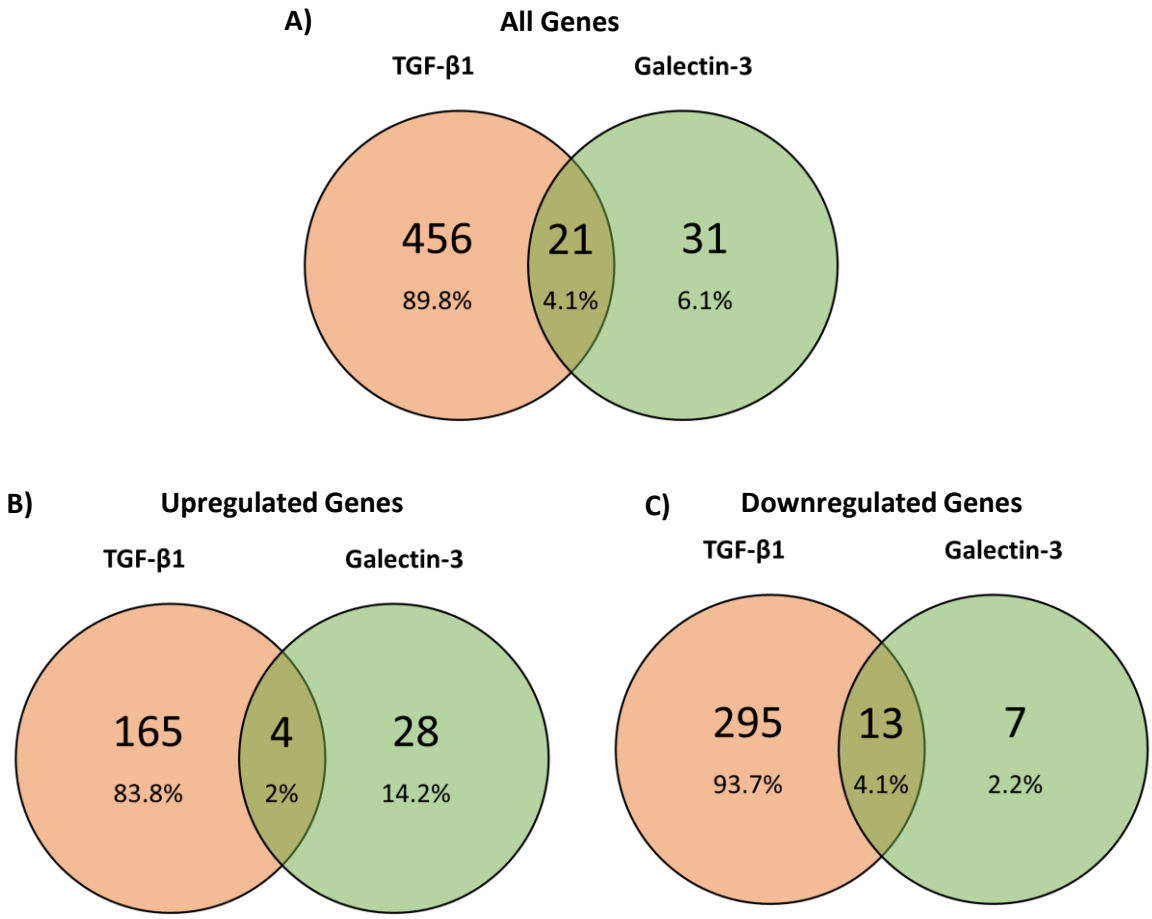

Figure 47. Galectin-3 and TGF-β1 challenge produce very distinct profiles in differentially expressed genes – Changes in gene expression were deemed significant if they had log 2 fold change > ± 1.5, >100 counts and padj≤0.01. Significant genes were inputted into Venny 2.1 BioInfoGP software (https://bioinfogp.cnb.csic.es/tools/venny/index.html). **A)** depicts all significantly differentially expressed genes in response to either TGF-β1 (orange) or Galectin-3 (green) treatment; **B)** genes upregulated in response to both treatments; **C)** downregulated genes in response to treatments.

Figure 48 heat map shows in more detail the differences in the expression profile of PCHS after TGF-β1 treatment. There are distinct differences between TGF-β1 and control, with the same profile consistent across all 5 donors. **Tables 7 and 8** provide details regarding the top 20 most significantly upregulated and downregulated genes. Some of the most strongly upregulated genes included a number of collagens, such as COL10A1, as well as IL-11 and the cardioactive growth factor Neuregulin-1. Expanding the significantly upregulated genes to more than the top 20 revealed many well-described pro-fibrotic markers such as CTGF, FGF and Endothelin-1. Some of these are depicted in **Figure 49** confirming that we are able to induce a fibrotic response in PCHS through TGF-β1 challenge. Further confirming the distinct profiles caused by either TGF-β1 or Galectin-3, apart from IL-6 expression, all genes significantly upregulated in response to TGF-β1 were unchanged in Galectin-3. In contrast to the mainly pro-fibrotic genes which were upregulated, the most differentially downregulated

genes included CCL14, CXCL6 and interestingly SMOC2 **(Table 8)**. Once again, genes downregulated with TGF-β1 were either unchanged or only slightly downregulated in Galectin-3, CCL14 was one of the only genes which was found to be downregulated in response to either treatment **(Figure 50)**.

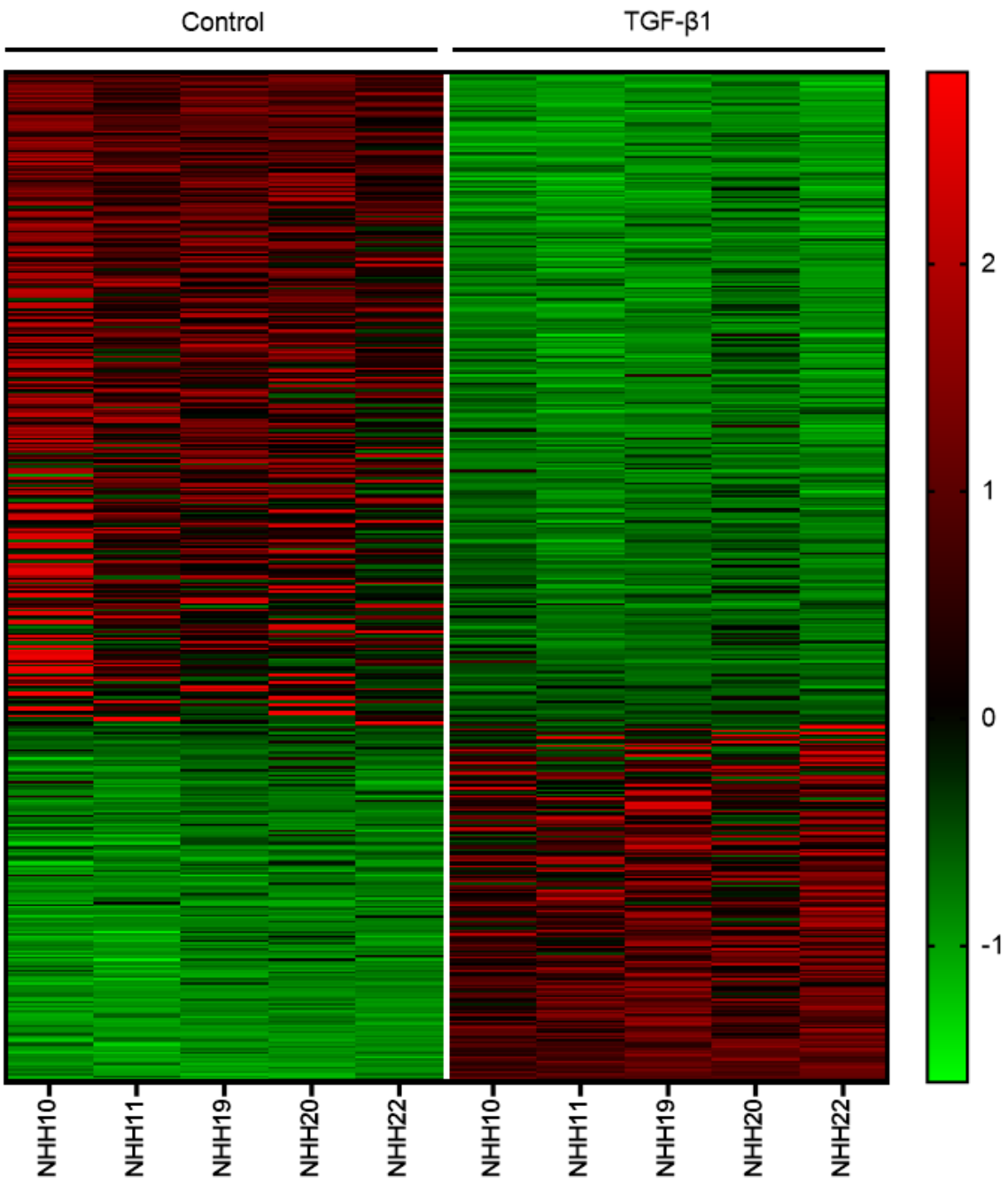

Figure 48. Heat map depicting distinct profile caused by TGF-β1 challenge – Z transformed gene expression changes from PCHS (n=5 donors) challenged with TGF-β1 or left untreated. Significance was determined by genes with log 2 fold change > ± 1.5, >100 counts and padj≤0.01.

Ensemble Gene ID	log2 FC	p-adj	Symbol	Description
ENSG00000275620	7.219	2.74E-14	FLJ16779	Uncharacterized LOC100192386
ENSG00000126562	7.208	1.12E-19	WNK4	WNK lysine deficient protein kinase 4
ENSG00000132854	6.366	2.38E-52	KANK4	KN motif and ankyrin repeat domains 4
ENSG00000060718	5.628	2.83E-10	COL11A1	Collagen type XI alpha 1 chain
ENSG00000123500	5.356	2.29E-07	COL10A1	Collagen type X alpha 1 chain
ENSG00000137868	5.281	7.25E-17	STRA6	Stimulated by retinoic acid 6
ENSG00000157168	5.238	1.40E-10	NRG1	Neuregulin 1
ENSG00000095752	5.038	5.27E-25	IL11	Interleukin 11
ENSG00000087494	4.946	2.97E-33	PTHLH	Parathyroid hormone like hormone
ENSG00000162873	4.892	5.66E-09	KLHDC8A	Kelch domain containing 8A
ENSG00000102385	4.869	4.08E-35	DRP2	Dystrophin related protein 2
ENSG00000105989	4.851	1.33E-19	WNT2	WNT family member 2
ENSG00000135480	4.832	6.13E-16	KRT7	Keratin 7
ENSG00000115290	4.61	8.15E-38	GRB14	Growth factor receptor bound protein 14
ENSG00000117586	4.507	1.20E-44	TNFSF4	TNF superfamily member 4
ENSG00000169436	4.462	3.13E-23	COL22A1	Collagen type XXII alpha 1 chain
ENSG00000118513	4.371	1.28E-19	MYB	MYB proto-oncogene, transcription factor
ENSG00000029559	4.318	1.42E-16	IBSP	Integrin binding sialoprotein
ENSG00000125869	4.301	5.24E-35	LAMP5	Lysosomal associated membrane protein family member 5
ENSG00000159217	4.29	1.11E-05	IGF2BP1	Insulin like growth factor 2 mRNA binding protein 1

Table 7. Top 20 genes significantly upregulated in response to TGF-β1 treatment – Shown is Ensemble gene ID, Log2 fold change, adjusted p-value, gene symbol and brief gene description.

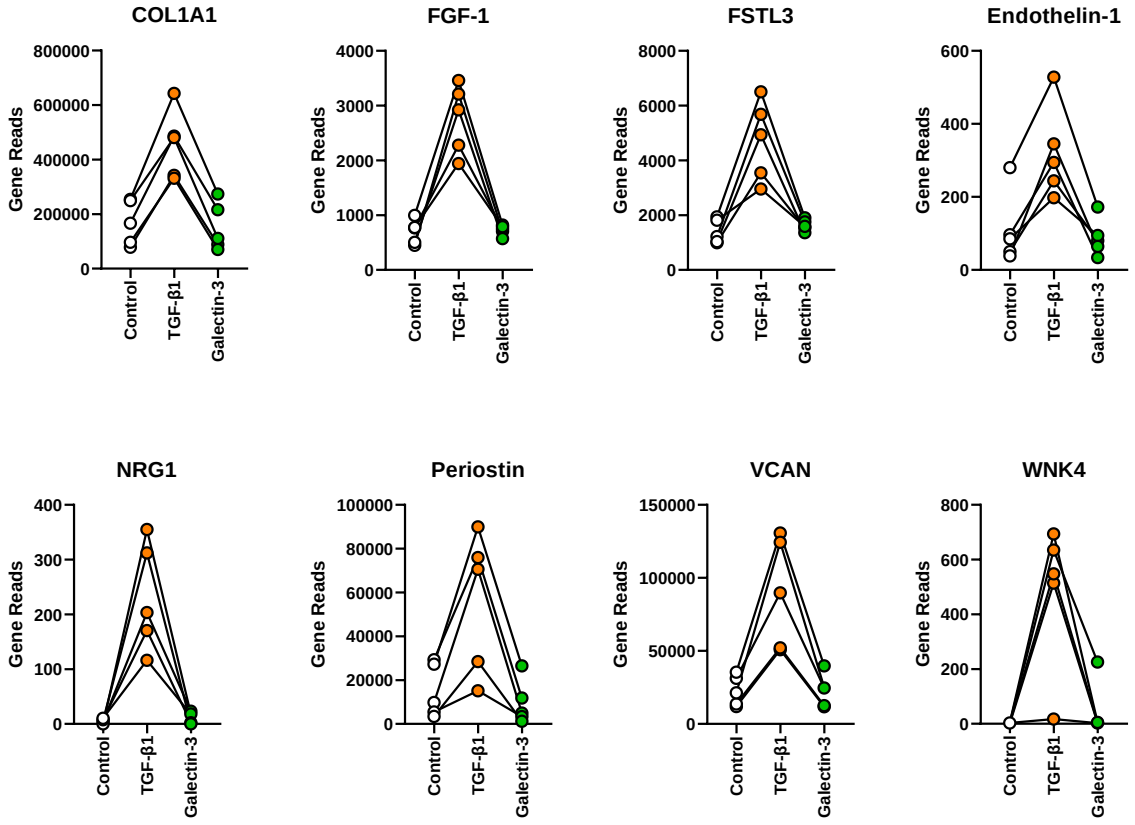

Figure 49. Representative graphs of genes upregulated in response to TGF-β1 treatment – Gene reads from RNA sequencing data after PCHS treated with either Galectin-3, TGF-β1 or control media for 72 hours. Gene expression was classed as significant if padj <0.01 and Log2 FC ±1.5. Data is shown for each individual donor; n=5 donors

Ensemble Gene ID	log2 FC	p-adj	Symbol	Description
ENSG00000276409	-5.975	3.44E-33	CCL14	C-C motif chemokine ligand 14
ENSG00000277494	-5.963	9.78E-32	GPIHBP1	Glycosylphosphatidylinositol anchored high density lipoprotein binding protein 1
ENSG00000075043	-5.726	0.00057	KCNQ2	Potassium voltage-gated channel subfamily Q member 2
ENSG00000196616	-5.306	2.73E-18	ADH1B	Alcohol dehydrogenase 1B (class I), beta polypeptide
ENSG00000171864	-5.057	7.99E-20	PRND	Prion like protein doppel
ENSG00000187955	-4.954	8.35E-62	COL14A1	Collagen type XIV alpha 1 chain
ENSG00000143248	-4.797	4.84E-47	RGS5	Regulator of G protein signalling 5
ENSG00000167434	-4.462	9.47E-51	CA4	Carbonic anhydrase 4
ENSG00000112936	-4.387	2.09E-18	C7	Complement C7
ENSG00000133048	-4.074	7.79E-12	CHI3L1	Chitinase 3 like 1
ENSG00000163815	-4.073	5.63E-16	CLEC3B	C-type lectin domain family 3 member B
ENSG00000129048	-4.069	3.23E-47	ACKR4	Atypical chemokine receptor 4
ENSG00000112562	-3.894	1.17E-55	SMOC2	SPARC related modular calcium binding 2
ENSG00000047457	-3.885	1.96E-08	CP	Ceruloplasmin
ENSG00000161649	-3.849	5.27E-17	CD300LG	CD300 molecule like family member g
ENSG00000145358	-3.839	6.18E-33	DDIT4L	DNA damage inducible transcript 4 like
ENSG00000151790	-3.814	2.55E-10	TDO2	Tryptophan 2,3-dioxygenase
ENSG00000124875	-3.798	5.08E-21	CXCL6	C-X-C motif chemokine ligand 6
ENSG00000197635	-3.743	4.66E-53	DPP4	Dipeptidyl peptidase 4
ENSG00000168309	-3.701	1.57E-17	FAM107A	Family with sequence similarity 107 member A

Table 8. Top 20 genes significantly downregulated in response to TGF-β1 treatment – Shown is Ensemble gene ID, Log2 fold change, adjusted p-value, gene symbol and brief gene description.

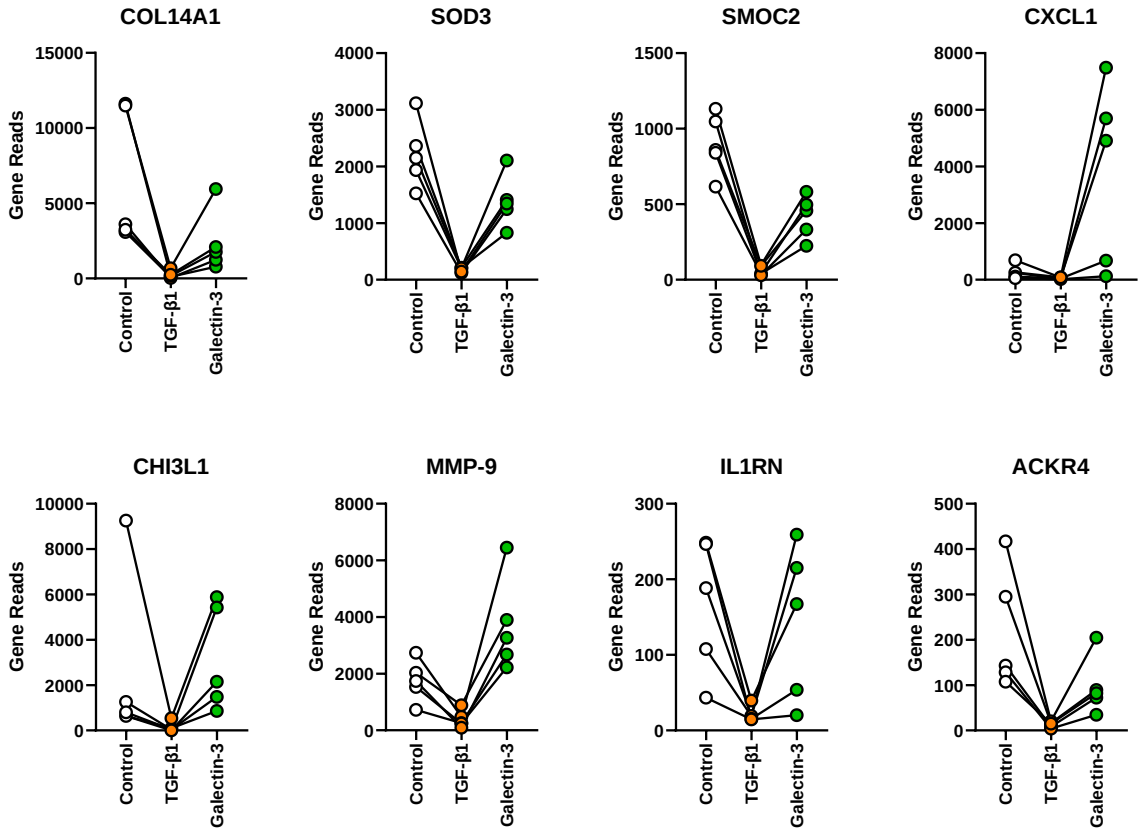

Figure 50. Representative graphs of genes downregulated in response to TGF-β1 treatment – Gene reads from RNA sequencing data after PCHS treated with either Galectin-3, TGF-β1 or control media for 72 hours. Gene expression was classed as significant if padj <0.01 and Log2 FC ±1.5. Data is shown for each individual donor; n=5 donors.

Comparing Galectin-3 differentially expressed genes to control heatmap shows that whilst there is a clear distinction between the conditions, donors NHH19 and NHH20 behaved differently to the other donors in respect to the upregulated genes **(Figure 51)**. With their profile mirroring that of control PCHS, interestingly however these differences did not apply to the downregulated genes, where they were consistent with the other donors. The results of the top 20 most differentially upregulated genes are in stark contrast to the equivalent results for TGF-β1 **(Table 9)**. Galectin-3 induces a potent inflammatory phenotype in PCHS, with a number of interleukins (IL-11, IL-24, IL-6 and IL-1B) and CXCL (CXCL1, CXCL3, CXCL6 and CXCL2) chemokines present **(Figure 52)**. Also significantly upregulated is the matrix degradation enzyme MMP-3 and peptidase inhibitor 3 (PI3). **Table 10** depicts the 20 most downregulated genes in response to treatment, these include Angiotensinogen, the ECM protein Asporin and interestingly two different apolipoproteins. A number of the genes downregulated in response to Galectin-3 were also seen to be downregulated after TGF-β1 treatment **(Figure 53)**. Those included WISP2, a matricellular protein able to inhibit TGF-β1 and MMP-2, COL14A1 and folate receptor 2 (FOLR2).

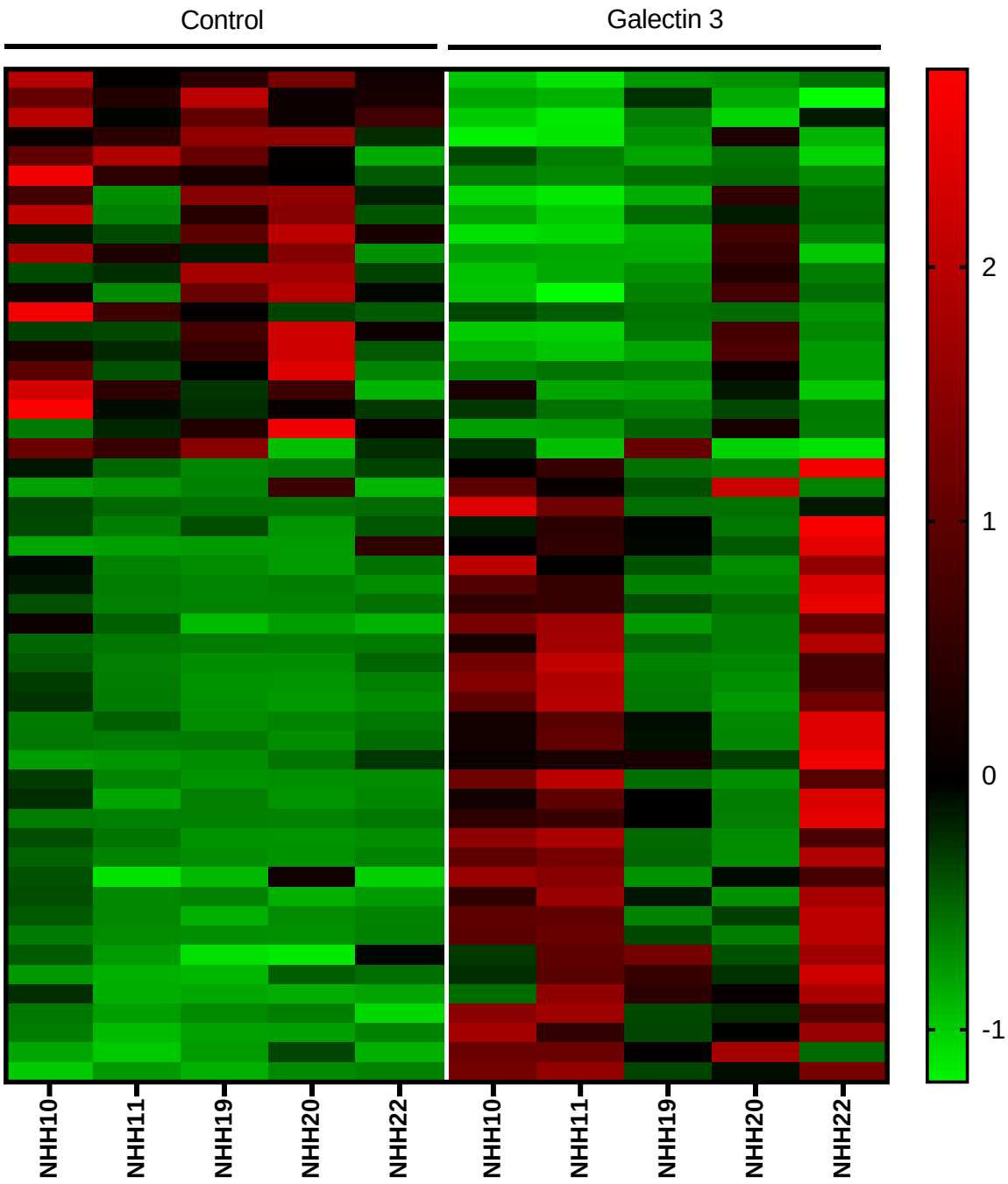

Figure 51. Heat map depicting distinct profile caused by Galectin-3 challenge – Z transformed gene expression changes from PCHS (n=5 donors) challenged with Galectin-3 or left untreated. Significance was determined by genes with log 2 fold change > ± 1.5, >100 counts and padj≤0.01.

Ensemble Gene ID	log2 FC	p-adj	Symbol	Description
ENSG00000124102	5.716	2.14E-17	PI3	Peptidase inhibitor 3
ENSG00000163735	4.264	1.15E-27	CXCL5	C-X-C motif chemokine ligand 5
ENSG00000149968	4.223	9.19E-11	MMP3	Matrix metallopeptidase 3
ENSG00000108342	3.990	4.57E-05	CSF3	Colony stimulating factor 3
ENSG00000028277	3.628	0.006503	POU2F2	POU class 2 homeobox 2
ENSG00000163739	3.480	3.63E-13	CXCL1	C-X-C motif chemokine ligand 1
ENSG00000125538	3.262	1.52E-05	IL1B	Interleukin 1 beta
ENSG00000124875	3.063	3.99E-15	CXCL6	C-X-C motif chemokine ligand 6
ENSG00000163734	3.056	4.69E-08	CXCL3	C-X-C motif chemokine ligand 3
ENSG00000162892	2.960	4.29E-07	IL24	Interleukin 24
ENSG00000169429	2.785	3.88E-07	CXCL8	C-X-C motif chemokine ligand 8
ENSG00000125730	2.550	2.33E-09	C3	Complement C3
ENSG00000163736	2.532	6.1E-08	PPBP	Pro-platelet basic protein
ENSG00000181374	2.443	0.000124	CCL13	C-C motif chemokine ligand 13
ENSG00000143546	2.441	5.76E-08	S100A8	S100 calcium binding protein A8
ENSG00000186407	2.378	9.38E-08	CD300E	CD300e molecule
ENSG00000108688	2.336	8.54E-07	CCL7	C-C motif chemokine ligand 7
ENSG00000081041	2.289	1.63E-05	CXCL2	C-X-C motif chemokine ligand 2
ENSG00000136244	2.190	1.98E-09	IL6	Interleukin 6
ENSG00000162706	2.097	1.69E-07	CADM3	Cell adhesion molecule 3

Table 9. Top 20 genes significantly upregulated in response to Galectin-3 treatment – Shown is Ensemble gene ID, Log2 fold change, adjusted p-value, gene symbol and brief gene description.

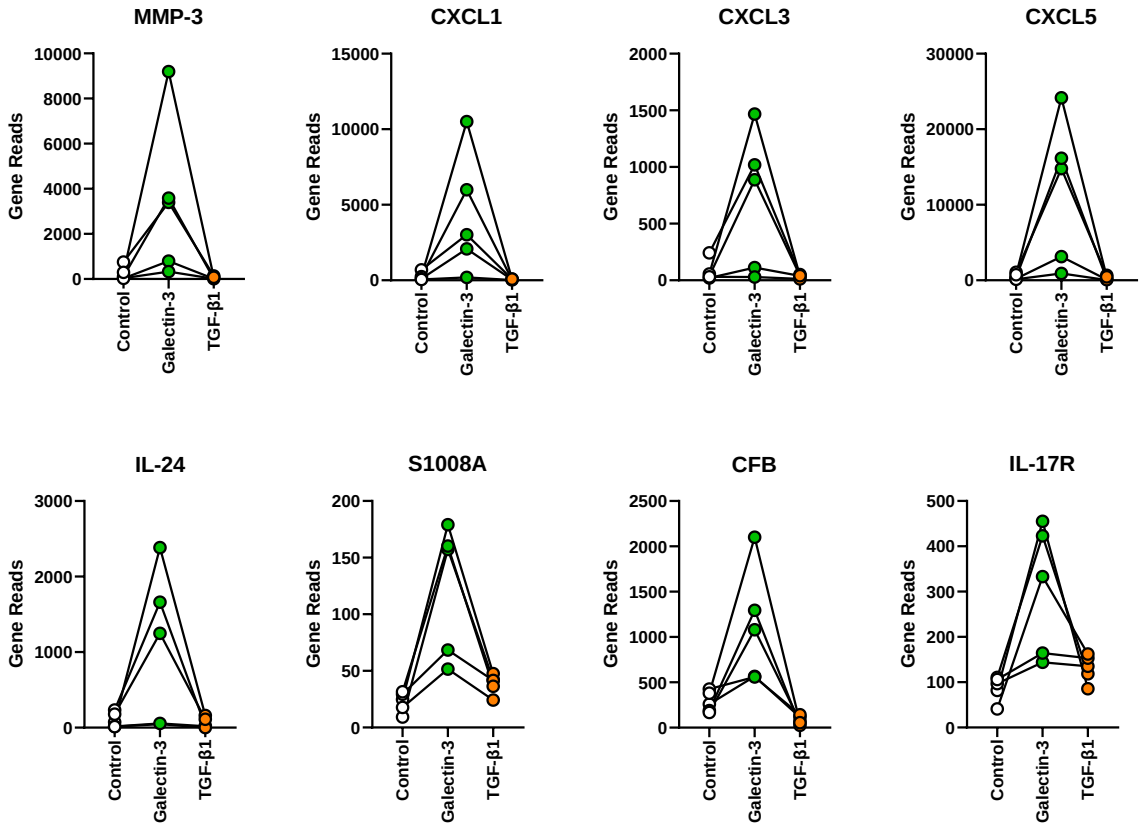

Figure 52. Representative graphs of genes upregulated in response to Galectin-3 treatment – Gene reads from RNA sequencing data after PCHS treated with either Galectin-3, TGF-β1 or control media for 72 hours. Gene expression was classed as significant if padj <0.01 and Log2 FC ±1.5. Data is shown for each individual donor; n=5 donors.

Ensemble Gene ID	log2 FC	p-adj	Symbol	Description
ENSG00000276409	-2.526	7.34E-09	CCL14	C-C motif chemokine ligand 14
ENSG00000095970	-2.382	1.24E-08	TREM2	Triggering receptor expressed on myeloid cells 2
ENSG00000169442	-2.301	0.000167	CD52	CD52 molecule
ENSG00000106819	-2.124	3.7E-05	ASPN	Asporin
ENSG00000130208	-2.054	1.79E-05	APOC1	Apolipoprotein C1
ENSG00000064205	-1.992	0.002372	WISP2	WNT1 inducible signalling pathway protein 2
ENSG00000130203	-1.889	6.14E-08	APOE	Apolipoprotein E
ENSG00000135744	-1.884	1.18E-07	AGT	Angiotensinogen
ENSG00000171864	-1.860	0.004033	PRND	Prion like protein doppel
ENSG00000005108	-1.855	0.003535	THSD7A	Thrombospondin type 1 domain containing 7A
ENSG00000167434	-1.732	4.82E-08	CA4	Carbonic anhydrase 4
ENSG00000165457	-1.719	8.19E-05	FOLR2	Folate receptor beta
ENSG00000130595	-1.712	0.005844	TNNT3	Troponin T3, fast skeletal type
ENSG00000135094	-1.694	1.48E-05	SDS	Serine dehydratase
ENSG00000277494	-1.643	5.03E-05	GPIHBP1	Glycosylphosphatidylinositol anchored high density lipoprotein binding protein 1
ENSG00000120457	-1.637	0.001234	KCNJ5	Potassium voltage-gated channel subfamily J member 5
ENSG00000187955	-1.623	9.24E-06	COL14A1	Collagen type XIV alpha 1 chain
ENSG00000174348	-1.578	1.55E-05	PODN	Podocan
ENSG00000135324	-1.561	7.89E-05	MRAP2	Melanocortin 2 receptor accessory protein 2
ENSG00000130592	-1.517	1.18E-06	LSP1	Lymphocyte-specific protein 1

Table 10. Top 20 genes significantly downregulated in response to Galectin-3 treatment – Shown is Ensemble gene ID, Log2 fold change, adjusted p-value, gene symbol and brief gene description.

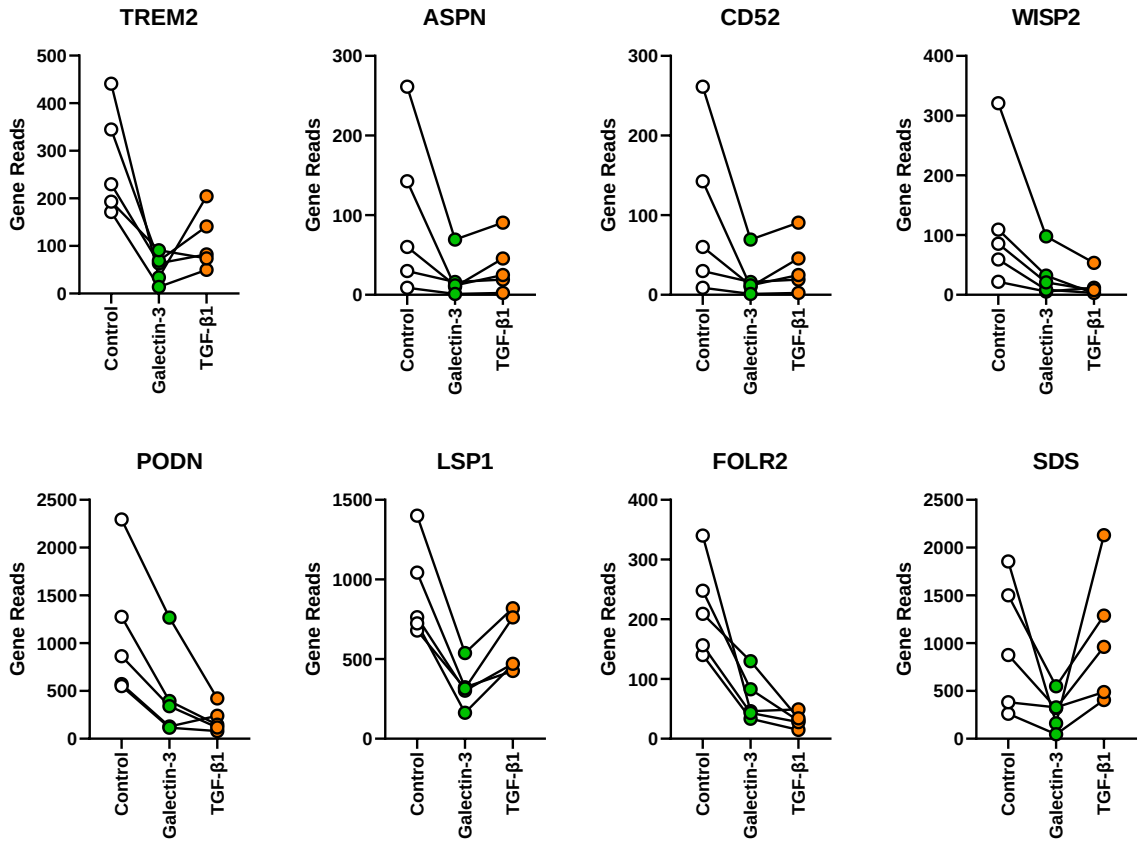

Figure 53. Representative graphs of genes downregulated in response to Galectin-3 treatment – Gene reads from RNA sequencing data after PCHS treated with either Galectin-3, TGF-β1 or control media for 72 hours. Gene expression was classed as significant if padj <0.01 and Log2 FC ±1.5. Data is shown for each individual donor; n=5 donors.

The RNA sequencing data confirms earlier results observed through quantification of the proteins secreted from PCHS in response to the different exogenous stimuli. TGF-β1 was able to illicit the strongest changes to gene expression, inducing the upregulation of a large number of genes involved in fibrosis and fibrotic signalling. This response was distinct to that of Galectin-3 with very little cross-over between upregulated genes, although there were a number of genes found to be downregulated in response to both TGF-β1 and Galectin-3. Once again Galectin-3 challenge induced a potent inflammatory response from the PCHS, with many genes involved in inflammation upregulated. Finally we confirmed that exogenous challenge with Angiotensin II, IL-11 or CTGF induced little to no response within our PCHS system.

5.4.2.2 Precision Cut Heart Slice Proteomics

Having demonstrated the ability to induce two distinct gene profiles within the PCHS in response to either TGF-β1 or Galectin-3 challenge we looked to confirm these findings in the total cell proteome. As previously described PCHS from n=6 donors were exogenously challenged with either control, TGF-β1, CTGF, Angiotensin II, IL-11 or Galectin-3 for a total of 72 hours. At the end of the culture period supernatants were removed, slices washed in PBS and FBS negative culture media applied before PCHS were cultured for an additional 3 hours. The use of BSA free media was key in preventing the masking of proteins by BSA contaminants therefore enabling the detection of proteins in the total cell lysate. Principal component analysis (PCA) from proteomic data initially did not show any clustering either between donor or treatment type. However, once removal of the patient batch effects had been applied donors NHH12, NHH14, NHH19 and NHH22 appeared to group in response to TGF-β1 treatment, whilst NHH11, NHH12, NHH19 and NHH22 clustered after Galectin-3 treatment **(Figures 54A and B)**. There was no clustering in response to IL-11, Angiotensin II or CTGF treatment. **Figures 54C and D** more clearly show the clustering of donors by treatment in response to either TGF-β1 or Galectin-3 in comparison to control.

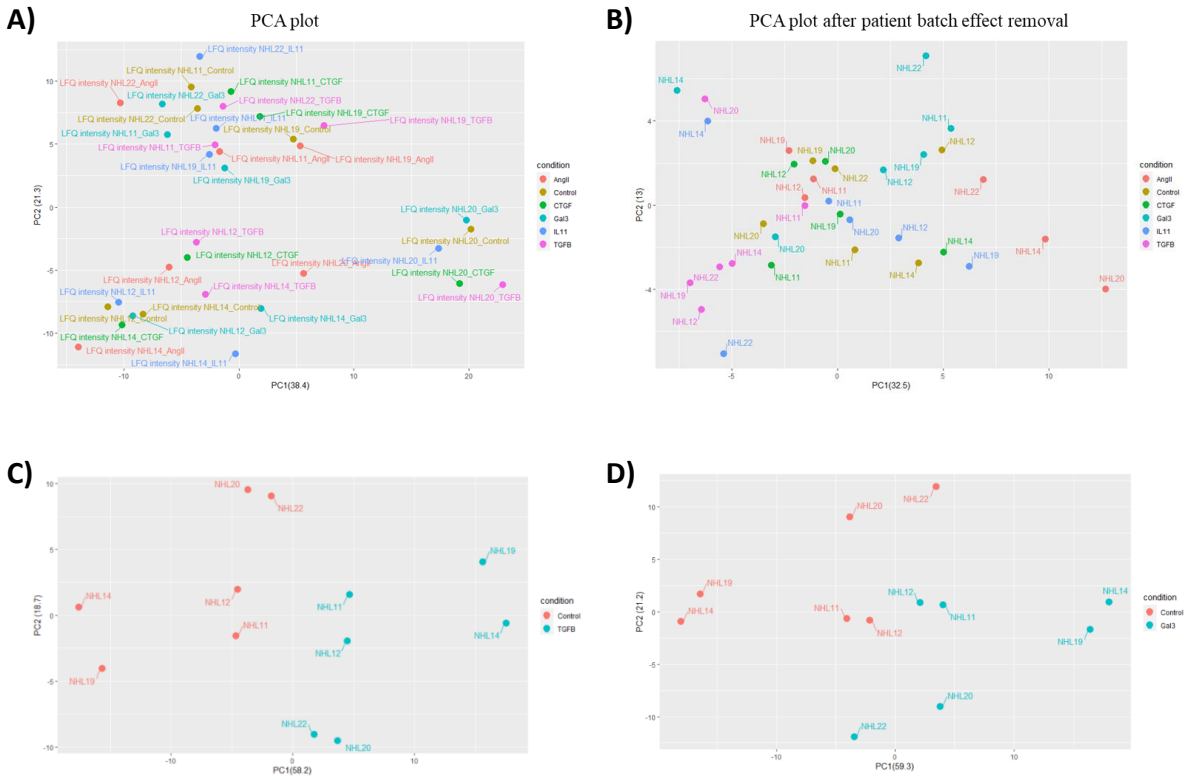

Figure 54. Exogenous TGF-β1 and Galectin-3 challenge dictates proteomics PCA clustering – PCHS (n=6 donors) were either unchallenged (Control) or treated with TGF-β1, Angiotensin II, CTGF, IL-11 or Galectin-3 for 72 hours prior to harvest of tissue for proteomic analysis. Proteomic data is shown as Principle Component Analysis (PCA) according to **A)** treatment applied or **B)** treatment for each donor after patient batch effect removal **C)** TGF-β1 vs Control **D)** Galectin-3 vs Control.

Exogenous challenge of PCHS with the different recombinant stimuli was able to induce differential protein expression compared to control PCHS and is visualised by volcano plots **(Figure 55)**. Once again CTGF, IL-11 and Angiotensin II resulted in the fewest number of significantly differential changes in protein expression (p value <0.05). Stimulation with CTGF only resulted in the significant change in 42 proteins, with 20 significantly increased and 22 significantly reduced. Angiotensin II treatment identified 114 proteins (18 upregulated and 96 downregulated) and IL-11 stimulation resulted in the identification of 63 significant proteins (23 upregulated and 40 downregulated). Whilst TGF-β1 once again elicited the greatest response from PCHS, with 424 significantly differential proteins identified. Of these proteins 271 were found to be increased whereas 153 decreased in response to challenge versus control. Galectin-3 treatment resulted in a total of 143 differentially expressed proteins (74 upregulated and 69 downregulated).

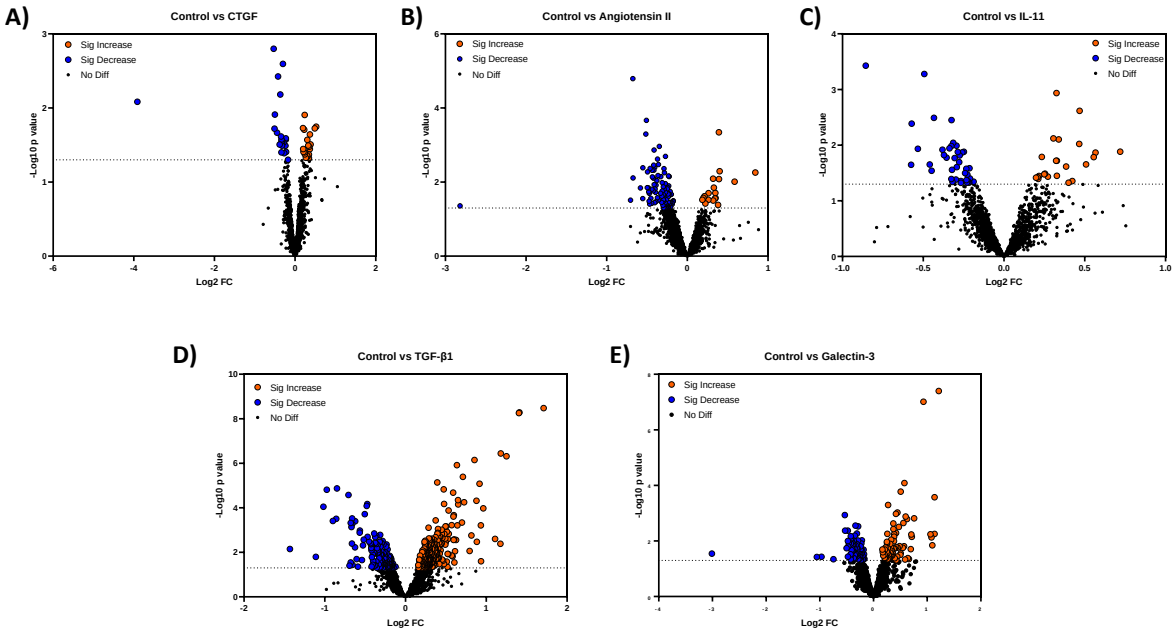

Figure 55. TGF-β1 and Galectin-3 treatment induce proteomic differences in PCHS – PCHS (n=6 donors) were either unchallenged (Control) or treated with TGF-β1, Angiotensin II, CTGF, IL-11 or Galectin-3 for 72 hours prior to harvest of tissue for proteomic analysis. Proteomic data is shown as volcano plots for each treatment versus control. Significantly differentially upregulated proteins = orange, significantly differentially downregulated proteins = blue and non-significant proteins = black. Proteins were termed significant by padj≤0.05 and Log 2 Fold Change (FC) ±1.5.

Upon comparison of the heat maps for TGF-β1 or Galectin-3 challenge versus control, both stimuli elicited distinct treatment based responses **(Figures 56 and 57)**. Once again there was little to no overlap between proteins significantly elevated or reduced in response to Galectin-3 or TGF-β1, nor between the other stimuli used. Of the proteins differentially expressed only 53 were found to be changed in both TGF-β1 and Galectin-3 **(Figure 58A)**. Proteins that were downregulated in response to either TGF-β1 or Galectin-3 provided the highest percentage (12.7%) of proteins common to both stimuli **(Figure 58C)**. These common proteins included Cathepsin Z, CXCR4 and Macrophage capping protein (CAPG). Some of the 14 proteins found to be upregulated in response to both stimuli included Transgelin, Integrin α-2 and ADAMTS4.

The heat maps depicting either TGF-β1 or Galectin-3 against control PCHS highlighted once more the ability to induce a distinct phenotype **(Figures 59 and 62)**. Whilst the response was mostly consistent across all 6 donors, NHH020 appeared to display a slightly different expression profile, with a number of proteins downregulated in NHH020 which were upregulated for the other donors.

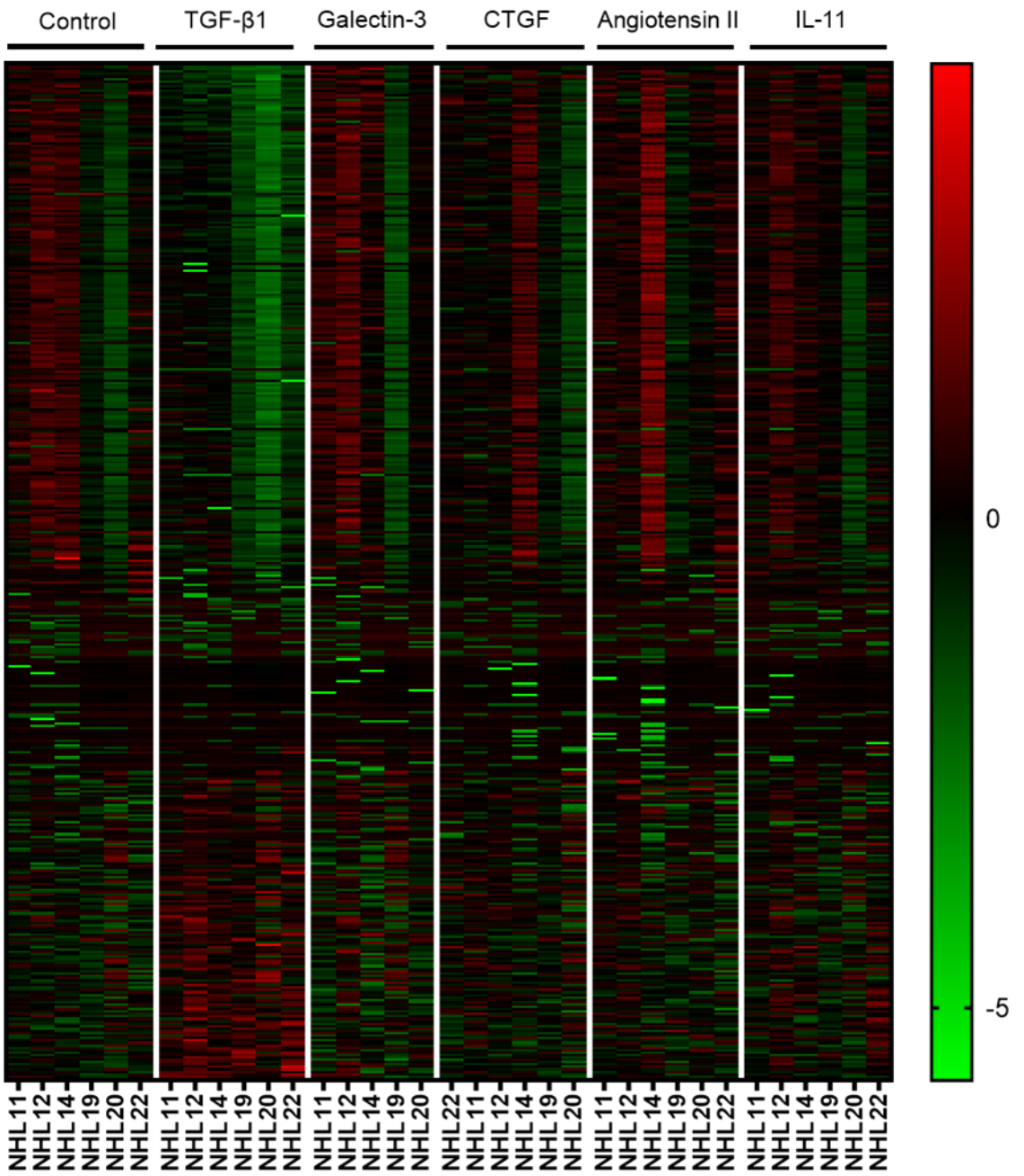

Figure 56. Heat map depicting distinct changes in protein expression induced by TGF-β1 challenge – PCHS (n=6 donors) were either untreated (control) or challenged with TGF-β1, Angiotensin II, CTGF, IL-11 or Galectin-3 for 72 hours prior to harvest of tissue for proteomic analysis. Heat map shows significant changes in differentially expressed proteins for TGF-β1 versus control. Proteins were deemed significant if log 2 FC ±>1.5, padj≤0.05.

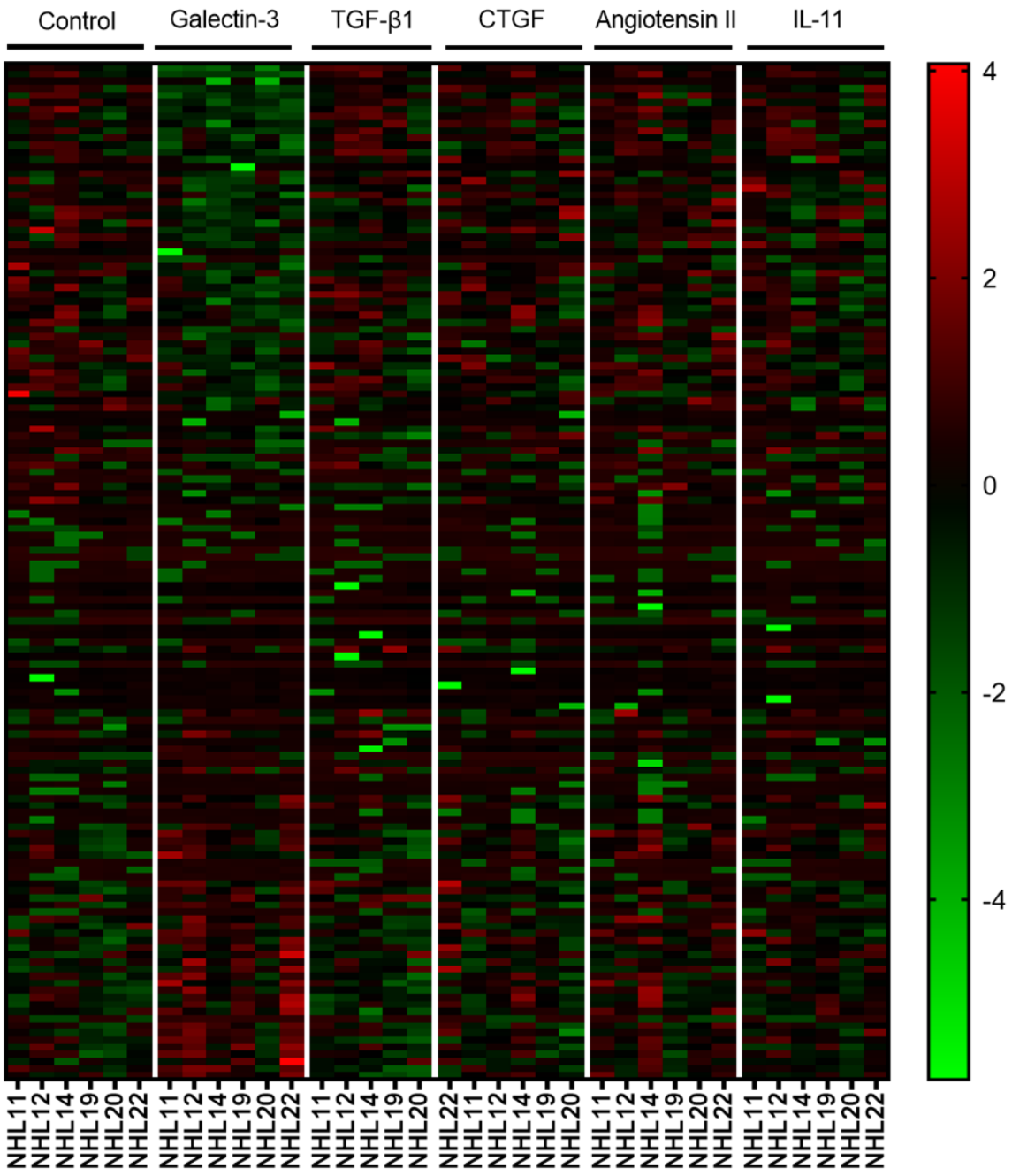

Figure 57. Heat map depicting distinct changes in differential protein changes induced by Galectin-3 challenge – PCHS (n=6 donors) were either untreated (control) or challenged with TGF-β1, Angiotensin II, CTGF, IL-11 or Galectin-3 for 72 hours prior to harvest of tissue for proteomic analysis. Heat map shows significant changes in differentially expressed proteins for Galectin-3 versus control. Proteins were deemed significant if log 2 FC ±>1.5, padj≤0.05.

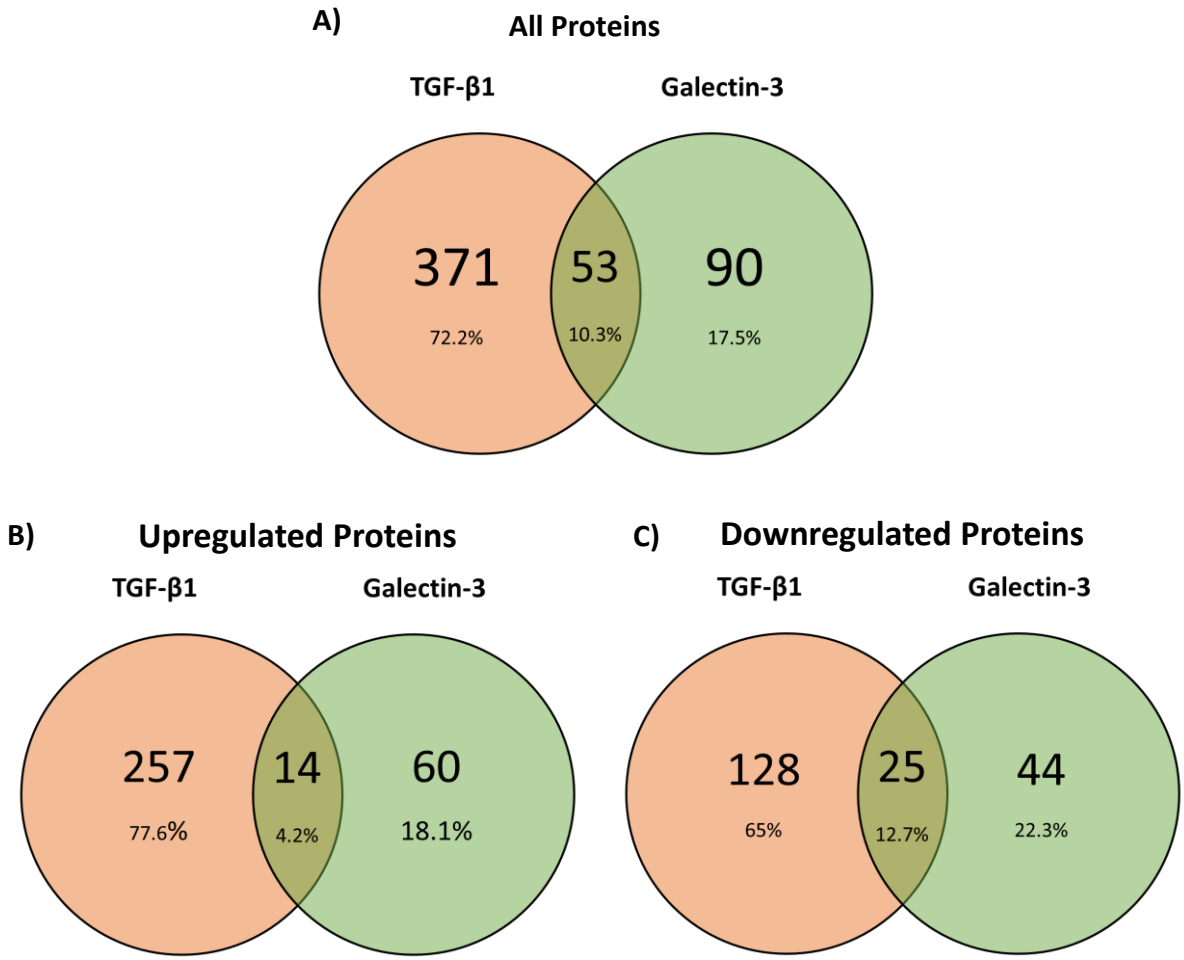

Figure 58. Galectin-3 and TGF-β1 challenge produce very distinct profiles in differentially expressed proteins – Changes in protein expression were deemed significant if they had log 2 fold change > ± 1.5 and padj≤0.05. Significant proteins were inputted into Venny 2.1 BioInfoGP software (https://bioinfogp.cnb.csic.es/tools/venny/index.html). **A)** depicts all significantly differentially expressed proteins in response to either TGF-β1 (orange) or Galectin-3 (green) treatment; **B)** proteins upregulated in response to both treatments; **C)** downregulated proteins in response to treatments.

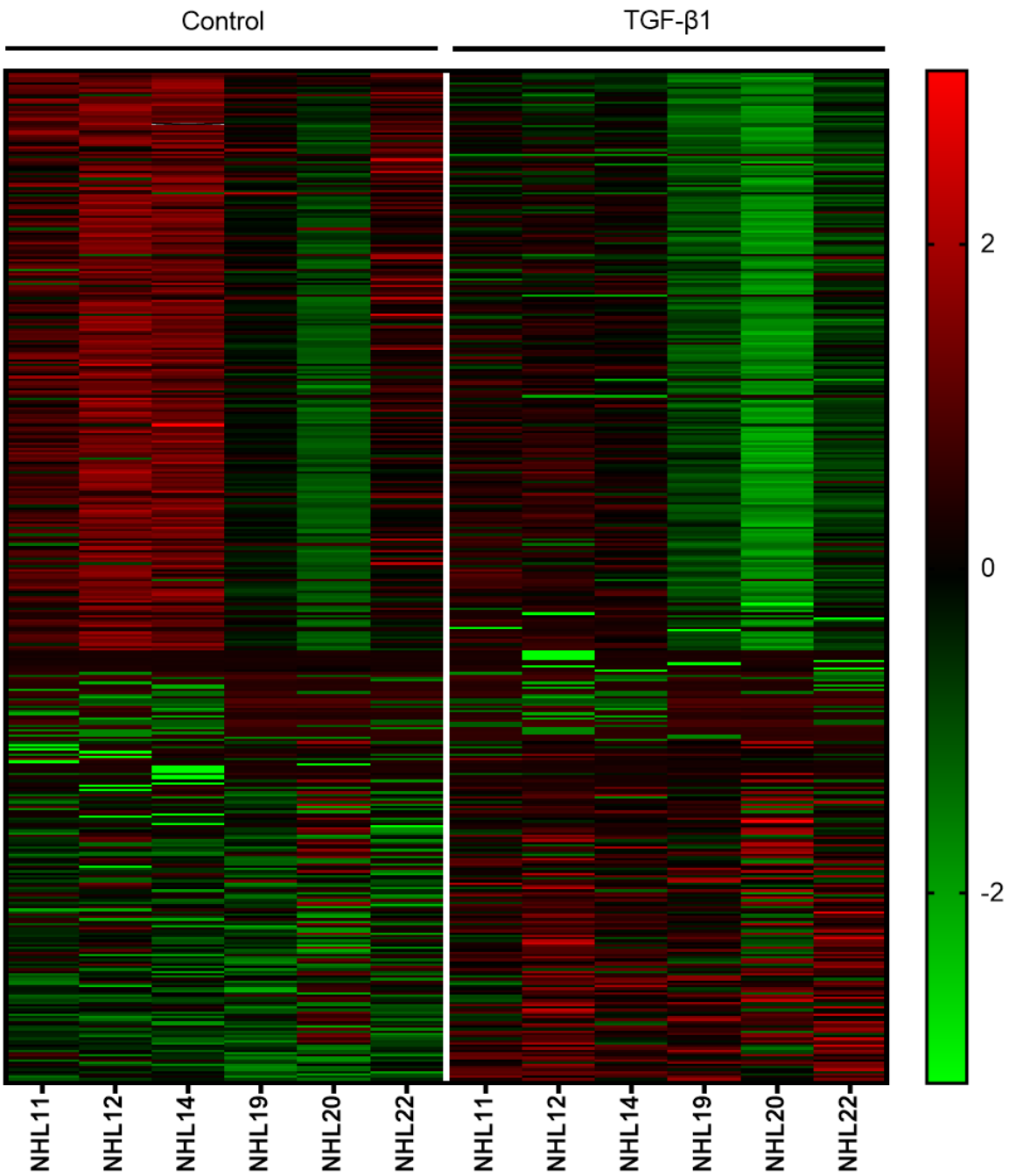

Figure 59. Heat map depicting distinct protein profile caused by TGF-β1 challenge – z transformed protein expression changes from PCHS (n=6 donors) challenged with TGF-β1 or untreated. Significance was determined by proteins with log 2 fold change > ± 1.5 and padj≤0.05.

When highlighting the top 20 most differently upregulated proteins in response to TGF-β1 treatment in **Table 11** it once again became obvious that many of the proteins present are involved in fibrotic pathways and the deposition of ECM. These proteins included Collagen 1a1, fibronectin, emilin-1 and the pro-fibrotic molecule SERPINE1 (plasminogen activator inhibitor 1), of which some are displayed in **Figure 60**. The pro-collagen fragment PLOD2, which is involved in the cross-linking of collagen fibres, was also one of the most significantly upregulated proteins. As was Thrombospondin-1, an important glycoprotein involved in both physiological and pathological wound repair.

As we observed with the transcriptomics, many of the proteins were only upregulated in response to TGF-β1, with levels remaining comparable to control PCHS in response to Galectin-3. **Table 12** depicts the top 20 most significantly downregulated proteins in response to TGF-β1, interestingly one of these proteins is Galectin-3. The inflammatory mediator S100A9, involved in the recruitment of leukocytes was significantly downregulated, in addition to a number of proteins involved in inflammation such as ICAM1 **(Figure 61)**. Interestingly S100A4, which is known to be a downstream signalling target of TGF-β1 was also found to be downregulated.

Accession	log2 FC	p-adj	Gene Name	Description
Q15582	1.709	3.68E-06	TGFBI	Transforming growth factor-beta-induced protein ig-h3
P02751	1.410	3.68E-06	FN1	Fibronectin
P05121	1.404	3.68E-06	SERPINE1	Plasminogen activator inhibitor 1
P13611	1.249	0.00019	VCAN	Versican core protein
P07996	1.179	0.00018	THBS1	Thrombospondin-1
P24821	1.175	0.00019	TNC	Tenascin
Q12884	1.109	0.00018	FAP	Prolyl endopeptidase FAP
P02452	0.962	0.07720	COL1A1	Collagen 1a1
Q9Y6C2	0.934	0.07215	EMILIN1	Emilin 1
O15460	0.932	0.00876	P4HA2	Prolyl 4-hydroxylase subunit alpha-2
P08195	0.916	0.17307	SLC3A2	4F2 cell-surface antigen heavy chain
O00469	0.883	0.03155	PLOD2	Procollagen-lysine,2-oxoglutarate 5-dioxygenase 2
Q13509	0.878	0.00166	TUBB3	Tubulin beta-3 chain
Q92626	0.854	0.07720	PXDN	Peroxidasin
Q9NR12	0.816	0.00564	PDLIM7	PDZ and LIM domain protein 7
Q01995	0.793	0.00024	TAGLN	Transgelin
Q16270	0.725	0.06223	IGFBP7	Insulin-like growth factor-binding protein 7
Q9BX97	0.710	0.10825	PLVAP	Plasmalemma vesicle-associated protein
P21291	0.698	0.00623	CSRP1	Cysteine and glycine-rich protein 1
Q9BQE3	0.652	0.00101	TUBA1C	Tubulin alpha-1C chain

Table 11. Top 20 most significantly upregulated proteins in response to TGF-β1 challenge – Shown is Accession ID, log 2 fold change, p-adj, gene name and brief description.

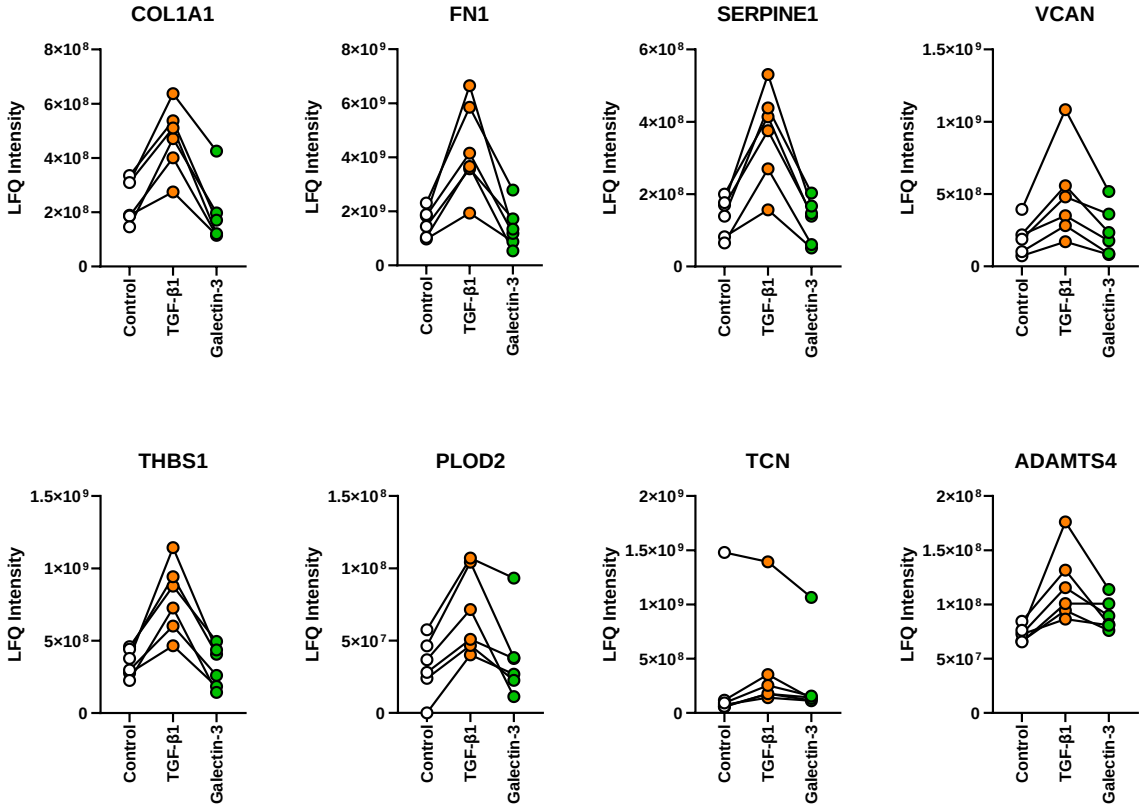

Figure 60. Representative graphs of proteins upregulated in response to TGF-β1 treatment – Protein intensity values from proteomic data after PCHS treated with either Galectin-3, TGF-β1 or control media for 72 hours. Protein expression was classed as significant if padj <0.05 and Log2 FC ±1.5. Data is shown for each individual donor; n=6 donors.

Accession	log2 FC	p-adj	Gene Name	Description
O43854	-1.432	0.09850	EDIL3	EGF-like repeat and discoidin I-like domain-containing protein 3
P40121	-1.111	0.14271	CAPG	Macrophage-capping protein
Q8WWM9	-1.017	0.00779	CYGB	Cytoglobin
Q04828	-0.975	0.00237	AKR1C1	Aldo-keto reductase family 1 member C1
P06702	-0.900	0.02426	S100A9	Protein S100-A9
Q8NHP8	-0.858	0.02067	PLBD2	Putative phospholipase B-like 2
P26022	-0.849	0.00237	PTX3	Pentraxin-related protein
P42330	-0.707	0.00354	AKR1C3	Aldo-keto reductase family 1 member C3
P59666	-0.693	0.21716	DEFA3	Neutrophil defensin 3
P10321	-0.679	0.18630	HLA-C	HLA class I histocompatibility antigen, Cw-7 alpha chain
P26447	-0.679	0.02730	S100A4	Protein S100-A4
P15559	-0.670	0.03479	NQO1	NAD(P)H dehydrogenase [quinone] 1
P05362	-0.664	0.07720	ICAM1	Intercellular adhesion molecule 1
Q92930	-0.662	0.02058	RAB8B	Ras-related protein Rab-8B
P17931	-0.660	0.02942	LGALS3	Galectin-3
P02461	-0.657	0.21068	COL3A1	Collagen alpha-1(III) chain
P08294	-0.626	0.09287	SOD3	Extracellular superoxide dismutase [Cu-Zn]
P36269	-0.623	0.02426	GGT5	Glutathione hydrolase 5 proenzyme
Q8IUG5	-0.605	0.15825	MYO18B	Unconventional myosin-XVIIIb
P30455	-0.590	0.22312	HLA-A	HLA class I histocompatibility antigen, A-36 alpha chain

Table 12. Top 20 most significantly downregulated proteins in response to TGF-β1 challenge – Shown is Accession ID, log 2 fold change, p-adj, gene name and brief description.

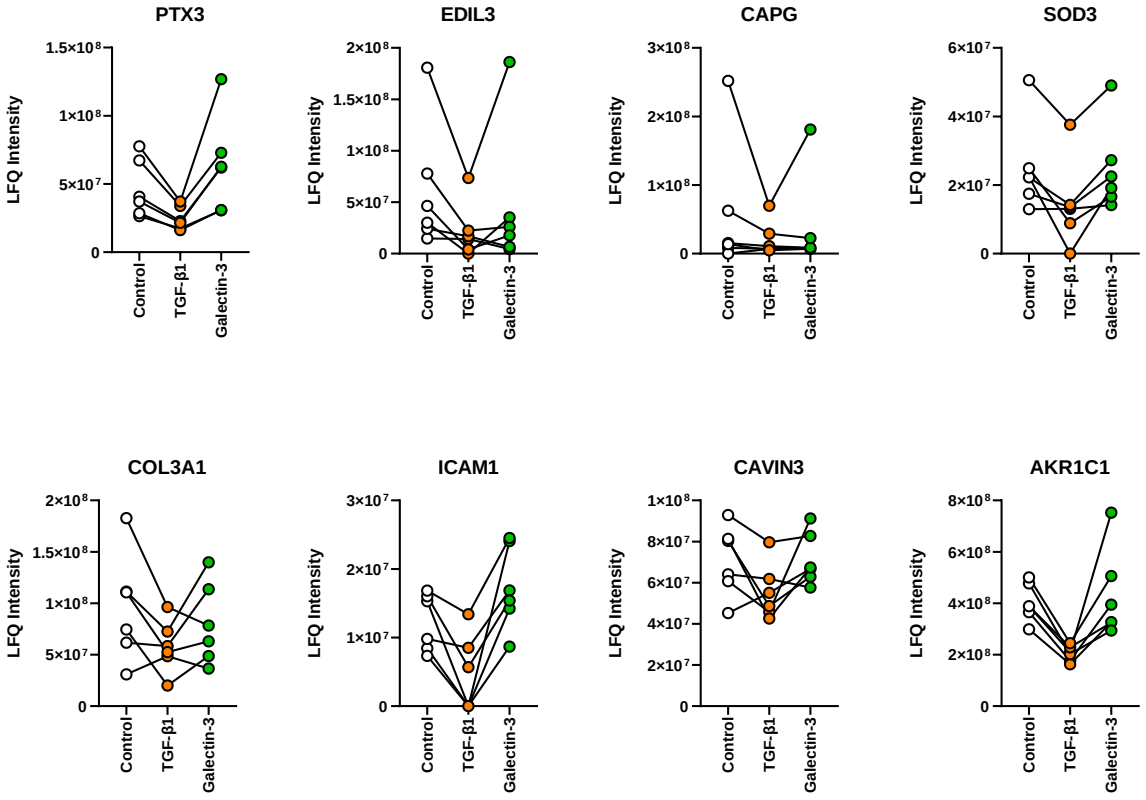

Figure 61. Representative graphs of proteins downregulated in response to TGF-β1 treatment – Protein intensity values from proteomic data after PCHS treated with either Galectin-3, TGF-β1 or control media for 72 hours. Protein expression was classed as significant if padj <0.0 and Log2 FC ±1.5. Data is shown for each individual donor; n=6 donors.

Whilst the transcriptomic analysis confirmed a potent inflammatory response in PCHS elicited by Galectin-3, many of the inflammatory genes expressed when translated to proteins are smaller than 10KDa in size and therefore undetectable through proteomic analysis due to absence of unique peptides. However despite this there were still a large number of proteins upregulated, with the most significant proteins shown in **Table 13**. Pentraxin-3, an acute phase protein involved in inflammatory responses and secreted from multiple cell types was shown to be upregulated **(Figure 63)**.

Interestingly Pentraxin-3 was also one of the most significantly downregulated proteins after TGF-β1 treatment. These results once again highlight our ability to change the profile of the PCHS in response to exogenous stimuli. Somewhat surprisingly, the ECM protein fibrillin is upregulated after Galectin-3 challenge, as are the basement membrane proteins Collagen 4a1 and Collagen 4a2. Whilst Collagen 4 was upregulated in response to Galectin-3, Collagen 1a1 was significantly downregulated as shown in **Table 14 and Figure 64**. The matricellular protein Thrombospondin-2 was also significantly downregulated, whilst remaining stable in the TGF-β1 treated PCHS.

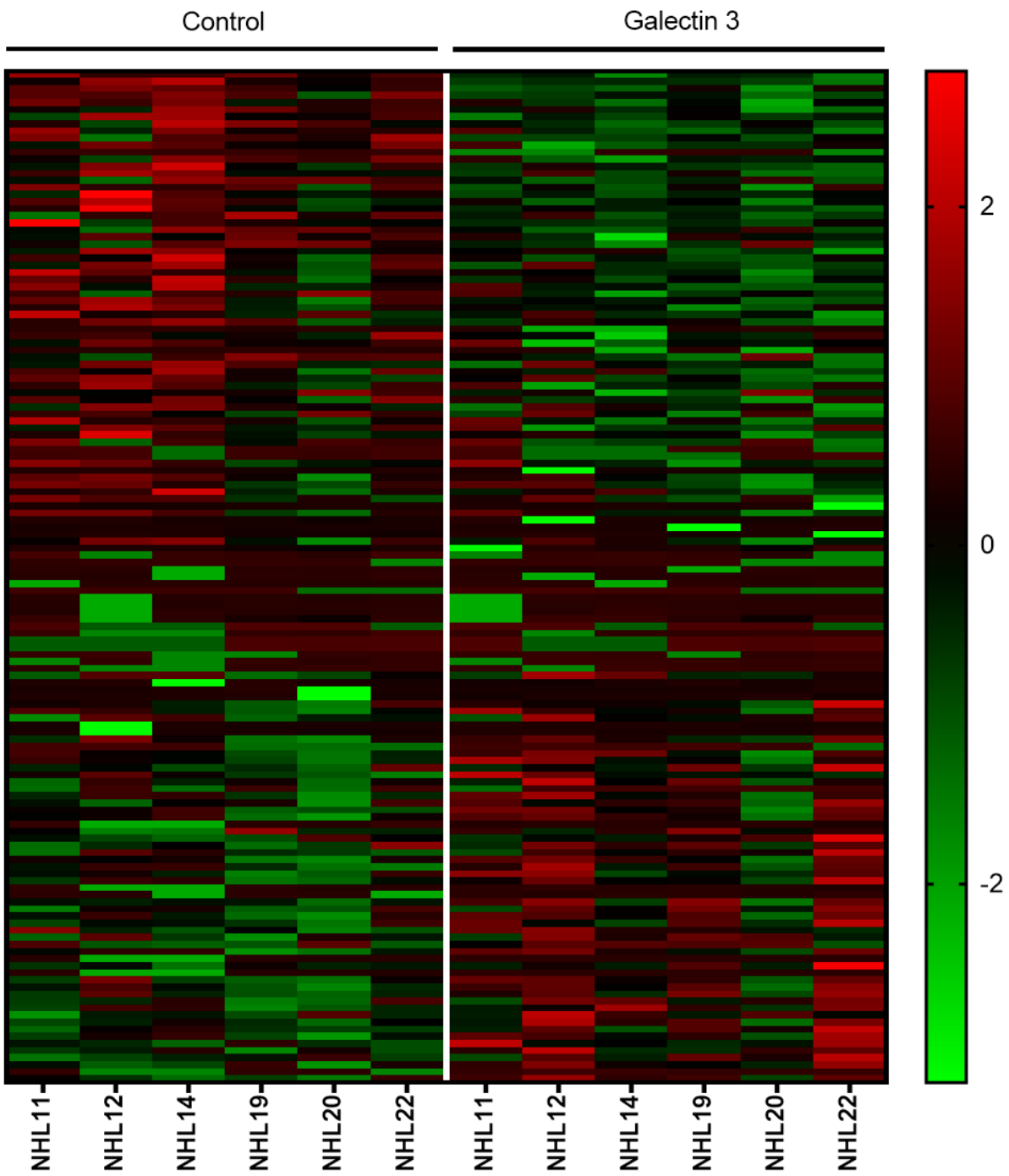

Figure 62. Heat map depicting distinct protein profile caused by Galectin-3 challenge – Z transformed protein expression changes from PCHS (n=6 donors) challenged with Galectin-3 or untreated. Significance was determined by proteins with log 2 fold change > ± 1.5 and padj≤0.05.

Accession	log2 FC	p-adj	Gene Name	Description
P42224	1.138	0.43050	STAT1	Signal transducer and activator of transcription 1-alpha/beta
P32455	1.137	0.10653	GBP1	Guanylate-binding protein 1
P02760	1.095	0.54112	AMBP	Protein AMBP
P35555	1.079	0.46235	FBN1	Fibrillin-1
P02795	1.061	0.43050	MT2A	Metallothionein-2
P43490	0.931	0.00010	NAMPT	Nicotinamide phosphoribosyl transferase
Q15631	0.756	0.26777	TSN	Translin
P08572	0.714	0.45533	COL4A2	Collagen alpha-2(IV) chain
P55083	0.705	0.43050	MFAP4	Microfibril-associated glycoprotein 4
P54652	0.694	0.54112	HSPA2	Heat shock-related 70 kDa protein 2
P02743	0.659	0.66070	APCS	Serum amyloid P-component
P35749	0.641	0.65659	MYH11	Myosin-11
P23381	0.624	0.26777	WARS	Tryptophan--tRNA ligase, cytoplasmic
P01889	0.598	0.26444	HLA-B	HLA class I histocompatibility antigen, B-7 alpha chain
Q01995	0.589	0.66267	TAGLN	Transgelin
Q9UL46	0.576	0.05463	PSME2	Proteasome activator complex subunit 2
P02462	0.568	0.54112	COL4A1	Collagen alpha-1(IV) chain
P29966	0.556	0.33339	MARCKS	Myristoylated alanine-rich C-kinase substrate
P08174	0.549	0.54112	CD55	Complement decay-accelerating factor
P56199	0.507	0.08381	IGTA1	Integrin alpha-1

Table 13. Top 20 most significantly upregulated proteins in response to Galectin-3 challenge – Shown is Accession ID, log 2 fold change, p-adj, gene name and brief description.

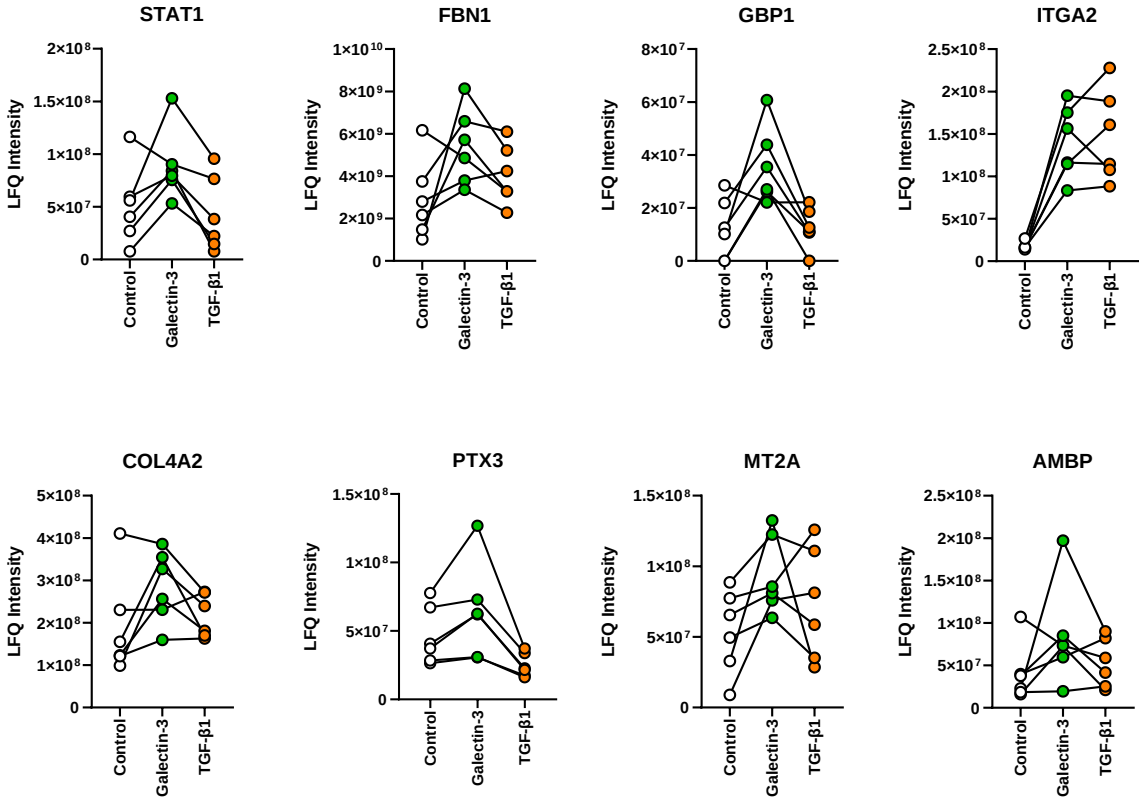

Figure 63. Representative graphs of proteins upregulated in response to Galectin-3 treatment – Protein intensity values from proteomic data after PCHS treated with either Galectin-3, TGF-β1 or control media for 72 hours. Protein expression was classed as significant if padj <0.05 and Log2 FC ±1.5. Data is shown for each individual donor; n=6 donors.

Accession	Log2 FC	p-adj	Gene Name	Description
Q96I25	-3.01084	0.615257	RBM17	Splicing Factor 45
O43854	-1.0551	0.646377	EDIL3	EGF-like repeat and discoidin I-like domain-containing protein 3
P40121	-0.96908	0.640952	CAPG	Macrophage-capping protein
P35442	-0.74685	0.660699	THBS2	Thrombospondin-2
Q9H299	-0.53452	0.258472	SH3BGRL3	SH3 domain-binding glutamic acid-rich-like protein 3
P46926	-0.5288	0.424363	GNPDA1	Glucosamine-6-phosphate isomerase 1
Q9NUQ9	-0.5005	0.541119	FAM49B	Protein FAM49B
Q16658	-0.47839	0.424363	FSCN1	Fascin
P02792	-0.47727	0.50372	FTL	Ferritin light chain
P02452	-0.47621	0.640952	COL1A1	Collagen alpha-1(I) chain
O76021	-0.47197	0.541119	RSL1D1	Ribosomal L1 domain-containing protein 1
Q08752	-0.46006	0.523813	PPID	Peptidyl-prolyl cis-trans isomerase D
Q13509	-0.42689	0.615257	TUBB3	Tubulin beta-3 chain
P50897	-0.42385	0.45533	PPT1	Palmitoyl-protein thioesterase 1
P61457	-0.42312	0.523813	PCBD1	Pterin-4-alpha-carbinolamine dehydratase
Q8NHP8	-0.42274	0.66267	PLBD2	Putative phospholipase B-like 2
Q9Y5L4	-0.42004	0.501438	TIMM13	Mitochondrial import inner membrane translocase subunit Tim13
Q9Y2W1	-0.41603	0.62741	THRAP3	Thyroid hormone receptor-associated protein 3
Q9UHQ4	-0.4148	0.50372	BCAP29	B-cell receptor-associated protein 29
O94832	-0.40841	0.541119	MYO1D	Unconventional myosin-Id

Table 14. Top 20 most significantly downregulated proteins in response to Galectin-3 challenge – Shown is Accession ID, log 2 fold change, p-adj, gene name and brief description.

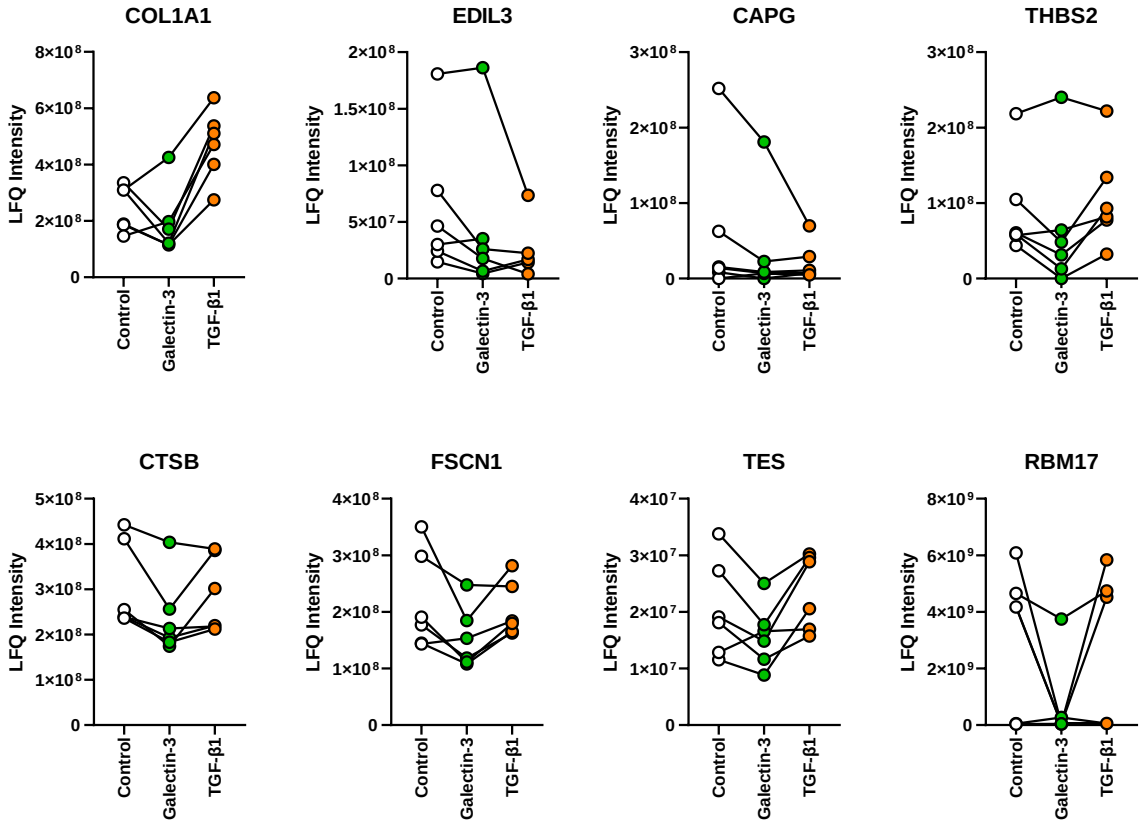

Figure 64. Representative graphs of proteins downregulated in response to Galectin-3 treatment – Protein intensity values from proteomic data after PCHS treated with either Galectin-3, TGF-β1 or control media for 72 hours. Protein expression was classed as significant if padj <0.0 and Log2 FC ±1.5. Data is shown for each individual donor; n=6 donors.

Taken together these data show the ability to modulate different phenotypes in PCHS in response to exogenous stimuli. Whilst CTGF, IL-11 and Angiotensin II induced a limited protein and transcriptional response in our system, the distinct effects induced through TGF-β1 and Galectin-3 treatment has provided us with the ability to investigate disease mechanisms occurring within primary human tissue in response to a pro-fibrotic or pro-inflammatory stimuli. Developing a greater understanding of both the genetic and protein changes occurring in the heart during disease is key to the development of novel therapies.

5.4.3 Investigating the inhibitory effect of compounds identified through IPA on primary cardiac fibroblasts.

Having demonstrated the ability to induce both inflammatory and fibrotic expression changes in the PCHS we next wanted the assess the ability to use the system to identify candidate compounds for the repurposing of therapies. In order to do this, the RNA sequencing results for TGF-β1 and Galectin-3 underwent Ingenuity Pathway Analysis (IPA). Core analysis was performed using log2 fold change for the z-score calculations. We focused our analysis on the Upstream Regulator Function from IPA. This function enables the identification of potential regulators responsible for gene expression changes within the dataset. IPA predicts whether an upstream regulated is either inhibited or activated to account for the upregulation or downregulation of particular genes in response to treatment. **Table 15** depicts the upstream regulators identified in response to either TGF-β1 or Galectin-3 challenge. Upstream regulators were limited to chemical drug, chemical reagent, biologic drug or chemical kinase inhibitors prior to sorting into predicted activation state and the activation z-score. In total we identified 20 upstream regulators of TGF-β1 and 13 upstream regulators of Galectin-3 to test on both cardiac fibroblasts and PCHS.

Upstream Regulator	Activation Z-Score	p-value overlap	TGF-β1 or Galectin-3
Ziritaxestat	2.309	4.18E-11	TGF-β1
Sorafenib	2.236	0.000552	TGF-β1
Geldanamycin	2.169	0.538	TGF-β1
GW9662	1.964	0.00000118	TGF-β1
Calcimycin (A23187)	1.876	0.135	TGF-β1
Aspirin	1.876	2.57E-11	TGF-β1
Tempol	1.732	0.0042	TGF-β1
Tamoxifen	1.731	0.00369	TGF-β1
BAY 11-7082	1.479	0.000488	TGF-β1
LY294002	1.404	5.63E-11	TGF-β1
H-7	1.387	0.000621	TGF-β1
AG490	1.386	0.000000131	TGF-β1
Dorsomorphin	1.363	0.0189	TGF-β1
Rottlerin	1.224	0.0111	TGF-β1
Triptolide	1.175	2.47E-08	TGF-β1
Rapamycin (Sirolimus)	1.173	0.00415	TGF-β1
Calphostin C	1.172	0.00595	TGF-β1
Dexamethasone	1.04	2.28E-36	TGF-β1
Napabucasin	1	0.0233	TGF-β1
Immethridine	1	0.000907	TGF-β1
Tetradecanoylphorbol acetate (PMA)	3.238	3.09E-11	Galectin-3
Tributyrin (Glycerol Tributyrate)	2.964	1.34E-14	Galectin-3
Mycophenolic acid	2.828	1.04E-11	Galectin-3
Resiquimod	2.806	9.23E-09	Galectin-3
Cycloheximide	2.698	5.16E-10	Galectin-3
Paclitaxel (Taxol)	2.695	1.69E-08	Galectin-3
Erlotinib	2.333	6.42E-16	Galectin-3
ABT-737	2.236	6.8E-10	Galectin-3
Camptothecin	1.941	4.28E-09	Galectin-3
PLX5622	1.941	0.0000236	Galectin-3
Capsaicin	1.67	0.0000248	Galectin-3
Acetaminophen (Paracetamol)	1.448	0.0000685	Galectin-3
Calcipotriene	1.25	0.000000348	Galectin-3

Table 15. Candidate compounds identified through the upstream regulators function during IPA – Table shows candidate compounds identified either in response to TGF-β1 or Galectin-3 treatment.

Initial experiments using the upstream regulator compounds took place in primary human cardiac fibroblasts isolated from LVAD tissue and unused donor hearts to assess fibroblast specific responses and toxicity. Briefly fibroblasts from 5 donors were seeded into 96 well plates and cultured overnight in serum free culture media prior to treatment with the different compounds. Each compound was applied in duplicate at either 10µM, 1µM or 0.1µM. After 24 hours media was collected for analysis *via* ELISA, whilst metabolic activity of the cells was assessed by resazurin assay.

Firstly it was important to ascertain whether any of the doses or compounds were toxic to the fibroblasts. Resazurin assay assessed metabolic activity of the cells in response to exposure to each compound, results were normalised to the values from untreated cells and presented as a percentage of control. **Table 16** depicts the viability of each donor for every compound and dose applied. Values closer to the control value, and therefore counted as viable, are visualised in green. As viability reduces, due to resazurin values falling below that of control, the values turn from green to yellow then orange and finally red.

Most of the compounds were well tolerated by the fibroblasts across multiple donors, for example Tempol had values remaining above 80% at all doses tested. Napabucasin appeared to be well tolerated at 0.1µM however at 1µM activity had dropped well below that of control, with the lowest value being 8.9% of control, interestingly though there was variability between the donors, with one donor remaining at 72% of control. Other compounds such as PMA were tolerated well at 0.1µM and 1µM however 10µM proved to be toxic. Cardiac fibroblasts isolated from Donor 1 appeared to be more sensitive to the different compounds across the three different doses with resazurin falling below 70% for a number of the compounds including Tamoxifen, Rapamycin, ABT-737 and Rottlerin. Due to this inter-donor variability, only drugs which maintained viability (defined as >70% of control) in at least three of the five donors were taken forward for further analysis *via* ELISA.

Compound Name	0.1µm					1µm					10µm				
	Donor 1	Donor 2	Donor 3	Donor 4	Donor 5	Donor 1	Donor 2	Donor 3	Donor 4	Donor 5	Donor 1	Donor 2	Donor 3	Donor 4	Donor 5
GW9662	90.0	99.6	84.0	91.8	109.1	88.4	95.4	86.3	97.4	107.0	105.9	106.0	93.6	92.2	96.2
Bay 11-7082	87.0	102.7	81.0	106.4	103.7	91.0	123.6	86.2	104.6	102.3	4.8	6.7	3.3	0.3	11.9
LY294002	81.9	105.6	85.0	93.1	91.9	80.2	105.1	91.4	92.4	92.5	70.6	91.1	97.3	73.0	75.6
GB1107	82.8	96.6	89.6	96.5	97.1	84.4	104.0	91.9	94.8	96.4	82.0	90.3	77.9	66.5	72.0
Taxol	66.3	101.1	71.3	80.1	82.2	63.9	100.9	71.5	82.7	86.8	70.0	93.4	70.3	66.9	91.4
Erlotinib	85.5	97.4	91.1	83.1	90.4	81.4	116.2	94.6	89.6	98.9	84.3	101.6	106.8	81.6	94.6
PLX5622	85.8	95.5	98.0	76.3	80.8	77.4	112.8	85.2	85.7	93.3	47.0	81.9	74.8	51.0	71.2
Tempol	86.6	99.7	94.0	94.4	110.6	95.4	105.9	107.2	103.9	106.0	92.8	96.6	100.7	101.9	82.8
Camptothecin	90.6	109.0	87.0	96.8	128.4	69.8	93.9	95.1	86.0	101.3	70.6	91.4	78.5	92.6	102.4
Cycloheximide	99.3	96.5	96.8	85.1	88.7	93.3	88.1	78.9	86.5	89.1	80.3	71.3	64.6	76.8	80.6
Mycophenolic Acid	101.3	101.4	101.5	84.0	104.6	91.4	106.1	100.2	97.1	104.5	105.4	103.2	99.2	100.8	97.6
AG-490	97.5	99.4	104.9	88.8	102.3	91.2	100.7	107.4	97.3	101.0	112.4	101.0	114.1	104.6	103.6
Aspirin	73.6	99.2	102.1	85.8	108.5	76.6	96.6	100.3	99.6	109.6	82.6	94.5	103.0	94.8	98.7
Napabucasin	83.3	101.7	98.4	90.4	81.7	65.4	8.9	39.3	37.0	72.5	10.8	5.2	7.2	2.2	78.1
Sorafenib	74.7	89.5	94.2	83.2	94.4	83.8	96.1	101.4	85.3	106.6	12.4	15.5	26.9	22.3	30.1
Dexamethasone	88.4	95.8	104.8	93.9	93.8	92.1	94.2	107.0	101.1	97.5	113.0	106.6	125.1	109.7	100.9
Tamoxifen	68.2	86.6	102.4	82.5	96.6	77.3	89.1	102.4	85.9	97.8	72.9	87.7	94.3	54.5	106.9
Rapamycin	59.7	91.2	84.1	74.1	94.0	66.6	89.6	88.5	82.4	102.1	81.2	101.0	107.5	92.5	120.9
ABT-737	61.8	110.0	86.3	77.8	107.3	68.2	107.4	87.1	82.8	115.7	62.0	98.2	77.5	64.5	110.6
Rottlerin	67.5	111.8	95.6	90.4	112.0	49.2	83.5	77.8	61.1	123.8	33.1	35.4	38.4	20.1	47.9
Ziritaxestat	72.2	99.0	84.4	86.7	92.0	76.9	91.7	88.3	89.0	98.2	77.6	85.8	89.0	83.0	94.8
Calcipotriene	64.4	92.6	88.9	83.3	108.6	79.0	110.3	103.4	91.4	116.1	4.1	4.8	3.4	2.3	14.8
Triptolide	40.2	85.4	82.6	76.4	104.2	38.3	74.2	57.0	71.1	98.9	43.6	78.6	68.7	74.2	92.0
Resiquimod	71.9	94.1	92.3	86.8	97.7	78.8	90.3	90.6	103.6	97.9	101.1	91.8	97.4	100.6	96.6
PMA	79.7	91.3	88.8	60.9	97.2	85.4	86.1	85.2	80.0	87.3	5.2	3.5	2.7	4.1	12.6
Geldanamycin	51.3	67.2	74.3	57.7	72.0	64.4	73.3	75.1	67.7	65.9	63.9	60.4	55.7	87.5	59.7
A23187	57.6	77.0	71.9	67.6	91.2	46.8	69.2	57.1	52.1	84.3	30.0	53.4	37.7	23.5	61.1
Capsaicin	77.9	93.5	88.0	92.5	121.8	76.4	101.2	85.7	97.7	112.3	89.4	103.1	91.9	93.8	100.6
Acetaminophen	76.7	94.1	82.2	96.2	116.3	77.8	98.3	85.0	97.2	121.0	95.6	106.0	88.9	104.0	110.3
Dorsomorphin	73.7	96.3	90.9	95.9	148.9	79.2	99.3	91.0	96.7	110.6	99.7	103.5	97.8	89.2	84.3
Immethridine Dihydrobromide	76.5	94.5	78.6	89.2	112.5	82.7	96.4	82.2	89.5	111.3	103.5	105.4	92.6	101.3	94.9
H-7	81.3	88.9	86.4	89.2	100.3	91.1	89.9	92.2	90.6	107.1	101.7	92.8	94.5	91.4	85.6

Table 16. Viability of cardiac fibroblasts in response to treatment with candidate compounds – Compounds were applied at either 0.1µM, 1µM or 10µM across 5 different donors for 24 hours. Metabolic activity was assessed *via* Resazurin assay which was applied to cells for 1 hour at the end of the culture period. Values were normalised to the control values for each donor and presented as a % of control.

Figure 65 depicts a number of compounds which have a range of tolerability depending on the dose applied. We determined any drug which resulted in the normalised resazurin value to be below 70% of the control to be toxic to the fibroblasts. The multi-kinase inhibitor and HCC therapy, Sorafenib, touted as a potential anti-fibrotic therapy for liver fibrosis was shown to reduce metabolic activity at 10µM, however it remained well tolerated at the lower doses **(Figure 65A)**. A number of the compounds tested reduced metabolic activity below the viability threshold at multiple doses. Geldanamycin and A23187 were the most toxic to the cells, with viability below the 70% threshold at all three doses tested, and therefore excluded from future analysis *via* ELISA. Overall, many of the candidate compounds were comparable to control at all doses **(Figure 65B)** including Taxol, Mycophenolic Acid and GW9662.

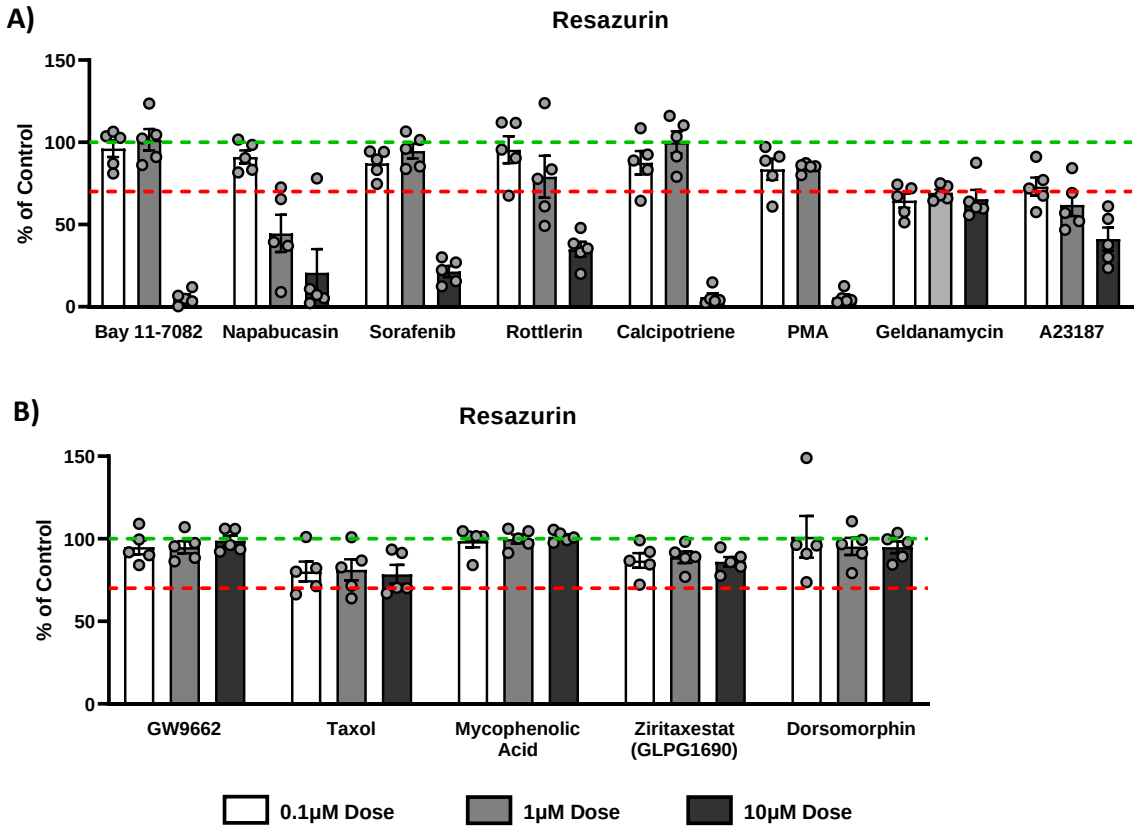

Figure 65. Metabolic activity of cardiac fibroblasts in response to treatment with candidate compounds – Primary human cardiac fibroblasts were treated for 24 hours with compounds identified from IPA Upstream regulator function. Compounds were used at 0.1μM, 1μM and 10μM, after 24 hours of culture, media was removed and stored for analysis by ELISA. Metabolic activity was assessed by Resazurin Assay, and results normalised to unstimulated cells. Data is presented as a percentage of control, n=5 donors. Green line marks 100%, red dashed lined marks 70% of control. Values below this line are designated as unviable.

Having assessed the metabolic activity of the cells in response to the different compounds we next proceeded to investigate the ability of the compounds to effect protein secretion. ELISA was performed on the cell culture supernatants to quantify changes in the secretion of pro-inflammatory (MCP-1) and pro-fibrotic (TGF-β1 and TIMP-1) proteins. Particular compounds, doses or donors were omitted from the analysis if the resazurin value had dropped below 70% of control. Those compounds omitted are depicted as grey blank cells **(Tables 17-19)**. **Table 17** depicts the individual donors response to each compound assessed at the three different doses, once again normalised to percentage of Collagen 1a1 secretion from untreated cells. The results show that across nearly all compounds tested Collagen 1a1 secretion was unable to be reduced by a 0.1µM treatment. Rottlerin was the only compound able to reduce collagen secretion across a number of donors at 1µM. However, it was found to be toxic at 10µM and ineffective at attenuating collagen 1a1 secretion at 0.1µM. Unsurprisingly the greatest inhibitory effects were observed in response to the 10µM dose with Taxol, Cycloheximide and Tamoxifen having the strongest responses. **Figure 66** depicts the changes in Collagen 1a1 secretion for a limited number of the compounds across the three doses tested.

Compound Name	0.1µm					1µm					10µm				
	Donor 1	Donor 2	Donor 3	Donor 4	Donor 5	Donor 1	Donor 2	Donor 3	Donor 4	Donor 5	Donor 1	Donor 2	Donor 3	Donor 4	Donor 5
GW9662	93.3	112.5	108.1	133.9	127.7	77.9	110.8	113.3	127.6	107.7	54.1	86.6	86.8	110.0	84.9
Bay 11-7082	86.6	117.0	131.7	132.2	126.6	86.5	106.1	139.0	129.4	133.5					
LY294002	93.4	113.9	126.6	117.7	116.3	84.5	115.2	127.6	113.0	108.5	54.8	98.0	72.0	66.4	74.6
GB1107	91.5	105.9	133.0	125.2	116.3	82.9	90.7	130.4	120.0	114.7	53.6	70.8	67.6		97.9
Taxol		98.9	100.8	107.8	126.0		79.2	99.0	108.0	120.7	31.1	48.8	64.6	59.8	75.1
Erlotinib	68.9	102.3	135.7	118.3	133.6	74.9	76.7	123.7	113.1	144.7	63.2	96.9	89.6	109.4	130.3
PLX5622	87.2	123.5	154.0	110.0	123.4	69.0	79.9	136.5	118.1	136.6		15.9	39.8		45.0
Tempol	96.6	122.4	120.9	138.3	138.1	86.3	103.8	131.1	142.2	128.8	70.9	68.2	87.6	127.0	87.4
Camptothecin	92.1	103.0	114.1	151.2	129.2		82.1	116.9	121.4	136.5	62.2	64.3	74.2	95.2	103.6
Cycloheximide	94.7	95.2	140.8	121.3	117.9	61.6	66.0	105.7	99.0	99.6	24.7	21.4	48.9	49.1	44.2
Mycophenolic Acid	101.5	105.5	131.4	143.7	132.1	91.6	104.9	143.8	141.6	111.3	71.2	61.4	109.5	132.3	95.5
AG-490	92.5	101.2	157.8	139.4	129.9	83.9	96.8	155.8	145.8	117.9	48.0	49.4	116.4	93.9	65.8
Aspirin	89.7	129.8	154.0	133.7	144.2	87.9	122.8	156.7	137.1	112.7	63.3	82.5	119.5	111.0	80.8
Napabucasin	86.4	133.0	196.2	177.4	141.2										
Sorafenib	94.0	114.4	167.9	131.0	126.5	75.2	137.1	172.6	143.0	166.6					
Dexamethasone	80.9	97.4	104.1	128.2	137.8	77.6	94.3	129.9	120.9	127.7	65.6	66.5	94.3	95.4	92.9
Tamoxifen		119.8	147.0	146.5	125.2	85.2	127.9	150.0	129.0	96.3	40.8	60.9	63.1		74.4
Rapamycin		190.6	134.0	131.7	149.9		183.9	132.7	126.4	142.7	70.7	105.2	108.5	81.4	122.6
ABT-737		212.1	145.3	133.8	141.7		166.5	149.4	154.7	156.5		106.2	94.7		137.8
Rottlerin		167.7	137.4	141.0	135.3		34.2	76.8	40.6	38.1					
Ziritaxestat		151.8	138.8	136.8	136.3	85.3	146.6	130.9	130.5	132.8	61.3	124.1	94.1	113.9	102.3
Calcipotriene		189.4	150.8	164.5	145.8	90.6	195.1	139.1	167.3	177.1					
Triptolide		137.9	116.6	133.7	120.6		128.8	80.7	107.0	118.4		98.3		80.4	96.0
Resiquimod		151.4	107.5	140.3	147.5	79.8	144.5	122.5	149.4	122.6	68.0	109.3	104.3	107.4	94.1
PMA		54.1	95.7		115.5	38.5	80.3	59.1	89.2	93.6					
Geldanamycin															
A23187															
Capsaicin	88.9	173.2	125.7	149.3	169.4	93.7	158.5	117.0	141.2	152.4	72.2	127.2	94.4	111.0	119.3
Acetaminophen	84.6	169.8	120.2	153.5	148.9	106.8	161.8	116.7	157.2	144.9	78.6	116.1	94.9	135.1	117.9
Dorsomorphin	110.0	180.4	124.0	144.5	165.5	106.9	154.9	120.4	135.3	142.3	76.8	104.9	86.4	86.2	102.4
Immethridine Dihydrobromide	97.0	170.9	111.6	143.7	163.5	112.4	174.8	107.4	139.2	148.5	75.5	122.4	81.1	120.9	107.1
H-7	103.8	171.5	142.5	135.1	144.6	100.0	171.4	135.2	130.3	148.4	75.3	100.1	75.7	103.0	109.0

Table 17. Collagen 1a1 secretion from cardiac fibroblasts in response to treatment with candidate compounds – Compounds were applied at either 0.1µM, 1µM or 10µM across 5 different donors for 24 hours. Collagen 1a1 secretion was quantified *via* ELISA. Values were normalised to the control values for each donor and presented as a % of control. Blank values represent results omitted from analysis due to cells being deemed unviable after resazurin assay.

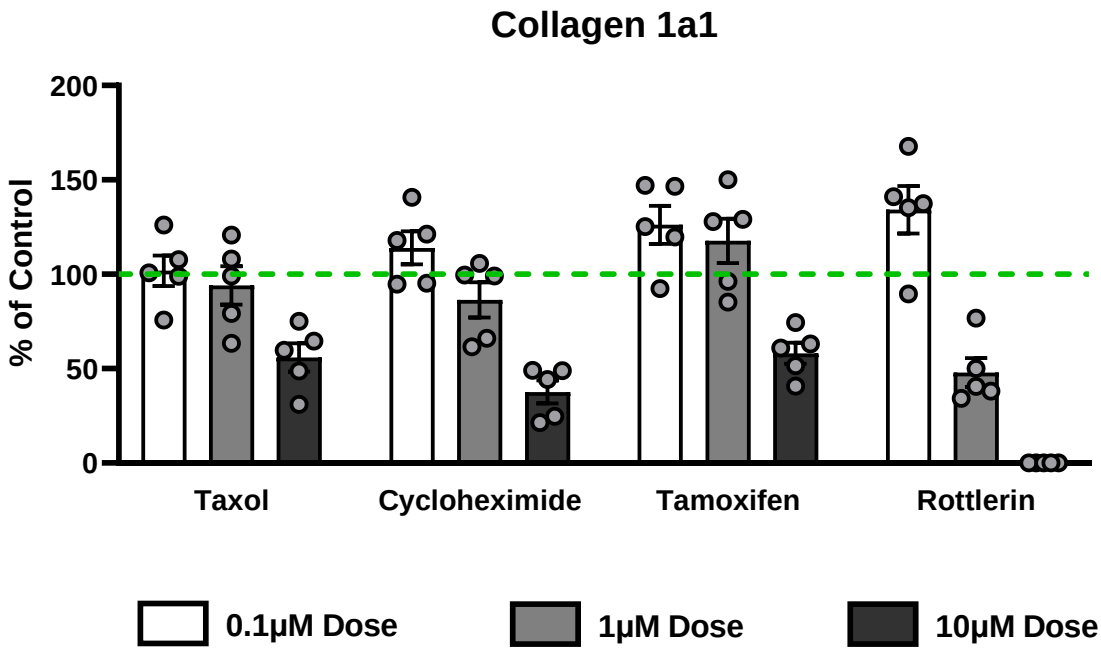

Figure 66. Collagen 1a1 secretion from cardiac fibroblasts in response to treatment with candidate compounds – Primary human cardiac fibroblasts were treated for 24 hours with compounds identified from IPA Upstream regulator function. Compounds were used at 0.1µM, 1µM and 10µM, after 24 hours of culture, media was removed and stored for analysis by ELISA. Results were normalised to unstimulated cells. Data is presented as a percentage of control, n=5 donors. Green line marks 100%.

To further investigate the anti-fibrotic capabilities of the compounds, TIMP-1 secretion was also quantified **(Table 18)**. These results demonstrated a similar profile to Collagen 1a1 secretion. Cycloheximide and rottlerin were able to potently attenuate TIMP-1 secretion at a dose of 1µM **(Figure 67)**. Other compounds which displayed potential anti-fibrotic efficacy were the colony stimulating factor receptor 1 (CSFR1) inhibitor PLX5622, rapamycin, ABT-737 and GB1107, a Galectin-3 inhibitor. Unsurprisingly the steroid Dexamethasone was one of a number of compounds to have no effect on TIMP-1 secretion.

Compound Name	0.1µm					1µm					10µm				
	Donor 1	Donor 2	Donor 3	Donor 4	Donor 5	Donor 1	Donor 2	Donor 3	Donor 4	Donor 5	Donor 1	Donor 2	Donor 3	Donor 4	Donor 5
GW9662	81.4	111.7	113.4	104.5	92.2	76.9	109.2	116.1	114.7	103.5	88.5	118.9	110.0	128.2	144.4
Bay 11-7082	82.4	104.0	111.6	107.0	94.8	81.6	98.0	107.0	92.6	96.3					
LY294002	78.3	105.5	105.0	108.0	90.4	75.8	94.1	105.4	110.6	74.8	95.2	97.5	119.5	104.4	94.1
GB1107	69.8	105.4	123.2	130.3	98.9	71.7	87.5	103.4	125.3	90.7	55.0	70.9	69.0		64.0
Taxol		101.7	121.4	101.9	91.4	54.5	93.1	110.9	94.8	98.7	79.0	108.9	124.2	98.1	97.6
Erlotinib	80.8	103.4	99.6	113.6	86.9		70.5	104.0	108.3	112.4	57.7	75.2	89.0	80.9	130.0
PLX5622	72.5	109.4	96.6	101.0	50.4	62.8	63.5	101.2	89.3	107.7		8.2	23.2		24.4
Tempol	111.1	98.0	78.8	95.6	100.6	106.1	88.1	112.2	105.3	91.3	115.5	84.8	89.4	109.3	103.0
Camptothecin	112.8	123.2	79.6	99.3	114.6	112.0	111.1	90.3	77.5	85.6	102.1	116.9	86.8	88.6	99.6
Cycloheximide	79.6	97.8	62.0	66.5	77.7		40.8	25.8	39.7	32.2	8.1	8.4	1.5	4.7	9.8
Mycophenolic Acid	107.6	115.8	55.9	87.5	107.5	104.8	100.7	80.4	93.7	108.1	120.3	103.8	82.4	108.3	112.6
AG-490	124.9	106.2	83.7	91.8	95.8	102.6	100.3	80.1	91.8	99.7	154.2	89.3	81.4	91.5	135.2
Aspirin	108.3	112.3	92.6	94.1	109.1	111.2	96.1	84.8	99.2	96.4	133.6	101.1	100.7	110.4	104.3
Napabucasin	111.5	101.2	96.4	102.5	105.6										
Sorafenib	92.9	115.5	87.9	102.6	82.9	70.0	77.1	67.4	65.1	69.1					
Dexamethasone	102.6	93.8	106.3	102.0	90.4	106.3	94.9	119.9	108.6	86.2	129.7	104.1	132.5	120.9	101.1
Tamoxifen	107.4	101.7	103.6	93.7	100.9	109.3	93.5	100.8	81.9	94.0	91.3	90.6	93.2		96.6
Rapamycin		98.3	94.7	79.3	107.0		88.0	91.9	80.1	111.9	41.6	49.4	50.1	55.8	80.7
ABT-737		114.5	108.1	105.7	98.6		95.1	97.2	99.1	99.2		62.1	60.9		61.7
Rottlerin		74.1	74.6	69.6	94.7		7.8	21.5	17.7	17.0					
Ziritaxestat		82.7	86.1	97.3	87.0	96.8	85.0	92.2	106.8	92.1	88.7	73.9	78.8	82.5	93.2
Calcipotriene		89.0	100.3	112.0	123.0	92.1	103.9	129.3	101.3	101.1					
Triptolide		84.4	76.3	89.9	91.1		61.8		61.0	64.9		68.2		59.9	70.8
Resiquimod		90.0	110.3	97.8	102.7	90.3	81.7	90.0	104.9	97.3	102.2	82.4	111.7	94.2	109.6
PMA		220.7	336.2		245.0	248.4	208.9	301.5	236.0	217.1					
Geldanamycin															
A23187															
Capsaicin	74.0	94.9	107.3	82.2	100.2	69.9	89.3	96.1	81.0	82.1	76.4	92.8	94.2	84.3	79.2
Acetaminophen	72.7	111.9	100.3	77.4	94.4	68.1	89.5	86.5	96.5	102.5	81.4	104.0	85.1	119.5	105.9
Dorsomorphin	71.9	108.8	110.7	103.5	109.4	67.7	92.5	99.8	87.7	96.4	65.8	88.3	75.8	58.5	81.9
Immethridine Dihydrobromide	93.4	91.1	106.8	82.2	89.9	92.7	91.1	100.2	91.6	100.8	103.3	99.3	90.8	90.4	103.1
H-7	77.2	91.9	104.2	83.1	81.7	81.0	79.5	105.4	90.2	82.2	82.4	86.5	96.0	85.3	74.8

Table 18. TIMP-1 secretion from cardiac fibroblasts in response to treatment with candidate compounds – Compounds were applied at either 0.1µM, 1µM or 10µM across 5 different donors for 24 hours. TIMP-1 secretion was quantified *via* ELISA .Values were normalised to the control values for each donor and presented as a % of control. Blank values represent results omitted from analysis due to cells being deemed unviable after resazurin assay.

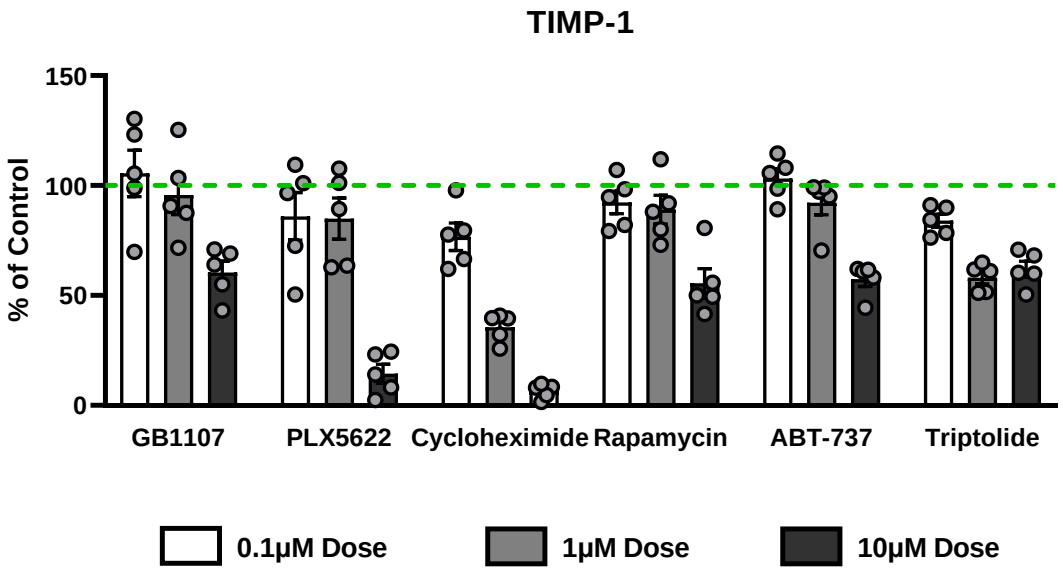

Figure 67. TIMP-1 secretion from cardiac fibroblasts in response to treatment with candidate compounds – Primary human cardiac fibroblasts were treated for 24 hours with compounds identified from IPA Upstream regulator function. Compounds were used at 0.1µM, 1µM and 10µM, after 24 hours of culture, media was removed and stored for analysis by ELISA. Results were normalised to unstimulated cells. Data is presented as a percentage of control, n=5 donors. Green line marks 100%.

Finally we explored the anti-inflammatory effects of the compounds through the quantification of MCP-1 secretion. Initial observations appear to show greater variability in the response between donors therefore making it difficult to interpret the anti-inflammatory effects of a number of the compounds **(Table 19)**. The effects of a number of the compounds are shown in **Figure 68**. Triptolide, a known anti-inflammatory compound, was found to be a potent inhibitor of MCP-1 production, with a consistent response across viable donors. Interestingly Dexamethasone, another potent anti-inflammatory compound resulted in a weaker inhibition of MCP-1. Despite this, Dexamethasone did appear to induce a response at all doses tested, with the 1µM dose resulting in a 32% reduction in MCP-1 secretion compared to control.

Compound Name	0.1µm					1µm					10µm				
	Donor 1	Donor 2	Donor 3	Donor 4	Donor 5	Donor 1	Donor 2	Donor 3	Donor 4	Donor 5	Donor 1	Donor 2	Donor 3	Donor 4	Donor 5
GW9662	89.5	102.6	163.2	118.1	86.4	71.4	73.8	155.1	128.1	72.2	94.8	90.4	114.0	122.0	52.5
Bay 11-7082	126.0	101.6	125.6	120.1	94.3	89.2	60.3	122.4	89.1	75.7					
LY294002	77.2	73.3	118.1	110.7	88.8	58.9	69.8	118.8	118.6	85.0	65.4	89.4	90.4	101.8	51.0
GB1107	81.3	84.5	113.0	118.1	82.1	88.1	17.3	98.6	125.8	99.1	73.0	16.6	81.6		59.3
Taxol		94.7	103.8	97.8	66.7		49.2	91.0	102.9	68.7	160.7	0.0	158.7	125.3	77.1
Erlotinib	104.2	83.2	101.3	110.8	79.8	86.8	73.0	102.6	121.4	105.7	87.6	69.7	93.2	106.8	86.6
PLX5622	101.6	93.6	89.9	97.1	111.6	78.1	93.0	147.4	100.4	112.1		206.8	59.3		28.4
Tempol	94.9	102.1	105.0	107.5	141.5	93.6	98.7	138.3	111.7	131.6	138.6	99.4	119.4	115.1	116.8
Camptothecin	72.9	109.5	68.8	72.9	61.0		92.7	44.0	52.7	51.4	84.6	69.5	65.6	75.4	95.2
Cycloheximide	68.4	74.6	61.3	88.5	113.1	64.9	84.2	64.7	87.7	76.0	88.5	50.8	75.6	63.7	179.6
Mycophenolic Acid	98.1	99.5	104.7	89.8	122.2	82.3	99.6	69.7	99.2	100.4	130.1	118.3	78.1	124.5	105.4
AG-490	105.3	82.3	73.4	90.2	127.5	87.5	73.0	65.7	102.2	218.0	106.0	1.5	77.8	109.9	74.5
Aspirin	90.6	120.4	78.1	96.0	146.5	95.0	64.7	98.7	105.5	132.9	143.2	72.9	82.3	116.8	119.0
Napabucasin	118.8	75.8	136.5	109.9	153.8										
Sorafenib	91.2	61.6	78.9	92.7	135.5	39.7	219.5	49.5	80.2	56.0					
Dexamethasone	76.8	75.3	54.4	71.4	109.8	79.6	42.5	61.1	73.0	83.5	84.1	73.1	51.8	85.7	78.6
Tamoxifen		111.2	99.6	80.9	147.1	102.4	103.5	87.4	74.9	176.3	197.2	164.7	153.9		69.3
Rapamycin		101.0	112.1	92.3	138.4		80.8	122.9	108.5	94.3	41.0	64.4	108.9	97.8	65.9
ABT-737		135.7	131.1	108.3	107.2		134.2	145.0	115.5	97.6		157.9	132.8		121.1
Rottlerin		87.0	89.0	87.4	59.0		13.4	68.6		8.5					
Ziritaxestat		80.4	75.3	98.5	67.4	94.9	111.3	93.2	74.8	56.5	84.0	190.0	89.9	85.8	57.2
Calcipotriene		89.6	70.8	98.7	81.8	85.8	108.1	91.3	104.9	60.7					
Triptolide		41.1	31.1	37.0	28.4		85.9		48.6	39.0		67.6		63.5	27.0
Resiquimod		104.1	105.0	86.7	99.3	92.8	141.4	81.6	89.9	102.1	71.3	116.6	97.7	97.7	103.3
PMA		298.5	166.4		159.1	150.4	336.0	176.8	48.0	128.4					
Geldanamycin															
A23187															
Capsaicin	60.3	69.2	107.9	86.7	125.2	66.1	67.8	105.4	95.6	125.5	82.0	92.5	120.6	98.6	91.0
Acetaminophen	62.9	71.7	120.2	99.7	108.9	59.6	62.8	113.8	110.6	77.2	82.3	99.5	103.8	110.6	73.2
Dorsomorphin	53.3	83.5	119.8	103.6	111.1	60.6	73.6	100.3	110.3	93.1	70.0	109.5	75.1	83.0	52.3
Immethridine Dihydrobromide	86.7	76.3	137.2	100.0	113.7	94.4	63.6	128.4	101.1	110.0	117.1	97.0	101.6	115.9	110.7
H-7	87.2	54.1	107.1	92.6	146.7	71.7	57.7	110.6	108.1	137.6	87.6	82.2	115.4	122.9	97.7

Table 19. MCP-1 secretion from cardiac fibroblasts in response to treatment with candidate compounds – Compounds were applied at either 0.1µM, 1µM and 10µM across 5 different donors for 24 hours. TIMP-1 secretion was quantified *via* ELISA .Values were normalised to the control values for each donor and presented as a % of control. Blank values represent results omitted from analysis due to cells being deemed unviable after resazurin assay.

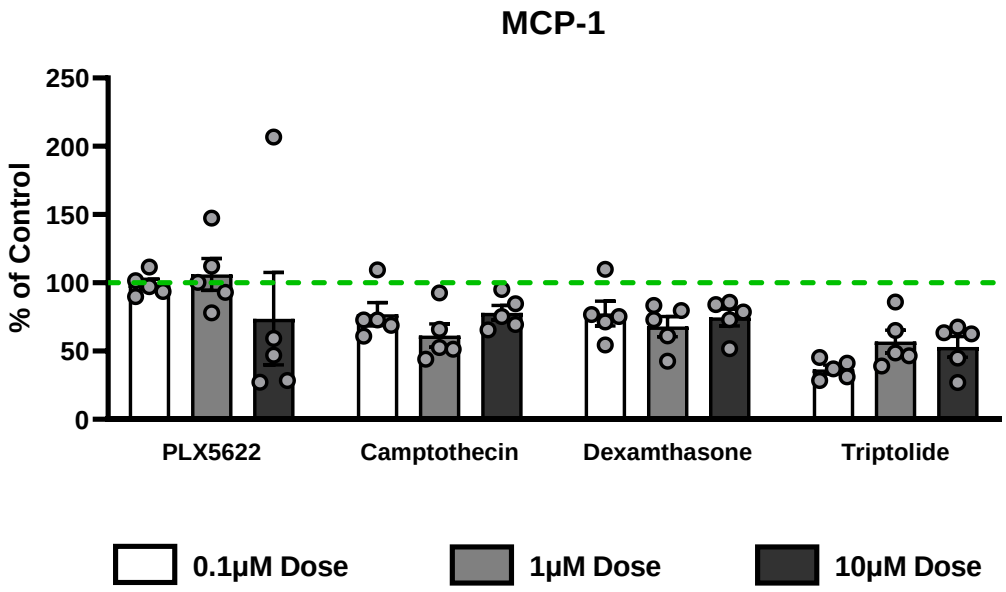

Figure 68. MCP-1 secretion from cardiac fibroblasts in response to treatment with candidate compounds – Primary human cardiac fibroblasts were treated for 24 hours with compounds identified from IPA Upstream regulator function. Compounds were used at 0.1µM, 1µM and 10µM, after 24 hours of culture, media was removed and stored for analysis by ELISA. Results were normalised to unstimulated cells. Data is presented as a percentage of control, n=5 donors. Green line marks 100%.

Taken together these data show the limited ability of the compounds identified through IPA to inhibit the secretion of pro-inflammatory and pro-fibrotic proteins from cardiac fibroblasts. Whilst we demonstrated that a large number of the compounds tested were well tolerated in the 2D culture system the majority of effective compounds needed to be applied at the high dose of 10µM to elicit a response. Only 4 of the compounds tested were able to attenuate secretion of fibrosis markers (Collagen 1a1 and TIMP-1) at 1µM and none were effective at 0.1µM. Data for MCP-1 attenuation was extremely variable between the different donors, making it difficult to make definitive conclusions.

5.4.4 IPA Compounds on PCHS

After assessing the ability of a number of the candidate compounds to effect protein secretion in cardiac fibroblasts we next moved onto investigating their efficacy in whole tissue through the use of PCHS. PCHS prepared from human hearts secrete proteins involved in both inflammation and fibrosis spontaneously throughout their time in culture. Whilst we have previously demonstrated the ability to further induce these responses through the application of recombinant proteins, in order not to bias the effects of the candidate compounds to a specific inflammation or fibrosis signalling pathway, PCHS were not stimulated with either Galectin-3 or TGF-β1. Therefore PCHS were simply treated after a 24 hour rest period with the different compounds at either 0.1µM, 1µM or 10µM for 72 hours. Supernatants were collected at every time point to assess protein secretion throughout the culture period. Our earlier experiments have already confirmed the efficacy of the ALK5 inhibitor and the two approved anti-fibrotic therapies Pirfenidone and Nintedanib, therefore we used these to provide a benchmark for the candidate compounds. As expected ALK5 inhibitor showed good anti-fibrotic effects, attenuating Collagen 1a1 and TIMP-1 secretion, as well as reducing levels of IL-6. Nintedanib also reaffirmed its ability to strongly reduce Collagen 1a1 and although to a lesser extent also effectively inhibited TIMP-1, IL-6 and IL-8. Finally Pirfenidone was strongly efficacious in blocking inflammation, inhibiting secretion of IL-8, IL-6 and MCP-1 by at least 60% compared to control. Collagen 1a1 and TIMP-1 secretion was also attenuated 35% and 20% respectively, confirming our earlier data detailing its anti-fibrotic effects to be less potent than that of Nintedanib and the ALK5 inhibitor.

Viability of slices after 72 hours of exposure to the compounds was assessed through resazurin assay of the PCHS at the end of the culture period and presented as a percentage of control slice viability **(Table 20)**. We accepted resazurin values of >70% of the control/untreated PCHS as viable, with values <70% deemed to have negatively impacted PCHS function. From this table it was very clear to see that the candidate compound Napabucasin was very toxic to the PCHS at 10µM, reducing resazurin to 6% of the control value. These toxic effects appear to be limited to 10µM, with viability for 0.1µM and 1µM on average remaining at 100.2% and 88.6% respectively.

Changes in protein secretion was assessed by ELISA for both pro-fibrotic (Collagen 1a1 and TIMP-1) and pro-inflammatory (IL-6, IL-8 and MCP-1) markers. In order to assess the effects of each compound on PCHS viability and function we plotted normalised resazurin values against protein secretion for each inflammatory and fibrotic marker assessed. The ability of each of the compounds to attenuate the secretion of inflammatory and fibrotic markers was subdivided using 3 different ranges of efficacy compared to control/untreated PCHS; 20-45% reduction (slight), 45-70% reduction (moderate), >70% reduction (strong). **Figures 69-73** depict the function and viability plots for each of the markers assessed, with results shown as compiled data, with all three doses plotted, and then also as a graph for each individual dose used. Unsurprisingly the greatest number of compounds which fell below the 70% of control resazurin and therefore deemed unviable were in response to the 10µM dose, with 9 compounds failing to reach this threshold **(Table 20)**. Napabucasin, a small molecule STAT3 inhibitor proved to have the greatest detrimental effect on resazurin levels from all the candidate compounds tested at 10µM, reaching just 7% of that of control. Whilst at the lower doses of 0.1µM and 1µM Napabucasin proved to be well tolerated, there was no inhibitory effect seen when secretion of Collagen 1a1, TIMP-1, IL-6, IL-8 or MCP-1 was quantified, in fact treatment often increased secretion of these proteins.

Compound Name	0.1µM		1µM		10µM	
GW9662	90.8	75.4	89.0	74.0	75.4	78.0
Bay 11-7082	70.0	91.1	103.5	88.6	50.8	94.7
LY294002	70.0	95.8	88.9	78.5	108.3	96.0
GB1107	92.3	94.9	79.9	82.8	101.2	92.1
Taxol	100.2	102.9	80.9	93.6	73.6	97.3
Erlotinib	87.4	96.7	86.5	88.8	91.5	80.0
PLX5622	96.0	78.3	79.3	98.2	93.6	65.7
Tempol	81.1	89.6	84.1	89.4	56.4	87.7
Camptothecin	115.4	109.2	93.0	55.6	76.3	61.4
Cycloheximide	57.9	85.4	57.5	103.5	52.0	71.5
Mycophenolic Acid	102.9	111.1	74.5	104.2	72.1	90.3
AG-490	123.8	91.3	84.9	100.5	100.7	81.5
Aspirin	88.8	81.9	69.5	58.4	96.3	66.9
Napabucasin	91.5	108.9	93.1	84.1	6.2	6.1
Sorafenib	148.4	67.1	86.7	94.8	101.7	100.9
Dexamethasone	112.5	95.6	95.2	82.6	97.2	88.9
Tamoxifen	61.0	75.1	78.6	75.4	69.6	72.1
Rapamycin	77.8	75.9	73.4	48.2	45.8	55.5
ABT-737	90.5	73.8	86.8	92.4	82.6	66.4
Rottlerin	76.9	81.9	60.0	66.2	36.8	47.6
Ziritaxestat	65.6	47.1	69.7	73.3	37.5	61.2
Calcipotriene	71.0	59.4	93.1	88.3	86.1	78.8
Triptolide	51.6	73.2	40.2	51.8	24.6	22.3
Resiquimod	78.8	89.7	90.6	75.9	73.4	90.7
PMA	110.0	89.9	80.0	81.3	67.6	75.6
Geldanamycin	98.0	106.1	51.7	84.1	36.6	35.3
A23187	71.3	50.4	83.5	81.4	48.1	14.4
Capsaicin	97.6	98.9	100.3	107.0	84.9	90.3
Acetaminophen	127.7	85.2	75.6	81.7	86.7	111.0
Dorsomorphin	96.3	117.3	98.6	91.2	100.1	124.9
Immethridine Dihydrobromide	80.7	105.0	101.0	95.2	130.1	94.4
H-7	90.7	111.4	102.4	79.9	74.2	105.5

Table 20. Viability of PCHS in response to treatment with candidate compounds – Compounds were applied to PCHS at either 0.1µM, 1µM or 10µM across 2 different donors for 72 hours. Metabolic activity was assessed *via* Resazurin assay which was applied to cells for 1 hour at the end of the culture period. Values were normalised to the control values for each donor and presented as a % of control.

In order to allow for the easier visualisation of the effects of specific candidate compounds at the three doses tested, results for each protein was presented in **Tables 21 and 22**. Only results which met the 70% viability threshold are shown. The strength of the inhibitory capabilities of each compound is shown by either one, two or three ticks. One tick represents 20-45% reduction (slight), two ticks show a 45-70% reduction (moderate), whilst three ticks represent the most potent attenuation in each marker, a >70% reduction (strong).

Whilst the 10µM dose was used to assess both toxicity and inhibitory effects of the candidate compounds, it remains, for the majority of compounds at least a dose which would be too high for translation into patients. Therefore when assessing the success of the inhibitory effects of the compounds, 0.1µM and 1µM provided a much more exciting prospect for

transfer into use in the clinic. We initially investigated the anti-fibrotic compounds, defined as those which successfully inhibited Collagen and TIMP-1 secretion. Interestingly Collagen secretion was more successfully inhibited compared to TIMP-1. Rapamycin, Geldanamycin, Taxol, Cycloheximide and Camptothecin all either had strong or moderate effects at 0.1µM and 1µM on collagen levels **(Figure 69 and Table 21)**. Whereas none of the candidate compounds tested were able to strongly inhibit TIMP-1 secretion at 0.1µM **(Figure 70)**. Only once the dose was increased to 1µM did we observe strong inhibitory effects (defined by a >70% reduction compared to control) from Geldanamycin, Cycloheximide, Mycophenolic Acid and Camptothecin. There was some parity between the cardiac fibroblast cultures and PCHS, in regard to the inhibition of Collagen secretion. Both Taxol and Cycloheximide, which were able to reduce Collagen 1a1 at 10µM in fibroblasts, were both shown to be efficacious in the PCHS at the lower doses of 0.1µM and 1µM. In total we identified n=9 compounds which were able to attenuate collagen or TIMP-1 secretion by at least 45% at either 0.1µM or 1µM doses.

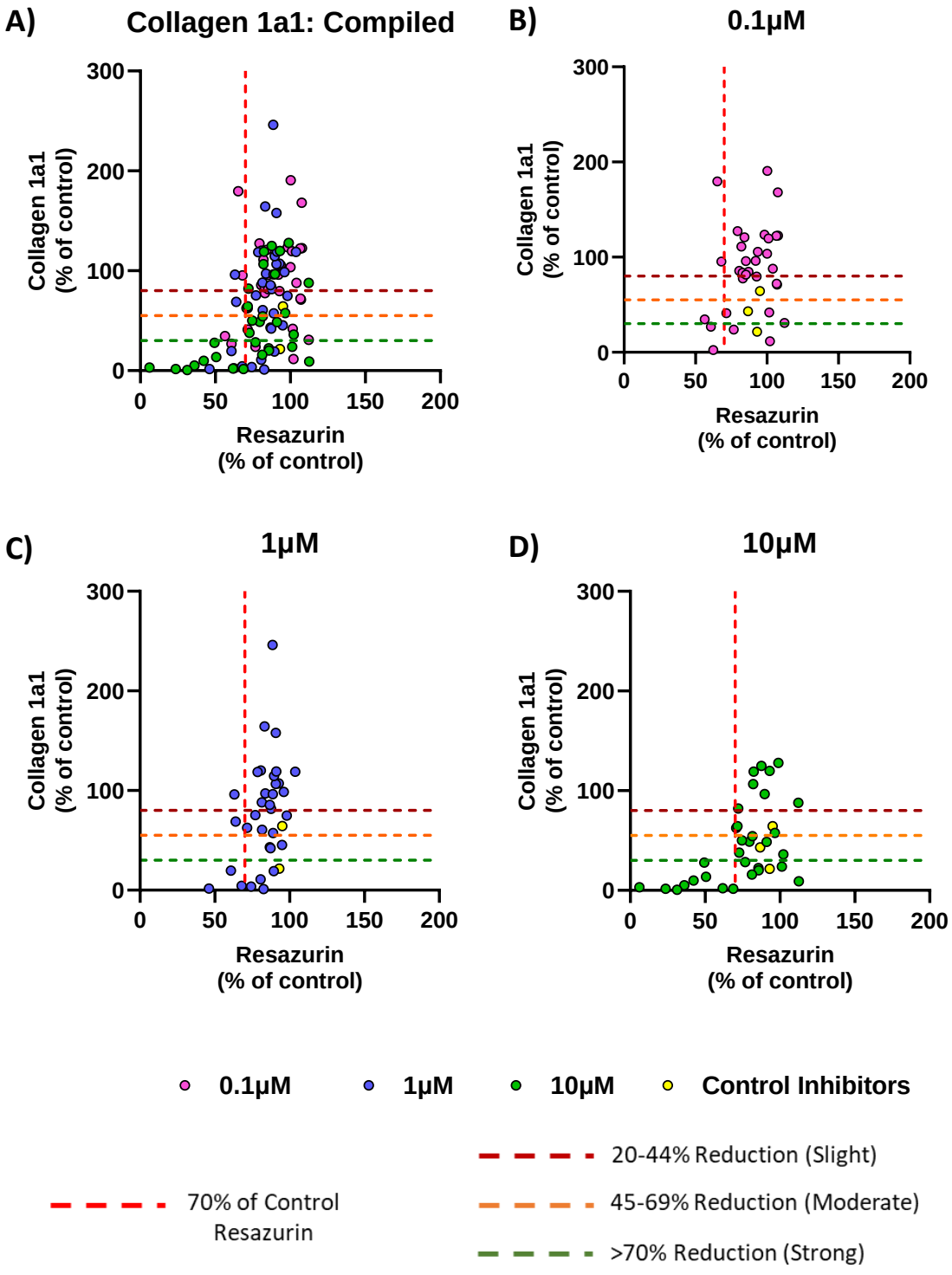

Figure 69. Efficacy and viability testing of candidate compounds identified through Ingenuity Pathway Analysis – Graphs depict resazurin, normalised to control, as a readout of slice viability versus collagen 1a1 secretion, normalised to control. Compounds were applied at 0.1µM, 1µM or 10µM for 72 hours. Control inhibitors were ALK5 inhibitor SB525334 (10µM), Pirfenidone (2.5mM) and Nintedanib (2.5µM). Red dashed line crossing x-axis at 70% marks threshold for viability (30% reduction compared to control). Dashed lines crossing y-axis mark 20% reduction (dark red), 45% reduction (orange) and 70% reduction (green) compared to collagen secretion from control slices.

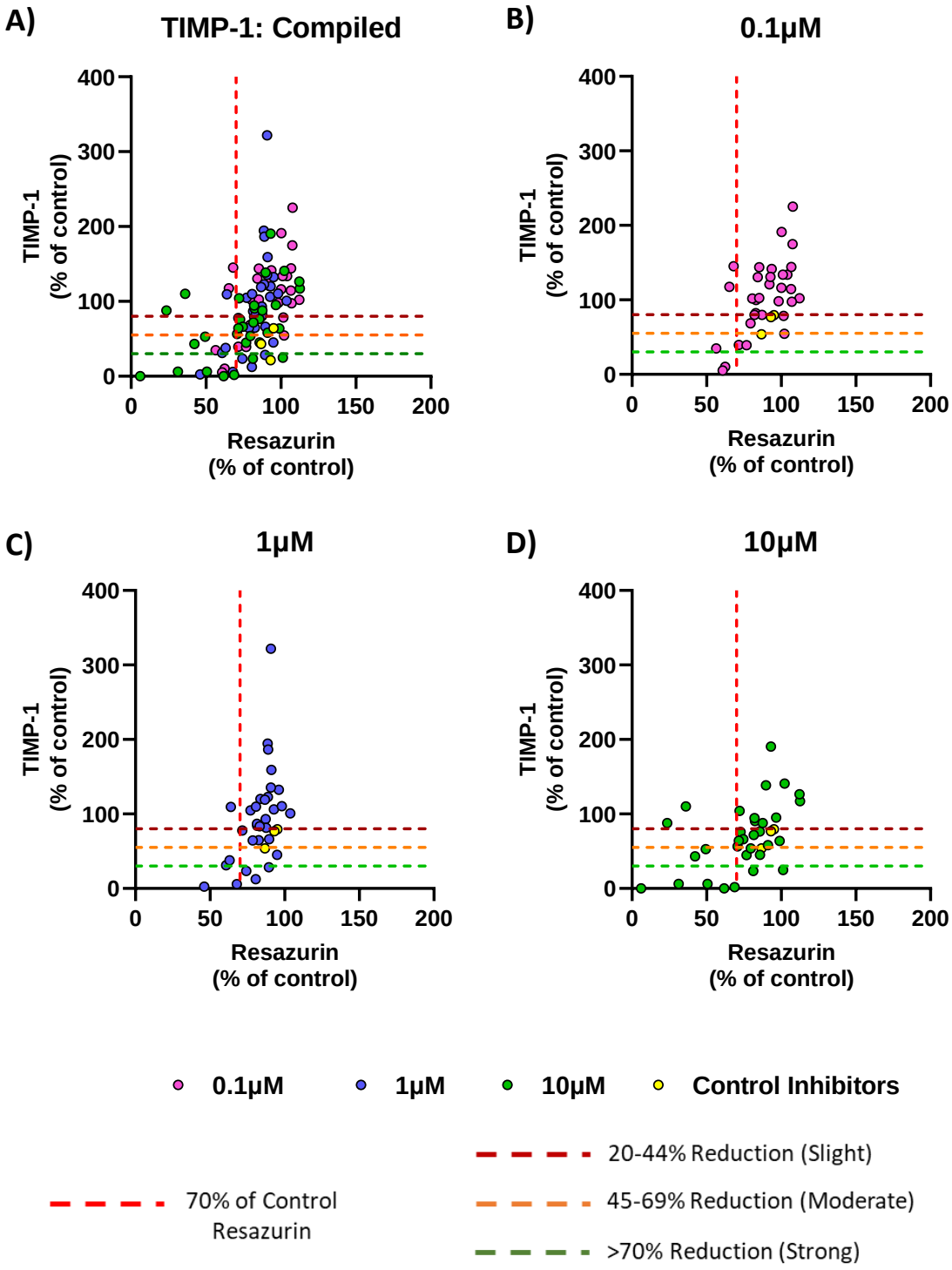

Figure 70. Efficacy and viability testing of candidate compounds identified through Ingenuity Pathway Analysis – Graphs depict resazurin, normalised to control, as a readout of slice viability versus TIMP-1 secretion, normalised to control. Compounds were applied at 0.1µM, 1µM or 10µM for 72 hours. Control inhibitors were ALK5 inhibitor SB525334 (10µM), Pirfenidone (2.5mM) and Nintedanib (2.5µM). Red dashed line crossing x-axis at 70% marks threshold for viability (30% reduction compared to control). Dashed lines crossing y-axis mark 20% reduction (dark red), 45% reduction (orange) and 70% reduction (green) compared to TIMP-1 secretion from control slices.

Inhibitor	Collagen 1a1			TIMP-1		
	0.1µm	1µm	10µm	0.1µm	1µm	10µm
GW9662	✓	✓	✓✓✓			
Bay 11-7082						✓
LY294002						
GB1107						
Taxol	✓✓	✓✓	✓✓✓			✓
Erlotinib			✓✓✓			✓✓
PLX5622						✓✓
Tempol						
Camptothecin	✓✓	✓✓✓			✓✓✓	
Cycloheximide	✓✓	✓✓✓			✓✓✓	
Mycophenolic Acid	✓	✓✓✓	✓✓✓		✓✓✓	✓✓✓
AG-490						✓
Aspirin						✓
Napabucasin						
Sorafenib			✓✓✓			✓✓✓
Dexamethasone		✓				
Tamoxifen		✓			✓	
Rapamycin	✓✓✓			✓✓		
ABT-737					✓	✓
Rottlerin						
Ziritaxestat		✓				
Calcipotriene						
Triptolide						
Resiquimod						
PMA						✓
Geldanamycin	✓✓✓			✓✓		
A23187		✓✓✓				
Capsaicin						
Acetaminophen					✓	✓
Dorsomorphin	✓	✓✓	✓✓✓		✓✓	
Immethridine Dihydrobromide	✓	✓				
H-7						

Table 21. Candidate compounds and their effect on secretion of fibrosis markers – Table shows compounds with effects at viable doses – one red tick for 20% reduction, two orange ticks for 45% reduction and three green ticks for 70% reduction in Collagen 1a1 or TIMP-1 secretion compared to control. Greyed out cells denote unviable doses (resazurin <70%).

Through the quantification of IL-6, IL-8 and MCP-1 protein secretion we assessed the candidate compounds anti-inflammatory potential **(Figures 71-73)**. Unsurprisingly the steroid Dexamethasone was both very well tolerated by PCHS and also exhibited broad anti-inflammatory effects **(Table 22)**. Across all three markers (IL-8, IL-6 and MCP-1) Dexamethasone at 0.1µM was able to reduce secretion by at least 65% compared to control, with IL-6 secretion the most potently attenuated. Another compound which displayed anti-inflammatory effects broadly across the three markers was Camptothecin, results showed strong inhibition of IL-6, IL-8 and MCP-1 secretion after PCHS were treated with a 1µM dose, with attenuation of MCP-1, IL-6 and IL-8 also present in response to the 0.1µM dose of Camptothecin.

There were a number of compounds which had elicited little to no ability to inhibit Collagen or TIMP-1 secretion, but were able to block secretion of either one or more of IL-8, IL-6 or MCP-1. These included Acetaminophen, Resiquimod and Capsaicin. All three of these compounds proved to only be effective at attenuating IL-8 secretion from PCHS, their effects on IL-6 or MCP-1 was limited. Geldanamycin, a Heat shock protein 90 (HSP-90) inhibitor was one of the most potent compounds we tested. It exhibited both strong anti-inflammatory and anti-fibrotic effects at only 0.1µM, whilst having toxic effects at the higher doses. Therefore the efficacy of Geldanamycin could continue to be explored further at doses below 0.1µM to reduce the possibility of adverse side effects and toxicity. This demonstrates the ability of PCHS as a model to identify effective but non-toxic doses of candidate and novel compounds.

Overall, we have identified n=11 compounds which demonstrated the ability to reduce the secretion of at least one of a number of pro-inflammatory markers by at least 45% when applied to PCHS at either 0.1µM or 1µM.

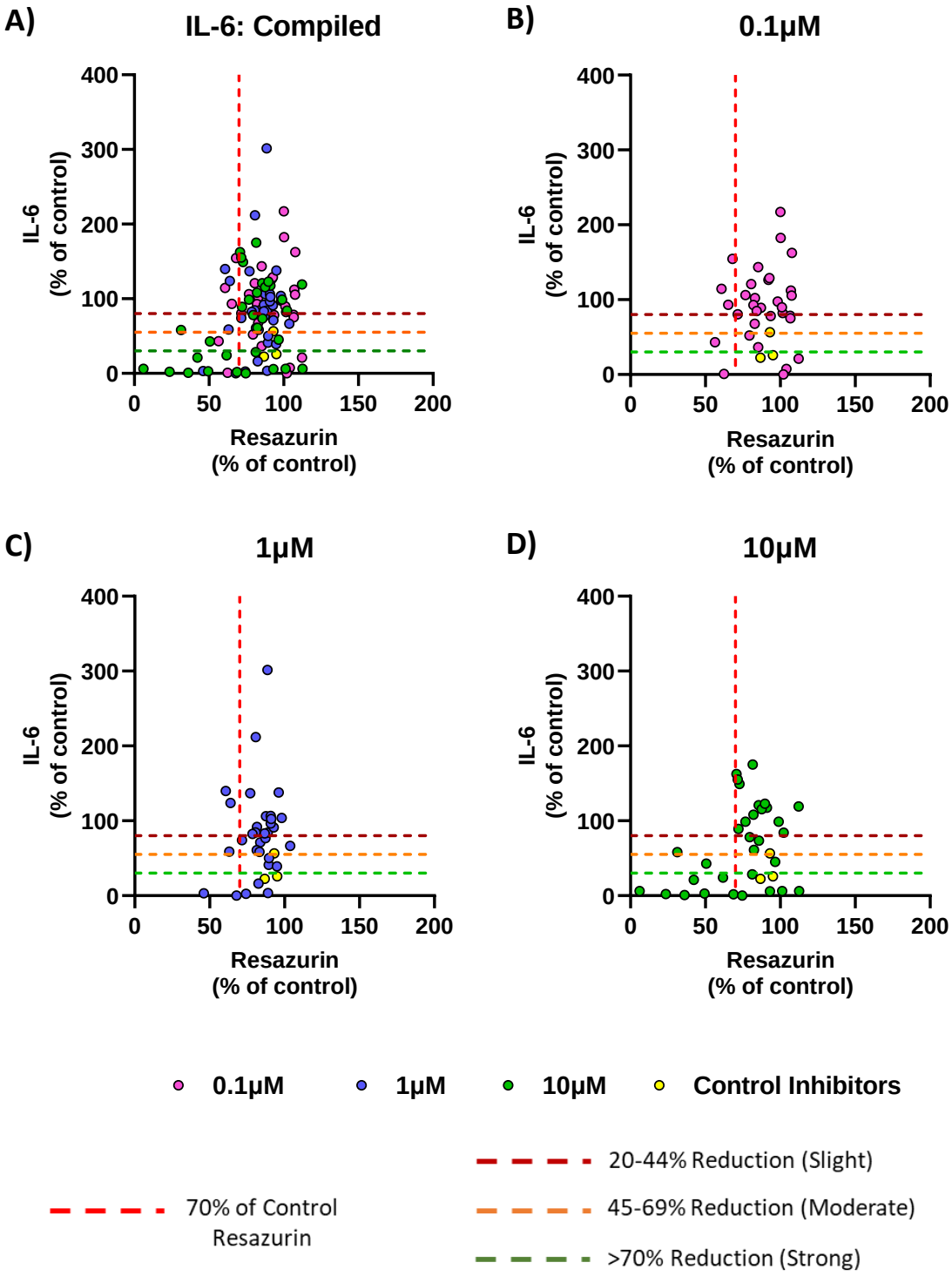

Figure 71. Efficacy and viability testing of candidate compounds identified through Ingenuity Pathway Analysis – Graphs depict resazurin, normalised to control, as a readout of slice viability versus IL-6 secretion, normalised to control. Compounds were applied at 0.1µM, 1µM or 10µM for 72 hours. Control inhibitors were ALK5 inhibitor SB525334 (10µM), Pirfenidone (2.5mM) and Nintedanib (2.5µM). Red dashed line crossing x-axis at 70% marks threshold for viability (30% reduction compared to control). Dashed lines crossing y-axis mark 20% reduction (dark red), 45% reduction (orange) and 70% reduction (green) compared to IL-6 secretion from control slices.

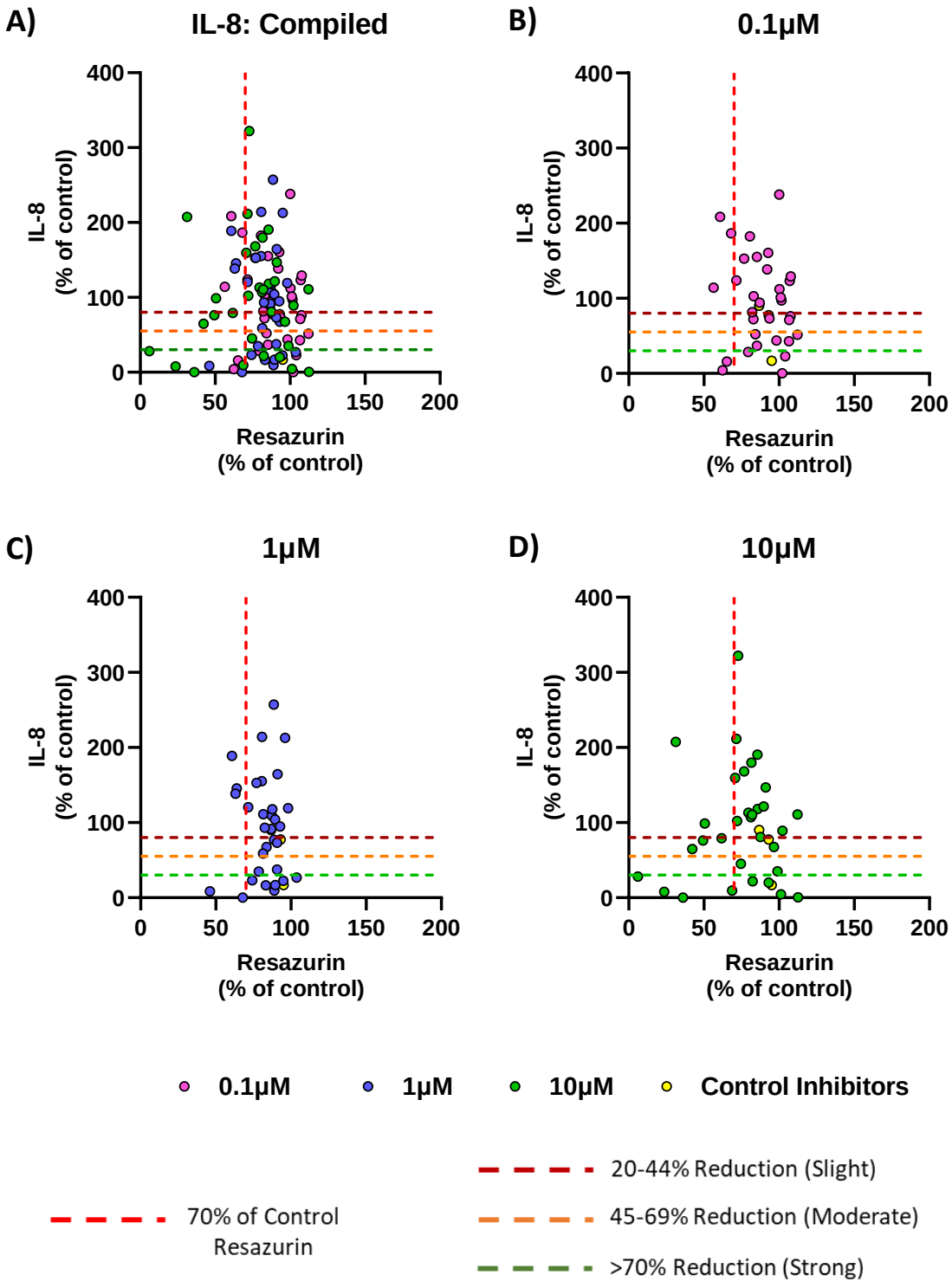

Figure 72. Efficacy and viability testing of candidate compounds identified through Ingenuity Pathway Analysis – Graphs depict resazurin, normalised to control, as a readout of slice viability versus IL-8 secretion, normalised to control. Compounds were applied at 0.1µM, 1µM or 10µM for 72 hours. Control inhibitors were ALK5 inhibitor SB525334 (10µM), Pirfenidone (2.5mM) and Nintedanib (2.5µM). Red dashed line crossing x-axis at 70% marks threshold for viability (30% reduction compared to control). Dashed lines crossing y-axis mark 20% reduction (dark red), 45% reduction (orange) and 70% reduction (green) compared to IL-8 secretion from control slices.

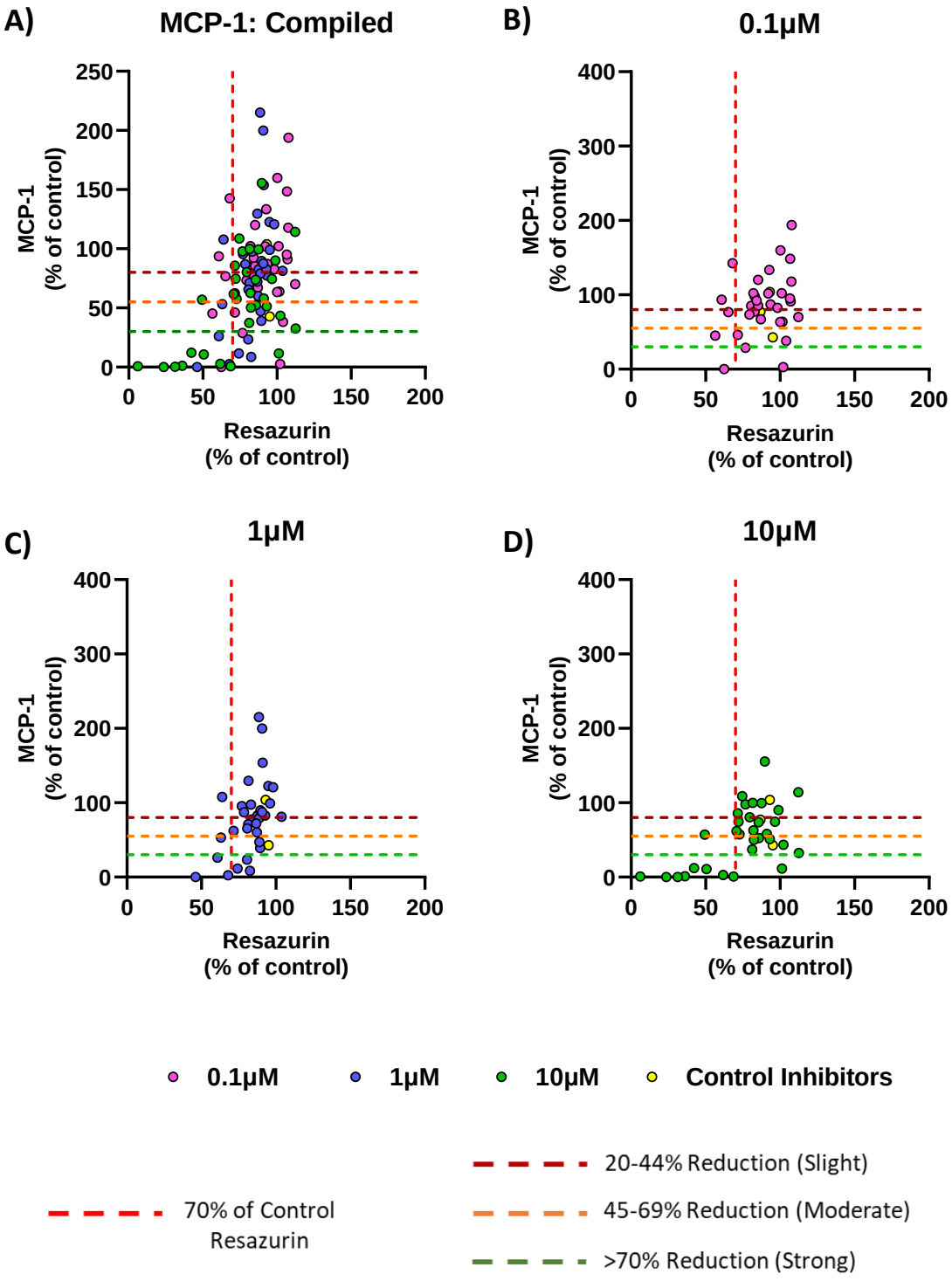

Figure 73. Efficacy and viability testing of candidate compounds identified through Ingenuity Pathway Analysis – Graphs depict resazurin, normalised to control, as a readout of slice viability versus MCP-1 secretion, normalised to control. Compounds were applied at 0.1µM, 1µM or 10µM for 72 hours. Control inhibitors were ALK5 inhibitor SB525334 (10µM), Pirfenidone (2.5mM) and Nintedanib (2.5µM). Red dashed line crossing x-axis at 70% marks threshold for viability (30% reduction compared to control). Dashed lines crossing y-axis mark 20% reduction (dark red), 45% reduction (orange) and 70% reduction (green) compared to MCP-1 secretion from control slices.

Inhibitor	IL-6			IL-8			MCP-1		
	0.1µm	1µm	10µm	0.1µm	1µm	10µm	0.1µm	1µm	10µm
GW9662									
Bay 11-7082									✓
LY294002	✓	✓		✓	✓		✓	✓	✓✓
GB1107	✓	✓	✓✓	✓	✓	✓		✓	✓
Taxol		✓					✓	✓	✓
Erlotinib			✓						✓✓
PLX5622			✓		✓		✓		
Tempol	✓✓			✓✓				✓	✓
Camptothecin	✓✓✓	✓✓✓		✓✓	✓✓✓		✓	✓✓✓	
Cycloheximide							✓✓	✓✓✓	
Mycophenolic Acid		✓✓	✓✓✓					✓✓	✓✓
AG-490				✓					✓
Aspirin									
Napabucasin									
Sorafenib			✓✓✓		✓	✓✓✓			✓✓✓
Dexamethasone	✓✓✓	✓✓✓	✓✓✓	✓✓✓	✓✓✓	✓✓✓	✓✓	✓✓	✓✓
Tamoxifen									✓
Rapamycin							✓✓✓		
ABT-737		✓✓	✓✓✓		✓✓✓	✓✓			
Rottlerin	✓✓			✓✓✓			✓		
Ziritaxestat		✓						✓	
Calcipotriene			✓		✓✓	✓✓✓			✓✓
Triptolide									
Resiquimod		✓		✓✓	✓✓✓				✓
PMA							✓	✓	
Geldanamycin	✓✓✓			✓✓✓			✓✓✓		
A23187		✓✓✓							
Capsaicin		✓		✓✓	✓✓✓				
Acetaminophen	✓			✓✓	✓✓	✓✓			
Dorsomorphin	✓	✓✓	✓✓✓	✓	✓✓✓	✓✓✓			✓✓
Immethridine Dihydrobromide									
H-7									

Table 22. Candidate compounds and their effect on secretion of inflammatory markers – Table shows compounds with effects at viable doses – one red tick for 20% reduction, two orange ticks for 45% reduction and three green ticks for 70% reduction in IL-6, IL-8 or MCP-1 secretion compared to control. Greyed out cells denote unviable doses (resazurin <70%).

Figures 74 and 75 depict the complete profile for a number of the more promising candidate compounds and approved therapies. The efficacy of these compounds is displayed alongside our positive control therapies (ALK5 inhibitor, Pirfenidone and Nintedanib). Taxol showed strong anti-fibrotic effects at both 0.1µM and 1µM as characterised by a reduction in Collagen 1α1 secretion after 72hrs of treatment. However this effect was exclusive to Collagen 1α1 as TIMP-1 secretion was unaffected. The mTOR inhibitor rapamycin was effective at attenuating secretion of Collagen 1α1, TIMP-1 and MCP-1, although no effect was observed on IL-8 secretion. Only the 0.1µM dose of Rapamycin is shown due to a significant reduction in the viability of the PCHS observed at increased doses. One the most potent anti-inflammatory compounds we tested was dexamethasone, which was very well tolerated at all doses tested and strongly attenuated MCP-1 and IL-8 secretion from PCHS.

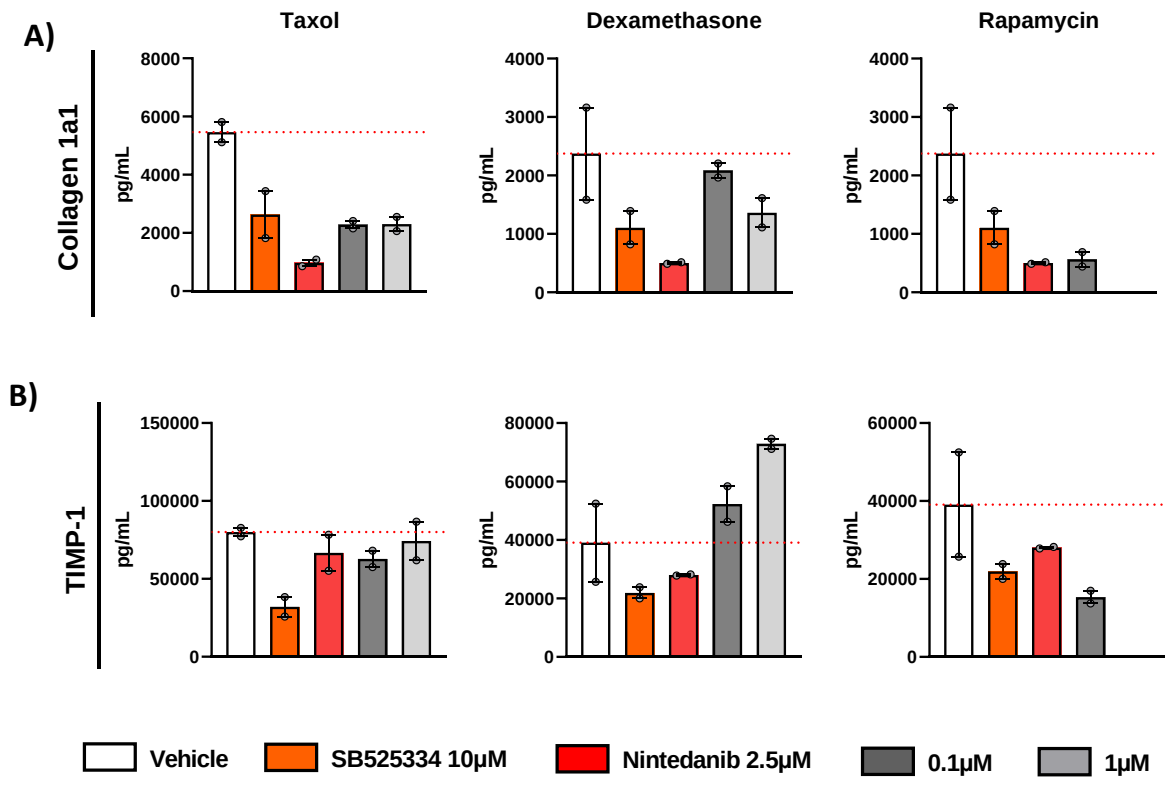

Figure 74. Attenuation of fibrosis by candidate compounds – Graphs depicting anti-fibrotic effects of 3 candidate compounds at doses of 0.1µM and 1µM compared to positive control therapies ALK5i (SB525334) and Nintedanib. **A)** Collagen 1a1 ELISA; **B)** TIMP-1 ELISA. N=2 donors; data is presented as Mean ± SEM; dashed red line shows mean value from vehicle control.

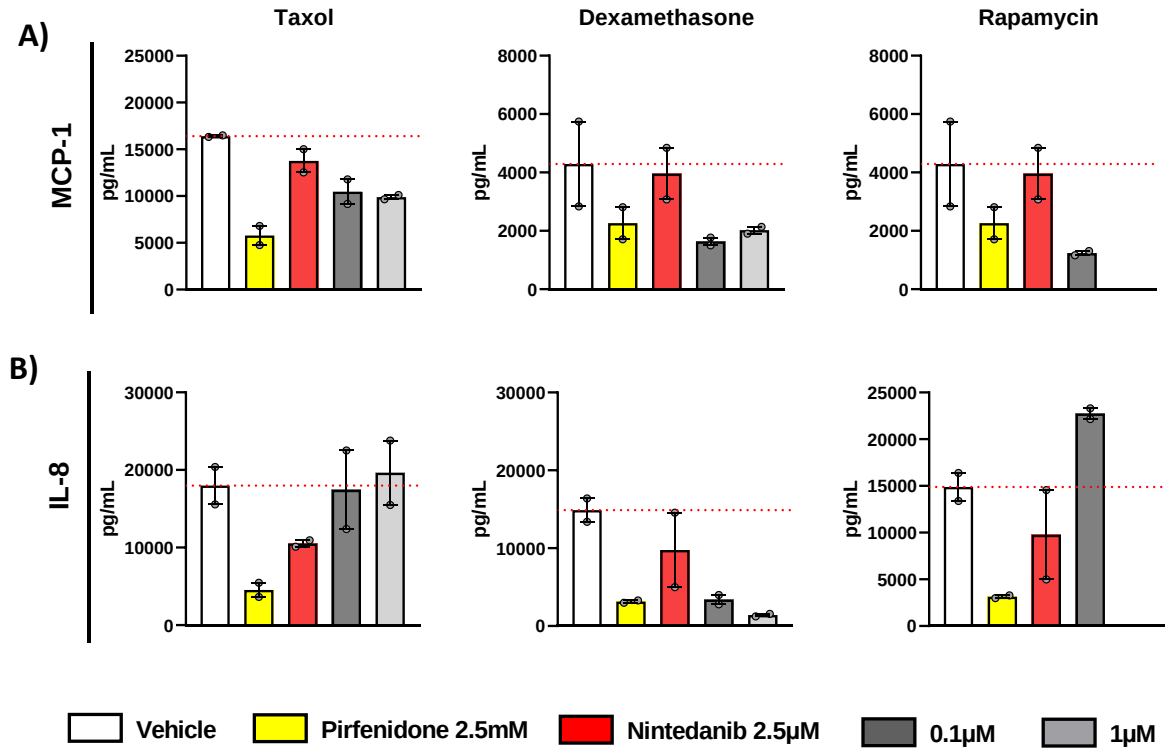

Figure 75. Attenuation of inflammation by candidate compounds – Graphs depicting anti-inflammatory effects of 3 candidate compounds at doses of 0.1µM and 1µM compared to positive control therapies Pirfenidone and Nintedanib. **A)** Collagen 1a1 ELISA; **B)** TIMP-1 ELISA. N=2 donors; data is presented as Mean ± SEM; dashed red line shows mean value from vehicle control.

To further investigate the potential genes involved for the inhibitors identified through the Upstream Regulator Analysis (URA), the mechanistic network for Dexamethasone in response to Galectin-3 treatment is shown in **Figure 76.** The network depicts that in response to Galectin-3 treatment, Dexamethasone is predicted to have inhibitory effects on a number of downstream genes shown to be upregulated. A number of cytokines, including IL-1β, IL-6 and CXCL1, depicted in the network are upregulated in response to Galectin-3 whilst being potential downstream targets of Dexamethasone. In addition to cytokines, a number of transcription regulators, including STAT3, NFKB1 and HIF1A, which are upregulated in response to Galectin-3, are also targets of inhibition by Dexamethasone.

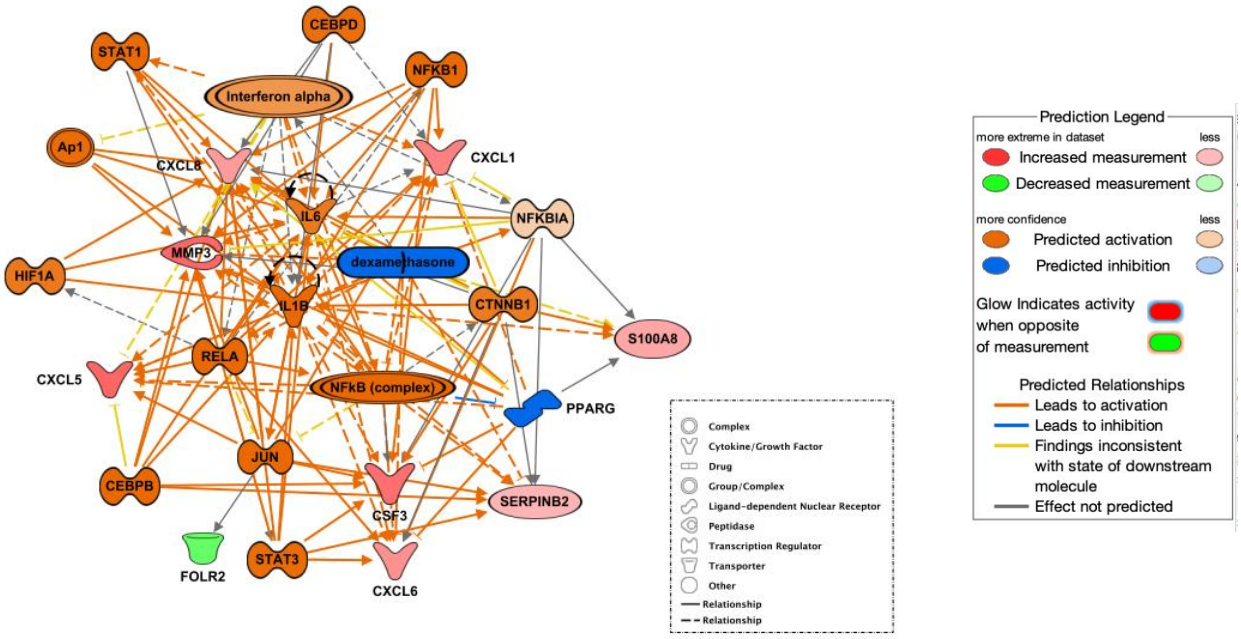

Figure 76. Mechanistic network of the predicted effects of Dexamethasone identified through Upstream Regulator Function – Predicted downstream effects of Dexamethasone in response to Galectin-3 treatment. Molecule and Prediction legends are included in the figure. Activation z-score is -3.366 with a p-value of overlap of 5.40E-13 calculated by a Fisher's Exact test (FET).

In order to highlight the importance of using PCHS in drug screening we compared we compared the efficacy of a number of the candidate compounds in PCHS and cardiac fibroblasts **(Figure 77)**. Cycloheximide and Taxol were able to potently attenuate Collagen 1a1 secretion at both 0.1µM and 1µM in PCHS, in addition Cycloheximide was also able to reduced MCP-1 secretion at these doses. However, these effects were not mirrored in cardiac fibroblasts. The anti-fibrotic effects of Rottlerin appeared only to be effective in fibroblasts as there was no attenuation of Collagen 1a1 secretion in the PCHS. The anti-inflammatory effects of Dexamethasone, assessed by MCP-1 secretion, was present in both PCHS and cardiac fibroblasts, however the effects were more pronounced in PCHS. These data highlight the risk of false negatives when using primary fibroblasts to test efficacy of novel therapeutics.

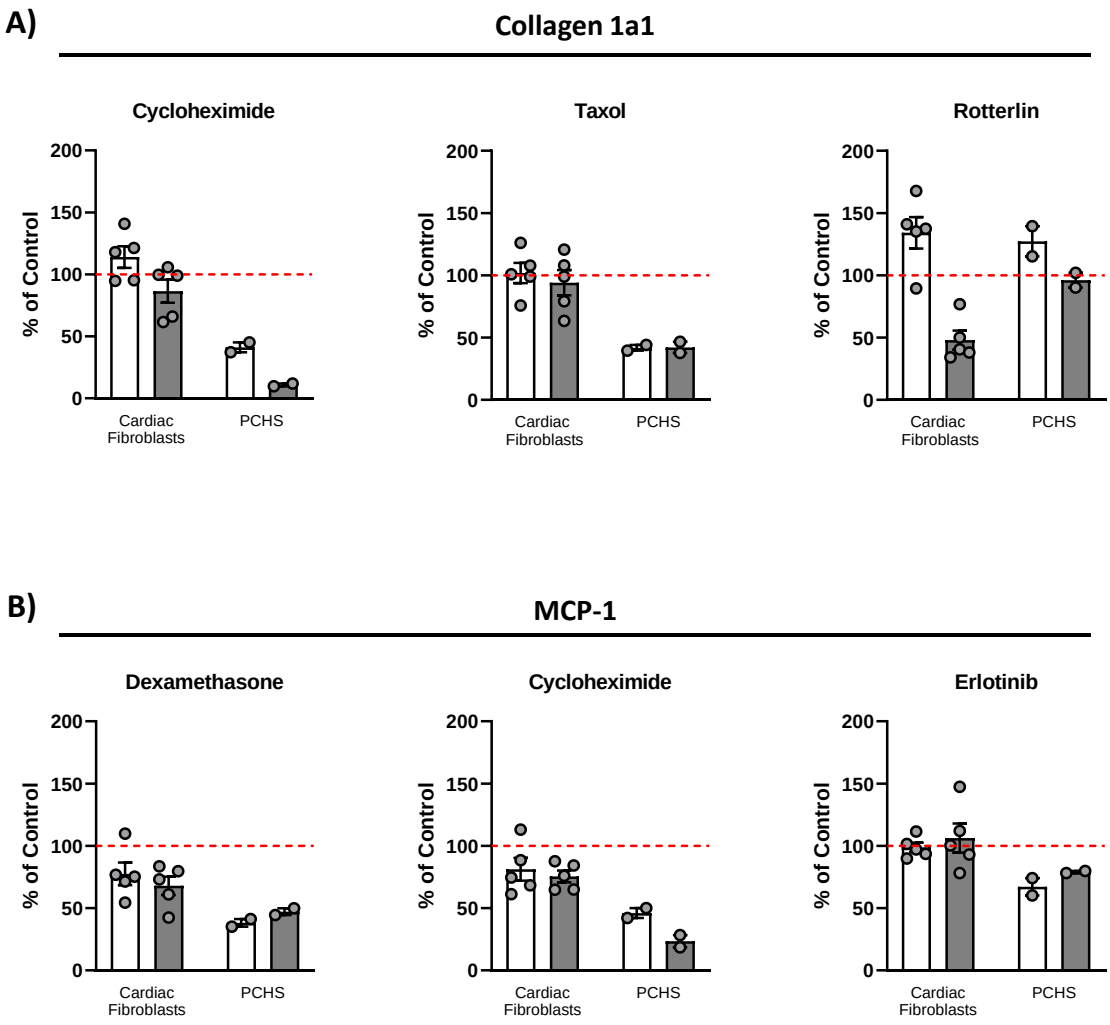

Figure 77. Differences in response between Cardiac fibroblasts and PCHS – Data comparing the attenuation of protein secretion (Collagen 1a1 and MCP-1) between cardiac fibroblasts and PCHS in response to treatment with candidate compounds. Values were normalised to the control values for each donor and presented as a % of control. Red dashed line depicts cardiac fibroblasts or PCHS treated with vehicle control.

Our data shows that through the use of the IPA upstream regulator function we have identified a number of candidate compounds, which when tested within the PCHS system have the ability to attenuate inflammatory and/or fibrotic responses. We have identified n=9 anti-fibrotic compounds which were shown to be efficacious at either 0.1µM or 1µM doses. Whilst n=11 compounds were able to inhibit inflammation. This provides the opportunity to utilise our system to help guide the repurposing of novel compounds for use in treating cardiac diseases.

5.5 Discussion

Cardiac fibrosis is the common endpoint in a number of cardiac diseases. Currently there are no approved anti-fibrotic therapies to reverse or halt disease progression approved for use within the fibrotic heart. Research investigating the disease mechanisms of fibrosis have centred on the use of either animal models or homogeneous 2D cultures. Whilst these techniques have enabled the understanding of a number of the disease mechanisms involved in the development of cardiac fibrosis they so far have been unable to produce an efficacious therapy. Rodent models are unable to completely mimic the disease process, whilst differences between the rodent model and human disease may result in the identification of proteins which play no role in human disease. For many years simple and cost-effective 2D cell culture models have been used to perform extensive drug screening or to investigate specific intracellular signalling pathways. However the major disadvantage of these models is the inability to accurately recapitulate the complex cellular interactions between different cell types and the ECM present within the human tissue and the use of an unnatural stiff matrix upon which cells are cultured. In regard to fibroblasts this results in the uncontrolled trans-differentiation of these cells into activated myofibroblasts, with the resultant changes in gene and protein expression. Within the first 24-48 hours of culture after the isolation of cardiac fibroblasts from the tissue the expression of α-SMA, a marker of myofibroblasts, is already present with in the culture. The development of more complex 3D and *ex vivo* models of cardiac fibrosis, such as PCHS, hope to bridge the gap between drug discovery and the clinic. The first aim of our study was to investigate the effectiveness of proposed drivers of cardiac fibrosis and interrogate the genomic and proteomic differences in response to treatment.

In our system we investigated the ability to modulate disease phenotypes through the application of a number of proposed drivers of inflammation and fibrosis in the human heart. Exogenous challenge of recombinant Angiotensin II had little to no ability to induce significant changes in the PCHS as assessed by bulk RNA and protein analysis. This was an unexpected result due to the extensive literature supporting its role in cardiac fibrosis. Angiotensin II treatment has been shown to stimulate the release of TGF-β1 and IL-6 from cardiac fibroblasts(345). These results have been confirmed *in vivo* by infusion of Angiotensin II. Mice were exposed to Angiotensin II through the use of a mini-pump for up to 7 days. TGF-β1 mRNA was significantly elevated in Angiotensin II mice along with increased deposition of collagen

matrix within the myocardium. In our system we were unable to identify any increase in collagen 1a1 secretion in response to 72 hours of Angiotensin II exposure(346). This could, in part, be explained by the short half-life of Angiotensin II, with research by van Kats *et al* (1997) demonstrating that *in vivo* it is as short as 15 minutes within the heart tissue, dropping to 30 seconds once present within the circulation(347). More recent work by Takayanagi further confirmed Angiotensin II's short half-life, this time *in vitro*. Angiotensin II was shown to be stable for less than 1hr in culture after 100nmol/l treatment, and after 4 hours it was no longer detectable(348). Therefore in order to chronically stimulate and see a response in PCHS, it may require multiple treatments within each 24 hour period, or application *via* constant as is used *in vivo*.

Seminal work by Schafer *et al* highlighted an important role for IL-11 in the development of cardiac fibrosis(254). IL-11 is known to be upregulated in response to TGF-β1 treatment, however for many years IL-11 was thought to have cardioprotective and anti-fibrotic effects in the heart. Early research by Kimura *et al* in a mouse model of ischemia demonstrated IL-11's protective role, preventing further injury following reperfusion(349). These findings were confirmed in other mouse models of cardiac disease, including a cold ischemia model mimicking conditions post-transplantation(350–352). However more recently these findings have been thrown into question upon discovery of the species specific effects of recombinant IL-11. The application of a recombinant human IL-11 (*rh*IL-11) induced potent pro-fibrotic response in primary human myofibroblasts, providing results in direct contrast to the earlier studies(254). In order to explore these results further, they produced a recombinant mouse IL-11 (*rm*IL-11) and applied this both *in vitro* and *in vivo* to mouse cells and models, comparing directly with the effect of *rh*IL-11. The results produced were striking in the differences in responses observed between the different recombinant IL-11. Potent fibrotic effects were present in both *in vivo* and *in vitro* mouse models in the *rm*IL-11 groups whereas those treated with *rh*IL-11 exhibited no pro-fibrotic effects(254). These species specific effects of recombinant IL-11 were also confirmed by other researchers when investigating the role of IL-11 in kidney and liver fibrosis(254,353). Interestingly, we were unable to induce a pro-fibrotic response from PCHS challenged with *rh*IL-11. However, IL-11 was upregulated at both the genetic and protein level in response to both TGF-β1 and Galectin-3 treatment from PCHS. Our protein secretion data from PCHS isolated from donor hearts unsuitable for transplant treated with *rh*IL-11 did appear to show a trend towards increased collagen 1a1 and TIMP-1

secretion, however variations between donors prevented statistical significance being attained. Whilst our work does complement earlier studies showing IL-11 present downstream of other pro-fibrotic signalling, it is unclear within our system whether IL-11 is driving fibrosis directly.

Whilst our data appears to demonstrate that Angiotensin II, CTGF and IL-11 are unable to drive inflammation or fibrosis within the PCHS model, Galectin-3 provided more promising results. Galectin-3 is a chimeric lectin known to have a number of intra- and extra-cellular functions within health and disease. It has been shown to be present within a number of tissues, such as the lungs and kidney, as well as being highly expressed in myeloid cells such as monocytes and macrophages, and other cell types including fibroblasts and epithelial cells. In the healthy heart it is expressed in low levels, with upregulation only observed upon the initiation of disease. This was initially discovered in a rat model of heart failure, which discovered that Galectin-3 was the strongest differentially regulated gene(315). These findings were confirmed in patient samples in the same study. A key finding from our study was the strong inflammatory response induced in the PCHS after exogenous Galectin-3 challenge. This response was consistent across all secreted inflammatory markers assessed, and was matched by the differentially expressed genetic changes. Through the use of RNA sequencing we identified many chemokine (CXCL5, CXCL1, CXCL6), cytokines (IL-1β, IL-6, IL-24) and other drivers of inflammation (Colony stimulating factor 3, complement C3) significantly upregulated in response to Galectin-3 treatment. Chronic inflammation leads to a dysregulation in the normal wound healing response and the initiation of tissue fibrosis. Galectin-3 is thought to be secreted from either resident or infiltrating macrophages and monocytes in response to injury and upon continued damage to the site of injury Galectin-3 can be involved in the transition from chronic inflammation to fibrosis. Our data confirms the inflammatory role of Galectin-3 in the heart however its ability to drive collagen deposition was less obvious in our system. Neither protein nor gene expression data supported a role for Galectin-3 directly in the secretion of collagen 1a1 from the PCHS, with collagen 1a1 secretion being downregulated in the proteomic analysis. Interestingly thought the proteomic analysis identified significant increase in a number of other proteins involved in fibrogenesis, including collagen IV, Transgelin and fibrillin. Interestingly we also observed TIMP-1 secretion becoming significantly upregulated. Our data has demonstrated that with prolonged treatment with Galectin-3 in PCHS, we are starting to observe a switch to a pro-fibrotic phenotype in response

to Galectin-3 induced chronic inflammation. These finding are in agreement with a number of other studies linking Galectin-3 induced inflammation to the development of fibrosis(354,355). Increasing the culture period of the PCHS as well as including the earlier timepoints (48 hours and 72 hours) for omics analysis could help to illuminate whether the responses we have observed are indeed the initiation of a fibrotic response.

Due to the difficulty in obtaining tissue from HF patients, there are currently only very limited datasets with which to compare the RNA sequencing and proteomic data sets produced in our study to. Work performed by Hua *et al* utilised multi-level transcriptomic sequencing using LV biopsies from 21 heart failure patients and compared results to 9 control patients(356). They identified a number of genes significantly upregulated in HF patients, such as COL1A1, POSTN, FSTL3 and FIBIN which were also identified in our datasets. Interestingly they also identified correlation between a number of these fibrotic genes and microRNAs, something which was beyond the scope of our present study, but could provide an area of future investigation. Comparing our pro-fibrotic (TGF-β1 treated PCHS) RNA sequencing dataset with other published fibrotic tissue profiles once again confirmed the ability to mimic fibrotic disease within the PCHS system. Significantly upregulated genes common between our dataset and those already published included POSTN, COL1A1, CCN2, FN1(141,357). These data provides confidence to our system, allowing us to identify potential novel drivers of fibrosis and future therapeutic targets.

There are currently a lack of suitable models in which to test potential therapies prior to their use in patients. Most studies rely on either animal models or simplistic 2D cell culture systems. A second aim of our study was to produce a model with closer proximity to patients in which therapies could be trialled. Our *ex vivo* PCHS model utilises human left ventricular tissue which can be processed to produce many individual slices enabling a medium throughput model for testing novel or repurposed therapeutics. We tested over 30 candidate compounds identified through IPA Upstream Regulator Analysis, using the TGF-β Receptor inhibitor SB525334 and approved IPF compounds (Pirfenidone and Nintedanib) for positive controls.

Mycophenolic Acid is a highly selective, non-competitive and reversible inhibitor of the inosine monophosphate dehydrogenase (IMPDH), resulting in the inhibition of lymphocyte proliferation. Due to its immunosuppressive capabilities it is widely used to prevent allograft

rejection after organ transplantation. More recently it has been identified as a potential therapy for various forms of fibrotic diseases, including IPF and Interstitial Lung Disease (IDL)(358). Early cell based studies focusing on anti-fibrotic actions included work by Johnsson *et al* on rat fibroblasts, observing almost complete abrogation of fibroblasts proliferation(359). A more recent study investigated the efficacy of a combination therapy of Mycophenolic Acid with the mTOR inhibitor Rapamycin to attenuate kidney fibrosis. Mice receiving the combination therapy had prolonged survival and increased kidney function. Whilst treatment in cultured human mesangial cells inhibited TGF-β1-induced fibrosis. Finally, patient studies have also been performed, mostly in patients with IPF or ILD, in which treatment has shown potential to reduce annual FVC decline in IPF patients(360). The anti-fibrotic effects reported in these studies were also observed in our PCHS model, with reductions in Collagen 1a1 and TIMP-1 secretion as well as anti-inflammatory effects as characterised by reduced IL-6 and MCP-1 secretion.

Camptothecin, a topoisomerase inhibitor, exhibited some of the most potent and broadest anti-fibrotic and anti-inflammatory effects in our system. The anti-inflammatory effects observed in our system are in agreement with a number of other studies investigating inflammation in a variety of diseases(361). The anti-fibrotic effects of Camptothecin are less well defined although research by Zhang *et al* demonstrated its ability to reduce collagen synthesis from fibroblasts isolated from patients with Keloids(362).

The most potent of the candidate compounds we tested was Geldanamycin, a HSP-90 inhibitor. In our PCHS it attenuated secretion of all markers we assessed at 0.1µM, interestingly it was deemed unsuitable at higher doses due to reducing the metabolic activity of the slices below 70% of control. Yun *et al* demonstrated the ability of Geldanamycin to inhibit TGF-β1 signalling through the induction of inducible HSP-70, which in turn interacts with the TGF-β receptors leading to their degradation and attenuation of downstream signalling(363). Blockade of the downstream signalling prevented the upregulation and secretion of the ECM and pro-fibrotic proteins fibronectin and PAI-1. Geldanamycin was also shown to regulate Angiotensin II-induced cardiac hypertrophy by inhibiting the activation of NF-κB(364). Whilst these studies have not specifically investigated the anti-fibrotic actions of Geldanamycin, they have involved pathways common to fibrotic disease, therefore providing an insight into the mechanism of action of Geldanamycin. The toxic effects we observed at the

doses of 1μM and 10μM Geldanamycin were in agreement with a number of cell culture based studies. Through the use of MTT assay, the cytotoxic effects of the Geldanamycin were evident in bladder cancer cell lines at 10μM after 24 and 48 hours of exposure(365). Therefore whilst demonstrating good potential as an anti-fibrotic compound, careful consideration to the dose would have to be taken prior to use in patients.

The importance of suitable pre-clinical models was highlighted by the novel autotaxin inhibitor, Ziritaxestat. It was a proposed therapy for IPF, with two important trials, the FLORA (ClinicalTrials.gov; trial registration number NCT02738801) and ISABELA 1 and 2 (ClinicalTrials.gov; trial registration numbers NCT03711162; NCT03733444) taking place to assess safety and efficacy(366,367). The initial trial, FLORA, did not identify any adverse effects of the treatment, supporting further development and Phase III trials of the drug(366). However during the two Phase III trials (ISABELA) adverse effects were detected in the participants, resulting in the early termination of the trial(367). Within our PCHS system we also identified reductions in metabolic activity which fell below our threshold for viability, therefore highlighting its toxicity. Whereas within our primary fibroblast cultures we identified no detrimental effects on fibroblast viability. This highlights the importance of suitable pre-clinical models which can identify adverse events prior to their transfer into clinical trials.

In conclusion we have shown through the use of RNA sequencing and proteomics that we are able to mimic cardiac disease pathways involved in inflammation and fibrosis. The datasets produced support results from published datasets of established disease from patient samples. Therefore, we propose we have developed a system in which we can identify potential novel drivers of fibrosis and inflammation whilst continuing to interrogate and understand known disease pathways. We have also demonstrated a strength of our PCHS system over 2D cultures currently used during drug development. We highlighted a number of candidate compounds viable in fibroblast cultures that were shown to not only be toxic in our PCHS system but also in clinical trials. Finally, the identification of a number of candidate compounds able to attenuate inflammation and fibrosis in our PCHS system highlights the potential of our system to act as a translational bridge between drug development and clinical trials.

6 Patient Biomarker Study

6.1 Introduction

6.1.1 Female Manifesting Carriers

Whilst DMD is a genetic disease in which the most severe effects are in young males, there is a small but significant number of female DMD carriers who display symptoms. The majority of female carriers are direct relatives of male DMD patients, usually either the mother, whom the mutated gene on the X chromosome is inherited from, or a sister(368). Daughters of female carriers have a 50% chance of being carriers themselves. Most female heterozygous DMD carriers are asymptomatic, those who develop symptoms are termed Manifesting Carriers (MC)(369). There is some disagreement about the incidence of MC in female DMD carriers, some estimate the range to be between 5-7.8%(369,370) but other studies have suggested the incidence of MC to be as high as 30%(371). In addition to female DMD carriers, carriers of the milder Becker's Muscular Dystrophy (BDM) have also been identified.

Unlike their male counterparts, female MC usually only present with mild skeletal muscle weakness, often proximally located, asymmetric and with an extremely variable age of onset of symptoms. Increased serum Creatine Kinase levels are often used to identify DMD carriers. Of greater concern is the more prevalent presentation of a cardiac pathology in female MC(372,373). Whilst in most patients this can remain as mild abnormalities, in around 8-18% of DMD MC this can progress to dilated cardiomyopathy (DCM) and in a small number of patients the requirement for cardiac transplantation(374,375). In female BMD carriers the figure of those with cardiomyopathies is believed to be as high as 13% (376).

The most common cause of symptomatic presentation is thought to be due to skewed X-chromosome inactivation (XCI). This occurs when the X-chromosome which carries the normal functional dystrophin gene is preferentially inactivated over the X-chromosome containing the mutated dystrophin gene. However, research by Brioschi et al (2012) showed no relationship between X-inactivation and the transcriptional pattern of dystrophin. They instead suggested protein amount is a greater determinant of symptomatic DMD carriers(377).

Dystrophin immunohistochemistry studies using muscle biopsies from MC show a mosaic pattern of dystrophin expression within the skeletal muscles. This presents as positive dystrophin membrane staining on some fibres, whilst others are uniformly unstained and some fibres have partial dystrophin staining(378). Distribution of these areas of abnormal fibres was non-uniform within the muscles(378,379).

6.1.2 Biomarkers

The National Institute of Health (NIH) defines a biomarker as 'a characteristic that is objectively measured and evaluated as an indicator of normal biological processes, pathogenic processes, or pharmacologic responses to a therapeutic intervention'(380). There are a wide range of different types of biomarker, ranging from magnetic resonance imaging (MRI) and computed tomography (CT) to biochemical analysis of markers in blood. Broadly, biomarkers are classified into 4 different groups; prognostic biomarkers, predictive biomarkers, pharmacodynamic biomarkers and surrogate endpoints.

A prognostic biomarker can be used to distinguish patients into groups dependent on whether they will have a good or poor outcome after the biomarker test or after any subsequent treatments they may undertake. However, it is important to highlight that a prognostic biomarker is unable to act as a guide to the type of treatment a patient should undergo. B-type natriuretic peptide (BNP) is an example of a prognostic biomarker, used during the screening and diagnosis of heart failure, it has been shown to be able to predict sudden death in patients(381). Whilst amyloid β peptide 1-42 (AB) is used in the diagnosis of prodromal Alzheimer's disease(382).

Predictive biomarkers on the other hand predict the outcome or likelihood of a response to a particular treatment. They are used in the treatment of breast cancer, to identify patients who are oestrogen receptor positive. In these patients the antioestrogen Tamoxifen has greater success at preventing the recurrence of breast cancer than in patients who are oestrogen receptor negative.

Pharmacodynamic biomarkers respond over time to the treatment or intervention that a patient is undergoing. In addition, they can also be used to optimise the dosing schedule of a

drug during its development stages. C-reactive protein (CRP) is one such example of a pharmacodynamic biomarker. It has been utilised in a number of clinical trials to assess the effectiveness of therapeutic interventions. The phase 3 TARGET study (NCT01709578) used CRP levels to investigate the efficacy of cotreatment of patients with Sarilumab and conventional synthetic disease-modifying antirheumatic drugs (csDMARDs) to treat Rheumatoid Arthritis(383).

The final class of biomarkers are Surrogate Endpoints. These biomarkers are used as a substitute for clinical endpoints. It is defined by the Biomarker Working Group as a 'biomarker intended to substitute for a clinical endpoint. A clinical investigator uses epidemiological, therapeutic, pathophysiological, or other scientific evidence to select a surrogate endpoint that is expected to predict clinical benefit, harm, or lack of benefit or harm'(380). One of the most widely used surrogate endpoints is low-density lipoprotein (LDL) cholesterol. It has been used in many clinical trials testing the safety and efficacy of statins. Reduced levels of LDL cholesterol was used as a surrogate for a reduction in cardiovascular events in study participants.

Neoepitope biomarkers are defined as 'pathology-specific post-translational modifications which occur to specific proteins to create disease-specific epitopes'(384). There are a number of proteins which are formed from pro-peptides, upon formation of the fully functioning peptide these pro-peptides are cleaved and able to be quantified in the circulation of patients. In addition to the quantification of the formation of peptides, neoepitopes also include small protein fragments released from larger protein complexes upon their degradation. Markers of collagen formation and degradation have been identified as important biomarkers for the identification of ECM remodelling which occurs during fibrosis in a variety of fibrotic diseases(384–386).

6.2 Rationale, Hypothesis and Objectives

6.2.1 Rationale

There is a current unmet need for the development of quick, safe and reliable methods to diagnose patients with cardiac fibrosis. Currently the gold standard for diagnosis is the use of myocardial biopsies, which carries the risk of complications, or by expensive cMRI with Late Gadolinium Enhancement (LGE). The identification of biomarkers capable of confirming myocardial involvement ahead of the development of structural changes or fibrosis would allow for earlier, more targeted therapies and potentially improve long-term prognosis for those affected. The identification of potential biomarkers requires a well characterised cohort of patients . Female carriers of mutations in the Dystrophin gene are routinely monitored for symptoms of disease and therefore provide a well-characterised cohort of patients in which to address this. Patients can either be Silent Carriers, meaning they develop no symptoms associated with the DMD mutation or symptomatic patients, termed Manifesting Carriers. These patients can present with cardiac abnormalities, with up to 7% of all female carriers reported to suffer from cardiomyopathies. We have identified a small but well characterised cohort of female DMD carriers in which the presence or absence of cardiac dysfunction and fibrosis has been confirmed by cMRI. The identification of specific neoepitopes or biomarkers in blood from female DMD carrier patients could prove a step increase in the sensitivity of testing in surveillance, disease progression and effects of different drug interventions. It has the potential to revolutionise how clinical trials are conducted, enabling measures of drug efficacy rapidly, potentially months in advance of any structural changes in the heart.

6.2.2 Hypothesis

We hypothesise that soluble factors released by the fibrotic heart will provide a molecular signature of cardiac fibrosis in the blood. The use of a well-characterised cohort of patients who represent a spectrum of disease will enable us to identify soluble factors secreted into the circulation from the heart, therefore providing a blood based molecular signature for effective early diagnosis and management of cardiac fibrosis in female DMD carriers.

6.2.3 Objectives

To achieve this we will:

1) Recruit female DMD carriers that have been classified into the following four groups:
    - Group 1: Female DMD carriers with no evidence of cardiac dysfunction on echo
    - Group 2: Female DMD carriers that have evidence of fibrosis on cMRI but with preserved left ventricular function on echo (LVEF $\geq$ 50%)
    - Group 3: Female DMD carriers with significant left ventricular dysfunction (LVEF < 50%) and evidence of fibrosis on cMRI
    - Group 4: Female DMD skeletal muscle manifesting carriers with no cardiac symptoms despite some having evidence of left ventricular dysfunction

2) Employ four distinct cutting-edge molecular biology approaches to identify specific markers of cardiac fibrosis to determine the molecular profile of the fibrotic human heart. The techniques used will be; Proteomics, Lipidomics, Nordic Bioscience Protein Fingerprint™ Technology and Mesoscale Discovery™ Multiplex ELISA.

6.3 Materials and Methods

6.3.1 Ethical approval and Patient Stratification and Recruitment

Ethical approval was granted to acquire blood/plasma from female DMD carriers (Newcastle University Biobank application NB-208). Participants were identified and recruited in collaboration with Dr John Bourke (Consultant Cardiologist at the Department of Cardiology, Freeman Hospital, Newcastle upon Tyne) from the Newcastle Female Carrier Cohort consisting of ~150 individuals. Female DMD carriers were classified into four distinct groups **(Table 23)**. Group 1: Female DMD carriers with no evidence of cardiac dysfunction on echo (n=17 patients). Group 2: Female DMD carriers that have evidence of fibrosis on cMRI but with preserved left ventricular function on echo (LVEF $\geq$ 50%) (n=8 patients). Group 3: Female DMD carriers with significant left ventricular dysfunction (LVEF < 50%) and evidence of fibrosis on cMRI (n=5 patients). Critically, Female DMD carriers in Groups 1-3 were selected with no muscle myopathy to minimize the potential confounding impacts of skeletal muscle biomarkers. Group 4: Female DMD skeletal muscle manifesting carriers with no evidence of left ventricular dysfunction and / or fibrosis on cMRI (n=7 patients). This particular group will allow us to determine which biomarkers are exclusive to cardiac involvement from those that can also originate from skeletal changes.

6.3.2 Sample collection and processing

Patient samples were collected by Research Nurses at the Freeman Hospital, Newcastle upon Tyne **(Figure 78)**. Two 9ml blood samples were collected in Vacutainer EDTA blood collection tubes and immediately transferred for storage at 4^{o}C. Tubes were spun at 3000rpm for 10 minutes. The separated plasma was transferred to clean 15ml Falcon tubes. The falcon tubes containing the plasma were spun at 3000rpm for a further 10 minutes. Plasma samples were pooled and transferred to a clean 15ml falcon and stored at -80^{o}C for future analysis.

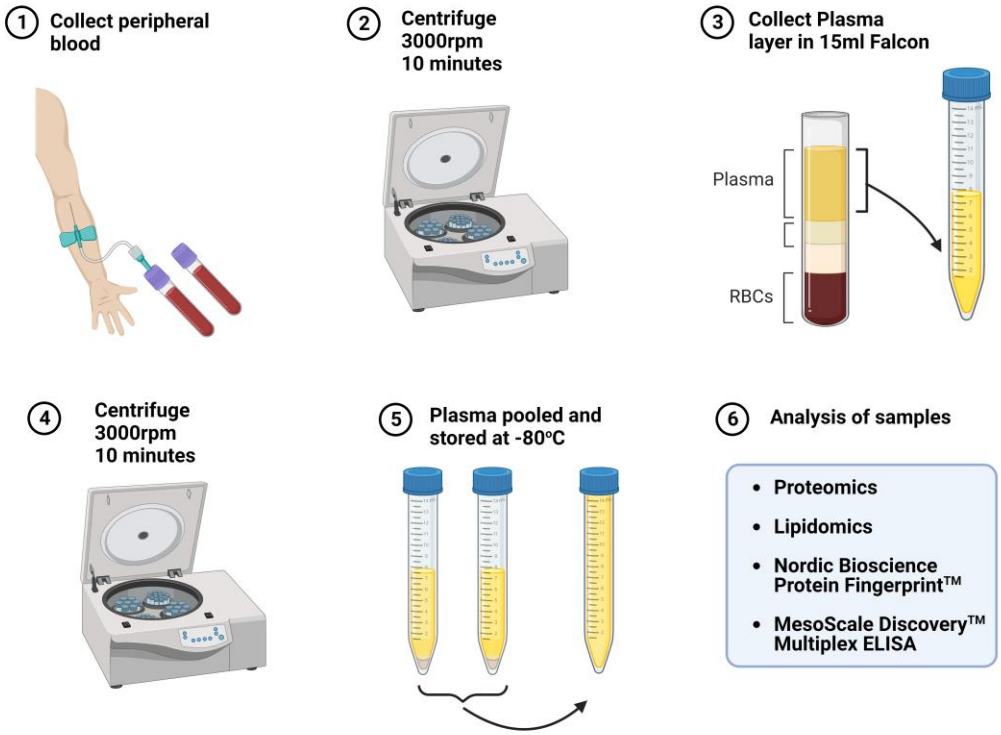

Figure 78. Workflow of sample collection and processing from donors – 1) Two 9ml blood samples are collected from donors; **2)** Tubes were centrifuged at 3000rpm for 10minutes; **3)** Plasma is removed from blood tubes and placed into fresh 15ml falcons; **4)** Plasma is centrifuged again at 3000rpm for 10 minutes; **5)** Plasma from the same donor is pooled into one 15ml falcon and stored at -80°C; **6)** Analysis of samples - Created with BioRender.com

Patient No.	Category of CM	Disease Groupings	Group 1-4	AGE (yrs)	BMI (K/m^2)	DMD / BMD
C-9001	ECM & MRI	Early CM	Group 2	53	N/A	DMD
C-9002	ACM & MRI	Early CM	Group 2	56	N/A	DMD
C-9003	Moderate CM	CM	Group 3	33	24.0	BMD
C-9004	No CM	Normal	Group 1	25	N/A	BMD
C-9005	No CM	Normal	Group 1	38	31.9	DMD
C-9006	ACM	CM	Group 3	49	37.8	DMD
C-9007	No CM	Normal	Group 1	50	24.5	BMD
C-9008	No CM	Normal	Group 1	30	34.7	DMD
C-9009	No CM	Normal	Group 1	41	31.4	BMD
C-9010	ECM & MRI	Early CM	Group 2	48	24.8	DMD
C-9011	MMC & wheelchair	MM	Group 4	41	29.4	DMD
C-9012	No CM	Normal	Group 1	26	22.6	DMD
C-9013	MMC & wheelchair	MM	Group 4	49	27.3	BMD
C-9014	ACM & MRI	Early CM	Group 2	61	24.8	DMD
C-9015	No CM	Normal	Group 1	78	26.8	DMD
C-9016	No CM	Normal	Group 1	36	23.8	DMD
C-9017	No CM	Normal	Group 1	49	50.8	DMD
C-9018	ECM	Early CM	Group 2	42	21.9	BMD
C-9019	No CM	Normal	Group 1	24	30.8	DMD
C-9020	MMC	MM	Group 4	44	N/A	DMD
C-9021	ECM & MRI	Early CM	Group 2	56	24.1	DMD
C-9022	No CM	Normal	Group 1	51	25.0	intermed DMD/BMD
C-9023	MMC & MRI	MM	Group 4	33	21.6	DMD
C-9024	No CM	Normal	Group 1	44	24.9	BMD
C-9025	No CM	Normal	Group 1	21	30.5	DMD
C-9026	ACM	CM	Group 3	50	53.5	DMD
C-9027	ACM	CM	Group 3	44	30.4	DMD
C-9028	No CM	Normal	Group 1	54	29.6	DMD
C-9029	Moderate CM	CM	Group 3	62	N/A	DMD
C-9030	No CM	Normal	Group 1	58	32.8	DMD
C-9031	No CM	Normal	Group 1	52	25.6	BMD
C-9032	MMC & MRI	MM	Group 4	62	38.1	BMD
C-9033	No CM	Normal	Group 1	50	24.3	DMD
C-9034	No CM	MM	Group 4	56	25.9	DMD
C-9035	ECM	Early CM	Group 2	45	28.7	BMD
C-9036	MM & No CM	MM	Group 4	56	53.7	DMD
C-9037	ECM & MRI	Early CM	Group 2	54	23.0	DMD

Table 23. Patient information and group stratification - CM – Cardiomyopathy; ECM – Early Cardiomyopathy; ACM – Advanced Cardiomyopathy; MM – Muscle Manifesting; MMC – Muscle Manifesting Carrier; MRI – Magnetic Resonance Imaging; DMD – Duchenne Muscular Dystrophy; BMD – Becker's Muscular Dystrophy.

6.3.3 Neoepitopes

Patient plasma samples (n=37) were sent to Nordic Bioscience to utilise their Protein Fingerprint™ Technology to quantify extracellular matrix neoepitopes. These markers covered degradation and formation markers of abundant extra cellular matrix proteins present in fibrotic tissue and provided an inclusive overview of fibrogenesis/fibrolysis in participants. Details of the specific markers are included in **Table 24**.

Nordic Biomarker	ECM Formation or Degradation	Description	Detectable
BGM	Degradation	Neo-epitope of MMP-9,12 mediated degradation of biglycan	Yes – 19
C3M	Degradation	Neo-epitope of MMP-9 mediated degradation of type III collagen	Yes
C4G	Degradation	Neo-epitope of Granzyme-B mediated degradation of type IV collagen	Yes
C4M	Degradation	Neo-epitope of MMP-2, 9, 12 mediated degradation of type IV collagen α1 chain	Yes
C5M	Degradation	Neo-epitope of MMP-2, 9 mediated degradation of type V collagen	Yes
C6M	Degradation	Neo-epitope of MMP-2 mediated degradation of type VI collagen	Yes
CPa9-HNE	Degradation	Neutrophil elastase degradation of the S100A9 dimer of calprotection	Yes – 15 Samples
LG1M	Degradation	Neo-epitope of MMP-9 mediated degradation of laminin gamma 1 chain	Yes
PRO-C1	Formation	Internal epitope in the N-terminal pro-peptide of type I collagen	Yes
PRO-C3	Formation	Released N-terminal pro-peptide of type III collagen	Yes
PRO-C4	Formation	Internal epitope in the 7S domain of type IV collagen	Yes
PRO-C5	Formation	Released C-terminal pro-peptide of type V collagen	Yes
PRO-C6	Formation	C-terminal C5 domain of type VI collagen α3 chain	Yes
PRO-C11	Formation	N-terminal pro-peptide of the α1-chain type XI collagen	Yes - 29 Samples
TIM	Formation	Neo-epitope of MMP-12 mediated degradation of titin (cardaic isoform)	Yes

Table 24. Nordic Bioscience Protein Fingerprint™ Technology – Neoepitopes quantified in patient plasma.

6.3.4 Mesoscale Discovery™ Multiplex ELISA

Multiplex ELISAs (MesoScale™ Discovery) were performed as described in **Chapter 3**. Patient samples (n=37) were analysed using the human Immuno-Oncology 111-plex assays, TGF triplex, Metabolic Group and Biomarker Group assays **(Table 25)**. Results were analysed using the MSD Discovery Workbench 4.0 analysis software.

6.3.5 Lipidomics

Lipidomic analysis of samples was performed by Dr Zoe Hall from Imperial University, London. Lipid and metabolite profiling was carried out following the protocol described here(387). Briefly, lipids and metabolites were initially extracted from the plasma samples using the Folch method(388) to create an organic lipid-containing layer. Untargeted liquid chromatography-mass spectrometry (LC-MS) was used to analyse the lipid-containing layer using an LTQ Orbitrap Elite. Lipid identification was performed using an in-house database containing lipid *m/z* ratios of all combinations of common fatty acids. Fatty acid composition and identity confirmation was performed by fragmentation with tandem MS and peak areas normalised to internal standards.

MSD Kit	Markers
Human Immuno-Oncology 111-plex	IL-17E/IL25; IL-17F; IL-21; IL-27; IL-29/IFN-λ1; IL-31; IL-33; IL-23; TSLP; IL-22
	GLP-1 (active); Eotaxin; Eotaxin-3; IP-10; MCP-1; MCP-4; MDC; MIP-1α; MIP-1β; IL-17A/F
	IL-1α; IL-7; IL-12/IL-23p40; IL-15; IL-16; TNF-β; G-CSF; IFN-α2a; IL-18; TPO
	GIP (active); IFN-β; EPO; IL-17C; FLT3L; IL-2Rα; IL-9; IL-3; IL-17D; IL-1RA
	IFN-γ; IL-1β; IL-2; IL-4; IL-6; IL-8; IL-10; IL-12p70; GM-CSF; IL-5
	Insulin; C-Peptide; Ghrelin (active); TNF-α; IL-17A; VEGF-A; SDF-1α; Fractalkine; CTACK; ENA-78
	GIP (total); Pro-Insulin; IL-13; GRO-α; I-309; MCP-2; Eotaxin-2; M-CSF; TRAIL
	gp130 (soluble); YKL-40; MIF; MIP-5; BCMA/TNFRSF17; HAVCR2/TIM-3; Tie-2
	GIP (inactive); GLP-1 (inactive); Ghrelin (total); Leptin; PP; PYY (total); I-TAC; VEGF-D
	BAFF; FGF-23; LH; FSH; BDNF; CD276/B7-H3; CD20; CD27; CD28
	BAFF-R/TNFRSF13C; CD40L (soluble); LAG3; Granzyme A; Granzyme B; CTLA-4; OX40/TNFRSF4; PD1 (epitope 1); FGF (basic); GITR/TNFRSF18
	TLR1; RANKL/TNFSF11; PD-L2; PIGF; GITRL/TNSF18; PD1 (Epitope 2); TIGIT; PD-L1 (Epitope 1)
TGF-β Triplex	TGF-β1; TGF-β2; TGF-β3
Metabolic Group 1	B-NGF; FGF-21; GLP-1 (total); Glucagon; TARC
Biomarker Group 1	IL-17B; MCP-3; MIP-3α; MIP-3β

Table 25. Details of Mesoscale Discovery™ multi-plex ELISAs used.

6.3.6 Proteomics

Proteomic analysis was performed by Dr Pawel Palmowski and Dr Andrew Porter from the Newcastle Protein and Proteomic Analysis (NUPPA) facility at Newcastle University.

Firstly, 50µg of protein was taken and reduced with 30mM DTT at 30°C for 30 min to break disulphide bridges. This was followed by alkylation with 10mM Iodoacetamide for 20min, in the dark, at room temperature. The pH was adjusted to 8 with the addition of 50mM ammonium bicarbonate. Proteins were digested to peptides with the addition of Trypsin (Worthington, TPCK treated) at a ratio of 20:1 (protein: trypsin), incubated overnight for 16hrs, 37°C. For the final 4hrs of digestion trypsin was added at a ratio of 50:1 (protein: trypsin). The digestion was stopped by the addition of 10 %(v/v) Trifluroacetic acid to a final

concentration of 1% (v/v). The solution was clarified by centrifugation at 13,000xg for 10 min at room temperature. The acidified peptide mixture was then adjusted to a concentration of 1µg/µl with 0.5% TFA.

The equivalent of 500ng was loaded per LCMS run, peptides were separated with a 65 min nonlinear gradient (3-40%, 0.1% formic acid (Line A) and 80% acetonitrile, 0.1% formic acid (LineB)) using an UltiMate 3000 RSLCnano HPLC. Samples were first loaded/ desalted onto a 300µm x 5mm C18 PepMap C18 trap cartridge in 0.1% formic acid at 10 µl/min for 3 min. Separated on a 75µmx50cm C18 column (Thermo EasySpray -C18 2 µm) with integrated emitter at 250nl/min. The eluent was directed to an Thermo Orbitrap Exploris 480 mass spectrometer through the EasySpray source at a temperature of 320^{o}C, spray voltage 1900V. The total LCMS run time was 90 min. A 45 window Data Independent Acquisition (DIA) method was used to improve quantitative accuracy of the data set.

A pool sample was used to generate a spectral library. This was a hybrid of DDA and DIA data. DIA were acquired as per previously described and with a Gas Phase Fractionation method(389). The pool sample was subject to 6 replicate injections of 1ug, each covering one of 6 gas phases in the acquisition range (400-500, 500-600, 600-700,700-800, 800-900, 900-1000). All data was searched with Spectonaut Pular (v15) to generate a hybrid library that contained 57648 fragments, 4285 precursors, 3229 peptides, 381 proteins.

6.3.7 Statistical Analysis

Statistical analysis was performed on datasets using GraphPad Prism 9.4.1. Results are presented as mean ± standard error of the mean (SEM). Statistical analysis comprised of unpaired t-tests. Data were considered statistically significant with a p value ≤0.05 *, p≤0.01 ** and p≤0.001 ***.

6.4 Results

6.4.1 Patient Demographics

Patients were recruited from the Newcastle Female Carrier Cohort, a well-characterised group of around 150 patients, who are continually monitored over many years. In total 37 patients were recruited into our study **(Table 26)**. Patient age ranged from 21 years up to 78 years, with the median age of 49 years. The Body Mass Index (BMI) of the participants ranged from 21.6 to 53.7 whilst the median BMI was 27. Whilst the majority of study participants were Duchenne Muscular Dystrophy carriers, a number of carriers of the milder Becker's Muscular Dystrophy were also recruited, 27% of total participants. This allowed for an increased number of participants to take part in the study due to the relatively small size of the patients available in the Newcastle Female Carrier cohort. The Normal cardiac group had the highest number of BMD carriers, totalling 29% of those in that group. However, there were no significant differences observed between any of the groups in respect to age, BMI or presence of BDM.

	All (n=37)	Normal (n=17)	Early CM (n=8)	CM (n=5)	MM (n=7)	p value
Age (Median) Range	49 (21-78)	44 (21-78)	54 (42-61)	49 (33-62)	49 (33-62)	0.3457
BMI (Median) Range	27 (21.6-53.7)	28 (22.6-50.8)	24 (21.9-28.7)	34 (24.0-53.5)	28 (21.6-53.7)	0.1718
BMD % of Group with BDM	10 of 37 27%	5 of 17 29%	2 of 8 25%	1 of 5 20%	2 of 7 28.50%	0.981

Table 26. Patient demographics – Details of patient age, BMI and DMD/BDM status. Data is shown as median and range.

6.4.2 Nordic Neoepitope Biomarkers

Nordic Bioscience have developed assays for the identification and quantification of disease-specific biomarkers in patient plasma samples. After carefully reviewing the literature, we identified 15 markers that were quantified in the plasma of study participants. These markers covered degradation and formation markers for the most abundant extra cellular matrix proteins present in fibrotic tissue and provided an inclusive overview of fibrogenesis/fibrolysis in participants. Of the 15 markers measured all were detectable in the samples. However, for 3 of the markers (Pro-C11, BGM and CPa9-HNE) the lower level of quantification (LLOQ) was only exceeded in 29, 19 and 15 of the samples respectively. None of the markers of ECM degradation were significantly changed between any of the disease groups **(Figure 79)**, with levels of each marker comparable across the four groups. Next we quantified the ECM

formation markers, of the six different markers measured, only Pro-C6, an epitope of collagen VI, had significant differences between groups **(Figure 80)**. Pro-C6 was significantly elevated in the patients with established CM compared to patients with no cardiac dysfunction, whilst the MM patients also appeared to trend to increased levels of Pro-C6.

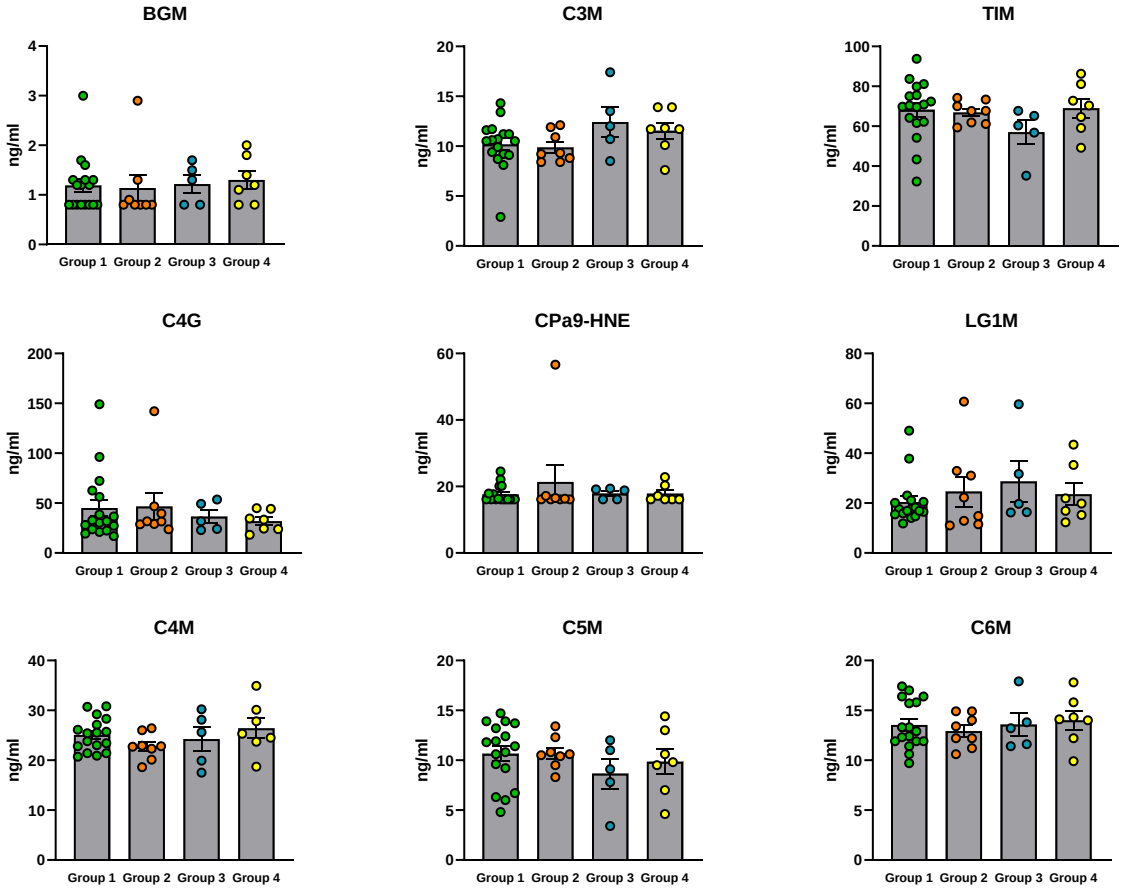

Figure 79. Neoepitopes of ECM Degradation – Patient plasma were quantified for levels of ECM degradation markers. Data is shown as Mean ± SEM n=37 donors.

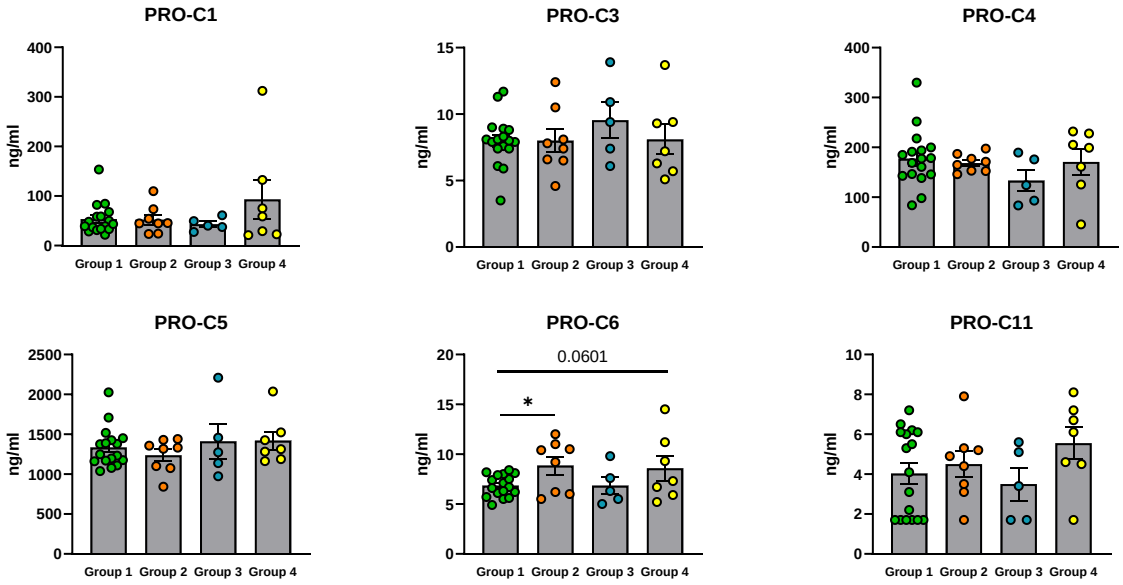

Figure 80. Neoepitopes of ECM formation – Patient plasma were quantified for levels of ECM degradation markers. Data is shown as Mean ± SEM, significant p values were calculated by unpaired student t tests *p≤0.05 ; n=37 donors.

Finally, in order to illuminate any differences in the turnover of the extracellular matrix, as assessed by the quantification of ECM formation or degradation, we compared the ratio between the degradation markers with their matched ECM formation marker **(Figure 81)**. The only differences observed were from patients with Early CM. These patients had an increased PRO-C6/C6M ratio compared to patients with normal cardiac function (Normal). Whilst the established CM patients had a reduced PRO-C4/C4M ratio compared to the patients with Early CM. Thus showing an increase in the formation of Collagen 4 and 6 compared to its breakdown.

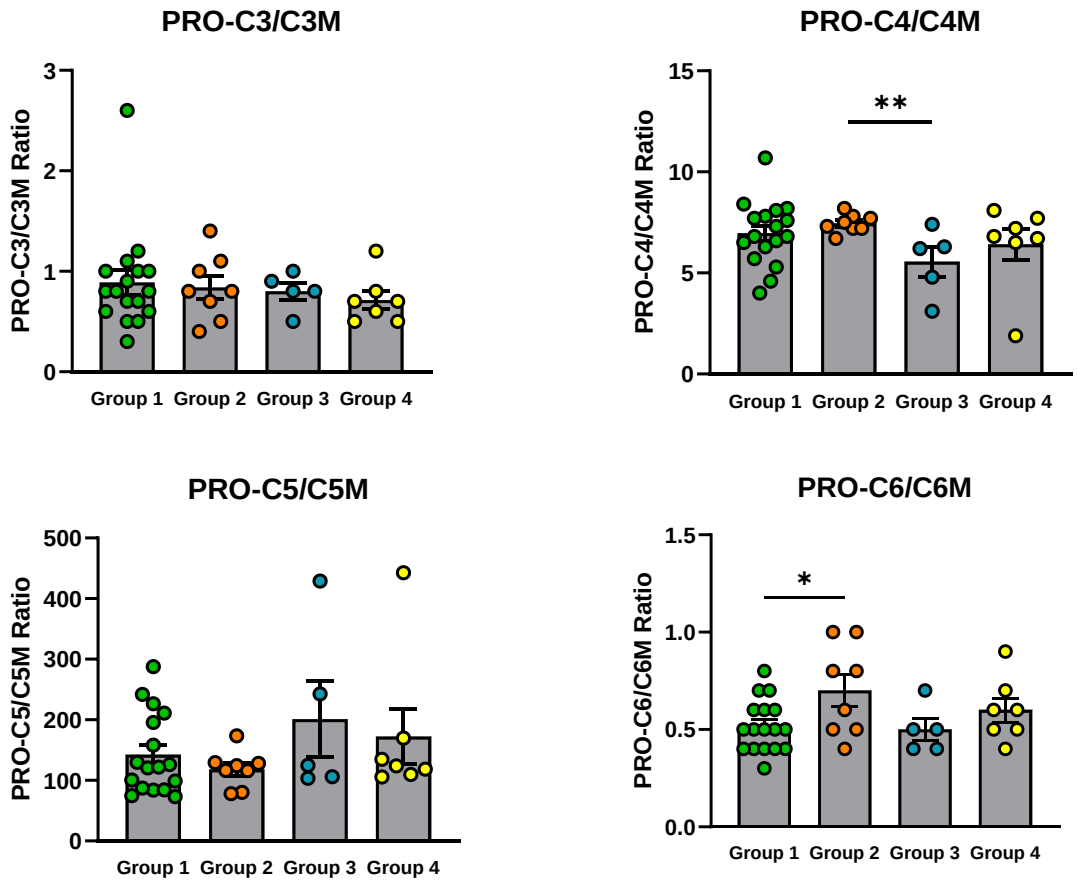

Figure 81. Ratio of neoepitope degradation/formation markers – Patient plasma were quantified for levels of ECM formation and degradation markers and presented as a ratio between the two. Data is shown as Mean ± SEM, significant p values were calculated by unpaired student t tests *p≤0.05; ** p≤0.01; n=37 donors.

These data have shown there to be an imbalance between the rate of formation and degradation of components of the ECM, specifically in the regard to Collagen 4 and 6, with increased amounts of these collagens being formed compared to the rate of their degradation. This provides the exciting prospect of utilising the measurement of neoepitopes as a blood based biomarker in female DMD carriers.

6.4.3 Multi-plex ELISA to quantify proteins present in patient plasma

MesoScale Discovery™ (MSD) assays combine electrochemiluminescence and multi-array technology for the high sensitivity measurement of molecules in biological samples to enable the high throughput profiling of potential biomarkers present within patient plasma samples. A total of n=122 different analytes were quantified in each patient sample, providing a broad disease profile across all patients. Samples from 36 of the 37 patients were included in our final analysis, 1 patient sample had a technical failure and was excluded from the final analysis. Of the 122 different analytes quantified, 39 did not reach the lower level of quantification (LLOQ) in at least 75% of the samples. The markers that were unable to be quantified are listed in **Table 27** and were excluded from further analysis.

MSD Kit	Markers below LLOQ (lower level of quantification)
Human Immuno-Oncology 111-plex	IL-21; IL-31; TSLP
	GLP-1 (active); Eotaxin-3; IL-17A/F
	IFN-β; IL-17C; IL-9; IL-3; IL-17D; IL-1RA
	IL-1β; IL-2; IL-4; IL-6; IL-10; IL-12p70; GM-CSF; IL-5
	IL-17A; ENA-78
	IL-13; I-309
	GLP-1 (inactive); I-TAC
	FGF (basic); GITR/TNFRSF18
	TLR1; PD-L2; PIGF; GITRL/TNSF18; PD-L1 (Epitope 1)
TGF-β Triplex	TGF-β3
Metabolic Group 1	B-NGF; GLP-1 (total); Glucagon
Biomarker Group 1	IL-17B; MCP-3

Table 27. Details of the analytes which fell below the lower level of quantification (LLOQ) and were therefore excluded from the results.

The heatmap depicts the z-transformed values from the quantifiable analytes **(Figure 82)**. While there is no obvious grouping of proteins present in the plasma in response to the disease profile of the donors, there were significant differences (p value ≤0.05) found in 8 markers, these are shown in **Figure 83**. In established CM patients the immune checkpoint protein PD-1 was significantly reduced in these donors compared to Early CM patients. Whilst macrophage colony-stimulating factor (M-CSF) was also found to be reduced in established CM patients when compared to the MM group. The early CM patients had significantly reduced levels of a number of the proteins quantified including Leptin, MIP-3β, FLT3L and C

peptide. Whilst MIP-3β and FLT3L are involved in immune system and inflammatory responses, C peptide is used as a biomarker of Diabetes in the clinic. Finally, in the MM patients, levels of M-CSF, MIP-3β and IL-29/IFNλ-1 were significantly increased compared to the donors with normal cardiac function.

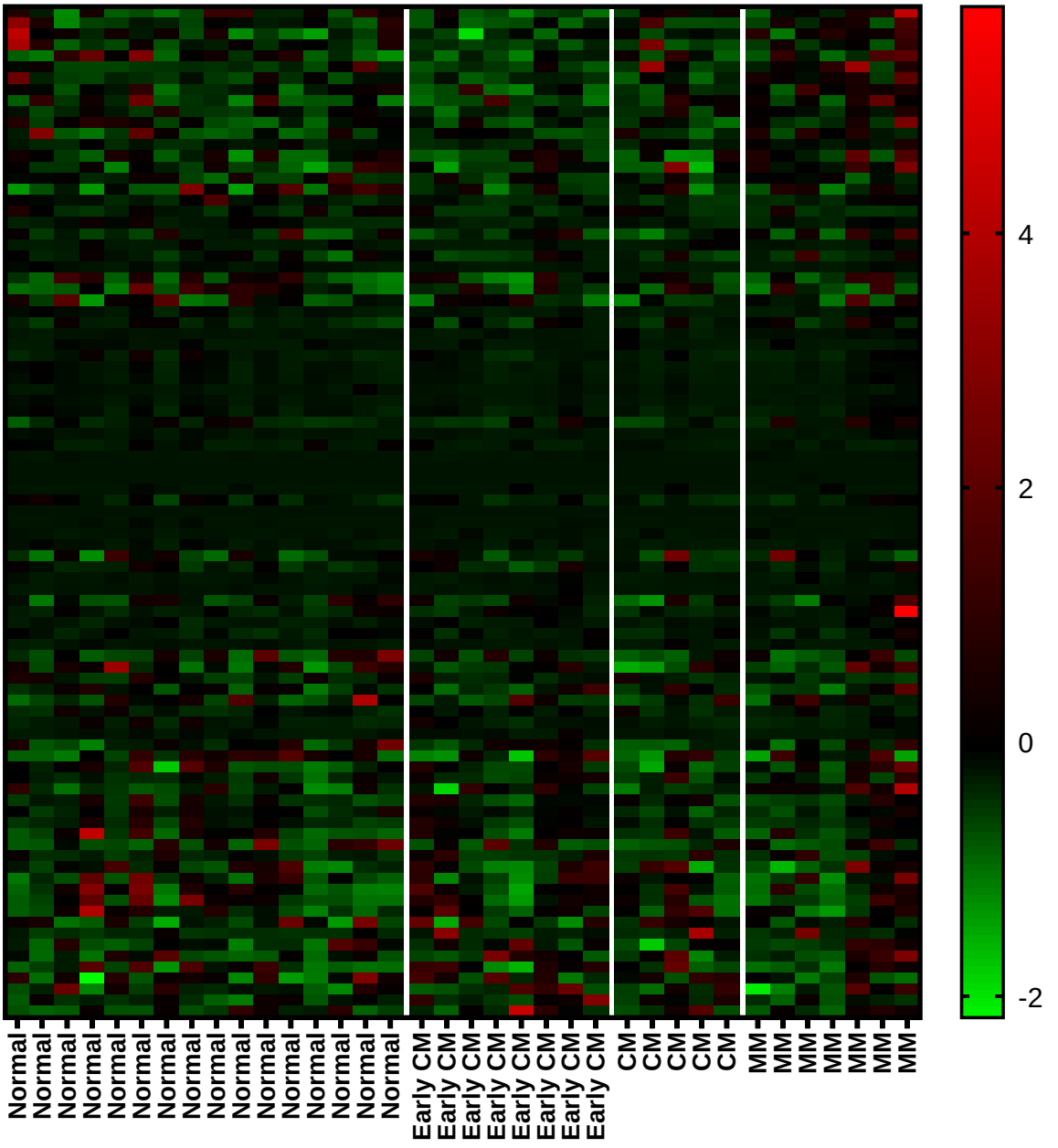

Figure 82. Heat map depicting the differences in proteins present in patient plasma depending on disease severity – Patient plasma (n=37) underwent Mesoscale Discovery™ Multi-plex ELSIA, data was z-transformed and normalised to the early CM group. Normal hearts on echo/No muscle symptoms (n=17 patients); Early Cardiomyopathy (Early CM) (n=8 patients); Established Cardiomyopathy (CM) (n=5 patients); Muscle Manifesting (MM) (n=7 patients).

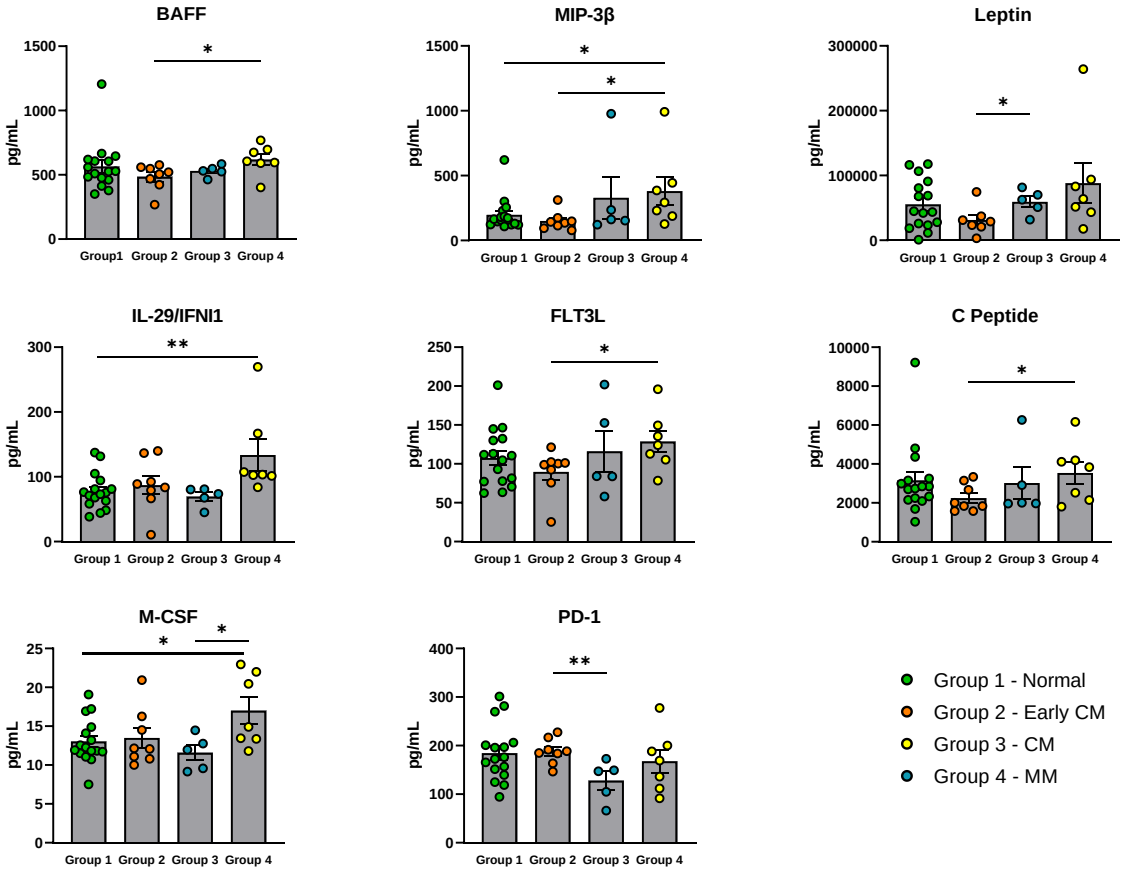

Figure 83. Representative graphs of proteins significantly changed in the plasma of female DMD carrier patients – Data is shown for each individual donor; n=37 donors; Normal hearts on echo/No muscle symptoms (n=17 patients); Early Cardiomyopathy (Early CM) (n=8 patients); Established Cardiomyopathy (CM) (n=5 patients); Muscle Manifesting (MM) (n=7 patients). Data are Mean ± SEM p values were calculated by unpaired student t tests; *p≤0.05.

Through the use of multi-plex ELISA we have identified a total of 8 proteins which are shown to have significant differences in the plasma of patients with a spectrum of cardiac disease. These markers have potential to be used as a blood based biomarker to identify cardiac fibrosis and/or progression in female DMD carriers.

6.4.4 Lipidomic profiles

To enable the characterisation of lipid metabolism, bulk lipidomic analysis targeting the metabolite profile was performed on the 37 patient samples. PCA plots of all patient groups and of Early CM, established CM and MM patients showed no clustering of samples in terms of lipid composition based on the disease severity of the patients **(Figure 84)**. The heat map in **Figure 85** depicts the levels of the many different isoforms of the lipids quantified during the lipidomic analysis, with the different isoforms clustered within their lipid grouping. There appeared to be little to no clustering of the different lipid isoforms in relation to the four disease groups. However within the patient groups it is possible to see differences in the presence of the different lipids between the individual donors. Next we looked at the difference in the levels of the total amount of different lipids between the disease groups **(Figure 86)**. A total of 7 different lipids were measured during the analysis, interestingly total mono-unsaturated fatty acid (MUFA)-containing Phosphatidylcholine (PC) and saturated fatty acid (SFA)-containing PC showed significant differences between patients with increasing disease severity. The levels of MUFA-PC were significantly elevated in patients with Early CM when compared to patients with no cardiac dysfunction (Normal), whilst SFA-PC were significantly elevated in the Early CM patients compared to patients with established CM. Although significance was not reached for the other total lipids, there were trends observed within the data. Patients with established CM appeared to have reduced levels of total PC, Phosphatidylethanolamine (PE) and Sphingomyelin (SM) compared to all other patient groups.

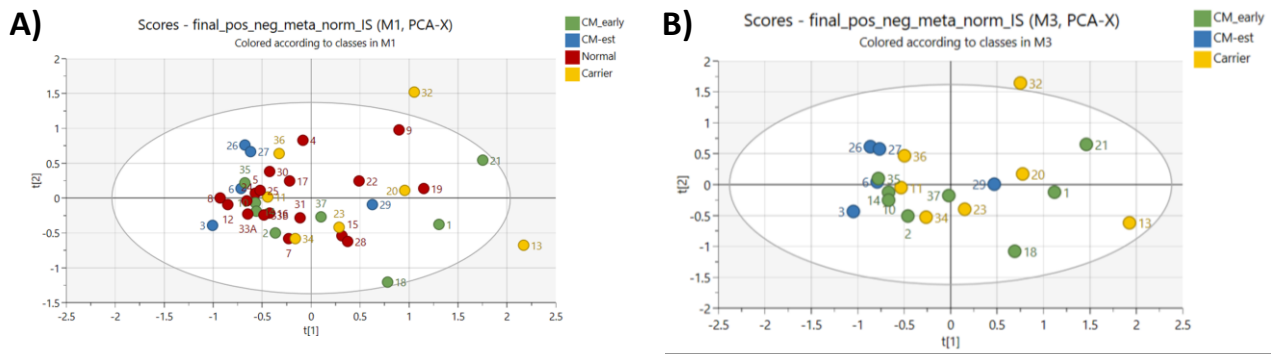

Figure 84. Disease severity had no effect on Lipidomic PCA clustering – Patient plasma (n=37) underwent lipidomic analysis; data is shown as Principle Component Analysis (PCA) plots for **A)** all disease groups **B)** Early CM, CM and MM groups.

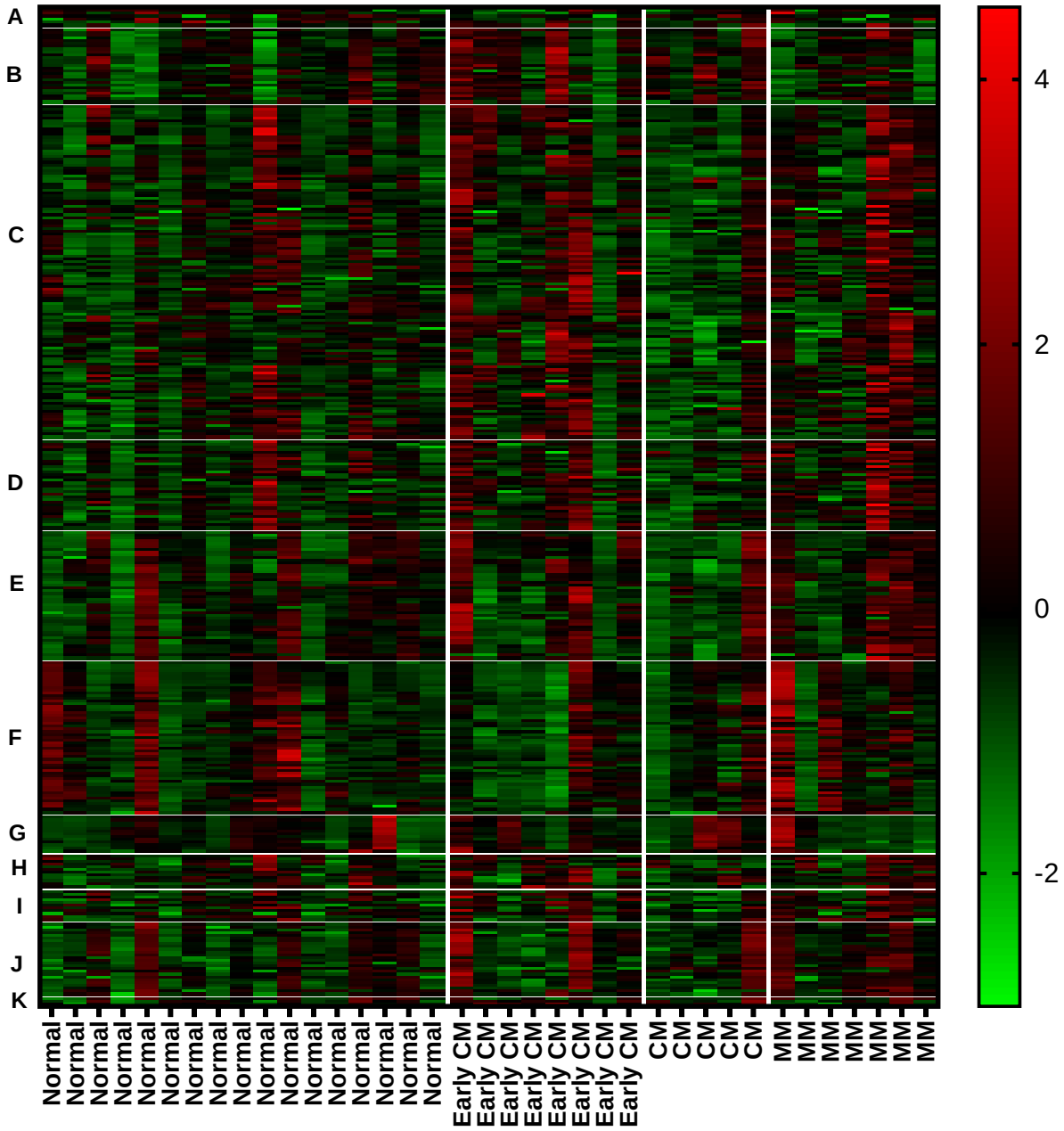

Figure 85. Heat map depicting the differences in lipid profiles between disease severity – Patient plasma (n=37) underwent lipidomics analysis, data was z-transformed. Normal hearts on echo/No muscle symptoms (n=17 patients); Early Cardiomyopathy (Early CM) (n=8 patients); Established Cardiomyopathy (CM) (n=5 patients); Muscle Manifesting (MM) (n=7 patients). **A** – Diacylglyceride; **B** – Lysophosphatidylcholine; **C** – Phosphatidylcholine; **D** – Phosphatidylethanolamine; **E** – Sphingomyelin; **F** – Triacylglyceride; **G** – Free Fatty Acids; **H** – Phosphatidylinositol; **I** – Phosphatidylserine; **J** – Ceramide and Hexose Ceramide; **K** – Lysphosphatidylethanolamine.

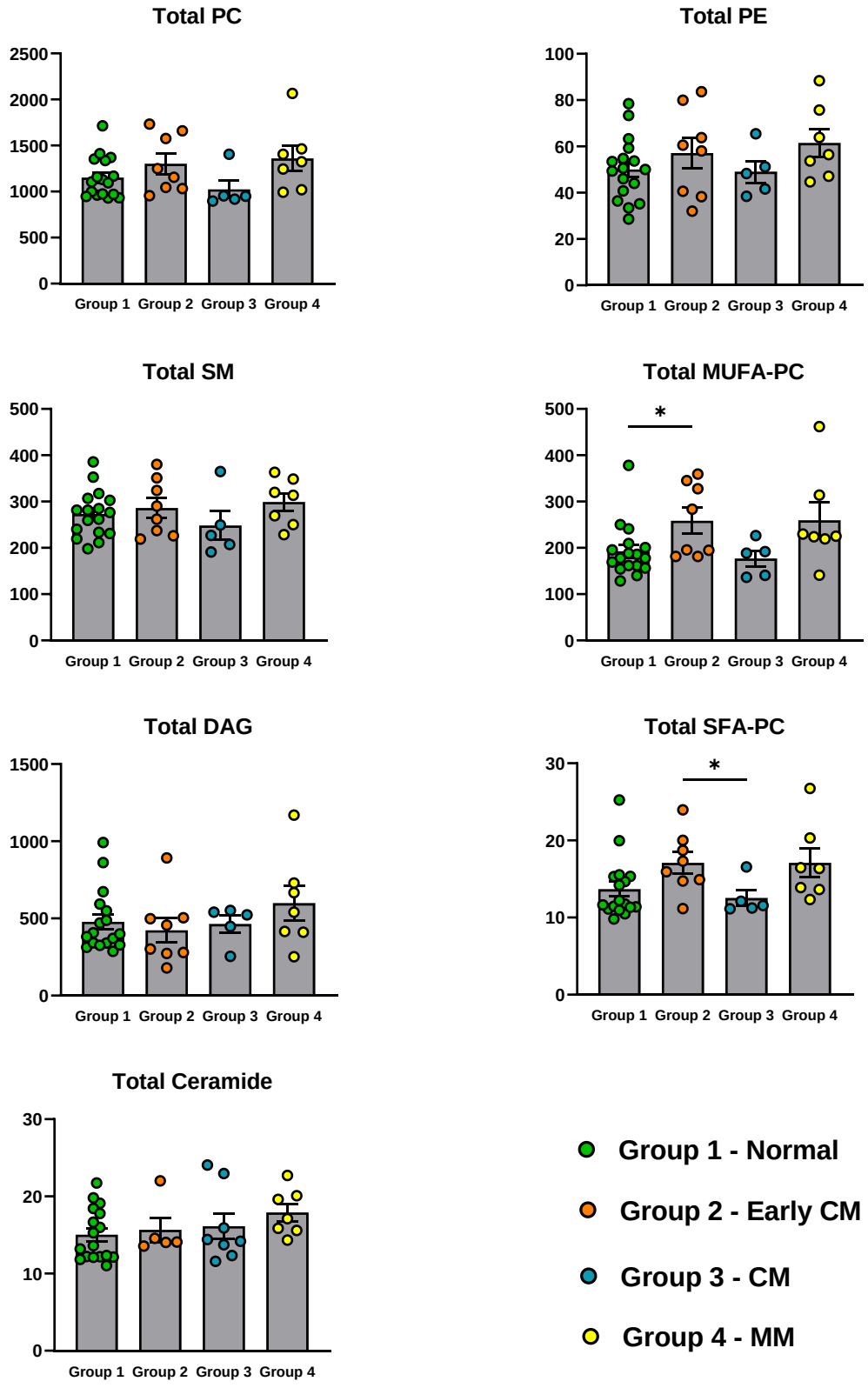

Figure 86. Comparisons of Total lipid levels between patients with different severities of cardiac disease – Patient plasma (n=37) underwent lipidomics analysis with the levels of total lipids compared between the four patient groups. Total PC – Phosphatidylcholine; Total DAG – Total Diacylglycerol; Total SFA-PC - saturated fatty acid-containing Phosphatidylcholine; Total MUFA-PC - Total mono-unsaturated fatty acid-containing Phosphatidylcholine; Total SM – Total Sphingomyelin; Total PE – Total Phosphatidylethanolamine. Data are Mean ± SEM p values were calculated by unpaired student t tests; *p≤0.05.

Finally we investigated the Omega 6/Omega 3 (n6/n3) ratios of the lipids **(Figure 87)**. The n6/n3 ratio is thought to be related to inflammation in patients, therefore differences between this ratio within patient groups could be indicative of differences in inflammatory profiles due to the severity of cardiac disease. In patients diagnosed with Early CM we observed a significant increase in the n6/n3 ratio of Free Fatty Acids (FFA) and Phosphatidylethanolamine (PE) whilst these patients also had a reduction in the n6/n3 ratio of Phosphatidylcholine (PC). Patients with established CM had a significant increase in Omega 6/Omega 3 ratio of Lysophosphatidylcholine (LPC). The MM patients had significantly increased levels of LPC, Phosphatidylethanolamine and Phosphatidylcholine when compared to the patients with normal cardiac and muscle function (Normal). Interestingly the MM patients had reduced n6/n3 ratio of FFA compared to normal cardiac function patients (Normal).

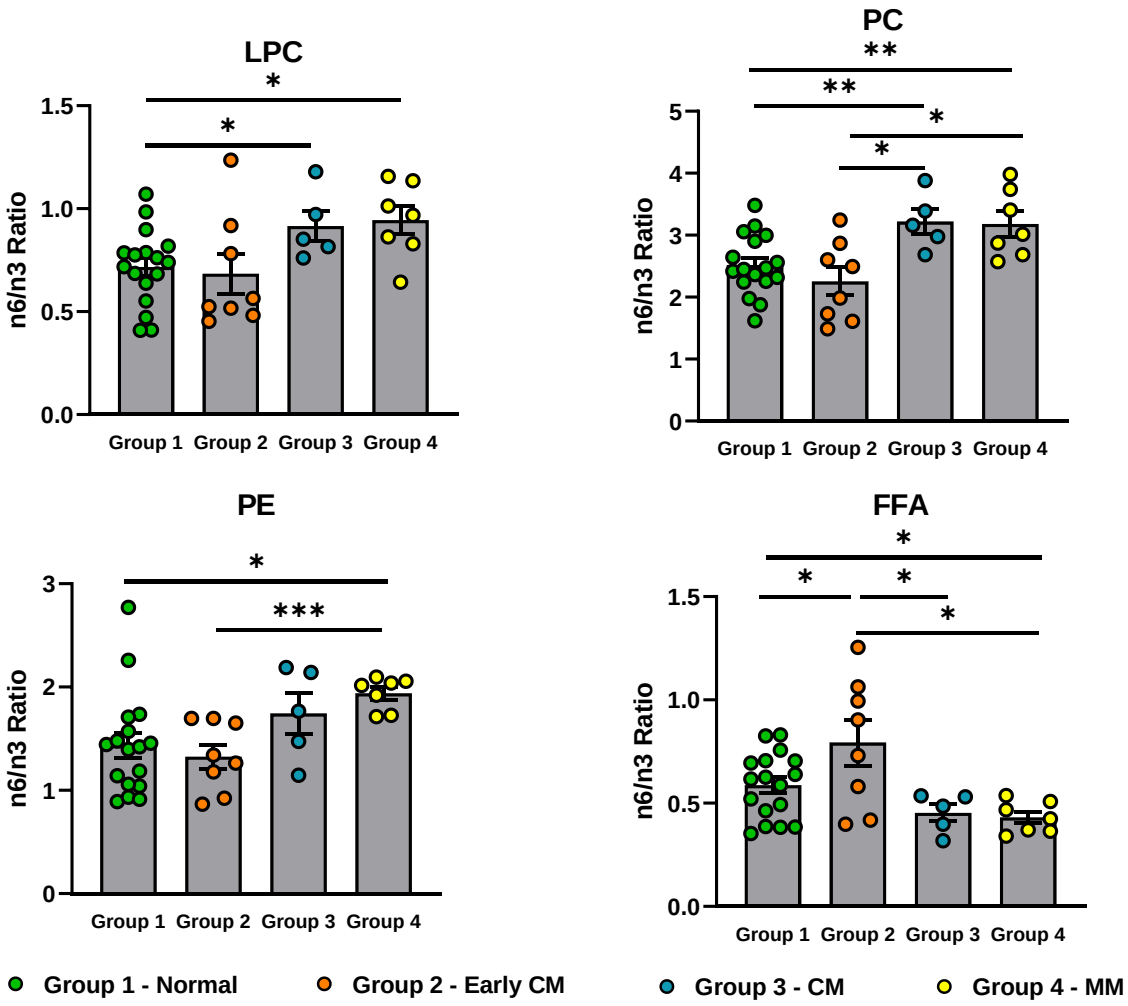

Figure 87. Changes in the n6/n3 ratio of different lipids depending of the cardiac disease severity of patients – Patient plasma (n=37) underwent lipidomics analysis with the levels of Omega 6 / Omega 3 ratios of lipids compared between the four patient groups. LPC – Lysophosphatidylcholine; PC – Phosphatidylcholine; PE – Phosphatidylethanolamine; FFA – Free Fatty Acid. Data are Mean ± SEM p values were calculated by unpaired student t tests; *p≤0.05; **p≤0.01; ***p≤0.001.

These data provide us with the opportunity to assess differences in the lipid profiles present within disease states. We have identified differences in the amount of two of the total lipids assessed, whilst also identifying a number of significant changes in the n6/n3 ratio of patients with different severities of cardiac damage. Therefore these result could help shed light on the presence of cardiac damage or to assess the progression of cardiac disease in female DMD patients.

6.4.5 Proteomic differences between severity of disease

In order to unbiasedly assess any differences in the amount and type of proteins present within the patient samples, we used unbiased proteomics. Principle component analysis (PCA) demonstrated there was no clustering of patient samples according to the disease severity of the donors **(Figure 88)**. In total proteomic analysis identified 338 total proteins across all runs. **Figure 89** depicts a heat map of all proteins identified, data was z-transformed, ordered depending on the disease severity and then normalised to the patients with evidence of Early CM. The heat map shows an area of upregulated proteins in the Early CM group compared to the other disease groups. It appears to be distinct in its profile compared to the patients with established CM as confirmed by cMRI (CM group), as well as the muscle manifesting (MM) patients. In addition to a cluster of upregulated proteins in the Early CM group there is also a cluster of downregulated proteins which is distinct to the other disease severity groups.

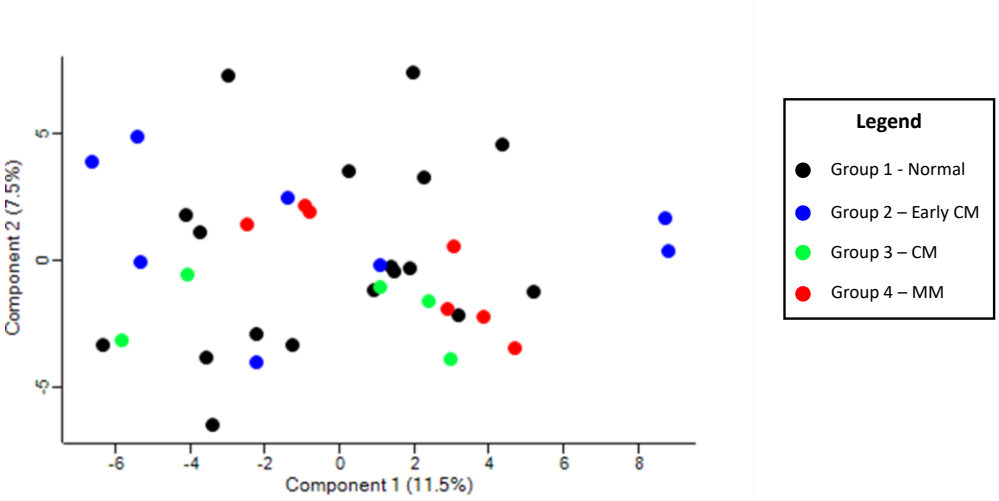

Figure 88. Disease severity had no effect on Proteomic PCA clustering – Patient plasma (n=37) underwent proteomic analysis. Group 1 – Normal hearts on echo/No muscle symptoms (n=17 patients); Group 2 – Early Cardiomyopathy (Early CM) (n=8 patients); Group 3 – Established Cardiomyopathy (CM) (n=5 patients); Group 4 – Muscle Manifesting (MM) (n=7 patients). Proteomic data is shown as Principle Component Analysis (PCA).

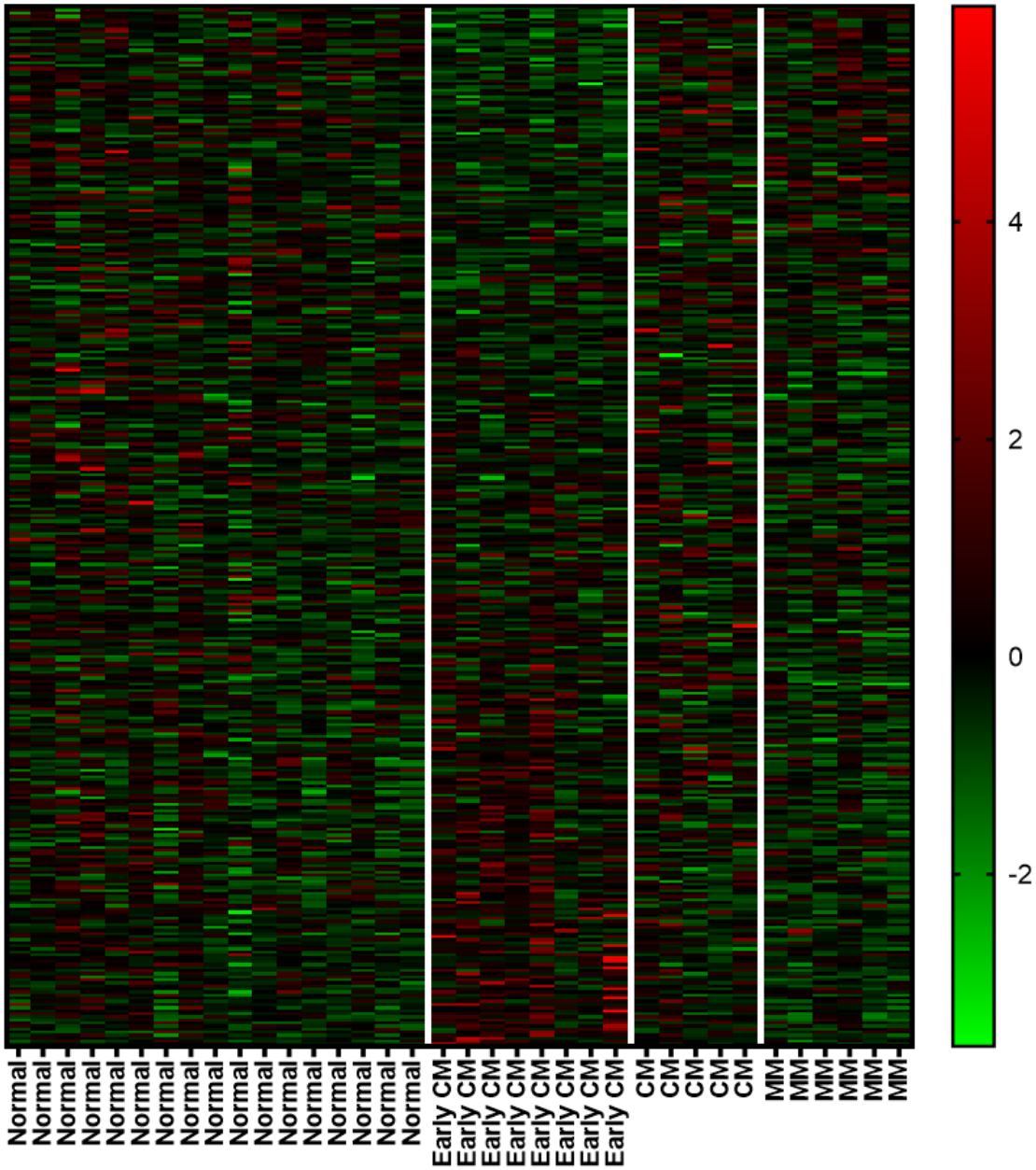

Figure 89. Heat map depicting the differences in protein expression between disease severity – Patient plasma (n=37) underwent proteomic analysis identifying 338 proteins present in all samples, data was z-transformed and normalised to the early CM group. Normal hearts on echo/No muscle symptoms (n=17 patients); Early Cardiomyopathy (Early CM) (n=8 patients); Established Cardiomyopathy (CM) (n=5 patients); Muscle Manifesting (MM) (n=7 patients).

Having initially assessed changes in the protein expression profile across all the different patient groups we next directly compared disease severity groups to investigate in more detail changes in protein expression. The first pair of groups we compared were the patients with Normal cardiac function with the patients with evidence of Early CM. This was to investigate whether there was protein signature distinct to the early stages of cardiomyopathy in patients. Out of the 338 proteins common across all donors and disease groups we identified 15 proteins which were significantly different in the Early CM patients compared to Normal cardiac function patients. Those with a padj of <0.05 were deemed to be statistically significant. Of these significantly different proteins, 11 were increased, whilst 4 were decreased in Early CM patients**. Figure 90** depicts these differences both as a volcano plot and heat map. The heat map clearly highlights the differences in protein expression between Normal cardiac function patients versus patients with evidence of Early CM.

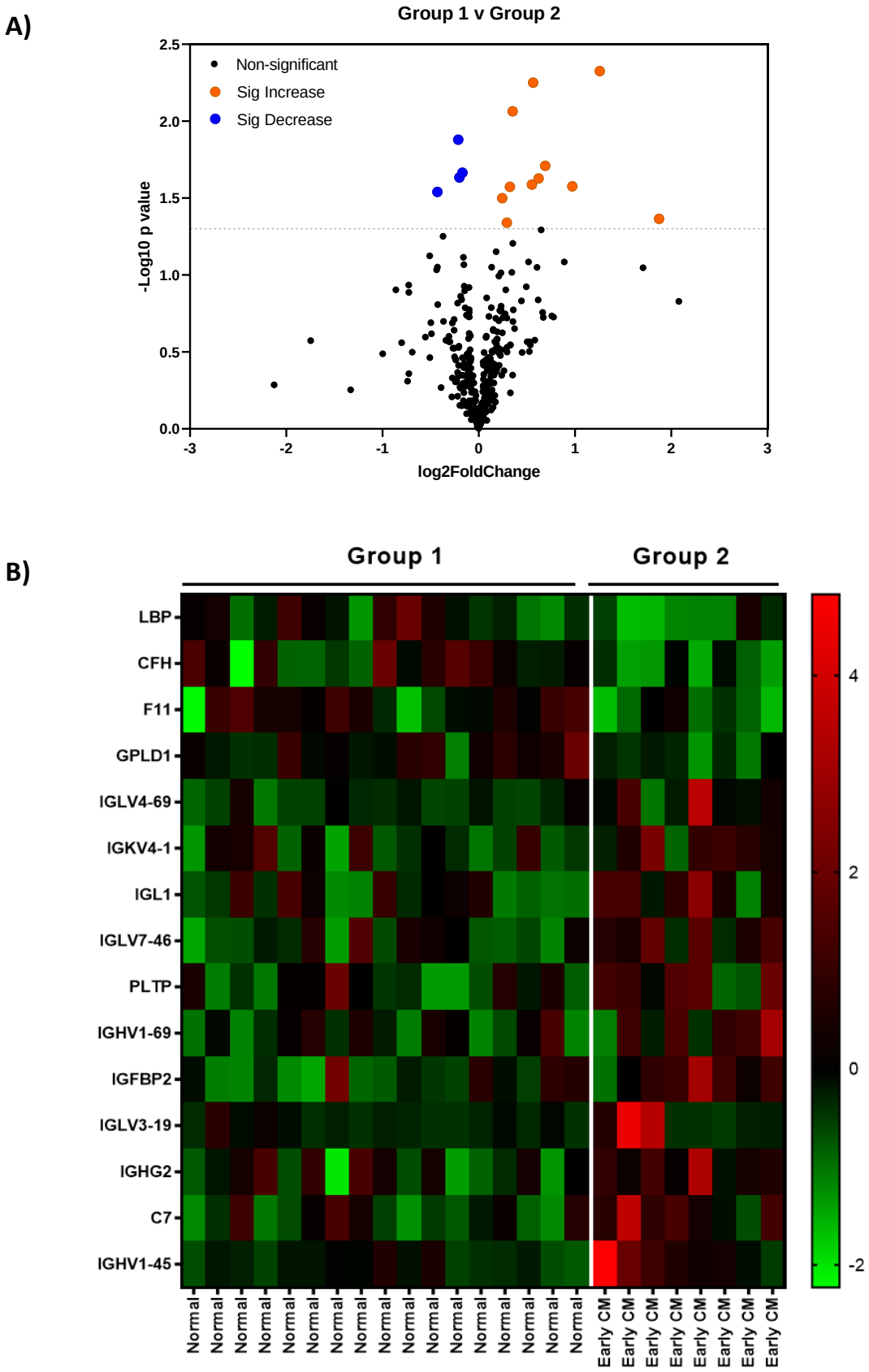

Figure 90. Significantly differentially expressed proteins between Normal and Early CM donors – Significantly differentially expressed proteins in Normal versus Early CM donors; Data is shown as **A)** Volcano Plot **B)** Heat Map. Proteins were deemed significant if padj value ≤0.05.

The levels of theses differentially regulated proteins was next assessed across all the disease severities with the majority of the proteins identified only differentially expressed in patients with evidence of Early CM. The proteins found to be significantly upregulated in these patients included IGLV7-46, C7, IGLV4-69, PLTP and IGLV3-19 **(Figure 92)**. Whilst in patients with evidence of Early CM the proteins GPLD1, CHF, F11 and LBP were found to be significantly downregulated **(Figure 91)**. Interestingly, there were a number of proteins also significantly different between patient groups with other disease severity, specifically the MM patients. Muscle Manifesting patients had significantly reduced levels of IGHG2 and IGL1 compared to patients with established CM **(Figure 92)**, whilst LBP was significantly elevated in MM patients compared to patients with normal cardiac function **(Figure 91)**.

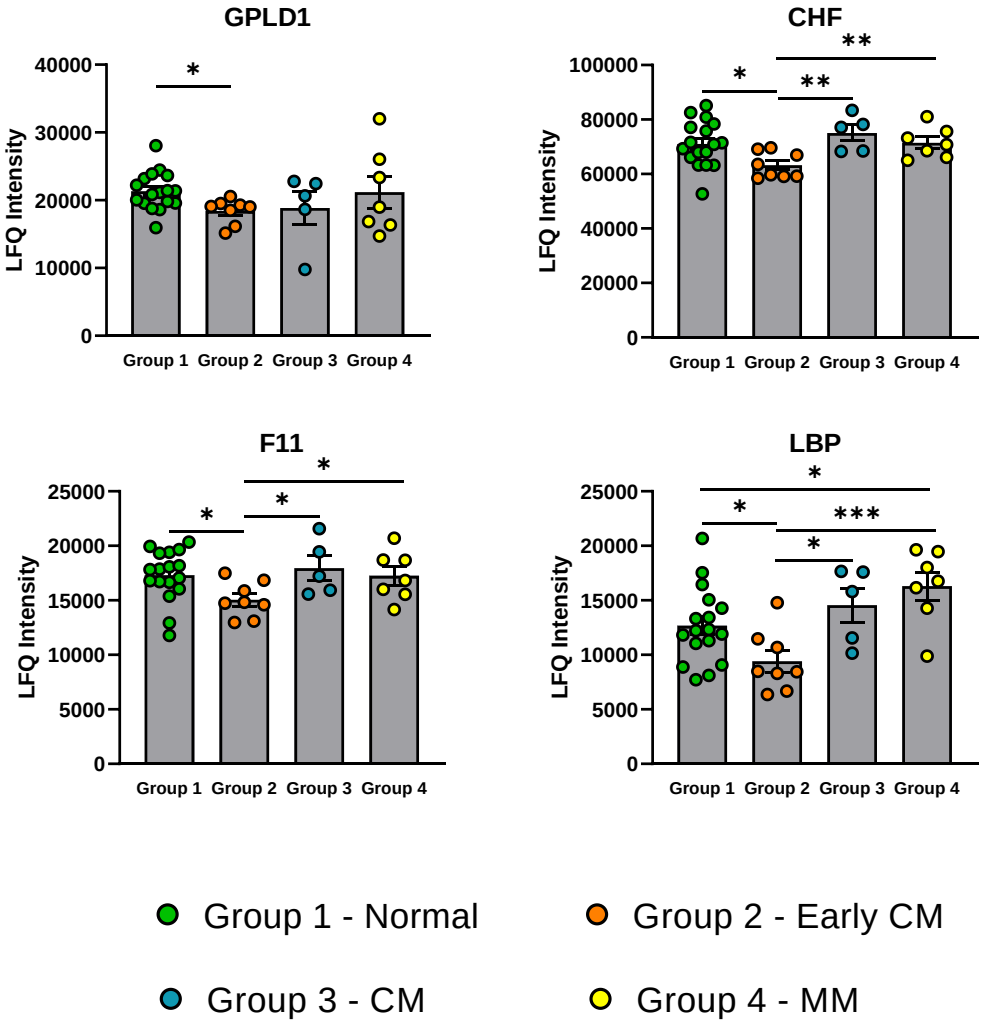

Figure 91. Representative graphs of proteins significantly downregulated in Early CM donors versus Normal cardiac donors – Protein intensity values from proteomic data. Protein expression was classed as significant if p value <0.05. Data is shown for each individual donor; n=37 donors; Normal hearts on echo/No muscle symptoms (n=17 patients); Early Cardiomyopathy (Early CM) (n=8 patients); Established Cardiomyopathy (CM) (n=5 patients); Muscle Manifesting (MM) (n=7 patients). Data are Mean ± SEM p values were calculated by unpaired student t tests; *p≤0.05; ***p≤0.001.

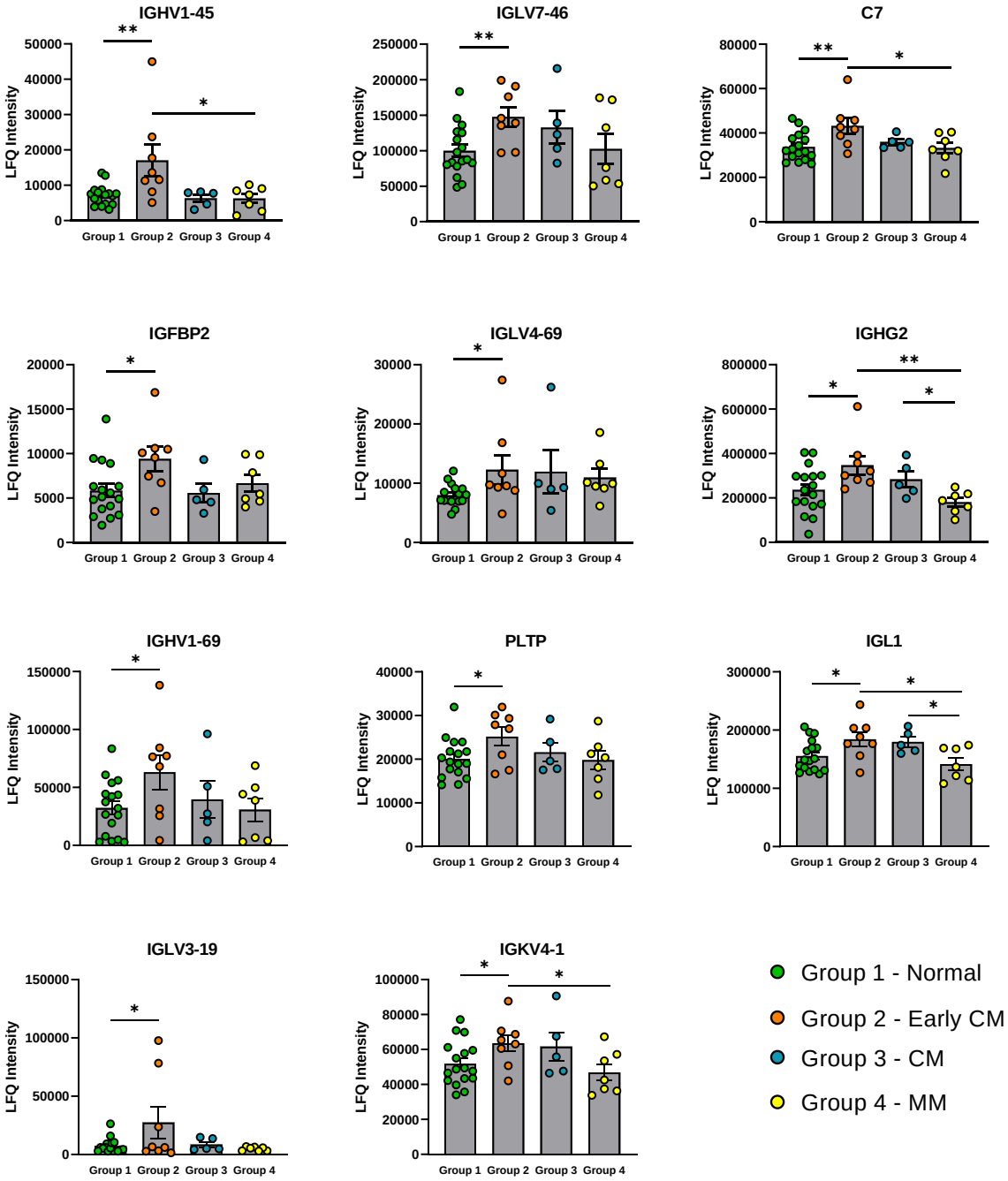

Figure 92. Representative graphs of proteins significantly upregulated in Early CM donors versus Normal cardiac donors – Protein intensity values from proteomic data. Protein expression was classed as significant if p value <0.05. Data is shown for each individual donor; n=37 donors; Normal hearts on echo/No muscle symptoms (n=17 patients); Early Cardiomyopathy (Early CM) (n=8 patients); Established Cardiomyopathy (CM) (n=5 patients); Muscle Manifesting (MM) (n=7 patients). Data are Mean ± SEM p values were calculated by unpaired student t tests; *p≤0.05; **p≤0.01.

The next groups we compared were the patients with no evidence of cardiac dysfunction (Normal) versus patients with established CM (CM) to investigate whether there was a profile of proteins specific to established cardiomyopathy. There was a total of 8 significantly differential proteins in established CM patients compared to patients with no cardiac dysfunction (Normal) **(Figure 93)**. Interestingly all the proteins identified were upregulated in the established CM patients. The heat map shows that this increase in the significant proteins was, on the whole, common to all five donors in the established CM group. The graphs in **Figure 94** show that for five of the upregulated proteins identified, their differential changes were unique to the established CM patients only. Whilst the remaining three proteins identified also have significant differences between the patients with differing disease severity. Histidine-rich glycoprotein (HRG) was the most differentially expressed protein across the four different groups. As well as being significantly upregulated in established CM patients compared to those with no cardiac dysfunction (Normal), it was also significantly elevated compared to both patients with early CM and also MM patients. There were also significant differences between the established CM and MM patients for the proteins IGA2 and IGKV1-27.

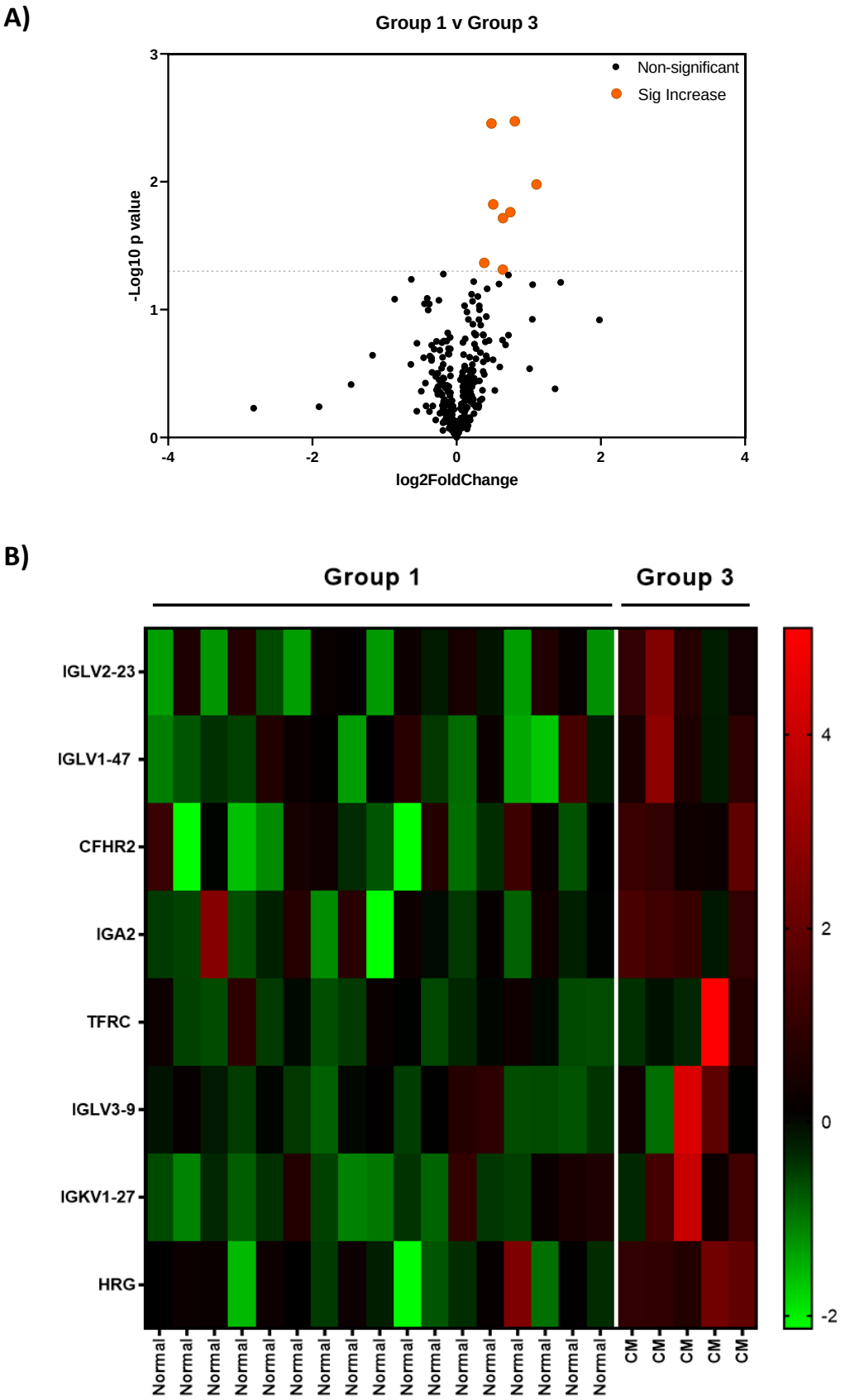

Figure 93. Significantly differentially expressed proteins between Normal and CM Donors – Significantly differentially expressed proteins in Normal versus established CM donors; Data is shown as **A)** Volcano Plot **B)** Heat Map. Proteins were deemed significant if p value ≤0.05.

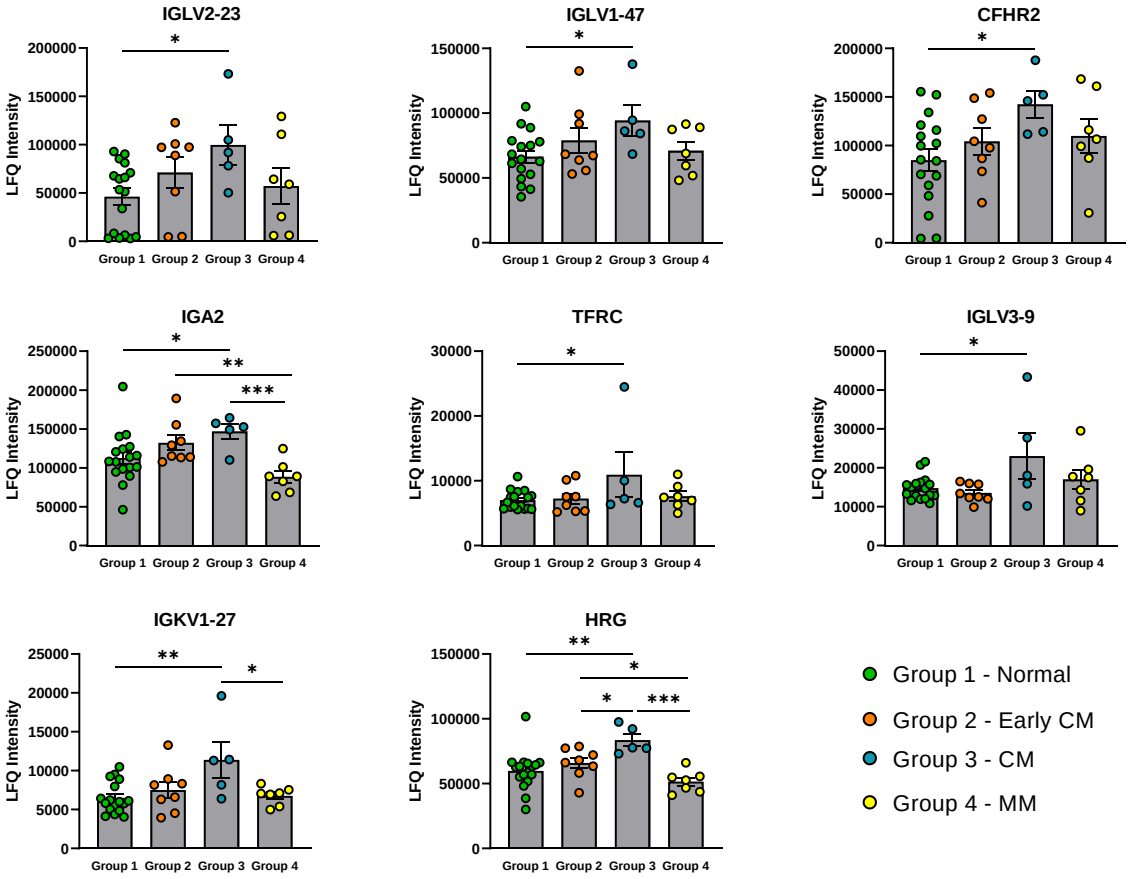

Figure 94. Representative graphs of proteins significantly upregulated in CM versus Normal donors – Protein intensity values from proteomic data. Protein expression was classed as significant if p value <0.05. Data is shown for each individual donor; n=37 donors; Normal hearts on echo/No muscle symptoms (n=17 patients); Early Cardiomyopathy (Early CM) (n=8 patients); Established Cardiomyopathy (CM) (n=5 patients); Muscle Manifesting (MM) (n=7 patients). Data are Mean ± SEM p values were calculated by unpaired student t tests; *p≤0.05; **p≤0.01; ***p≤0.001.

Lastly, we compared the patients with Early CM to those with established CM. In total there were 13 significant proteins identified to be either upregulated or downregulated in early CM patients **(Figure 95)**. The heat map shows the distinct profile between the early CM and established CM patients, with all donors having the same profile within the groups. Whilst the volcano plot depicts that of the 13 significantly differentially expressed proteins, 9 of them are upregulated in established CM patients whilst 4 are downregulated. The graphs showing the response of the upregulated proteins across all the groups interestingly highlights that IGHV3-20 and IGLV1-51 are the only two proteins to be significantly changed between only one pair of patient groups, the early CM patients and established CM patients **(Figure 96)**. Similar to what we have seen in the earlier figures LPS-binding protein (LBP) and HRG expression is significantly different across multiple patient groups including between patients with established CM and MM patients, and early CM patients and MM patients. **Figure 97** depicts the 4 proteins significantly downregulated in established CM patients compared to early CM

patients. These proteins are Leucine-rich α-2 glycoprotein 1 (LRG1), Serglycin (SRGN), Apolipoprotein M (APOM) and Cysteine Rich Secretory Protein 3 (CRISP3). Of these 4 proteins only LRG1, SRGN and APOM were uniquely changed between the early CM and established CM patients.

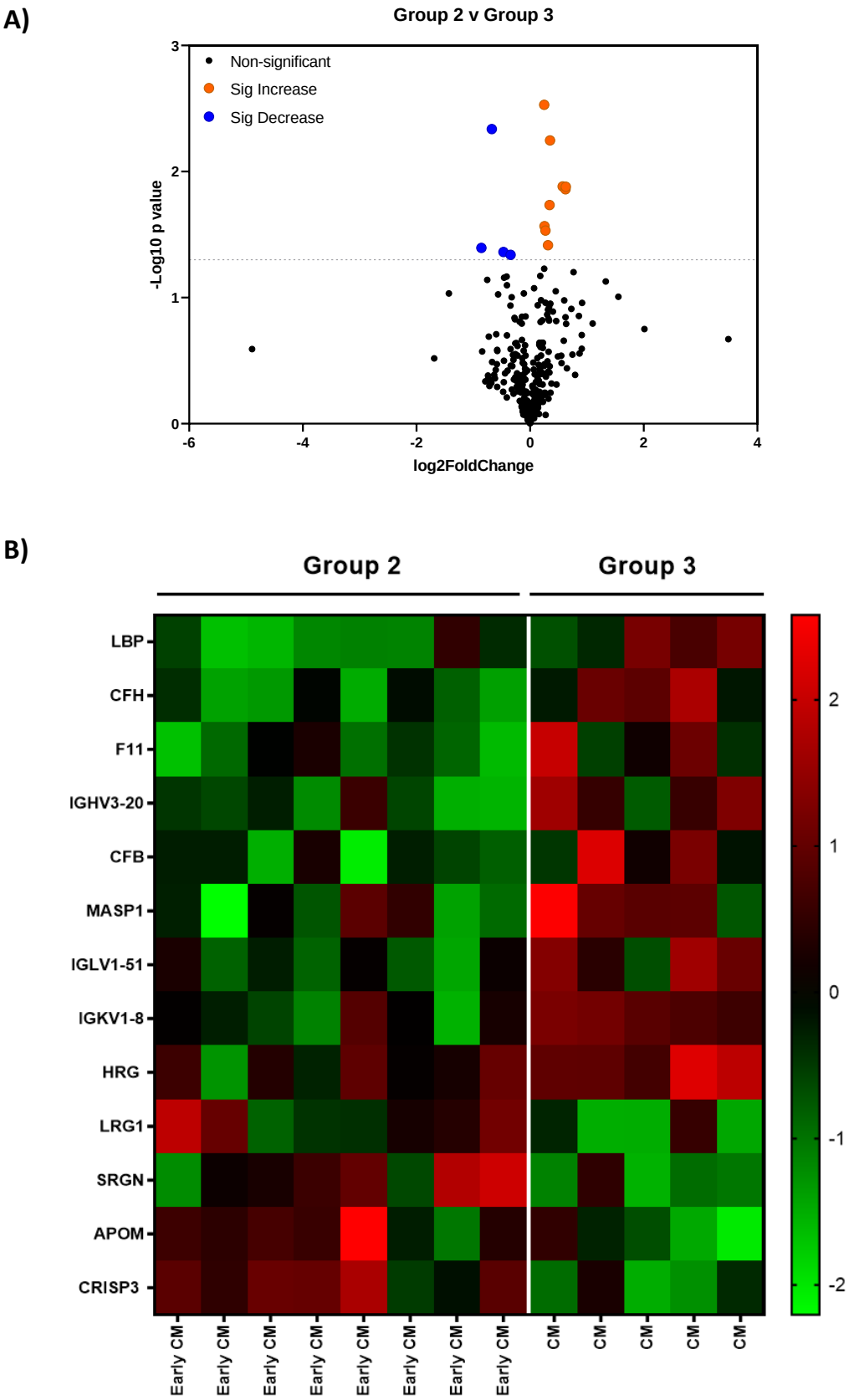

Figure 95. Significantly differentially expressed proteins between Early CM and established CM donors – Significantly differentially expressed proteins in Early CM versus Established CM donors; Data is shown as **A)** Volcano Plot **B)** Heat Map. Proteins were deemed significant if p value ≤0.05.

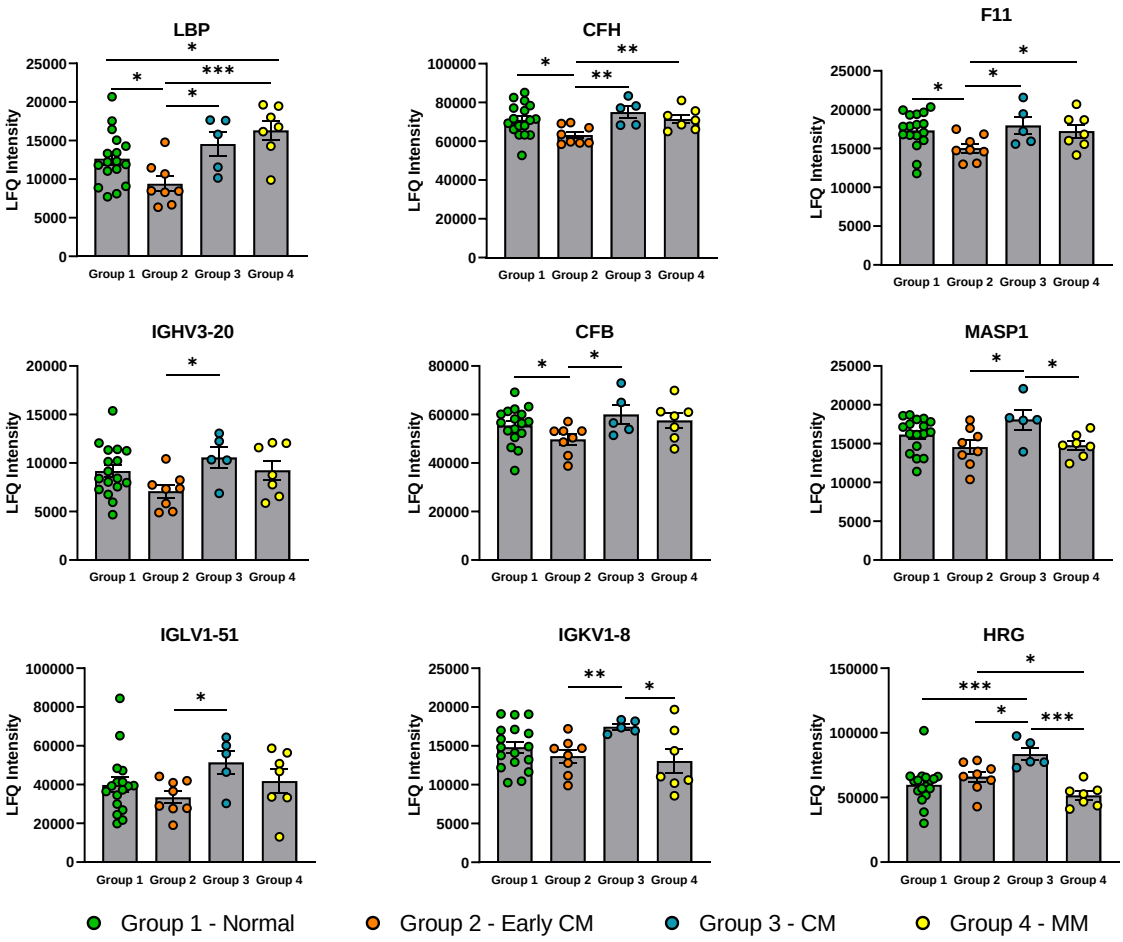

Figure 96. Representative graphs of proteins significantly upregulated in established CM donors versus early CM donors – Protein intensity values from proteomic data. Protein expression was classed as significant if p value <0.05. Data is shown for each individual donor; n=37 donors; Normal hearts on echo/No muscle symptoms (n=17 patients); Early Cardiomyopathy (Early CM) (n=8 patients); Established Cardiomyopathy (CM) (n=5 patients); Muscle Manifesting (MM) (n=7 patients). Data are Mean ± SEM p values were calculated by unpaired student t tests; *p≤0.05; **p≤0.01; ***p≤0.001.

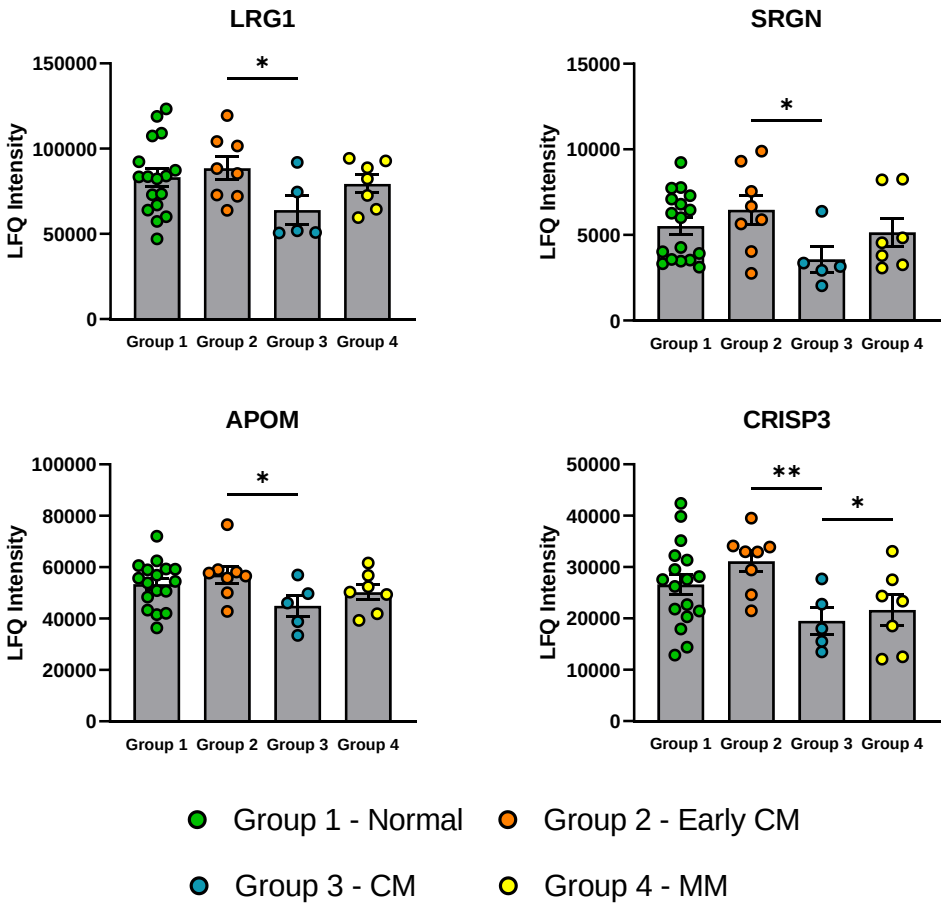

Figure 97. Representative graphs of proteins significantly downregulated in CM donors versus CM donors – Protein intensity values from proteomic data. Protein expression was classed as significant if p value <0.05. Data is shown for each individual donor; n=37 donors; Normal hearts on echo/No muscle symptoms (n=17 patients); Early Cardiomyopathy (Early CM) (n=8 patients); Cardiomyopathy (CM) (n=5 patients); Muscle Manifesting (MM) (n=7 patients). Data are Mean ± SEM p values were calculated by unpaired student t tests; *p≤0.05; **p≤0.01; ***p≤0.001.

These data have shown that we are able to identify 338 proteins within the patient plasma, of which 32 were significantly differentially expressed between the four patient groupings we compared. The identification of dynamic and differentially expressed proteins within our well-characterised but relatively small cohort provide the exciting potential to use blood based biomarkers to identify cardiac involvement in female DMD carriers enabling earlier pharmacological intervention or better disease monitoring.

6.5 Discussion

In recent years an ever increasing amount of research has focused upon the identification of biomarkers to aid medical diagnosis and to monitor therapeutic interventions, disease prognosis and disease progression. In regard to cardiac fibrosis and other cardiovascular diseases both diagnosis and progression of disease relies upon the use of either expensive cMRI or cardiac biopsies, which themselves carry a risk of complications. There is therefore a current unmet need for the identification of reliable, fast and cost-effective methods for the early and accurate detection of cardiomyopathies. Through the use of a small but well-characterised cohort of female DMD carriers we hoped to identify differences in protein or lipid expression in patient plasma that could potentially be used as biomarkers to identify the presence or progression of cardiac disease. The identification of cardiac specific circulating biomarkers would allow for early diagnosis in patients and obviate the need for less-sensitive and more expensive testing at the earlier surveillance phase for these patients. To achieve this we employed four distinct cutting-edge molecular biology approaches to identify specific markers of cardiac fibrosis to determine the molecular profile of the fibrotic human heart.

The use of proteomics in biomarker discovery research has advanced dramatically over recent years, especially in regard to cancer, cardiovascular diseases and diabetes research(390,391). Proteomic analysis of patient plasma in our study identified 32 significant differentially expressed proteins, around 10% of the total number of proteins identified in our cohort. Other studies have looked to utilise proteomics to identify biomarkers in DMD patients associated with muscle pathogenesis and disease progression. The majority of this research has focused on the skeletal muscle damage, with very little research investigating cardiac fibrosis biomarkers in patients. Work by Dang *et al* identified potential blood based biomarkers in DMD patients which correlated with increased disease severity, namely skeletal muscle fibrosis(392). A number of the proteins identified within our study have been suggested as potential biomarkers in a range of different diseases. Apolipoprotein M (apoM), a member of the lipocalin family, has been associated with a wide range of conditions, including cardiovascular disease. Although most recently apoM has been suggested as a biomarker for mortality in diabetes patients(393). A study by Ayoglu *et al* has utilised proteomics to identify potential biomarkers in DMD patients. Through this method they identified 11 potential markers, including 5 which proved to be novel(394). Work by Hathout *et al* used a combination of mass spec-based proteomics and a higher throughput method called SomaScan. Whilst

both methods were able to identify a large number of proteins, SomaScan discovered many more, with 44 blood based biomarkers identified and found to be present within two different cohorts(395).

The Nordic Bioscience Protein Fingerprint^{TM} technology has been used to identify biomarkers of ECM formation and breakdown products in a wide range of different diseases. In our samples we found Pro-C6, a marker of Collagen VI formation, to be differentially expressed between patient groups. Excitingly this is in agreement with other studies investigating biomarkers to identify cardiac fibrosis in patients. In the TOPCAT study, pro-C6 was found to be significantly predictive of rehospitalisation and risk of mortality in HFpEF patients with greater accuracy than accepted biomarker NT-proBNP(120). A large number of the neoepitopes quantified in our study were used in a study investigating cardiac fibrosis biomarkers in women with angina pectoris. Once again Pro-C6 was found to be elevated in the patients with cardiac fibrosis, interestingly the degradation markers C3M and C4M were also elevated in this group(396). However, in our study we found no differences between our disease groups for these markers when looking at them in isolation. Upon comparison of the ratio between the formation and degradation markers found an imbalance in the turnover of both Collagen 4 and 6.

The use of lipidomic analysis to identify biomarkers of disease has been previously used in a cohort of female DMD carriers. Evidence of dyslipidaemia, lipid imbalance, was found in the female carriers. In our study we identified a number of lipids to be altered between the different disease profiles. The Omega-3 fatty acids in Elderly patients with Myocardial Infarction (OMEMI) trial investigated the levels of n-3 and n-6 PUFA and their correlation with known biomarkers of cardiac fibrosis. Interestingly Galectin-3, a marker of cardiac remodelling, was found to be inversely proportional to n-3 PUFA levels in patient serums. This finding led researchers to conclude that n-3 PUFAs may have cardioprotective effects(397).

The use of multi-plex ELISAs enabled the high-throughput quantification of the levels of a wide range of proteins. Whilst quantifying 122 different analytes, a total of 8 proteins were found to have significant differences in at least one group. Interestingly these proteins were found to be reduced in either the early CM or CM groups. One of the proteins identified, leptin has been shown to increase collagen secretion and fibrosis in liver disease, whilst Wannamethee

et al suggested elevated plasma levels of leptin can cause cardiovascular complications(398). In patients with dilated cardiomyopathy, leptin was found to be increased, and has been used as a biomarker of disease progression(399). However, in our study leptin was reduced in patients with early CM group compared to established CM patients, whilst the patients with established CM were no different to patients with Normal cardiac function.

In this study we have identified a number of different molecules which are significantly changed in response to disease severity despite the small cohort size. However further validation of these biomarkers is required in additional, larger cohorts of female DMD carriers and also in other groups with the presence of cardiac fibrosis to ensure the changes observed are due to the changes occurring in fibrotic hearts.

7 Final Conclusions, Limitations and Future Work

7.1 Final Conclusions and Limitations

The work carried out in this thesis aimed to develop and utilise an *ex vivo* precision cut heart tissue slice model as an improvement on current translational and pre-clinical models of cardiac fibrosis. Our initial work focused on the optimisation of culture conditions to enable the extended culture of viable tissue slices prepared from human left ventricular tissue. Current PCHS models are able to keep tissue viable for a limited time, up to 48 hours, or use complex and highly specialised equipment which reduces the number of tissue slices able to be used in studies. Through careful investigation we tested a range of different commercially available culture mediums, which are designed specifically for use in human tissue culture. This was twinned with investigating whether the PCHS viability is improved with the use of a bioreactor rocking system developed and used by our laboratory(223). We showed that PCHS remained viable in culture for at least 96 hours when cultured in the bioreactor rocking system. Thus providing us with the longevity to model disease pathways and identify pathways engaged during the development of cardiac disease. A limitation of all PCHS models centres around the lack of circulation within the PCHS. Whilst the PCHS maintain the range of cell types present within the left ventricle, including immune cells present in the tissue at the time of slicing, the lack of a circulatory system means we are unable to monitor the effects of ingress and egress of immune cells present in the blood or from sources other than the heart.

Other groups using PCHS to investigate cardiac diseases have struggled to generate a response from exogenous challenge with recombinant proteins. In contrast we demonstrated a large number of broad pro-inflammatory (IL-1α, IL-1β, LPS and Poly-IC) and pro-fibrotic (TGF-β1) recombinant proteins are able to induce robust responses in PCHS. One of our aims was to develop a pre-clinical model to allow for the testing of novel compounds to treat cardiac fibrosis. In order to test this we tested approved anti-fibrotic therapies Pirfenidone and Nintedanib, in addition to known anti-inflammatory (IKK 2 inhibitor VIII) and anti-fibrotic (ALK5 inhibitor) compounds. These were applied in the presence of exogenous inflammatory (recombinant human IL-1α or LPS) or fibrotic (recombinant human TGF-β1) stimuli. We observed significant attenuation of protein markers of fibrosis, whilst Pirfenidone and IKK2 inhibitor VIII also displayed anti-inflammatory effects. Furthermore, these data confirmed results observed in HFpEF patients in clinical trials assessing the repurposing of Pirfenidone to

treat cardiac fibrosis in patients. A limitation of our system is that despite having extended the viable culture period compared to other models, were are still limited to a total of 96 hours. Fibrosis is a disease which occurs after repeated and uncontrolled damage to an organ over a long period of time, often years in patients. Therefore this system, along with many pre-clinical models, mimics an accelerated development and progression of fibrosis. This may result in some effects which occur in patients being absent or missed in our *ex vivo* system and vice versa.

Having demonstrated the ability to culture PCHS for an extended period and manipulate their responses to exogenous challenge, it was important to investigate the effect of a number of drivers of cardiac fibrosis identified from the literature and very well characterised *in vitro* and *in vivo* in our PCHS system. We achieved this through the identification and application of a number of proposed cardiac fibrosis stimuli (recombinant human TGF-β1, CTGF, Angiotensin II, Galectin-3 and IL-11). Initial experiments quantified the levels of secreted proteins from PCHS in response to each challenge. We found that the only stimuli to elicit reproducible and robust responses across PCHS from a number of donors were TGF-β1 and Galectin-3. In order to ensure we were not biasing ourselves due to the markers chosen we undertook unbiased transcriptomic and TCL proteomic analysis. Very minimal effects were observed in both the proteome and transcriptome in response to exogenous challenge with CTGF, IL-11 and Angiotensin II. Our data did confirm the ability to induce two distinct phenotypes within the PCHS in response to TGF-β1 or Galectin-3 treatment, confirming the pro-fibrotic effects of TGF-β1 and the pro-inflammatory response of Galectin-3.

Through the use of Ingenuity Pathway Analysis (IPA) on the RNA sequencing data from TGF-β1 and Galectin-3 treated PCHS, we identified a number of candidate compounds which when applied to PCHS could have anti-inflammatory and/or anti-fibrotic effects. Of the 32 compounds identified, n=11 of these compounds were found to be broadly anti-inflammatory, whilst n=9 compounds attenuated fibrotic responses. We did observe a number of the compounds to be equally effective at all doses tested, highlighting the need to titre doses of a number of the compounds to identify the minimal effective dose in the PCHS. We are currently missing key information regarding the mode of action of these compounds including identifying their targets within the heart tissue. In addition further work is required to understand the minimum effect dose (MED) in PCHS, achieved by measuring the

concentrations of the drug in the tissue instead of within the culture media. Answers to these questions would provide increased certainty that the anti-inflammatory and anti-fibrotic effects observed *ex vivo* would translate to patient populations.

The final aim of the PhD study was to use a well-characterised cohort of patients (female DMD carriers) with a spectrum of cardiac disease to identify potential blood based markers which could be used to diagnose cardiac involvement or monitor disease progression. This was achieved through the use of four distinct cutting-edge techniques; proteomics, lipidomic analysis, Nordic Bioscience Protein Fingerprint™ Technology and Mesoscale Discovery™ multiplex ELISA. Through this approach we identified a total of 32 proteins differentially expressed from the proteomics and 6 differences in the lipidomics profiles between disease severity. The collagen VI formation marker Pro-C6 was the only neoepitope to display any significant differences in the protein fingerprint analysis. However, when the ratio of formation to degradation were compared for a number of the markers, imbalances in the formation/degradation of Collagen IV and Collagen VI were observed. Through the use of the MSD multiplex ELISA 8 analytes were identified as potential biomarkers. Whilst the identification of significant differences between patients with differing severity of cardiac fibrosis is a potentially exciting prospect, data from this study should be treated with caution. The major limitations of this study is the small size of the cohort, with only 37 patients from a single centre. A much larger study is required to confirm whether the results found of the pilot study hold true when investigated in a much larger cohort.

7.2 Future Directions

The **optimisation of the culture conditions required to maintain viable PCHS** was completed in its entirety. We demonstrated the advantages of using the bioreactor rocking system to improve the viability of PCHS compared to other techniques. We were also able to manipulate the response from PCHS after treatment with pro-inflammatory and pro-fibrotic stimuli whilst being able to modulate these responses through the application of approved anti-fibrotic therapies Pirfenidone and Nintedanib.

Our work investigating the ability of **cardiac specific stimuli to induce inflammation and fibrosis** was robust, although despite large amounts of evidence in the literature, recombinant human Angiotensin II treatment was unable to induce a response in the PCHS. We believe this is due to the short half-life of Angiotensin II, shown to be a little as 20 minutes *in vitro.* Further work could be carried out, such as more frequent treatments with Angiotensin II, to investigate whether this would result in changes in gene expression and protein secretion similar to those seen both in patients and other pre-clinical models. Another addition to the work we performed would be the full integration of the 'omics' data, including secretomic and proteomic data, to fully elucidate and further interrogate our datasets. Our current work focused on the identification of candidate compounds with potential anti-inflammatory and anti-fibrotic effects. Further work is required to understand the mode of action of the compounds showing promise within our system, to identify doses which would be tolerable within patients and to understand the half-maximal inhibitory concentration (IC50) within the PCHS. We have currently focused on whole tissue effects in response to both exogenous recombinant protein stimulation and the application of the candidate compounds, further work could interrogate the different cell types effected by the treatments through the use of single cell sequencing for example, which in turn could provide more information regarding the pathways and proteins involved in the responses to the candidate compounds. Finally, due to the reduction in the availability of donor tissue caused by the Covid-19 pandemic, the experiments involving the candidate compounds were only able to be performed using two donors. Therefore further repeats using more donors are required to validate the current finding and ensure the effects are consistent in multiple donors.

The final section of the PhD project involved the **patient biomarkers study**, which aimed to identify potential biomarkers of cardiac fibrosis in a cohort of female DMD carriers. The major limitation of this work, centres around the small size of the patient cohort. Despite identifying many differences between the patient groups, we are likely to be missing some trends due to the small sample size of the disease groups. In order to investigate whether any of the potential biomarkers identified in the study have the potential be used in the clinic in the future, a much larger scale study is required, with patients recruited from multiple different centres around the country or world. Due to the delays in the recruitment and analysis of samples due to the Covid-19 pandemic, we have only been able to provide a high-level overview of the data produced. Future work will involve detailed interrogation to fully

elucidate the data and guide the future directions of the project. Cross referencing the data produced in the biomarker study with the multi-omics data produced in response to cardiac specific stimuli on PCHS would provide the opportunity to investigate whether our *ex vivo* model provides the opportunity to confirm results and further investigate the data produced in the patient biomarker study. Finally, there would be benefit to undertake a longitudinal study in order to identify potential blood based biomarkers during the development of disease in patients.

We have demonstrated that we have been able to create an improved method for the extended culture of PCHS. This improved methodology has enabled us to develop two distinct inflammatory and fibrotic phenotypes within the PCHS to allow for the identification of pathways involved in the development of cardiac inflammation and fibrosis. In addition we have been able to use the system to identify and test novel compounds, investigating their effectiveness to attenuate inflammation and fibrosis in the PCHS. Finally, we have highlighted a number of potential biomarkers of cardiac fibrosis within a cohort of female DMD carrier patients, paving the way for further in depth analysis and studies to confirm the accuracy of the potential biomarkers identified.

8 References

1. Borthwick LA, Wynn TA, Fisher AJ. Cytokine mediated tissue fibrosis. Biochimica et Biophysica Acta (BBA) - Molecular Basis of Disease. 2013 Jul;1832(7):1049–60.

2. Wynn T. Cellular and molecular mechanisms of fibrosis. J Pathol [Internet]. 2008 Jan;214(2):199–210. Available from: https://onlinelibrary.wiley.com/doi/10.1002/path.2277

3. Wynn TA. Fibrotic disease and the TH1/TH2 paradigm. Nat Rev Immunol. 2004 Aug;4(8):583–94.

4. Mozaffarian D, Benjamin EJ, Go AS, Arnett DK, Blaha MJ, Cushman M, et al. Heart Disease and Stroke Statistics—2016 Update. Circulation. 2016 Jan 26;133(4).

5. Wilkins E, Wilson L, Wickramasinghe K, Bhatnagar P, Leal J, Luengo-Fernandez R, et al. European Cardiovascular Disease Statistics 2017. 2017.

6. Bashey RI, Martinez-Hernandez A, Jimenez SA. Isolation, characterization, and localization of cardiac collagen type VI. Associations with other extracellular matrix components. Circ Res. 1992 May;70(5):1006–17.

7. Weber KT. Cardiac interstitium in health and disease: The fibrillar collagen network. J Am Coll Cardiol. 1989 Jun;13(7):1637–52.

8. Mewton N, Liu CY, Croisille P, Bluemke D, Lima JAC. Assessment of Myocardial Fibrosis With Cardiovascular Magnetic Resonance. J Am Coll Cardiol. 2011 Feb;57(8):891–903.

9. Brooks A. Interstitial fibrosis in the dilated non-ischaemic myocardium. Heart. 2003 Oct 1;89(10):1255–6.

10. Marijianowski MMH, Teeling P, Mann J, Becker AE. Dilated cardiomyopathy is associated with an increase in the type I/type III collagen ratio: A quantitative assessment. J Am Coll Cardiol. 1995 May;25(6):1263–72.

11. Sutton MGStJ, Sharpe N. Left Ventricular Remodeling After Myocardial Infarction. Circulation. 2000 Jun 27;101(25):2981–8.

12. Pinto AR, Ilinykh A, Ivey MJ, Kuwabara JT, D'Antoni ML, Debuque R, et al. Revisiting Cardiac Cellular Composition. Circ Res. 2016 Feb 5;118(3):400–9.

13. Bergmann O, Zdunek S, Felker A, Salehpour M, Alkass K, Bernard S, et al. Dynamics of Cell Generation and Turnover in the Human Heart. Cell. 2015 Jun;161(7):1566–75.

14. Zhou B, von Gise A, Ma Q, Hu YW, Pu WT. Genetic fate mapping demonstrates contribution of epicardium-derived cells to the annulus fibrosis of the mammalian heart. Dev Biol. 2010 Feb;338(2):251–61.

15. Kohl P. Heterogeneous Cell Coupling in the Heart. Circ Res. 2003 Sep 5;93(5):381–3.

16. Gaudesius G, Miragoli M, Thomas SP, Rohr S. Coupling of Cardiac Electrical Activity Over Extended Distances by Fibroblasts of Cardiac Origin. Circ Res. 2003 Sep 5;93(5):421–8.

17. Feld Y, Melamed-Frank M, Kehat I, Tal D, Marom S, Gepstein L. Electrophysiological Modulation of Cardiomyocytic Tissue by Transfected Fibroblasts Expressing Potassium Channels. Circulation. 2002 Jan 29;105(4):522–9.

18. Fredj S, Bescond J, Louault C, Potreau D. Interactions between cardiac cells enhance cardiomyocyte hypertrophy and increase fibroblast proliferation. J Cell Physiol. 2005 Mar;202(3):891–9.

19. Lucas JA, Zhang Y, Li P, Gong K, Miller AP, Hassan E, et al. Inhibition of transforming growth factor-β signaling induces left ventricular dilation and dysfunction in the pressure-overloaded heart. American Journal of Physiology-Heart and Circulatory Physiology. 2010 Feb;298(2):H424–32.

20. Zeisberg EM, Tarnavski O, Zeisberg M, Dorfman AL, McMullen JR, Gustafsson E, et al. Endothelial-to-mesenchymal transition contributes to cardiac fibrosis. Nat Med. 2007 Aug 29;13(8):952–61.

21. Kisanuki YY, Hammer RE, Miyazaki J ichi, Williams SC, Richardson JA, Yanagisawa M. Tie2-Cre Transgenic Mice: A New Model for Endothelial Cell-Lineage Analysis in Vivo. Dev Biol. 2001 Feb;230(2):230–42.

22. Alva JA, Zovein AC, Monvoisin A, Murphy T, Salazar A, Harvey NL, et al. VE-Cadherin-Cre-recombinase transgenic mouse: A tool for lineage analysis and gene deletion in endothelial cells. Developmental Dynamics. 2006 Mar;235(3):759–67.

23. Lugus JJ, Park C, Ma YD, Choi K. Both primitive and definitive blood cells are derived from Flk-1+ mesoderm. Blood. 2009 Jan 15;113(3):563–6.

24. Kramann R, Schneider RK, DiRocco DP, Machado F, Fleig S, Bondzie PA, et al. Perivascular Gli1+ Progenitors Are Key Contributors to Injury-Induced Organ Fibrosis. Cell Stem Cell. 2015 Jan;16(1):51–66.

25. Verma SK, Garikipati VNS, Krishnamurthy P, Schumacher SM, Grisanti LA, Cimini M, et al. Interleukin-10 Inhibits Bone Marrow Fibroblast Progenitor Cell–Mediated Cardiac Fibrosis in Pressure-Overloaded Myocardium. Circulation. 2017 Sep 5;136(10):940–53.

26. Kong P, Christia P, Saxena A, Su Y, Frangogiannis NG. Lack of specificity of fibroblast-specific protein 1 in cardiac remodeling and fibrosis. American Journal of Physiology-Heart and Circulatory Physiology. 2013 Nov 1;305(9):H1363–72.

27. Haider N, Boscá L, Zandbergen HR, Kovacic JC, Narula N, González-Ramos S, et al. Transition of Macrophages to Fibroblast-Like Cells in Healing Myocardial Infarction. J Am Coll Cardiol. 2019 Dec;74(25):3124–35.

28. Zeisberg EM, Kalluri R. Origins of Cardiac Fibroblasts. Circ Res. 2010 Nov 26;107(11):1304–12.

29. Ali SR, Ranjbarvaziri S, Talkhabi M, Zhao P, Subat A, Hojjat A, et al. Developmental Heterogeneity of Cardiac Fibroblasts Does Not Predict Pathological Proliferation and Activation. Circ Res. 2014 Sep 12;115(7):625–35.

30. Moore-Morris T, Guimarães-Camboa N, Banerjee I, Zambon AC, Kisseleva T, Velayoudon A, et al. Resident fibroblast lineages mediate pressure overload–induced cardiac fibrosis. Journal of Clinical Investigation. 2014 Jul 1;124(7):2921–34.

31. Moore-Morris T, Cattaneo P, Guimarães-Camboa N, Bogomolovas J, Cedenilla M, Banerjee I, et al. Infarct Fibroblasts Do Not Derive From Bone Marrow Lineages. Circ Res. 2018 Feb 16;122(4):583–90.

32. Vasan RS, Xanthakis V, Lyass A, Andersson C, Tsao C, Cheng S, et al. Epidemiology of Left Ventricular Systolic Dysfunction and Heart Failure in the Framingham Study. JACC Cardiovasc Imaging. 2018 Jan;11(1):1–11.

33. Ponikowski P, Voors AA, Anker SD, Bueno H, Cleland JGF, Coats AJS, et al. 2016 ESC Guidelines for the diagnosis and treatment of acute and chronic heart failure. Eur Heart J. 2016 Jul 14;37(27):2129–200.

34. Dunlay SM, Roger VL, Redfield MM. Epidemiology of heart failure with preserved ejection fraction. Nat Rev Cardiol. 2017 Oct 11;14(10):591–602.

35. Streng KW, Nauta JF, Hillege HL, Anker SD, Cleland JG, Dickstein K, et al. Non-cardiac comorbidities in heart failure with reduced, mid-range and preserved ejection fraction. Int J Cardiol. 2018 Nov;271:132–9.

36. Kanagala P, Cheng ASH, Singh A, Khan JN, Gulsin GS, Patel P, et al. Relationship Between Focal and Diffuse Fibrosis Assessed by CMR and Clinical Outcomes in Heart Failure With Preserved Ejection Fraction. JACC Cardiovasc Imaging. 2019 Nov;12(11):2291–301.

37. Cho JH, Zhang R, Aynaszyan S, Holm K, Goldhaber JI, Marbán E, et al. Ventricular Arrhythmias Underlie Sudden Death in Rats With Heart Failure and Preserved Ejection Fraction. Circ Arrhythm Electrophysiol. 2018 Aug;11(8).

38. Kosmas CE, Silverio D, Sourlas A, Montan PD, Guzman E. Role of spironolactone in the treatment of heart failure with preserved ejection fraction. Ann Transl Med. 2018 Dec;6(23):461–461.

39. Pitt B, Pfeffer MA, Assmann SF, Boineau R, Anand IS, Claggett B, et al. Spironolactone for Heart Failure with Preserved Ejection Fraction. New England Journal of Medicine. 2014 Apr 10;370(15):1383–92.

40. Dobaczewski M, Gonzalez-Quesada C, Frangogiannis NG. The extracellular matrix as a modulator of the inflammatory and reparative response following myocardial infarction. J Mol Cell Cardiol. 2010 Mar;48(3):504–11.

41. Kong P, Christia P, Frangogiannis NG. The pathogenesis of cardiac fibrosis. Cellular and Molecular Life Sciences. 2014 Feb 7;71(4):549–74.

42. Frangogiannis N. Chemokines in ischemia and reperfusion. Thromb Haemost. 2007 Nov 24;97(05):738–47.

43. Nahrendorf M, Swirski FK, Aikawa E, Stangenberg L, Wurdinger T, Figueiredo JL, et al. The healing myocardium sequentially mobilizes two monocyte subsets with divergent and complementary functions. Journal of Experimental Medicine. 2007 Nov 26;204(12):3037–47.

44. Ren G, Michael LH, Entman ML, Frangogiannis NG. Morphological Characteristics of the Microvasculature in Healing Myocardial Infarcts. Journal of Histochemistry & Cytochemistry. 2002 Jan 26;50(1):71–9.

45. Zymek P, Bujak M, Chatila K, Cieslak A, Thakker G, Entman ML, et al. The Role of Platelet-Derived Growth Factor Signaling in Healing Myocardial Infarcts. J Am Coll Cardiol. 2006 Dec;48(11):2315–23.

46. van den Borne SWM, Diez J, Blankesteijn WM, Verjans J, Hofstra L, Narula J. Myocardial remodeling after infarction: the role of myofibroblasts. Nat Rev Cardiol. 2010 Jan 1;7(1):30–7.

47. Holmes JW, Borg TK, Covell JW. Structure and Mechanics of Healing Myocardial Infarcts. Annu Rev Biomed Eng. 2005 Aug 15;7(1):223–53.

48. Mendell JR, Shilling C, Leslie ND, Flanigan KM, al-Dahhak R, Gastier-Foster J, et al. Evidence-based path to newborn screening for Duchenne muscular dystrophy. Ann Neurol. 2012 Mar;71(3):304–13.

49. Fairclough RJ, Wood MJ, Davies KE. Therapy for Duchenne muscular dystrophy: renewed optimism from genetic approaches. Nat Rev Genet. 2013 Jun 23;14(6):373–8.

50. Millay DP, Sargent MA, Osinska H, Baines CP, Barton ER, Vuagniaux G, et al. Genetic and pharmacologic inhibition of mitochondrial-dependent necrosis attenuates muscular dystrophy. Nat Med. 2008 Apr 16;14(4):442–7.

51. Guiraud S, Davies KE. Pharmacological advances for treatment in Duchenne muscular dystrophy. Curr Opin Pharmacol. 2017 Jun;34:36–48.

52. Mercuri E, Bönnemann CG, Muntoni F. Muscular dystrophies. The Lancet. 2019 Nov;394(10213):2025–38.

53. Duan D, Goemans N, Takeda S, Mercuri E, Aartsma-Rus A. Duchenne muscular dystrophy. Nat Rev Dis Primers. 2021 Feb 18;7(1):13.

54. Yilmaz A, Sechtem U. Cardiac involvement in muscular dystrophy: advances in diagnosis and therapy. Heart. 2012 Mar 1;98(5):420–9.

55. Finsterer J, Stöllberger C. The Heart in Human Dystrophinopathies. Cardiology. 2003;99(1):1–19.

56. Kaspar RW, Allen HD, Ray WC, Alvarez CE, Kissel JT, Pestronk A, et al. Analysis of Dystrophin Deletion Mutations Predicts Age of Cardiomyopathy Onset in Becker Muscular Dystrophy. Circ Cardiovasc Genet. 2009 Dec;2(6):544–51.

57. Eagle M, Bourke J, Bullock R, Gibson M, Mehta J, Giddings D, et al. Managing Duchenne muscular dystrophy – The additive effect of spinal surgery and home nocturnal ventilation in improving survival. Neuromuscular Disorders. 2007 Jun;17(6):470–5.

58. Kamdar F, Garry DJ. Dystrophin-Deficient Cardiomyopathy. J Am Coll Cardiol. 2016 May;67(21):2533–46.

59. Nigro G, Comi LI, Politano L, Bain RJI. The incidence and evolution of cardiomyopathy in Duchenne muscular dystrophy. Int J Cardiol. 1990 Mar;26(3):271–7.

60. Amoasii L, Hildyard JCW, Li H, Sanchez-Ortiz E, Mireault A, Caballero D, et al. Gene editing restores dystrophin expression in a canine model of Duchenne muscular dystrophy. Science (1979). 2018 Oct 5;362(6410):86–91.

61. Long C, Li H, Tiburcy M, Rodriguez-Caycedo C, Kyrychenko V, Zhou H, et al. Correction of diverse muscular dystrophy mutations in human engineered heart muscle by single-site genome editing. Sci Adv. 2018 Jan 5;4(1).

62. Nelson CE, Wu Y, Gemberling MP, Oliver ML, Waller MA, Bohning JD, et al. Long-term evaluation of AAV-CRISPR genome editing for Duchenne muscular dystrophy. Nat Med. 2019 Mar 18;25(3):427–32.

63. Young CS, Hicks MR, Ermolova NV, Nakano H, Jan M, Younesi S, et al. A Single CRISPR-Cas9 Deletion Strategy that Targets the Majority of DMD Patients Restores Dystrophin Function in hiPSC-Derived Muscle Cells. Cell Stem Cell. 2016 Apr;18(4):533–40.

64. Townsend D, Yasuda S, Metzger J. Cardiomyopathy of Duchenne muscular dystrophy: pathogenesis and prospect of membrane sealants as a new therapeutic approach. Expert Rev Cardiovasc Ther. 2007 Jan 10;5(1):99–109.

65. Weinberg M, Fell E, Lynfield J. Diagnostic Biopsy of the Pericardium and Myocardium. Archives of Surgery. 1958 May 1;76(5):825.

66. Sakakibara S, Konno S. Endomyocardial Biopsy. Jpn Heart J. 1962;3(6):537–43.

67. Bulloch RT, Murphy ML, Pearce MB. Intracardiac needle biopsy of the ventricular septum. Am J Cardiol. 1965 Aug;16(2):227–33.

68. Fowles RE, Mason JW. Endomyocardial Biopsy. Ann Intern Med. 1982 Dec 1;97(6):885.

69. Vöhringer M, Mahrholdt H, Yilmaz A, Sechtem U. Significance of Late Gadolinium Enhancement in Cardiovascular Magnetic Resonance Imaging (CMR). Herz Kardiovaskuläre Erkrankungen. 2007 Mar;32(2):129–37.

70. Haaf P, Garg P, Messroghli DR, Broadbent DA, Greenwood JP, Plein S. Cardiac T1 Mapping and Extracellular Volume (ECV) in clinical practice: a comprehensive review. Journal of Cardiovascular Magnetic Resonance. 2017 Jan 30;18(1):89.

71. Kim RJ, Wu E, Rafael A, Chen EL, Parker MA, Simonetti O, et al. The Use of Contrast-Enhanced Magnetic Resonance Imaging to Identify Reversible Myocardial Dysfunction. New England Journal of Medicine. 2000 Nov 16;343(20):1445–53.

72. Parsai C, O'Hanlon R, Prasad SK, Mohiaddin RH. Diagnostic and prognostic value of cardiovascular magnetic resonance in non-ischaemic cardiomyopathies. Journal of Cardiovascular Magnetic Resonance. 2012 Dec 2;14(1):54.

73. Judd RM, Lugo-Olivieri CH, Arai M, Kondo T, Croisille P, Lima JAC, et al. Physiological Basis of Myocardial Contrast Enhancement in Fast Magnetic Resonance Images of 2-Day-Old Reperfused Canine Infarcts. Circulation. 1995 Oct;92(7):1902–10.

74. Kim RJ, Fieno DS, Parrish TB, Harris K, Chen EL, Simonetti O, et al. Relationship of MRI Delayed Contrast Enhancement to Irreversible Injury, Infarct Age, and Contractile Function. Circulation. 1999 Nov 9;100(19):1992–2002.

75. Flacke SJ, Fischer SE, Lorenz CH. Measurement of the Gadopentetate Dimeglumine Partition Coefficient in Human Myocardium in Vivo: Normal Distribution and Elevation in Acute and Chronic Infarction. Radiology. 2001 Mar;218(3):703–10.

76. Wong TC, Piehler K, Puntil KS, Moguillansky D, Meier CG, Lacomis JM, et al. Effectiveness of late gadolinium enhancement to improve outcomes prediction in patients referred for cardiovascular magnetic resonance after echocardiography. Journal of Cardiovascular Magnetic Resonance. 2013 Dec 16;15(1):6.

77. Assomull RG, Prasad SK, Lyne J, Smith G, Burman ED, Khan M, et al. Cardiovascular Magnetic Resonance, Fibrosis, and Prognosis in Dilated Cardiomyopathy. J Am Coll Cardiol. 2006 Nov;48(10):1977–85.

78. Rubinshtein R, Glockner JF, Ommen SR, Araoz PA, Ackerman MJ, Sorajja P, et al. Characteristics and Clinical Significance of Late Gadolinium Enhancement by Contrast-Enhanced Magnetic Resonance Imaging in Patients With Hypertrophic Cardiomyopathy. Circ Heart Fail. 2010 Jan;3(1):51–8.

79. Monti CB, Codari M, Cozzi A, Alì M, Saggiante L, Sardanelli F, et al. Image quality of late gadolinium enhancement in cardiac magnetic resonance with different doses of contrast material in patients with chronic myocardial infarction. Eur Radiol Exp. 2020 Dec 3;4(1):21.

80. Alfano G, Fontana F, Ferrari A, Solazzo A, Perrone R, Giaroni F, et al. Incidence of nephrogenic systemic fibrosis after administration of gadoteric acid in patients on renal replacement treatment. Magn Reson Imaging. 2020 Jul;70:1–4.

81. Messroghli DR, Radjenovic A, Kozerke S, Higgins DM, Sivananthan MU, Ridgway JP. Modified Look-Locker inversion recovery (MOLLI) for high-resolutionT1 mapping of the heart. Magn Reson Med. 2004 Jul;52(1):141–6.

82. Messroghli DR, Radjenovic A, Kozerke S, Higgins DM, Sivananthan MU, Ridgway JP. Modified Look-Locker inversion recovery (MOLLI) for high-resolutionT1 mapping of the heart. Magn Reson Med. 2004 Jul;52(1):141–6.

83. Piechnik SK, Ferreira VM, Dall'Armellina E, Cochlin LE, Greiser A, Neubauer S, et al. Shortened Modified Look-Locker Inversion recovery (ShMOLLI) for clinical myocardial T1-mapping at 1.5 and 3 T within a 9 heartbeat breathhold. Journal of Cardiovascular Magnetic Resonance. 2010 Dec 19;12(1):69.

84. Chow K, Yang Y, Shaw P, Kramer CM, Salerno M. Robust free-breathing SASHA T1 mapping with high-contrast image registration. Journal of Cardiovascular Magnetic Resonance. 2016 Dec 17;18(1):47.

85. Garg P. Role of Cardiac T1 Mapping and Extracellular Volume (ECV) in the Assessment of Myocardial Infarction. The Anatolian Journal of Cardiology. 2018;

86. Moon JC, Messroghli DR, Kellman P, Piechnik SK, Robson MD, Ugander M, et al. Myocardial T1 mapping and extracellular volume quantification: a Society for Cardiovascular Magnetic Resonance (SCMR) and CMR Working Group of the European Society of Cardiology consensus statement. Journal of Cardiovascular Magnetic Resonance. 2013 Dec 14;15(1):92.

87. Yasue H, Yoshimura M, Sumida H, Kikuta K, Kugiyama K, Jougasaki M, et al. Localization and mechanism of secretion of B-type natriuretic peptide in comparison with those of A-type natriuretic peptide in normal subjects and patients with heart failure. Circulation. 1994 Jul;90(1):195–203.

88. Goetze JP, Bruneau BG, Ramos HR, Ogawa T, de Bold MK, de Bold AJ. Cardiac natriuretic peptides. Nat Rev Cardiol. 2020 Nov 22;17(11):698–717.

89. Castiglione V, Aimo A, Vergaro G, Saccaro L, Passino C, Emdin M. Biomarkers for the diagnosis and management of heart failure. Heart Fail Rev. 2022 Mar 14;27(2):625–43.

90. Palazzuoli A. Natriuretic peptides (BNP and NT-proBNP): measurement and relevance in heart failure. Vasc Health Risk Manag. 2010 May;411.

91. McKie PM, Burnett JC. NT-proBNP. J Am Coll Cardiol. 2016 Dec;68(22):2437–9.

92. Liu CY, Heckbert SR, Lai S, Ambale-Venkatesh B, Ostovaneh MR, McClelland RL, et al. Association of Elevated NT-proBNP With Myocardial Fibrosis in the Multi-Ethnic Study of Atherosclerosis (MESA). J Am Coll Cardiol. 2017 Dec;70(25):3102–9.

93. Sasaki T, Izumaru K, Hata J, Sakata S, Oishi E, Nagata T, et al. Serum NT-proBNP levels and histopathological myocardial fibrosis in autopsied cases from a Japanese community: The Hisayama Study. J Cardiol. 2021 Sep;78(3):237–43.

94. Katrukha IA. Human cardiac troponin complex. Structure and functions. Biochemistry (Moscow). 2013 Dec 12;78(13):1447–65.

95. Bertinchant JP, Larue C, Pernel I, Ledermann B, Fabbro-Peray P, Beck L, et al. Release kinetics of serum cardiac troponin i in ischemic myocardial injury. Clin Biochem. 1996 Dec;29(6):587–94.

96. Laugaudin G, Kuster N, Petiton A, Leclercq F, Gervasoni R, Macia JC, et al. Kinetics of high-sensitivity cardiac troponin T and I differ in patients with ST-segment elevation myocardial infarction treated by primary coronary intervention. Eur Heart J Acute Cardiovasc Care. 2016 Aug 5;5(4):354–63.

97. Filion KB, Agarwal SK, Ballantyne CM, Eberg M, Hoogeveen RC, Huxley RR, et al. High-sensitivity cardiac troponin T and the risk of incident atrial fibrillation: The Atherosclerosis Risk in Communities (ARIC) study. Am Heart J. 2015 Jan;169(1):31-38.e3.

98. deFilippi CR, de Lemos JA, Christenson RH, Gottdiener JS, Kop WJ, Zhan M, et al. Association of Serial Measures of Cardiac Troponin T Using a Sensitive Assay With Incident Heart Failure and Cardiovascular Mortality in Older Adults. JAMA. 2010 Dec 8;304(22):2494.

99. Johannessen TR, Atar D, Vallersnes OM, Larstorp ACK, Mdala I, Halvorsen S. Comparison of a single high-sensitivity cardiac troponin T measurement with the HEART score for rapid rule-out of acute myocardial infarction in a primary care emergency setting: a cohort study. BMJ Open. 2021 Feb 24;11(2):e046024.

100. Hijazi Z, Wallentin L, Siegbahn A, Andersson U, Alexander JH, Atar D, et al. High-Sensitivity Troponin T and Risk Stratification in Patients With Atrial Fibrillation During Treatment With Apixaban or Warfarin. J Am Coll Cardiol. 2014 Jan;63(1):52–61.

101. Askin L. Clinical Importance of High-Sensitivity Troponin T in Patients without Coronary Artery Disease. North Clin Istanb. 2019;

102. Kawasaki T, Sakai C, Harimoto K, Yamano M, Miki S, Kamitani T. Usefulness of High-Sensitivity Cardiac Troponin T and Brain Natriuretic Peptide as Biomarkers of Myocardial Fibrosis in Patients With Hypertrophic Cardiomyopathy. Am J Cardiol. 2013 Sep;112(6):867–72.

103. Seliger SL, Hong SN, Christenson RH, Kronmal R, Daniels LB, Lima JAC, et al. High-Sensitive Cardiac Troponin T as an Early Biochemical Signature for Clinical and Subclinical Heart Failure. Circulation. 2017 Apr 18;135(16):1494–505.

104. Vergaro G, Prud'homme M, Fazal L, Merval R, Passino C, Emdin M, et al. Inhibition of Galectin-3 Pathway Prevents Isoproterenol-Induced Left Ventricular Dysfunction and Fibrosis in Mice. Hypertension. 2016 Mar;67(3):606–12.

105. Meijers WC, Januzzi JL, deFilippi C, Adourian AS, Shah SJ, van Veldhuisen DJ, et al. Elevated plasma galectin-3 is associated with near-term rehospitalization in heart failure: A pooled analysis of 3 clinical trials. Am Heart J. 2014 Jun;167(6):853-860.e4.

106. Lok DJA, van der Meer P, de la Porte PWBA, Lipsic E, van Wijngaarden J, Hillege HL, et al. Prognostic value of galectin-3, a novel marker of fibrosis, in patients with chronic heart failure: data from the DEAL-HF study. Clinical Research in Cardiology. 2010 May 4;99(5):323–8.

107. van der Velde AR, Gullestad L, Ueland T, Aukrust P, Guo Y, Adourian A, et al. Prognostic Value of Changes in Galectin-3 Levels Over Time in Patients With Heart Failure. Circ Heart Fail. 2013 Mar;6(2):219–26.

108. Yancy CW, Jessup M, Bozkurt B, Butler J, Casey DE, Drazner MH, et al. 2013 ACCF/AHA Guideline for the Management of Heart Failure. J Am Coll Cardiol. 2013 Oct;62(16):e147–239.

109. Weir RAP, Petrie CJ, Murphy CA, Clements S, Steedman T, Miller AM, et al. Galectin-3 and Cardiac Function in Survivors of Acute Myocardial Infarction. Circ Heart Fail. 2013 May;6(3):492–8.

110. Srivatsan V, George M, Shanmugam E. Utility of galectin-3 as a prognostic biomarker in heart failure: where do we stand? Eur J Prev Cardiol. 2015 Sep 29;22(9):1096–110.

111. Griesenauer B, Paczesny S. The ST2/IL-33 Axis in Immune Cells during Inflammatory Diseases. Front Immunol. 2017 Apr 24;8.

112. Borthwick LA. The IL-1 cytokine family and its role in inflammation and fibrosis in the lung. Semin Immunopathol. 2016 Jul 21;38(4):517–34.

113. Weinberg EO, Shimpo M, de Keulenaer GW, MacGillivray C, Tominaga S ichi, Solomon SD, et al. Expression and Regulation of ST2, an Interleukin-1 Receptor Family Member, in Cardiomyocytes and Myocardial Infarction. Circulation. 2002 Dec 3;106(23):2961–6.

114. Ky B, French B, McCloskey K, Rame JE, McIntosh E, Shahi P, et al. High-Sensitivity ST2 for Prediction of Adverse Outcomes in Chronic Heart Failure. Circ Heart Fail. 2011 Mar;4(2):180–7.

115. Bayes-Genis A, de Antonio M, Vila J, Peñafiel J, Galán A, Barallat J, et al. Head-to-Head Comparison of 2 Myocardial Fibrosis Biomarkers for Long-Term Heart Failure Risk Stratification. J Am Coll Cardiol. 2014 Jan;63(2):158–66.

116. Wu AHB, Wians F, Jaffe A. Biological variation of galectin-3 and soluble ST2 for chronic heart failure: Implication on interpretation of test results. Am Heart J. 2013 Jun;165(6):995–9.

117. Gawor M, Śpiewak M, Kubik A, Wróbel A, Lutyńska A, Marczak M, et al. Circulating biomarkers of hypertrophy and fibrosis in patients with hypertrophic cardiomyopathy assessed by cardiac magnetic resonance. Biomarkers. 2018 Oct 3;23(7):676–82.

118. Quick S, Waessnig NK, Kandler N, Poitz DM, Schoen S, Ibrahim K, et al. Soluble ST2 and myocardial fibrosis in 3T cardiac magnetic resonance. . Scand Cardiovasc J. 2015;49(6):361–6.

119. Münch J, Avanesov M, Bannas P, Säring D, Krämer E, Mearini G, et al. Serum Matrix Metalloproteinases as Quantitative Biomarkers for Myocardial Fibrosis and Sudden Cardiac Death Risk Stratification in Patients With Hypertrophic Cardiomyopathy. J Card Fail. 2016 Oct;22(10):845–50.

120. Chirinos JA, Orlenko A, Zhao L, Basso MD, Cvijic ME, Li Z, et al. Multiple Plasma Biomarkers for Risk Stratification in Patients With Heart Failure and Preserved Ejection Fraction. J Am Coll Cardiol. 2020 Mar;75(11):1281–95.

121. Fan D, Takawale A, Lee J, Kassiri Z. Cardiac fibroblasts, fibrosis and extracellular matrix remodeling in heart disease. Fibrogenesis Tissue Repair. 2012 Dec 3;5(1):15.

122. Eghbali M. Cardiac fibroblasts: function, regulation of gene expression, and phenotypic modulation. In: Cardiac Adaptation in Heart Failure. Heidelberg: Steinkopff; 1992. p. 183–9.

123. Canty EG, Kadler KE. Procollagen trafficking, processing and fibrillogenesis. J Cell Sci. 2005 Apr 1;118(7):1341–53.

124. Leung MK, Fessler LI, Greenberg DB, Fessler JH. Separate amino and carboxyl procollagen peptidases in chick embryo tendon. Journal of Biological Chemistry. 1979 Jan;254(1):224–32.

125. Ding Y, Wang Y, Zhang W, Jia Q, Wang X, Li Y, et al. Roles of Biomarkers in Myocardial Fibrosis. Aging Dis. 2020;11(5):1157.

126. Yang C, Qiao S, Song Y, Liu Y, Tang Y, Deng L, et al. Procollagen type I carboxy-terminal propeptide (PICP) and MMP-2 are potential biomarkers of myocardial fibrosis in patients with hypertrophic cardiomyopathy. Cardiovascular Pathology. 2019 Nov;43:107150.

127. Querejeta R, López B, González A, Sánchez E, Larman M, Martínez Ubago JL, et al. Increased Collagen Type I Synthesis in Patients With Heart Failure of Hypertensive Origin. Circulation. 2004 Sep 7;110(10):1263–8.

128. Raafs AG, Verdonschot JAJ, Henkens MTHM, Adriaans BP, Wang P, Derks K, et al. The combination of carboxy-terminal propeptide of procollagen type I blood levels and late gadolinium enhancement at cardiac magnetic resonance provides additional prognostic information in idiopathic dilated cardiomyopathy – A multilevel assessment of myocardial fibrosis in dilated cardiomyopathy. Eur J Heart Fail. 2021 Jun 24;23(6):933–44.

129. Ferreira JP, Verdonschot J, Wang P, Pizard A, Collier T, Ahmed FZ, et al. Proteomic and Mechanistic Analysis of Spironolactone in Patients at Risk for HF. JACC Heart Fail. 2021 Apr;9(4):268–77.

130. Cleland JGF, Ferreira JP, Mariottoni B, Pellicori P, Cuthbert J, Verdonschot JAJ, et al. The effect of spironolactone on cardiovascular function and markers of fibrosis in people at increased risk of developing heart failure: the heart 'OMics' in AGEing (HOMAGE) randomized clinical trial. Eur Heart J. 2021 Feb 11;42(6):684–96.

131. Lee RC, Feinbaum RL, Ambros V. The C. elegans heterochronic gene lin-4 encodes small RNAs with antisense complementarity to lin-14. Cell. 1993 Dec;75(5):843–54.

132. Ladomery MR, Maddocks DG, Wilson ID. MicroRNAs: their discovery, biogenesis, function and potential use as biomarkers in non-invasive prenatal diagnostics. Int J Mol Epidemiol Genet. 2011 Aug 30;2(3):253–60.

133. Szemraj-Rogucka ZM, Szemraj J, Masiarek K, Majos A. Circulating microRNAs as biomarkers for myocardial fibrosis in patients with left ventricular non-compaction cardiomyopathy. Archives of Medical Science. 2019;15(2):376–84.

134. Peterlin A, Počivavšek K, Petrovič D, Peterlin B. The Role of microRNAs in Heart Failure: A Systematic Review. Front Cardiovasc Med. 2020 Oct 15;7.

135. Fang L, Ellims AH, Moore X lei, White DA, Taylor AJ, Chin-Dusting J, et al. Circulating microRNAs as biomarkers for diffuse myocardial fibrosis in patients with hypertrophic cardiomyopathy. J Transl Med. 2015 Dec 24;13(1):314.

136. Cao W, Shi P, Ge JJ. miR-21 enhances cardiac fibrotic remodeling and fibroblast proliferation via CADM1/STAT3 pathway. BMC Cardiovasc Disord. 2017 Dec 23;17(1):88.

137. Yuan J, Chen H, Ge D, Xu Y, Xu H, Yang Y, et al. Mir-21 Promotes Cardiac Fibrosis After Myocardial Infarction Via Targeting Smad7. Cellular Physiology and Biochemistry. 2017;42(6):2207–19.

138. Cavarretta E, Condorelli G. miR-21 and cardiac fibrosis: another brick in the wall?: Figure 1. Eur Heart J. 2015 Aug 21;36(32):2139–41.

139. Villar A v., García R, Merino D, Llano M, Cobo M, Montalvo C, et al. Myocardial and circulating levels of microRNA-21 reflect left ventricular fibrosis in aortic stenosis patients. Int J Cardiol. 2013 Sep;167(6):2875–81.

140. Akhurst RJ, Hata A. Targeting the TGFβ signalling pathway in disease. Nat Rev Drug Discov [Internet]. 2012 Oct 24;11(10):790–811. Available from: http://www.nature.com/articles/nrd3810

141. Travers JG, Kamal FA, Robbins J, Yutzey KE, Blaxall BC. Cardiac Fibrosis. Circ Res [Internet]. 2016 Mar 18;118(6):1021–40. Available from: https://www.ahajournals.org/doi/10.1161/CIRCRESAHA.115.306565

142. Dobaczewski M, Bujak M, Li N, Gonzalez-Quesada C, Mendoza LH, Wang XF, et al. Smad3 Signaling Critically Regulates Fibroblast Phenotype and Function in Healing Myocardial Infarction. Circ Res. 2010 Aug 6;107(3):418–28.

143. See F, Thomas W, Way K, Tzanidis A, Kompa A, Lewis D, et al. p38 mitogen-activated protein kinase inhibition improves cardiac function and attenuates left ventricular remodeling following myocardial infarction in the rat. J Am Coll Cardiol. 2004 Oct;44(8):1679–89.

144. Ono K, Ohtomo T, Ninomiya-Tsuji J, Tsuchiya M. A dominant negative TAK1 inhibits cellular fibrotic responses induced by TGF-β. Biochem Biophys Res Commun. 2003 Jul;307(2):332–7.

145. Picard F, Brehm M, Fassbach M, Pelzer B, Scheuring S, Küry P, et al. Increased cardiac mRNA expression of matrix metalloproteinase-1 (MMP–1) and its inhibitor (TIMP–1) in DCM patients. Clinical Research in Cardiology. 2006 May 3;95(5):261–9.

146. Lindsay MM, Maxwell P, Dunn FG. TIMP-1: a marker of left ventricular diastolic dysfunction and fibrosis in hypertension. Hypertension. 2002 Aug;40(2):136–41.

147. Parichatikanond W, Luangmonkong T, Mangmool S, Kurose H. Therapeutic targets for the treatment of cardiac fibrosis and cancer: Focusing on tgf-β Signaling. Vol. 7, Frontiers in Cardiovascular Medicine. Frontiers Media S.A.; 2020.

148. Frantz S, Hu K, Adamek A, Wolf J, Sallam A, KG Maier S, et al. Transforming growth factor beta inhibition increases mortality and left ventricular dilatation after myocardial infarction. Basic Res Cardiol. 2008 Sep 23;103(5):485–92.

149. Kuwahara F, Kai H, Tokuda K, Kai M, Takeshita A, Egashira K, et al. Transforming Growth Factor-β Function Blocking Prevents Myocardial Fibrosis and Diastolic Dysfunction in Pressure-Overloaded Rats. Circulation. 2002 Jul 2;106(1):130–5.

150. Tan SM, Zhang Y, Connelly KA, Gilbert RE, Kelly DJ. Targeted inhibition of activin receptor-like kinase 5 signaling attenuates cardiac dysfunction following myocardial infarction. American Journal of Physiology-Heart and Circulatory Physiology. 2010 May;298(5):H1415–25.

151. Frazier K, Thomas R, Scicchitano M, Mirabile R, Boyce R, Zimmerman D, et al. Inhibition of ALK5 Signaling Induces Physeal Dysplasia in Rats. Toxicol Pathol. 2007 Feb 25;35(2):284–95.

152. Lacouture ME, Morris JC, Lawrence DP, Tan AR, Olencki TE, Shapiro GI, et al. Cutaneous keratoacanthomas/squamous cell carcinomas associated with neutralization of transforming growth factor β by the monoclonal antibody fresolimumab (GC1008). Cancer Immunology, Immunotherapy. 2015 Apr 13;64(4):437–46.

153. Nguyen DT, Ding C, Wilson E, Marcus GM, Olgin JE. Pirfenidone mitigates left ventricular fibrosis and dysfunction after myocardial infarction and reduces arrhythmias. Heart Rhythm. 2010 Oct;7(10):1438–45.

154. Miric G, Dallemagne C, Endre Z, Margolin S, Taylor SM, Brown L. Reversal of cardiac and renal fibrosis by pirfenidone and spironolactone in streptozotocin-diabetic rats. Br J Pharmacol. 2001 Jul;133(5):687–94.

155. Mirkovic S, Seymour AML, Fenning A, Strachan A, Margolin SB, Taylor SM, et al. Attenuation of cardiac fibrosis by pirfenidone and amiloride in DOCA-salt hypertensive rats. Br J Pharmacol. 2002 Feb;135(4):961–8.

156. Wang Y, Wu Y, Chen J, Zhao S, Li H. Pirfenidone Attenuates Cardiac Fibrosis in a Mouse Model of TAC-Induced Left Ventricular Remodeling by Suppressing NLRP3 Inflammasome Formation. Cardiology. 2013;126(1):1–11.

157. Lewis GA, Schelbert EB, Naish JH, Bedson E, Dodd S, Eccleson H, et al. Pirfenidone in Heart Failure with Preserved Ejection Fraction—Rationale and Design of the PIROUETTE Trial. Cardiovasc Drugs Ther. 2019 Aug 8;33(4):461–70.

158. Lewis GA, Dodd S, Clayton D, Bedson E, Eccleson H, Schelbert EB, et al. Pirfenidone in heart failure with preserved ejection fraction: a randomized phase 2 trial. Nat Med. 2021 Aug 12;27(8):1477–82.

159. Kelly DJ, Zhang Y, Connelly K, Cox AJ, Martin J, Krum H, et al. Tranilast attenuates diastolic dysfunction and structural injury in experimental diabetic cardiomyopathy. American Journal of Physiology-Heart and Circulatory Physiology. 2007 Nov;293(5):H2860–9.

160. MARTIN J, KELLY D, MIFSUD S, ZHANG Y, COX A, SEE F, et al. Tranilast attenuates cardiac matrix deposition in experimental diabetes: role of transforming growth factor-β. Cardiovasc Res. 2005 Feb 15;65(3):694–701.

161. Kagitani S, Ueno H, Hirade S, Takahashi T, Takata M, Inoue H. Tranilast attenuates myocardial fibrosis in association with suppression of monocyte/macrophage infiltration in DOCA/salt hypertensive rats. J Hypertens. 2004 May;22(5):1007–15.

162. Holmes DR, Savage M, LaBlanche JM, Grip L, Serruys PW, Fitzgerald P, et al. Results of Prevention of REStenosis with Tranilast and its Outcomes (PRESTO) Trial. Circulation. 2002 Sep 3;106(10):1243–50.

163. Hall JE. Historical Perspective of the Renin-Angiotensin System. Mol Biotechnol. 2003;24(1):27–39.

164. Bader M, Peters J, Baltatu O, Müller DN, Luft FC, Ganten D. Tissue renin-angiotensin systems: new insights from experimental animal models in hypertension research. J Mol Med. 2001 Apr 9;79(2–3):76–102.

165. Murphy AM, Wong AL, Bezuhly M. Modulation of angiotensin II signaling in the prevention of fibrosis. Fibrogenesis Tissue Repair. 2015 Dec 23;8(1):7.

166. Gao X, He X, Luo B, Peng L, Lin J, Zuo Z. Angiotensin II increases collagen I expression via transforming growth factor-beta1 and extracellular signal-regulated kinase in cardiac fibroblasts. Eur J Pharmacol. 2009 Mar;606(1–3):115–20.

167. Schultz JEJ, Witt SA, Glascock BJ, Nieman ML, Reiser PJ, Nix SL, et al. TGF-β1 mediates the hypertrophic cardiomyocyte growth induced by angiotensin II. Journal of Clinical Investigation. 2002 Mar 15;109(6):787–96.

168. Baudino TA, Carver W, Giles W, Borg TK. Cardiac fibroblasts: friend or foe? American Journal of Physiology-Heart and Circulatory Physiology [Internet]. 2006 Sep;291(3):H1015–26. Available from: https://www.physiology.org/doi/10.1152/ajpheart.00023.2006

169. Iwata M, Cowling RT, Gurantz D, Moore C, Zhang S, Yuan JXJ, et al. Angiotensin-(1–7) binds to specific receptors on cardiac fibroblasts to initiate antifibrotic and antitrophic effects. American Journal of Physiology-Heart and Circulatory Physiology. 2005 Dec;289(6):H2356–63.

170. Crawford MH. Combination Therapy as First-Line Treatment for Hypertension. American Journal of Cardiovascular Drugs. 2009 Jan 17;9(1):1–6.

171. Nehme A, Zibara K. Efficiency and specificity of RAAS inhibitors in cardiovascular diseases: how to achieve better end-organ protection? Hypertension Research. 2017 Nov 6;40(11):903–9.

172. Shimada YJ, Passeri JJ, Baggish AL, O'Callaghan C, Lowry PA, Yannekis G, et al. Effects of Losartan on Left Ventricular Hypertrophy and Fibrosis in Patients With Nonobstructive Hypertrophic Cardiomyopathy. JACC Heart Fail. 2013 Dec;1(6):480–7.

173. Oliveira-Junior SA, Martinez PF, Guizoni DM, Campos DHS, Fernandes T, Oliveira EM, et al. AT1 Receptor Blockade Attenuates Insulin Resistance and Myocardial Remodeling in Rats with Diet-Induced Obesity. PLoS One. 2014 Jan 23;9(1):e86447.

174. Brilla CG, Funck RC, Rupp H. Lisinopril-Mediated Regression of Myocardial Fibrosis in Patients With Hypertensive Heart Disease. Circulation. 2000 Sep 19;102(12):1388–93.

175. Chevalier B, Heudes D, Heymes C, Basset A, Dakhli T, Bansard Y, et al. Trandolapril Decreases Prevalence of Ventricular Ectopic Activity in Middle-Aged SHR. Circulation. 1995 Oct;92(7):1947–53.

176. Brilla CG, Janicki JS, Weber KT. Cardioreparative effects of lisinopril in rats with genetic hypertension and left ventricular hypertrophy. Circulation. 1991 May;83(5):1771–9.

177. Piacentini L, Gray M, Honbo NY, Chentoufi J, Bergman M, Karliner JS. Endothelin-1 Stimulates Cardiac Fibroblast Proliferation Through Activation of Protein Kinase C. J Mol Cell Cardiol. 2000 Apr;32(4):565–76.

178. Shi-wen X, Denton CP, Holmes AM, Black CM, Abraham DJ, Dashwood MR, et al. Fibroblast Matrix Gene Expression and Connective Tissue Remodeling: Role of Endothelin-1. Journal of Investigative Dermatology. 2001 Mar;116(3):417–25.

179. Shi-wen X, Kennedy L, Renzoni EA, Bou-Gharios G, du Bois RM, Black CM, et al. Endothelin is a downstream mediator of profibrotic responses to transforming growth factor β in human lung fibroblasts. Arthritis Rheum. 2007 Dec;56(12):4189–94.

180. Leask A. Potential Therapeutic Targets for Cardiac Fibrosis. Circ Res. 2010 Jun 11;106(11):1675–80.

181. Alvarez D, Briassouli P, Clancy RM, Zavadil J, Reed JH, Abellar RG, et al. A Novel Role of Endothelin-1 in Linking Toll-like Receptor 7-mediated Inflammation to Fibrosis in Congenital Heart Block. Journal of Biological Chemistry. 2011 Sep;286(35):30444–54.

182. Zhao Y, Du D, Chen S, Chen Z, Zhao J. New Insights into the Functions of MicroRNAs in Cardiac Fibrosis: From Mechanisms to Therapeutic Strategies. Genes (Basel). 2022 Aug 4;13(8):1390.

183. Pan Z wei, Lu Y jie, Yang B feng. MicroRNAs: a novel class of potential therapeutic targets for cardiovascular diseases. Acta Pharmacol Sin. 2010 Jan 7;31(1):1–9.

184. Thum T, Gross C, Fiedler J, Fischer T, Kissler S, Bussen M, et al. MicroRNA-21 contributes to myocardial disease by stimulating MAP kinase signalling in fibroblasts. Nature. 2008 Dec 30;456(7224):980–4.

185. van Rooij E, Sutherland LB, Thatcher JE, DiMaio JM, Naseem RH, Marshall WS, et al. Dysregulation of microRNAs after myocardial infarction reveals a role of miR-29 in cardiac fibrosis. Proceedings of the National Academy of Sciences. 2008 Sep 2;105(35):13027–32.

186. Liang H, Zhang C, Ban T, Liu Y, Mei L, Piao X, et al. A novel reciprocal loop between microRNA-21 and TGFβRIII is involved in cardiac fibrosis. Int J Biochem Cell Biol. 2012 Dec;44(12):2152–60.

187. Hinkel R, Ramanujam D, Kaczmarek V, Howe A, Klett K, Beck C, et al. AntimiR-21 Prevents Myocardial Dysfunction in a Pig Model of Ischemia/Reperfusion Injury. J Am Coll Cardiol. 2020 Apr;75(15):1788–800.

188. Zhang Y, Huang XR, Wei LH, Chung AC, Yu CM, Lan HY. miR-29b as a Therapeutic Agent for Angiotensin II-induced Cardiac Fibrosis by Targeting TGF-β/Smad3 signaling. Molecular Therapy. 2014 May;22(5):974–85.

189. Valkov N, King ME, Moeller J, Liu H, Li X, Zhang P. MicroRNA-1-Mediated Inhibition of Cardiac Fibroblast Proliferation Through Targeting Cyclin D2 and CDK6. Front Cardiovasc Med. 2019 May 17;6.

190. Shan H, Zhang Y, Lu Y, Zhang Y, Pan Z, Cai B, et al. Downregulation of miR-133 and miR-590 contributes to nicotine-induced atrial remodelling in canines. Cardiovasc Res. 2009 Aug 1;83(3):465–72.

191. Carè A, Catalucci D, Felicetti F, Bonci D, Addario A, Gallo P, et al. MicroRNA-133 controls cardiac hypertrophy. Nat Med. 2007 May 29;13(5):613–8.

192. Duisters RF, Tijsen AJ, Schroen B, Leenders JJ, Lentink V, van der Made I, et al. miR-133 and miR-30 Regulate Connective Tissue Growth Factor. Circ Res. 2009 Jan 30;104(2):170–8.

193. Matkovich SJ, Wang W, Tu Y, Eschenbacher WH, Dorn LE, Condorelli G, et al. MicroRNA-133a Protects Against Myocardial Fibrosis and Modulates Electrical Repolarization Without Affecting Hypertrophy in Pressure-Overloaded Adult Hearts. Circ Res. 2010 Jan 8;106(1):166–75.

194. Kang J, Park H, Kim H, Mun D, Park H, Yun N, et al. Human peripheral blood-derived exosomes for microRNA delivery. Int J Mol Med. 2019 Mar 28;

195. Li RQ, Wu Y, Zhi Y, Yang X, Li Y, Xu FJ, et al. PGMA-Based Star-Like Polycations with Plentiful Hydroxyl Groups Act as Highly Efficient miRNA Delivery Nanovectors for Effective Applications in Heart Diseases. Advanced Materials. 2016 Nov;28(43):9452–9452.

196. Gyöngyösi M, Winkler J, Ramos I, Do Q, Firat H, McDonald K, et al. Myocardial fibrosis: biomedical research from bench to bedside. Eur J Heart Fail. 2017 Feb 3;19(2):177–91.

197. Liu F, Mih JD, Shea BS, Kho AT, Sharif AS, Tager AM, et al. Feedback amplification of fibrosis through matrix stiffening and COX-2 suppression. Journal of Cell Biology. 2010 Aug 23;190(4):693–706.

198. Smithmyer ME, Cassel SE, Kloxin AM. Bridging 2D and 3D culture: Probing impact of extracellular environment on fibroblast activation in layered hydrogels. AIChE Journal. 2019 Dec 4;65(12).

199. Campbell M, Chabria M, Figtree GA, Polonchuk L, Gentile C. Stem Cell-Derived Cardiac Spheroids as 3D In Vitro Models of the Human Heart Microenvironment. In 2018. p. 51–9.

200. Polonchuk L, Chabria M, Badi L, Hoflack JC, Figtree G, Davies MJ, et al. Cardiac spheroids as promising in vitro models to study the human heart microenvironment. Sci Rep. 2017 Dec 1;7(1):7005.

201. Lee MO, Jung KB, Jo SJ, Hyun SA, Moon KS, Seo JW, et al. Modelling cardiac fibrosis using three-dimensional cardiac microtissues derived from human embryonic stem cells. J Biol Eng. 2019 Dec 13;13(1):15.

202. Mastikhina O, Moon BU, Williams K, Hatkar R, Gustafson D, Mourad O, et al. Human cardiac fibrosis-on-a-chip model recapitulates disease hallmarks and can serve as a platform for drug testing. Biomaterials. 2020 Mar;233:119741.

203. Rai V, Sharma P, Agrawal S, Agrawal DK. Relevance of mouse models of cardiac fibrosis and hypertrophy in cardiac research. Mol Cell Biochem. 2017 Jan 20;424(1–2):123–45.

204. Westermann D, Becher PM, Lindner D, Savvatis K, Xia Y, Fröhlich M, et al. Selective PDE5A inhibition with sildenafil rescues left ventricular dysfunction, inflammatory immune response and cardiac remodeling in angiotensin II-induced heart failure in vivo. Basic Res Cardiol. 2012 Nov 2;107(6):308.

205. Redfield MM, Chen HH, Borlaug BA, Semigran MJ, Lee KL, Lewis G, et al. Effect of Phosphodiesterase-5 Inhibition on Exercise Capacity and Clinical Status in Heart Failure With Preserved Ejection Fraction. JAMA. 2013 Mar 27;309(12):1268.

206. Martin TP, Hortigon-Vinagre MP, Findlay JE, Elliott C, Currie S, Baillie GS. Targeted disruption of the heat shock protein 20-phosphodiesterase 4D (PDE4D) interaction protects against pathological cardiac remodelling in a mouse model of hypertrophy. FEBS Open Bio. 2014 Jan 1;4(1):923–7.

207. deAlmeida AC, van Oort RJ, Wehrens XHT. Transverse Aortic Constriction in Mice. Journal of Visualized Experiments. 2010 Apr 21;(38).

208. Im W. Differential expression of dystrophin isoforms in strains of mdx mice with different mutations. Hum Mol Genet. 1996 Aug 1;5(8):1149–53.

209. Shirokova N, Niggli E. Cardiac phenotype of Duchenne Muscular Dystrophy: Insights from cellular studies. J Mol Cell Cardiol. 2013 May;58:217–24.

210. Quinlan JG, Hahn HS, Wong BL, Lorenz JN, Wenisch AS, Levin LS. Evolution of the mdx mouse cardiomyopathy: physiological and morphological findings. Neuromuscular Disorders. 2004 Sep;14(8–9):491–6.

211. Danialou G, Comtois AS, Dudley R, Karpati G, Vincent G, des Rosiers C, et al. Dystrophin-deficient cardiomyocytes are abnormally vulnerable to mechanical stress-induced contractile failure and injury. The FASEB Journal. 2001 Jul 29;15(9):1655–7.

212. Zhang W, ten Hove M, Schneider JE, Stuckey DJ, Sebag-Montefiore L, Bia BL, et al. Abnormal cardiac morphology, function and energy metabolism in the dystrophic mdx mouse: An MRI and MRS study. J Mol Cell Cardiol. 2008 Dec;45(6):754–60.

213. Bia BL, Cassidy PJ, Young ME, Rafael JA, Leighton B, Davies KE, et al. Decreased Myocardial nNOS, Increased iNOS and Abnormal ECGs in Mouse Models of Duchenne Muscular Dystrophy. J Mol Cell Cardiol. 1999 Oct;31(10):1857–62.

214. Chu V, Otero JM, Lopez O, Sullivan MF, Morgan JP, Amende I, et al. Electrocardiographic findings inmdx mice: A cardiac phenotype of Duchenne muscular dystrophy. Muscle Nerve. 2002 Oct;26(4):513–9.

215. Dixon JA, Spinale FG. Large Animal Models of Heart Failure. Circ Heart Fail. 2009 May;2(3):262–71.

216. Houser SR, Margulies KB, Murphy AM, Spinale FG, Francis GS, Prabhu SD, et al. Animal Models of Heart Failure. Circ Res. 2012 Jun 22;111(1):131–50.

217. Pleger ST, Brinks H, Ritterhoff J, Raake P, Koch WJ, Katus HA, et al. Heart Failure Gene Therapy. Circ Res. 2013 Aug 30;113(6):792–809.

218. Parrish AR, Gandolfi AJ, Brendel K. Precision-cut tissue slices: Applications in pharmacology and toxicology. Life Sci. 1995 Oct;57(21):1887–901.

219. Parrish AR, Shipp NG, Spall RD, Dorr RT, Krumdieck CL, Gandolfi AJ, et al. Organ Culture of Rat Myocardial Slices: An Alternative in Vitro Tool in Organ-Specific Toxicology. Toxicology Methods. 1992 Jan 27;2(2):101–11.

220. Krumdieck CL, dos Santos J, Ho KJ. A new instrument for the rapid preparation of tissue slices. Anal Biochem. 1980 May;104(1):118–23.

221. Olinga P, Meijer DKF, Slooff MJH, Groothuis GMM. Liver slices in in vitro pharmacotoxicology with special reference to the use of human liver tissue. Toxicology in Vitro. 1997 Jan;12(1):77–100.

222. Zimmermann M, Lampe J, Lange S, Smirnow I, Königsrainer A, Hann-von-Weyhern C, et al. Improved reproducibility in preparing precision-cut liver tissue slices. Cytotechnology. 2009 Dec 20;61(3):145–52.

223. Paish HL, Reed LH, Brown H, Bryan MC, Govaere O, Leslie J, et al. A Bioreactor Technology for Modeling Fibrosis in Human and Rodent Precision-Cut Liver Slices. Hepatology [Internet]. 2019 Oct 28;70(4):1377–91. Available from: https://onlinelibrary.wiley.com/doi/10.1002/hep.30651

224. Klassen LW, Thiele GM, Duryee MJ, Schaffert CS, DeVeney AL, Hunter CD, et al. An in vitro method of alcoholic liver injury using precision-cut liver slices from rats. Biochem Pharmacol. 2008 Aug;76(3):426–36.

225. Clouzeau-Girard H, Guyot C, Combe C, Moronvalle-Halley V, Housset C, Lamireau T, et al. Effects of bile acids on biliary epithelial cell proliferation and portal fibroblast activation using rat liver slices. Laboratory Investigation. 2006 Mar 9;86(3):275–85.

226. Pillekamp F, Reppel M, Dinkelacker V, Duan Y, Jazmati N, Bloch W, et al. Establishment and Characterization of a Mouse Embryonic Heart Slice Preparation. Cellular Physiology and Biochemistry. 2005;16(1–3):127–32.

227. Halbach M, Pillekamp F, Brockmeier K, Hescheler J, Müller-Ehmsen J, Reppel M. Ventricular Slices of Adult Mouse Hearts - a new Multicellular In Vitro Model for Electrophysiological Studies. Cellular Physiology and Biochemistry. 2006;18(1–3):1–8.

228. Bussek A, Wettwer E, Christ T, Lohmann H, Camelliti P, Ravens U. Tissue Slices from Adult Mammalian Hearts as a Model for Pharmacological Drug Testing. Cellular Physiology and Biochemistry. 2009;24(5–6):527–36.

229. Brandenburger M, Wenzel J, Bogdan R, Richardt D, Nguemo F, Reppel M, et al. Organotypic slice culture from human adult ventricular myocardium. Cardiovasc Res. 2012 Jan 1;93(1):50–9.

230. Watson SA, Duff J, Bardi I, Zabielska M, Atanur SS, Jabbour RJ, et al. Biomimetic electromechanical stimulation to maintain adult myocardial slices in vitro. Nat Commun. 2019 Dec 15;10(1):2168.

231. Perbellini F, Thum T. Living myocardial slices: a novel multicellular model for cardiac translational research. Eur Heart J. 2020 Jul 1;41(25):2405–8.

232. Fischer C, Milting H, Fein E, Reiser E, Lu K, Seidel T, et al. Long-term functional and structural preservation of precision-cut human myocardium under continuous electromechanical stimulation in vitro. Nat Commun. 2019 Dec 10;10(1):117.

233. Perbellini F, Watson SA, Scigliano M, Alayoubi S, Tkach S, Bardi I, et al. Investigation of cardiac fibroblasts using myocardial slices. Cardiovasc Res. 2018 Jan 1;114(1):77–89.

234. Agocha A, Sigel A v., Eghbali-Webb M. Characterization of adult human heart fibroblasts in culture: a comparative study of growth, proliferation and collagen production in human and rabbit cardiac fibroblasts and their response to transforming growth factor-beta 1. Cell Tissue Res. 1997 Mar 11;288(1):87–93.

235. Marinković A, Liu F, Tschumperlin DJ. Matrices of Physiologic Stiffness Potently Inactivate Idiopathic Pulmonary Fibrosis Fibroblasts. Am J Respir Cell Mol Biol. 2013 Apr;48(4):422–30.

236. Antoni D, Burckel H, Josset E, Noel G. Three-Dimensional Cell Culture: A Breakthrough in Vivo. Int J Mol Sci. 2015 Mar 11;16(12):5517–27.

237. de Graaf IAM, Olinga P, de Jager MH, Merema MT, de Kanter R, van de Kerkhof EG, et al. Preparation and incubation of precision-cut liver and intestinal slices for application in drug metabolism and toxicity studies. Nat Protoc. 2010 Sep 19;5(9):1540–51.

238. Umachandran M, Howarth J, Ioannides C. Metabolic and structural viability of precision-cut rat lung slices in culture. Xenobiotica. 2004 Aug 22;34(8):771–80.

239. Poosti F, Pham BT, Oosterhuis D, Poelstra K, van Goor H, Olinga P, et al. Precision-cut kidney slices (PCKS) to study development of renal fibrosis and efficacy of drug targeting *ex vivo*. Dis Model Mech. 2015 Jan 1;

240. Watson SA, Scigliano M, Bardi I, Ascione R, Terracciano CM, Perbellini F. Preparation of viable adult ventricular myocardial slices from large and small mammals. Nat Protoc. 2017 Dec 30;12(12):2623–39.

241. Perbellini F, Watson SA, Scigliano M, Alayoubi S, Tkach S, Bardi I, et al. Investigation of cardiac fibroblasts using myocardial slices. Cardiovasc Res. 2018 Jan 1;114(1):77–89.

242. Mullard A. Parsing clinical success rates. Nat Rev Drug Discov. 2016 Jul 30;15(7):447–447.

243. Burnashev NA, Edwards FA, Verkhratsky AN. Patch-clamp recordings on rat cardiac muscle slices. Pfl�gers Archiv European Journal of Physiology. 1990 Sep;417(1):123–5.

244. Camelliti P, Al-Saud SA, Smolenski RT, Al-Ayoubi S, Bussek A, Wettwer E, et al. Adult human heart slices are a multicellular system suitable for electrophysiological and pharmacological studies. J Mol Cell Cardiol. 2011 Sep;51(3):390–8.

245. Leslie J, Macia MG, Luli S, Worrell JC, Reilly WJ, Paish HL, et al. c-Rel orchestrates energy-dependent epithelial and macrophage reprogramming in fibrosis. Nat Metab. 2020 Nov 9;2(11):1350–67.

246. Maalouf R, Bailey S. A review on B-type natriuretic peptide monitoring: assays and biosensors. Heart Fail Rev. 2016 Sep 15;21(5):567–78.

247. Yücel G, Zhao Z, El-Battrawy I, Lan H, Lang S, Li X, et al. Lipopolysaccharides induced inflammatory responses and electrophysiological dysfunctions in human-induced pluripotent stem cell derived cardiomyocytes. Sci Rep. 2017 Dec 7;7(1):2935.

248. Bao M, Hofsink N, Plösch T. LPS versus Poly I:C model: comparison of long-term effects of bacterial and viral maternal immune activation on the offspring. American Journal of Physiology-Regulatory, Integrative and Comparative Physiology. 2022 Feb 1;322(2):R99–111.

249. Maelfait J, Vercammen E, Janssens S, Schotte P, Haegman M, Magez S, et al. Stimulation of Toll-like receptor 3 and 4 induces interleukin-1β maturation by caspase-8. Journal of Experimental Medicine. 2008 Sep 1;205(9):1967–73.

250. Yamagami K, Oka T, Wang Q, Ishizu T, Lee JK, Miwa K, et al. Pirfenidone exhibits cardioprotective effects by regulating myocardial fibrosis and vascular permeability in pressure-overloaded hearts. American Journal of Physiology-Heart and Circulatory Physiology. 2015 Aug 1;309(3):H512–22.

251. Wollin L, Wex E, Pautsch A, Schnapp G, Hostettler KE, Stowasser S, et al. Mode of action of nintedanib in the treatment of idiopathic pulmonary fibrosis. European Respiratory Journal. 2015 May;45(5):1434–45.

252. Baxter A, Brough S, Cooper A, Floettmann E, Foster S, Harding C, et al. Hit-to-lead studies: the discovery of potent, orally active, thiophenecarboxamide IKK-2 inhibitors. Bioorg Med Chem Lett. 2004 Jun;14(11):2817–22.

253. Bonafoux D, Bonar S, Christine L, Clare M, Donnelly A, Guzova J, et al. Inhibition of IKK-2 by 2-[(aminocarbonyl)amino]-5-acetylenyl-3-thiophenecarboxamides. Bioorg Med Chem Lett. 2005 Jun;15(11):2870–5.

254. Schafer S, Viswanathan S, Widjaja AA, Lim WW, Moreno-Moral A, DeLaughter DM, et al. IL-11 is a crucial determinant of cardiovascular fibrosis. Nature. 2017 Dec 13;552(7683):110–5.

255. Gwathmey JK, Tsaioun K, Hajjar RJ. Cardionomics: a new integrative approach for screening cardiotoxicity of drug candidates. Expert Opin Drug Metab Toxicol. 2009 Jun 15;5(6):647–60.

256. Brandenburger M, Wenzel J, Bogdan R, Richardt D, Nguemo F, Reppel M, et al. Organotypic slice culture from human adult ventricular myocardium. Cardiovasc Res. 2012 Jan 1;93(1):50–9.

257. Kang C, Qiao Y, Li G, Baechle K, Camelliti P, Rentschler S, et al. Human Organotypic Cultured Cardiac Slices: New Platform For High Throughput Preclinical Human Trials. Sci Rep. 2016 Sep 30;6(1):28798.

258. Koch A, Saran S, Tran DDH, Klebba-Färber S, Thiesler H, Sewald K, et al. Murine precision-cut liver slices (PCLS): a new tool for studying tumor microenvironments and cell signaling ex vivo. Cell Communication and Signaling. 2014 Dec 7;12(1):73.

259. Hanna A, Frangogiannis NG. Inflammatory Cytokines and Chemokines as Therapeutic Targets in Heart Failure. Cardiovasc Drugs Ther. 2020 Dec 9;34(6):849–63.

260. Dewald O, Frangogiannis NG, Zoerlein M, Duerr GD, Klemm C, Knuefermann P, et al. Development of murine ischemic cardiomyopathy is associated with a transient inflammatory reaction and depends on reactive oxygen species. Proceedings of the National Academy of Sciences. 2003 Mar 4;100(5):2700–5.

261. Dewald O, Zymek P, Winkelmann K, Koerting A, Ren G, Abou-Khamis T, et al. CCL2/Monocyte Chemoattractant Protein-1 Regulates Inflammatory Responses Critical to Healing Myocardial Infarcts. Circ Res. 2005 Apr 29;96(8):881–9.

262. Stumpf C, Lehner C, Raaz D, Yilmaz A, Anger T, Daniel WG, et al. Platelets contribute to enhanced MCP-1 levels in patients with chronic heart failure. Heart. 2008 Jan 1;94(1):65–9.

263. Damås J. Myocardial expression of CC- and CXC-chemokines and their receptors in human end-stage heart failure. Cardiovasc Res. 2000 Sep;47(4):778–87.

264. Damås J. Myocardial expression of CC- and CXC-chemokines and their receptors in human end-stage heart failure. Cardiovasc Res. 2000 Sep;47(4):778–87.

265. Damås J. CXC-chemokines, a new group of cytokines in congestive heart failure — possible role of platelets and monocytes. Cardiovasc Res. 2000 Jan 14;45(2):428–36.

266. Cappuzzello C, di Vito L, Melchionna R, Melillo G, Silvestri L, Cesareo E, et al. Increase of plasma IL-9 and decrease of plasma IL-5, IL-7, and IFN-γ in patients with chronic heart failure. J Transl Med. 2011 Dec 21;9(1):28.

267. Nymo SH, Hulthe J, Ueland T, McMurray J, Wikstrand J, Askevold ET, et al. Inflammatory cytokines in chronic heart failure: interleukin-8 is associated with adverse outcome. Results from CORONA. Eur J Heart Fail. 2014 Jan;16(1):68–75.

268. Gullestad L, Ueland T, Brunsvig A, Kjekshus J, Simonsen S, Frøland SS, et al. Effect of metoprolol on cytokine levels in chronic heart failure—A substudy in the Metoprolol Controlled-Release Randomised Intervention Trial in Heart Failure (MERIT-HF). Am Heart J. 2001 Mar;141(3):418–21.

269. Kuo FY, Lee SP, Cheng JT, Wu MC. The direct effect of lipopolysaccharide on an isolated heart is different from the effect on cardiac myocytes in vitro. Archives of Medical Science. 2019 Aug 2;

270. Chen CJ, Kono H, Golenbock D, Reed G, Akira S, Rock KL. Identification of a key pathway required for the sterile inflammatory response triggered by dying cells. Nat Med. 2007 Jul 17;13(7):851–6.

271. Suwara MI, Green NJ, Borthwick LA, Mann J, Mayer-Barber KD, Barron L, et al. IL-1α released from damaged epithelial cells is sufficient and essential to trigger inflammatory responses in human lung fibroblasts. Mucosal Immunol. 2014 May 30;7(3):684–93.

272. Petrov V v, Fagard RH, Lijnen PJ. Transforming growth factor-β1 induces angiotensin-converting enzyme synthesis in rat cardiac fibroblasts during their differentiation to myofibroblasts. Journal of the Renin-Angiotensin-Aldosterone System. 2000 Dec 22;1(4):342–52.

273. Yamagami K, Oka T, Wang Q, Ishizu T, Lee JK, Miwa K, et al. Pirfenidone exhibits cardioprotective effects by regulating myocardial fibrosis and vascular permeability in pressure-overloaded hearts. American Journal of Physiology-Heart and Circulatory Physiology. 2015 Aug 1;309(3):H512–22.

274. Yamazaki T, Yamashita N, Izumi Y, Nakamura Y, Shiota M, Hanatani A, et al. The antifibrotic agent pirfenidone inhibits angiotensin II-induced cardiac hypertrophy in mice. Hypertension Research. 2012 Jan 25;35(1):34–40.

275. Seifirad S. Pirfenidone: A novel hypothetical treatment for COVID-19. Med Hypotheses. 2020 Nov;144:110005.

276. Zhang F, Wei Y, He L, Zhang H, Hu Q, Yue H, et al. A trial of pirfenidone in hospitalized adult patients with severe coronavirus disease 2019. Chin Med J (Engl). 2022 Feb 5;135(3):368–70.

277. Flores-Contreras L, Sandoval-Rodríguez AS, Mena-Enriquez MG, Lucano-Landeros S, Arellano-Olivera I, Álvarez-Álvarez A, et al. Treatment with pirfenidone for two years decreases fibrosis, cytokine levels and enhances CB2 gene expression in patients with chronic hepatitis C. BMC Gastroenterol. 2014 Dec 27;14(1):131.

278. Flaherty KR, Wells AU, Cottin V, Devaraj A, Walsh SLF, Inoue Y, et al. Nintedanib in Progressive Fibrosing Interstitial Lung Diseases. New England Journal of Medicine. 2019 Oct 31;381(18):1718–27.

279. Huang J, Beyer C, Palumbo-Zerr K, Zhang Y, Ramming A, Distler A, et al. Nintedanib inhibits fibroblast activation and ameliorates fibrosis in preclinical models of systemic sclerosis. Ann Rheum Dis. 2016 May;75(5):883–90.

280. Liu F, Wang L, Qi H, Wang J, Wang Y, Jiang W, et al. Nintedanib, a triple tyrosine kinase inhibitor, attenuates renal fibrosis in chronic kidney disease. Clin Sci. 2017 Aug 15;131(16):2125–43.

281. Öztürk Akcora B, Storm G, Prakash J, Bansal R. Tyrosine kinase inhibitor BIBF1120 ameliorates inflammation, angiogenesis and fibrosis in CCl4-induced liver fibrogenesis mouse model. Sci Rep. 2017 Apr 14;7(1):44545.

282. Rangarajan S, Kurundkar A, Kurundkar D, Bernard K, Sanders YY, Ding Q, et al. Novel Mechanisms for the Antifibrotic Action of Nintedanib. Am J Respir Cell Mol Biol. 2016 Jan;54(1):51–9.

283. Wollin L, Maillet I, Quesniaux V, Holweg A, Ryffel B. Antifibrotic and Anti-inflammatory Activity of the Tyrosine Kinase Inhibitor Nintedanib in Experimental Models of Lung Fibrosis. Journal of Pharmacology and Experimental Therapeutics. 2014 May;349(2):209–20.

284. Biernacka A, Dobaczewski M, Frangogiannis NG. TGF-β signaling in fibrosis. Growth Factors. 2011 Oct 11;29(5):196–202.

285. Margadant C, Sonnenberg A. Integrin–TGF-β crosstalk in fibrosis, cancer and wound healing. EMBO Rep. 2010 Feb 15;11(2):97–105.

286. Saadat S, Noureddini M, Mahjoubin-Tehran M, Nazemi S, Shojaie L, Aschner M, et al. Pivotal Role of TGF-β/Smad Signaling in Cardiac Fibrosis: Non-coding RNAs as Effectual Players. Front Cardiovasc Med. 2021 Jan 25;7.

287. Dennler S. Direct binding of Smad3 and Smad4 to critical TGFbeta -inducible elements in the promoter of human plasminogen activator inhibitor-type 1gene. EMBO J. 1998 Jun 1;17(11):3091–100.

288. Chen Y, Blom IE, Sa S, Goldschmeding R, Abraham DJ, Leask A. CTGF expression in mesangial cells: Involvement of SMADs, MAP kinase, and PKC. Kidney Int. 2002 Oct;62(4):1149–59.

289. Khan S, Joyce J, Margulies KB, Tsuda T. Enhanced Bioactive Myocardial Transforming Growth Factor-β in Advanced Human Heart Failure. Circulation Journal. 2014;78(11):2711–8.

290. Yoshida K, Matsuzaki K, Mori S, Tahashi Y, Yamagata H, Furukawa F, et al. Transforming Growth Factor-β and Platelet-Derived Growth Factor Signal via c-Jun N-Terminal Kinase-Dependent Smad2/3 Phosphorylation in Rat Hepatic Stellate Cells after Acute Liver Injury. Am J Pathol. 2005 Apr;166(4):1029–39.

291. Furukawa F. p38 MAPK mediates fibrogenic signal through Smad3 phosphorylation in rat myofibroblasts. Hepatology. 2003 Oct;38(4):879–89.

292. Li Q, Xu Y, Li X, Guo Y, Liu G. Inhibition of Rho-kinase ameliorates myocardial remodeling and fibrosis in pressure overload and myocardial infarction: Role of TGF-β1–TAK1. Toxicol Lett. 2012 Jun;211(2):91–7.

293. Moulik S, Speth R, Turner B, Rowe B. Angiotensin II receptor subtype distribution in the rabbit brain. Exp Brain Res. 2002 Jan 1;142(2):275–83.

294. Kramár EA, Harding JW, Wright JW. Angiotensin II- and IV-induced changes in cerebral blood flow. Regul Pept. 1997 Jan;68(2):131–8.

295. van Kats JP, Danser AHJ, van Meegen JR, Sassen LMA, Verdouw PD, Schalekamp MADH. Angiotensin Production by the Heart. Circulation. 1998 Jul 7;98(1):73–81.

296. Paz Ocaranza M, Riquelme JA, García L, Jalil JE, Chiong M, Santos RAS, et al. Counter-regulatory renin–angiotensin system in cardiovascular disease. Nat Rev Cardiol. 2020 Feb 19;17(2):116–29.

297. Kurisu S, Ozono R, Oshima T, Kambe M, Ishida T, Sugino H, et al. Cardiac Angiotensin II Type 2 Receptor Activates the Kinin/NO System and Inhibits Fibrosis. Hypertension. 2003 Jan;41(1):99–107.

298. Ohkubo N, Matsubara H, Nozawa Y, Mori Y, Murasawa S, Kijima K, et al. Angiotensin Type 2 Receptors Are Reexpressed by Cardiac Fibroblasts From Failing Myopathic Hamster Hearts

and Inhibit Cell Growth and Fibrillar Collagen Metabolism. Circulation. 1997 Dec 2;96(11):3954–62.

299. Forrester SJ, Booz GW, Sigmund CD, Coffman TM, Kawai T, Rizzo V, et al. Angiotensin II Signal Transduction: An Update on Mechanisms of Physiology and Pathophysiology. Physiol Rev. 2018 Jul 1;98(3):1627–738.

300. Kawai T, Forrester SJ, O'Brien S, Baggett A, Rizzo V, Eguchi S. AT1 receptor signaling pathways in the cardiovascular system. Pharmacol Res. 2017 Nov;125:4–13.

301. Zhou Y, Poczatek MH, Berecek KH, Murphy-Ullrich JE. Thrombospondin 1 mediates angiotensin II induction of TGF-β activation by cardiac and renal cells under both high and low glucose conditions. Biochem Biophys Res Commun. 2006 Jan;339(2):633–41.

302. Sopel MJ, Rosin NL, Lee TD, Légaré JF. Myocardial fibrosis in response to Angiotensin II is preceded by the recruitment of mesenchymal progenitor cells. Laboratory Investigation. 2011 Apr 29;91(4):565–78.

303. Díez J, Querejeta R, López B, González A, Larman M, Martínez Ubago JL. Losartan-Dependent Regression of Myocardial Fibrosis Is Associated With Reduction of Left Ventricular Chamber Stiffness in Hypertensive Patients. Circulation. 2002 May 28;105(21):2512–7.

304. Yamazaki T, Yamashita N, Izumi Y, Nakamura Y, Shiota M, Hanatani A, et al. The antifibrotic agent pirfenidone inhibits angiotensin II-induced cardiac hypertrophy in mice. Hypertension Research. 2012 Jan 25;35(1):34–40.

305. Messerli FH, Staessen JA, Zannad F. Of fads, fashion, surrogate endpoints and dual RAS blockade. Eur Heart J. 2010 Sep 2;31(18):2205–8.

306. Telmisartan, Ramipril, or Both in Patients at High Risk for Vascular Events. New England Journal of Medicine. 2008 Apr 10;358(15):1547–59.

307. Wan Y, Wallinder C, Plouffe B, Beaudry H, Mahalingam AK, Wu X, et al. Design, Synthesis, and Biological Evaluation of the First Selective Nonpeptide AT_2 Receptor Agonist. J Med Chem. 2004 Nov 1;47(24):5995–6008.

308. Rehman A, Leibowitz A, Yamamoto N, Rautureau Y, Paradis P, Schiffrin EL. Angiotensin Type 2 Receptor Agonist Compound 21 Reduces Vascular Injury and Myocardial Fibrosis in Stroke-Prone Spontaneously Hypertensive Rats. Hypertension. 2012 Feb;59(2):291–9.

309. Lauer D, Slavic S, Sommerfeld M, Thöne-Reineke C, Sharkovska Y, Hallberg A, et al. Angiotensin Type 2 Receptor Stimulation Ameliorates Left Ventricular Fibrosis and Dysfunction via Regulation of Tissue Inhibitor of Matrix Metalloproteinase 1/Matrix Metalloproteinase 9 Axis and Transforming Growth Factor β1 in the Rat Heart. Hypertension. 2014 Mar;63(3).

310. Park JW. Association of galectin-1 and galectin-3 with Gemin4 in complexes containing the SMN protein. Nucleic Acids Res. 2001 Sep 1;29(17):3595–602.

311. Dagher SF, Wang JL, Patterson RJ. Identification of galectin-3 as a factor in pre-mRNA splicing. Proceedings of the National Academy of Sciences. 1995 Feb 14;92(4):1213–7.

312. Nakahara S, Oka N, Raz A. On the role of galectin-3 in cancer apoptosis. Apoptosis. 2005 Mar;10(2):267–75.

313. Menon RP, Hughes RC. Determinants in the N-terminal domains of galectin-3 for secretion by a novel pathway circumventing the endoplasmic reticulum-Golgi complex. Eur J Biochem. 1999 Sep;264(2):569–76.

314. Johannes L, Jacob R, Leffler H. Galectins at a glance. J Cell Sci. 2018 May 1;131(9).

315. Sharma UC, Pokharel S, van Brakel TJ, van Berlo JH, Cleutjens JPM, Schroen B, et al. Galectin-3 Marks Activated Macrophages in Failure-Prone Hypertrophied Hearts and Contributes to Cardiac Dysfunction. Circulation. 2004 Nov 9;110(19):3121–8.

316. Liu YH, D'Ambrosio M, Liao T dong, Peng H, Rhaleb NE, Sharma U, et al. *N* -acetyl-seryl-aspartyl-lysyl-proline prevents cardiac remodeling and dysfunction induced by galectin-3, a mammalian adhesion/growth-regulatory lectin. American Journal of Physiology-Heart and Circulatory Physiology. 2009 Feb;296(2):H404–12.

317. Yu L, Ruifrok WPT, Meissner M, Bos EM, van Goor H, Sanjabi B, et al. Genetic and Pharmacological Inhibition of Galectin-3 Prevents Cardiac Remodeling by Interfering With Myocardial Fibrogenesis. Circ Heart Fail. 2013 Jan;6(1):107–17.

318. Lopez-Andrès N, Rossignol P, Iraqi W, Fay R, Nuée J, Ghio S, et al. Association of galectin-3 and fibrosis markers with long-term cardiovascular outcomes in patients with heart failure, left ventricular dysfunction, and dyssynchrony: insights from the CARE-HF (Cardiac Resynchronization in Heart Failure) trial. Eur J Heart Fail. 2012 Jan;14(1):74–81.

319. de Boer RA, van Veldhuisen DJ, Gansevoort RT, Muller Kobold AC, van Gilst WH, Hillege HL, et al. The fibrosis marker galectin-3 and outcome in the general population. J Intern Med. 2012 Jul;272(1):55–64.

320. Ho JE, Liu C, Lyass A, Courchesne P, Pencina MJ, Vasan RS, et al. Galectin-3, a Marker of Cardiac Fibrosis, Predicts Incident Heart Failure in the Community. J Am Coll Cardiol. 2012 Oct;60(14):1249–56.

321. Srivatsan V, George M, Shanmugam E. Utility of galectin-3 as a prognostic biomarker in heart failure: where do we stand? Eur J Prev Cardiol. 2015 Sep 29;22(9):1096–110.

322. Yancy CW, Jessup M, Bozkurt B, Butler J, Casey DE, Drazner MH, et al. 2013 ACCF/AHA Guideline for the Management of Heart Failure. J Am Coll Cardiol. 2013 Oct;62(16):e147–239.

323. Holbourn KP, Acharya KR, Perbal B. The CCN family of proteins: structure–function relationships. Trends Biochem Sci. 2008 Oct;33(10):461–73.

324. Chen MM, Lam A, Abraham JA, Schreiner GF, Joly AH. CTGF Expression is Induced by TGF- β in Cardiac Fibroblasts and Cardiac Myocytes: a Potential Role in Heart Fibrosis. J Mol Cell Cardiol. 2000 Oct;32(10):1805–19.

325. Wang CH, Weng CM, Chung KF, Kuo HP. TGF-β1-Mediated CTGF Upregulation Through Transactivation of EGFR in Fibrocytes of Chronic Obstructive Asthma. In: Airway Cell Biology and Immunopathology. European Respiratory Society; 2017. p. PA4917.

326. Adler SG, Schwartz S, Williams ME, Arauz-Pacheco C, Bolton WK, Lee T, et al. Phase 1 Study of Anti-CTGF Monoclonal Antibody in Patients with Diabetes and Microalbuminuria. Clinical Journal of the American Society of Nephrology. 2010 Aug;5(8):1420–8.

327. Gressner OA, Gressner AM. Connective tissue growth factor: a fibrogenic master switch in fibrotic liver diseases. Liver International. 2008 Aug 6;28(8):1065–79.

328. Uchio K, Graham M, Dean NM, Rosenbaum J, Desmoulière A. Down-regulation of connective tissue growth factor and type I collagen mRNA expression by connective tissue growth factor antisense oligonucleotide during experimental liver fibrosis. Wound Repair and Regeneration. 2004 Jan;12(1):60–6.

329. Brigstock DR. Connective tissue growth factor (CCN2, CTGF) and organ fibrosis: lessons from transgenic animals. J Cell Commun Signal. 2010 Mar 2;4(1):1–4.

330. Tong Z, Chen R, Alt DS, Kemper S, Perbal B, Brigstock DR. Susceptibility to liver fibrosis in mice expressing a connective tissue growth factor transgene in hepatocytes. Hepatology. 2009 Sep;50(3):939–47.

331. Leask A, Parapuram SK, Shi-wen X, Abraham DJ. Connective tissue growth factor (CTGF, CCN2) gene regulation: a potent clinical bio-marker of fibroproliferative disease? J Cell Commun Signal. 2009 Jun 21;3(2):89–94.

332. Dorn LE, Petrosino JM, Wright P, Accornero F. CTGF/CCN2 is an autocrine regulator of cardiac fibrosis. J Mol Cell Cardiol. 2018 Aug;121:205–11.

333. Chen MM, Lam A, Abraham JA, Schreiner GF, Joly AH. CTGF Expression is Induced by TGF- β in Cardiac Fibroblasts and Cardiac Myocytes: a Potential Role in Heart Fibrosis. J Mol Cell Cardiol. 2000 Oct;32(10):1805–19.

334. Yoon PO, Lee MA, Cha H, Jeong MH, Kim J, Jang SP, et al. The opposing effects of CCN2 and CCN5 on the development of cardiac hypertrophy and fibrosis. J Mol Cell Cardiol. 2010 Aug;49(2):294–303.

335. Accornero F, van Berlo JH, Correll RN, Elrod JW, Sargent MA, York A, et al. Genetic Analysis of Connective Tissue Growth Factor as an Effector of Transforming Growth Factor β Signaling and Cardiac Remodeling. Mol Cell Biol. 2015 Jun 15;35(12):2154–64.

336. Mori T, Kawara S, Shinozaki M, Hayashi N, Kakinuma T, Igarashi A, et al. Role and interaction of connective tissue growth factor with transforming growth factor-? in persistent fibrosis: A mouse fibrosis model. J Cell Physiol. 1999 Oct;181(1):153–9.

337. Isaacs C, Robert NJ, Bailey FA, Schuster MW, Overmoyer B, Graham M, et al. Randomized placebo-controlled study of recombinant human interleukin-11 to prevent chemotherapy-induced thrombocytopenia in patients with breast cancer receiving dose-intensive cyclophosphamide and doxorubicin. Journal of Clinical Oncology. 1997 Nov;15(11):3368–77.

338. Smith JW. Tolerability and side-effect profile of rhIL-11. Oncology (Williston Park). 2000 Sep;14(9 Suppl 8):41–7.

339. Liu N wei, Huang X, Liu S, Liu W jian, Wang H, Wang W da, et al. Elevated BNP caused by recombinant human interleukin-11 treatment in patients with chemotherapy-induced thrombocytopenia. Supportive Care in Cancer. 2019 Nov 15;27(11):4293–8.

340. Obana M, Maeda M, Takeda K, Hayama A, Mohri T, Yamashita T, et al. Therapeutic Activation of Signal Transducer and Activator of Transcription 3 by Interleukin-11 Ameliorates Cardiac Fibrosis After Myocardial Infarction. Circulation. 2010 Feb 9;121(5):684–91.

341. Tamura Y, Kohno H, Mohri T, Fujio Y, Matsumiya G. The cardioprotective effect of interleukin-11 against ischemia-reperfusion injury in a heart donor model. Ann Cardiothorac Surg. 2018 Jan;7(1):99–105.

342. Ye J, Wang Z, Ye D, Wang Y, Wang M, Ji Q, et al. Increased Interleukin-11 Levels Are Correlated with Cardiac Events in Patients with Chronic Heart Failure. Mediators Inflamm. 2019 Jan 8;2019:1–8.

343. Obana M, Miyamoto K, Murasawa S, Iwakura T, Hayama A, Yamashita T, et al. Therapeutic administration of IL-11 exhibits the postconditioning effects against ischemia-reperfusion injury via STAT3 in the heart. American Journal of Physiology-Heart and Circulatory Physiology. 2012 Sep 1;303(5):H569–77.

344. Kimura R, Maeda M, Arita A, Oshima Y, Obana M, Ito T, et al. Identification of cardiac myocytes as the target of interleukin 11, a cardioprotective cytokine. Cytokine. 2007 May;38(2):107–15.

345. Sano M, Fukuda K, Kodama H, Pan J, Saito M, Matsuzaki J, et al. Interleukin-6 Family of Cytokines Mediate Angiotensin II-induced Cardiac Hypertrophy in Rodent Cardiomyocytes. Journal of Biological Chemistry. 2000 Sep;275(38):29717–23.

346. Sopel MJ, Rosin NL, Lee TD, Légaré JF. Myocardial fibrosis in response to Angiotensin II is preceded by the recruitment of mesenchymal progenitor cells. Laboratory Investigation. 2011 Apr 29;91(4):565–78.

347. van Kats JP, de Lannoy LM, Danser AHJ, van Meegen JR, Verdouw PD, Schalekamp MADH. Angiotensin II Type 1 (AT1) Receptor–Mediated Accumulation of Angiotensin II in Tissues and Its Intracellular Half-life In Vivo. Hypertension. 1997 Jul;30(1):42–9.

348. Takayanagi T, Bourne AM, Kimura K, Takaguri A, Elliott KJ, Eguchi K, et al. Constitutive Stimulation of Vascular Smooth Muscle Cells by Angiotensin II Derived From an Adenovirus Encoding a Furin-Cleavable Fusion Protein. Am J Hypertens. 2012 Mar 1;25(3):280–3.

349. Kimura R, Maeda M, Arita A, Oshima Y, Obana M, Ito T, et al. Identification of cardiac myocytes as the target of interleukin 11, a cardioprotective cytokine. Cytokine. 2007 May;38(2):107–15.

350. Tamura Y, Kohno H, Mohri T, Fujio Y, Matsumiya G. The cardioprotective effect of interleukin-11 against ischemia-reperfusion injury in a heart donor model. Ann Cardiothorac Surg. 2018 Jan;7(1):99–105.

351. Obana M, Miyamoto K, Murasawa S, Iwakura T, Hayama A, Yamashita T, et al. Therapeutic administration of IL-11 exhibits the postconditioning effects against ischemia-reperfusion injury via STAT3 in the heart. American Journal of Physiology-Heart and Circulatory Physiology. 2012 Sep 1;303(5):H569–77.

352. Obana M, Maeda M, Takeda K, Hayama A, Mohri T, Yamashita T, et al. Therapeutic Activation of Signal Transducer and Activator of Transcription 3 by Interleukin-11 Ameliorates Cardiac Fibrosis After Myocardial Infarction. Circulation. 2010 Feb 9;121(5):684–91.

353. Widjaja AA, Singh BK, Adami E, Viswanathan S, Dong J, D'Agostino GA, et al. Inhibiting Interleukin 11 Signaling Reduces Hepatocyte Death and Liver Fibrosis, Inflammation, and Steatosis in Mouse Models of Nonalcoholic Steatohepatitis. Gastroenterology. 2019 Sep;157(3):777-792.e14.

354. Suthahar N, Meijers WC, Silljé HHW, Ho JE, Liu FT, de Boer RA. Galectin-3 Activation and Inhibition in Heart Failure and Cardiovascular Disease: An Update. Theranostics. 2018;8(3):593–609.

355. Sygitowicz G, Maciejak-Jastrzębska A, Sitkiewicz D. The Diagnostic and Therapeutic Potential of Galectin-3 in Cardiovascular Diseases. Biomolecules. 2021 Dec 29;12(1):46.

356. Hua X, Wang YY, Jia P, Xiong Q, Hu Y, Chang Y, et al. Multi-level transcriptome sequencing identifies COL1A1 as a candidate marker in human heart failure progression. BMC Med. 2020 Dec 6;18(1):2.

357. Frangogiannis NG. Cardiac fibrosis: Cell biological mechanisms, molecular pathways and therapeutic opportunities. Vol. 65, Molecular Aspects of Medicine. Elsevier Ltd; 2019. p. 70–99.

358. Morath C, Schwenger V, Beimler J, Mehrabi A, Schmidt J, Zeier M, et al. Antifibrotic actions of mycophenolic acid. Clin Transplant. 2006 Dec;20(s17):25–9.

359. JOHNSSON C, GERDIN B, TUFVESON G. Effects of commonly used immunosuppressants on graft-derived fibroblasts. Clin Exp Immunol. 2004 May 4;136(3):405–12.

360. Nambiar AM, Anzueto AR, Peters JI. Effectiveness and safety of mycophenolate mofetil in idiopathic pulmonary fibrosis. PLoS One. 2017 Apr 25;12(4):e0176312.

361. Wang Y, Liu K, Qi Z, Chen T, Yu W, Jiang Y, et al. Therapeutic Mechanism and Effect of Camptothecin on Dextran Sodium Sulfate-Induced Ulcerative Colitis in Mice. J Immunol Res. 2021 Apr 24;2021:1–13.

362. Zhang GY, Gao WY, Li X, Yi CG, Zheng Y, Li Y, et al. Effect of Camptothecin on Collagen Synthesis in Fibroblasts From Patients With Keloid. Ann Plast Surg. 2009 Jul;63(1):94–9.

363. Yun CH, Yoon SY, Nguyen TT, Cho HY, Kim TH, Kim ST, et al. Geldanamycin inhibits TGF-β signaling through induction of Hsp70. Arch Biochem Biophys. 2010 Mar;495(1):8–13.

364. Lee KH, Jang Y, Chung JH. Heat shock protein 90 regulates IκB kinase complex and NF-κB activation in angiotensin II-induced cardiac cell hypertrophy. Exp Mol Med. 2010;42(10):703.

365. Karkoulis PK, Stravopodis DJ, Konstantakou EG, Voutsinas GE. Targeted inhibition of heat shock protein 90 disrupts multiple oncogenic signaling pathways, thus inducing cell cycle arrest and programmed cell death in human urinary bladder cancer cell lines. Cancer Cell Int. 2013 Dec 8;13(1):11.

366. Maher TM, van der Aar EM, van de Steen O, Allamassey L, Desrivot J, Dupont S, et al. Safety, tolerability, pharmacokinetics, and pharmacodynamics of GLPG1690, a novel autotaxin inhibitor, to treat idiopathic pulmonary fibrosis (FLORA): a phase 2a randomised placebo-controlled trial. Lancet Respir Med. 2018 Aug;6(8):627–35.

367. Maher TM, Kreuter M, Lederer DJ, Brown KK, Wuyts W, Verbruggen N, et al. Rationale, design and objectives of two phase III, randomised, placebo-controlled studies of GLPG1690, a novel autotaxin inhibitor, in idiopathic pulmonary fibrosis (ISABELA 1 and 2). BMJ Open Respir Res. 2019 May 21;6(1):e000422.

368. Ligon AH, Kashork CD, Richards CS, Shaffer LG. Identification of female carriers for Duchenne and Becker muscular dystrophies using a FISH-based approach. European Journal of Human Genetics. 2000 Apr 15;8(4):293–8.

369. Moser H, Emery AEH. The manifesting carrier in Duchenne muscular dystrophy. Clin Genet. 2008 Apr 23;5(4):271–84.

370. Norman A, Harper P. A survey of manifesting carriers of Duchenne and Becker muscular dystrophy in Wales. Clin Genet. 2008 Jun 28;36(1):31–7.

371. Hoogerwaard E, Bakker E, Ippel P, Oosterwijk J, Majoor-Krakauer D, Leschot N, et al. Signs and symptoms of Duchenne muscular dystrophy and Becker muscular dystrophy among carriers in the Netherlands: a cohort study. The Lancet. 1999 Jun;353(9170):2116–9.

372. Kinoshita H, Goto Y ichi, Ishikawa M, Uemura T, Matsumoto K, Hayashi YK, et al. A carrier of Duchenne muscular dystrophy with dilated cardiomyopathy but no skeletal muscle symptom. Brain Dev. 1995 May;17(3):202–5.

373. Comi LI, Nigro G, Politano L, Petretta VR. The cardiomyopathy of Duchenne/Becker consultands. Int J Cardiol. 1992 Mar;34(3):297–305.

374. Mah ML, Cripe L, Slawinski MK, Al-Zaidy SA, Camino E, Lehman KJ, et al. Duchenne and Becker muscular dystrophy carriers: Evidence of cardiomyopathy by exercise and cardiac MRI testing. Int J Cardiol. 2020 Oct;316:257–65.

375. Lim KRQ, Sheri N, Nguyen Q, Yokota T. Cardiac Involvement in Dystrophin-Deficient Females: Current Understanding and Implications for the Treatment of Dystrophinopathies. Genes (Basel). 2020 Jul 8;11(7):765.

376. Ishizaki M, Kobayashi M, Adachi K, Matsumura T, Kimura E. Female dystrophinopathy: Review of current literature. Neuromuscul Disord. 2018;28(7):572–81.

377. Brioschi S, Gualandi F, Scotton C, Armaroli A, Bovolenta M, Falzarano MS, et al. Genetic characterization in symptomatic female DMD carriers: lack of relationship between X-inactivation, transcriptional DMD allele balancing and phenotype. BMC Med Genet. 2012 Dec 16;13(1):73.

378. Arahata K, Ishihara T, Kamakura K, Tsukahara T, Ishiura S, Baba C, et al. Mosaic Expression of Dystrophin in Symptomatic Carriers of Duchenne's Muscular Dystrophy. New England Journal of Medicine. 1989 Jan 19;320(3):138–42.

379. Soltanzadeh P, Friez MJ, Dunn D, von Niederhausern A, Gurvich OL, Swoboda KJ, et al. Clinical and genetic characterization of manifesting carriers of DMD mutations. Neuromuscular Disorders. 2010 Aug;20(8):499–504.

380. Biomarkers and surrogate endpoints: Preferred definitions and conceptual framework. Clin Pharmacol Ther. 2001 Mar;69(3):89–95.

381. Berger R, Huelsman M, Strecker K, Bojic A, Moser P, Stanek B, et al. B-Type Natriuretic Peptide Predicts Sudden Death in Patients With Chronic Heart Failure. Circulation. 2002 May 21;105(20):2392–7.

382. Frank R, Hargreaves R. Clinical biomarkers in drug discovery and development. Nat Rev Drug Discov. 2003 Jul;2(7):566–80.

383. Gabay C, Msihid J, Zilberstein M, Paccard C, Lin Y, Graham NMH, et al. Identification of sarilumab pharmacodynamic and predictive markers in patients with inadequate response to TNF inhibition: a biomarker substudy of the phase 3 TARGET study. RMD Open. 2018 Mar 14;4(1):e000607.

384. Arvanitidis A, Henriksen K, Karsdal MA, Nedergaard A. Neo-epitope Peptides as Biomarkers of Disease Progression for Muscular Dystrophies and Other Myopathies. J Neuromuscul Dis. 2016 Aug 30;3(3):333–46.

385. Leeming DJ, Sand JM, Nielsen MJ, Genovese F, Martinez FJ, Hogaboam CM, et al. Serological Investigation of the Collagen Degradation Profile of Patients with Chronic Obstructive Pulmonary Disease or Idiopathic Pulmonary Fibrosis. Biomark Insights. 2012 Jan 13;7:BMI.S9415.

386. Genovese F, Manresa AA, Leeming DJ, Karsdal MA, Boor P. The extracellular matrix in the kidney: a source of novel non-invasive biomarkers of kidney fibrosis? Fibrogenesis Tissue Repair. 2014 Dec 28;7(1):4.

387. Hall Z, Chiarugi D, Charidemou E, Leslie J, Scott E, Pellegrinet L, et al. Lipid Remodeling in Hepatocyte Proliferation and Hepatocellular Carcinoma. Hepatology. 2021 Mar 3;73(3):1028–44.

388. Folch J, Lees M, Sloane Stanley G. A simple method for the isolation and purification of total lipids from animal tissues. J Biol Chem. 1957;226(1):497–503.

389. Searle BC, Swearingen KE, Barnes CA, Schmidt T, Gessulat S, Küster B, et al. Generating high quality libraries for DIA MS with empirically corrected peptide predictions. Nat Commun. 2020 Dec 25;11(1):1548.

390. Merchant ML, Klein JB. Proteomic Discovery of Diabetic Nephropathy Biomarkers. Adv Chronic Kidney Dis. 2010 Nov;17(6):480–6.

391. Hanash S, Taguchi A. Application of Proteomics to Cancer Early Detection. The Cancer Journal. 2011 Nov;17(6):423–8.

392. Dang UJ, Ziemba M, Clemens PR, Hathout Y, Conklin LS, Hoffman EP. Serum biomarkers associated with baseline clinical severity in young steroid-naïve Duchenne muscular dystrophy boys. Hum Mol Genet. 2020 Aug 29;29(15):2481–95.

393. Christoffersen C. Apolipoprotein M—A Marker or an Active Player in Type II Diabetes? Front Endocrinol (Lausanne). 2021 May 21;12.

394. Ayoglu B, Chaouch A, Lochmüller H, Politano L, Bertini E, Spitali P, et al. Affinity proteomics within rare diseases: a <scp>BIO</scp> - <scp>NMD</scp> study for blood biomarkers of muscular dystrophies. EMBO Mol Med. 2014 Jul 11;6(7):918–36.

395. Hathout Y, Brody E, Clemens PR, Cripe L, DeLisle RK, Furlong P, et al. Large-scale serum protein biomarker discovery in Duchenne muscular dystrophy. Proceedings of the National Academy of Sciences. 2015 Jun 9;112(23):7153–8.

396. Nielsen SH, Mygind ND, Michelsen MM, Bechsgaard DF, Suhrs HE, Genovese F, et al. Accelerated collagen turnover in women with angina pectoris without obstructive coronary artery disease: An iPOWER substudy. Eur J Prev Cardiol. 2018 May 13;25(7):719–27.

397. Laake K, Seljeflot I, Schmidt E, Myhre P, Tveit A, Norseth J, et al. Galectin-3, a marker of cardiac remodeling, is inversely related to serum levels of marine omega-3 fatty acids. A cross-sectional study. JRSM Cardiovasc Dis. 2017 Jan 12;6:204800401772998.

398. Wannamethee SG, Tchernova J, Whincup P, Lowe GDO, Kelly A, Rumley A, et al. Plasma leptin: Associations with metabolic, inflammatory and haemostatic risk factors for cardiovascular disease. Atherosclerosis. 2007 Apr;191(2):418–26.

399. Bobbert P, Jenke A, Bobbert T, Kühl U, Rauch U, Lassner D, et al. High leptin and resistin expression in chronic heart failure: adverse outcome in patients with dilated and inflammatory cardiomyopathy. Eur J Heart Fail. 2012 Nov 18;14(11):1265–75.